Design and Synthesis of Orally Bioavailable Sphingosine Kinase 2 Selective Inhibitors

Christopher David Sibley

Dissertation submitted to the faculty of the Virginia Polytechnic Institute and State University in partial fulfillment of the requirements for the degree of

Doctor of Philosophy
In
Chemistry

Webster L. Santos, Chair
Paul R. Carlier
David G. I. Kingston
Andrew N. Lowell

June 15, 2020
Blacksburg, VA

Keywords: Sphingosine Kinase, SphK2, Sphingosine, Sphingosine 1-Phosphate, S1P, Inhibitor, SAR, Molecular Docking, Guanidine, Prodrug, Oral Bioavailability

Design and Synthesis of Orally Bioavailable Sphingosine Kinase 2 Selective Inhibitors

Christopher David Sibley

Abstract

In humans, mammals, and perhaps all vertebrates, sphingolipids exist as a family of cellular signaling molecules and have been shown to be involved in a wide range of biological processes ranging from proliferation to apoptosis. As such, sphingolipid signaling has garnered the attention of numerous researchers as an attractive candidate for pharmacological manipulation. The synthetic pathway of one prominent sphingolipid, sphingosine 1-phosphate (S1P), has been implicated in a variety of disease states such as cancer, sickle cell disease, multiple sclerosis, and renal fibrosis. Formation of S1P is facilitated from the ATP dependent phosphorylation of sphingosine (Sph) through its generative enzyme's sphingosine kinase 1 and 2 (SphK1 and SphK2). Inhibition of SphK1 and SphK2 results in the manipulation of S1P levels, which has been shown to be therapeutic in various animal models of disease. While there are multiple examples of potent SphK1-selective and dual SphK1/2 inhibitors, SphK2-selective inhibitors are scarce.

Herein, we describe the design, synthesis and biological testing of SphK2-selective inhibitors. We first describe the discovery that introducing a trifluoromethyl group onto the internal aryl ring of our inhibitor scaffold led to superior selectivity and potency towards SphK2. We demonstrate that the trifluoromethyl moiety is interacting with a previously unknown side cavity in the substrate binding site of SphK2 that is unique and could be exploited in the design of SphK2-selective inhibitors. The synthesis of 21 derivatives with various substituents spanning off the internal aryl ring was completed, therefore characterizing the preferred size and chemical nature of moieties positioned in that portion of the binding site. This work led to the development

of the most potent SphK2-selective inhibitor known at the time. We then describe the transformation of our SphK2-selective inhibitors into an orally bioavailable drug. We explain how the guanidine functionality on our inhibitor scaffold hinders our compounds from being orally bioavailable. Consequently, a library of 24 derivatives with various modifications to the guanidine functionality was synthesized and evaluated for improved orally bioavailability. Highlighted in this work is the development of the most potent SphK2-selective inhibitor currently known **3.14** (**SLS1081832**), which displays a hSphK2 K_i of 82 nM and 122-fold selectivity for SphK2. Chemical modification and *in vivo* assessment of **3.14** (**SLS1081832**) prodrugs was explored.

Design and Synthesis of Orally Bioavailable Sphingosine Kinase 2 Selective Inhibitors

Christopher David Sibley

General Audience Abstract

In humans, sphingosine 1-phosphate (S1P) is a signaling molecule that is generated through an ATP dependent reaction of sphingosine (Sph) *via* sphingosine kinase 1 and 2 (SphK1 and SphK2). Furthermore, S1P has been shown to be implicated in various diseases such as cancer, sickle cell disease, multiple sclerosis, and renal fibrosis. Inhibition of SphK1 and SphK2 has been shown to be therapeutic towards the symptoms of these diseases. Therefore, in order to alleviate these disorders, the concentrations of S1P must be controlled through pharmacological inhibition of SphK1 and SphK2. There are multiple reported examples of potent SphK1-selective and dual SphK1/2 inhibitors; however, SphK2-selective inhibitors are scarce. This work describes the synthesis and biological assessment of 21 compounds for their effectiveness in selectively targeting and inhibiting SphK2. The work led to the discovery of a previously unrecognized side cavity in the binding pocket of SphK2 that enhances inhibitor potency and selectivity towards SphK2. Furthermore, studies characterizing the preferred size and chemical nature of moieties positioned in that portion of the binding site led to the development of the most potent SphK2-selective inhibitor known at the time. Building on this work, we next focused on the transformation of our SphK2-selective inhibitors into a drug that could be administered orally. We describe the synthesis of 24 compounds with various modifications to one portion of our scaffold and their effect on improved orally bioavailability. This work led to the development of the most potent SphK2-selective inhibitor currently known **3.14** (**SLS1081832**)

Acknowledgements

I would first like to thank my committee advisor Dr. Webster L. Santos for his years of mentorship and support. As an undergraduate junior at Virginia Tech looking for a chemistry laboratory to receive research credit, he took me under his wing and provided the knowledge, guidance, and support I needed to enter into graduate school and traverse through the program. I would next like to thank my committee members Dr. Paul R. Carlier, Dr. David G. I. Kingston, and Dr. Andrew N. Lowell. Through my lecture course work and research progress over the past five years, they have provided me fantastic constructive criticism and advice to fine-tune my abilities as a chemist and scientific professional.

Next, I would like to thank our collaborators for the wonderful work they have provided for our research campaigns. First, from the Department of Pharmacology at the University of Virginia, Dr. Kevin R. Lynch, Dr. Yugesh Kharel, and Dr. Tao Huang for their biological contributions pertaining to sphingosine kinase. Second, from the Department of Biochemistry at Virginia Tech, Dr. Anne M. Brown, and Dr. David R. Bevan for their computational modeling work with sphingosine kinase and our inhibitors.

Additionally, I would like to thank the Santos lab research assistant Karen Iannaccone, as well as the Virginia Tech Graduate Chemistry Program Coordinator Joli Huynh. Without their help and organizational skills, I would have been lost and wouldn't have made it past the first year of the program. Furthermore, I would like to thank all of the Santos lab members, both past and present, through my seven years with the group. Namely, Dr. Elizabeth Childress, Dr. Molly Congdon, Kenneth Knott, Dr. Hao Li, Emily Morris, Dr. Cheryl Peck, Dr. Jessica Wynn, Dr. Amanda Nelson, Dr. Russell Snead, Dr. Yumin Dai, Dr. Srinath Pashikanti, Dr. Astha Verma, Dr.

Jan Nekvinda, Dr. Ashley Peralta, Dr. Russell Fritzemeier, Dr. Ashley Gates, Justin Grams, Eric Medici, Jose Santiago-Rivera, Jacob Murray, Christopher Garcia, Daniel Foster, Johnathan Bowen, Connor Szwetkowski, Swetha Jos, Ariel Burgio, Kyle Dunnavant, Michael Payette, Christopher Shrader, Carol Ann Rosenblum, Annalise Pham, and Laura Wonilowicz. They have all provided me countless laughs, guidance (some helpful, some not), leadership, wisdom, and friendship. I know that without them, coming into work every day wouldn't be the same.

Finally, I would like to give special acknowledgements to my family and girlfriend Jessie. Since I was a little kid, my parents Janice and David Sibley have fostered and encouraged my scientific curiosity. As a child, they supported me countless times by purchasing books for me to read, helping me out with my grade school science fairs, teaching me about all the amazing plants and animals in this world, and bringing me to "take your child to work day" at the NIH. They had more of an impact for me to become a chemist than they realize. I would like to thank my brother Mike, and my sister Robin for their support throughout my college and graduate career. The two of them were always there to provide advice and support when I needed it. Lastly, I would like to thank my girlfriend Jessie, and our dog Colby. For the last eight years of our relationship, and three with Colby, they have given me endless laughs, love, and support that I could never repay. Looking back, I was constantly in awe and inspired from watching Jessie climb the mountain that is veterinary school and become a Doctor of Veterinary Medicine, as well as witnessing Colby climb the mountain that is getting out of her bed in the morning. From observing Jessie every day, I truly witnessed what the definition of hard work is. Words cannot express how much they both mean to me and how important they were for my graduate studies.

Table of Contents

List of Figures

List of Tables

List of Schemes

1 The Sphingosine 1-Phosphate Synthetic Pathway

1.1 Introduction

In order to execute biological processes within a living system, both intra- and extracellular communication is essential. Cellular signaling is one mechanism of a complex arrangement of chemical communication that regulates various activities within and between cells. One prominent class of signaling molecules are sphingolipids, which play vital roles in both health and disease processes. One member of the sphingolipid family, sphingosine 1-phospahte (S1P), has been shown to be involved in a broad range of signaling cascades resulting in both cellular proliferation and pro-survival to cell arrest and apoptosis.[1,2] Production of S1P is exclusively due to the ATP dependent phosphorylation of sphingosine (Sph) by sphingosine kinase (SphK) (Figure 1.1). SphK exists in two isoforms, namely, sphingosine kinase 1 (SphK1) and sphingosine kinase 2 (SphK2). A multitude of studies have implicated SphK1 and SphK2 to various diseases including cancer,[3–8] multiple sclerosis,[9,10] sickle cell disease,[11,12] and fibrosis.[13–15] Furthermore, inhibition of SphKs in animal models of these diseases have shown to have therapeutic effects towards alleviating the symptoms of these disorders.[1,16] While there are numerous examples of potent SphK1-selective and dual SphK1/2 inhibitors, SphK2-selective inhibitors are sparse, thus highlighting the need for further study. Taken altogether, the S1P synthetic pathway stands as an attractive target for pharmacological intervention and drug therapy. This review will focus on elucidating the S1P synthetic pathway, its role in disease, and notable SphK2-selective inhibitors.

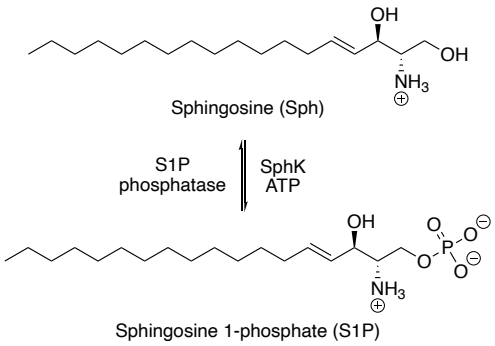

Figure 1.1. The synthesis of S1P and the Sph/S1P equilibrium.

1.2 Sphingolipids

Sphingolipids are simple polar lipids characterized by the presence of a long nonpolar carbon chain accompanied by a terminal amino alcohol. Sphingolipids exist on the cellular membrane in humans, and presumably all mammals and can be utilized as potent signaling molecules for the cell.[17] Numerous studies have implicated sphingolipids to be key players in a broad spectrum of signaling cascades ranging from proliferation and growth to cellular stress and apoptosis.[3,11,17] Noteworthy examples include ceramide (Cer), Sph, and S1P. These three sphingolipids are part of a hypothesized Cer/S1P rheostat that regulates cellular fate.[18] In general, elevated concentrations of Cer and Sph have been correlated with pro-apoptotic pathways, whereas increased S1P levels are associated with pro-survival pathways. Controlling the equilibrium between Sph and S1P, thus controlling the balance of cellular death or survival, remains an interesting target for further investigation.

The production of S1P is exclusively from the action of one synthetic pathway beginning with Cer. As shown in Figure 1.2, Sph is synthesized from a ceramidase-catalyzed amide cleavage of Cer. Next, the newly synthesized Sph can be reversibly metabolized back to Cer *via* ceramide synthase, or proceed further down the synthetic pathway. Subsequently, S1P generation is

accomplished *via* the SphK-catalyzed phosphorylation of Sph with ATP. S1P can be utilized to regenerate Sph through S1P phosphatase or be permanently metabolized by S1P lyase into its degradation products hexadecenal and phosphoethanolamine. Alternatively, S1P can be utilized as an intra- or extracellular signaling molecule for a multitude of cellular processes.[2]

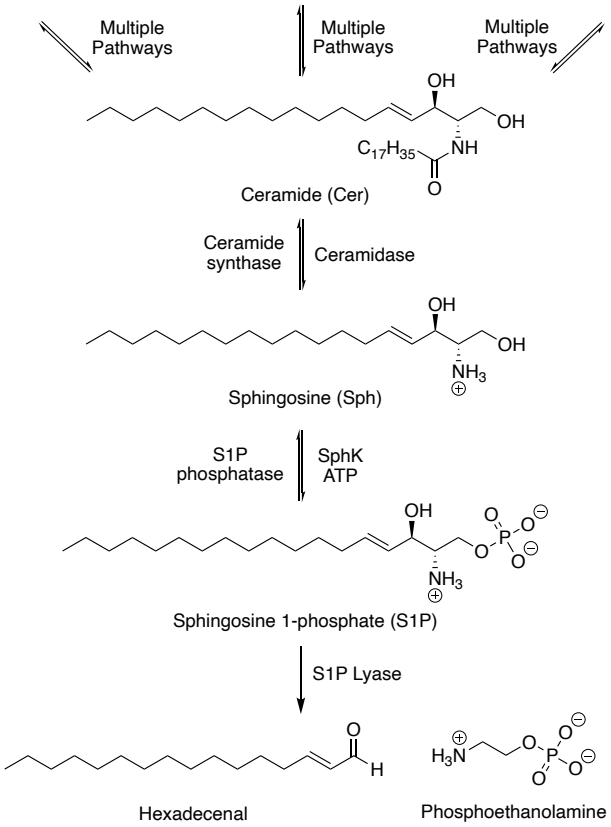

Figure 1.2. Biologic equilibrium of sphingolipids.

S1P circulates in the blood of humans, rodents and other mammals at low micromolar concentrations.[2] Although found throughout the body, the primary source of S1P is from erythrocytes. Interestingly, these cells lack S1P lyase, express high levels of SphK1, and possess their own unique S1P transporter Mfsd2b.[19] As shown in Figure 1.3, varying concentrations of both intra- and extracellular S1P can elicit either pro-survival or pro-apoptotic effects. For example, Laviad *et al.* published evidence that S1P produced inside of the endoplasmic reticulum

led to an up-regulation of ceramide synthase 2 (CerS2) activity. CerS2 is one of multiple ceramide synthase enzymes that catalyzes the synthesis of ceramide, a pro-apoptotic signaling molecule. S1P has been shown to induce CerS2 and increase the production of ceramide within the cell, leading to apoptotic events.[20] Likewise, studies performed by Chipuk *et al.* have demonstrated that mitochondrial S1P can interact with Bcl-2 homologous antagonist killer (BAK) protein resulting in elevated mitochondrial membrane permeabilization. This increased permeabilization leads to the release of the pro-apoptotic messenger cytochrome *c* into the cytosol, thus inducing cell death.[21] On the contrary, cytosolic S1P has been shown to promote proliferative effects for the cell. Experiments published by Alvarez *et al.* demonstrated that cytosolic S1P could stimulate tumor necrosis factor receptor-associated factor 2 (TRAF2).[22] Activation of TRAF2 produces an up-regulation of the protein complex NF-κB resulting in positive anti-apoptotic and immune processes.[22]

Notably, with the exclusion of erythrocytes, S1P can also be transported to the extracellular space *via* spinster homolog 2 (SPNS2). Upon translocation outside of the cell, S1P has a high affinity for five native G-protein coupled receptors $S1P_{1\text{-}5}$ resulting in a cascade of downstream signaling leading to cell survival and growth effects (Figure 1.3).[1,23] Recently, evidence published by Bruno *et al.* present a correlation between extracellular $S1P/S1P_2$ interactions and heightened β3-adrenoreceptor (β3-AR) activity.[24] The β3-AR subtype has shown to be heavily involved with sustaining the pathogenesis of various cancers such as neuroblastoma. Their experiments show evidence of S1P-induced $S1P_2$ cross-talk with β3-AR resulting in increased neuroblastoma tumor progression.[24] Furthermore, blockade of S1P synthesis through SphK inhibition has displayed therapeutic benefits. Among other pathways, S1P has been implicated in signaling events relevant to Alzheimer's disease,[25–28] fibrosis,[29–31] and some viral infections.[32,33]

Taken altogether, S1P and its generative enzyme SphK have been proven to be particularly interesting targets for pharmaceutical manipulation. In the examples stated above, each disease or pathway was commonly reliant on the relationship between S1P and SphK. Pharmacological control of the S1P/SphK synthetic pathway could enable command over pro-survival or pro-apoptotic pathways where signaling events have gone awry.

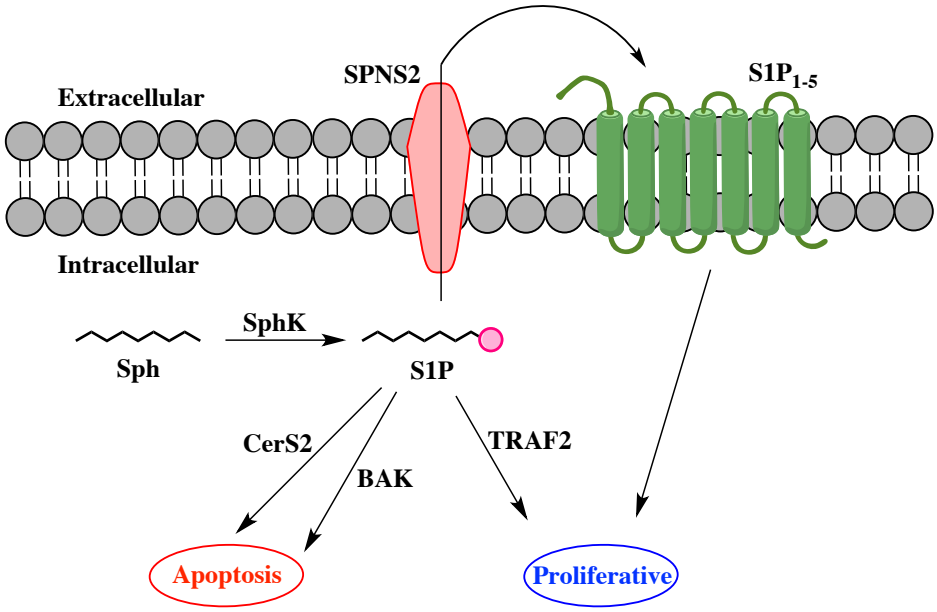

Figure 1.3. Intra- and extracellular signaling of S1P.

1.3 Sphingosine Kinase

Regulation of Sph and S1P levels to induce either pro-survival or pro-apoptotic cellular consequences is tightly controlled through the hypothesized Cer/S1P rheostat.[18] Two essential enzymes involved in the rheostat are SphK1 and SphK2. The function of these two kinases is somewhat redundant in that both catalyze the ATP dependent phosphorylation of Sph to S1P. Genetic knockout of SphKs in mice demonstrated that deletion of a single kinase isoform was not disadvantageous in any way, and mice remined fertile and phenotypically indistinguishable. However, it was observed that genetic knockout of both kinase isoforms was embryonically lethal

at about day E13.5.[34,35] Biochemically, SphK1 and SphK2 share a 47% amino acid sequence identity and 83% sequence similarity.[36] Illustrated in Figure 1.4, sequence comparison of the two isoforms reveals that both enzymes have five conserved domains (C1-C5). Furthermore, both kinases contain a catalytic domain in the C1-C3 region that encompasses the ATP binding site. However, distinctive differences can be seen with SphK2 with the addition of four transmembrane domains (TM1-TM4), as well as an additional proline-rich region resulting in an overall longer sequence length of 618 residues (384 in SphK1).[37]

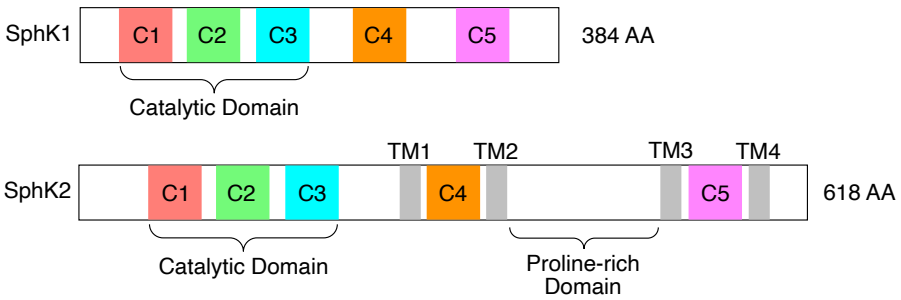

Figure 1.4. Sequence comparison of SphK1 versus SphK2.

SphK1 and SphK2 also differ in their substrate binding affinity (K_m) for Sph. Measured Sph affinity for SphK1 has been reported to be 10 μM, while SphK2 is around 5 μM.[36] Interestingly, substrate specificity has been shown to be fairly distinct between SphK1 and SphK2. Studies conducted with both isoforms have determined that SphK1 is substrate-specific for the native form for Sph, D-*erythro*-sphingosine. Conversely, SphK2 is somewhat more promiscuous and will phosphorylate a variety of substrates including D-*erythro*-sphingosine, D-*erythro*-dihydrosphingosine, phytosphingosine, and DL-*threo*-dihydrosphingosine (Figure 1.5).[36]

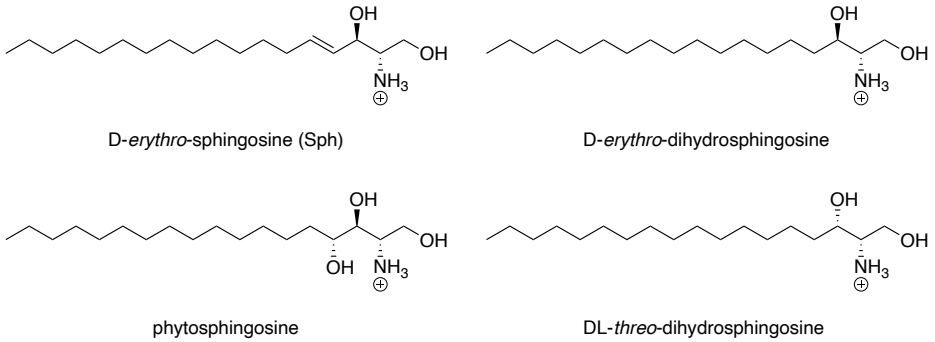

Figure 1.5. Structures of D-*erythro*-sphingosine, D-*erythro*-dihydrosphingosine, phytosphingosine, and DL-*threo*-dihydrosphingosine.

1.3.1 Sphingosine Kinase 1

Sphingosine Kinase 1 is commonly associated with cellular proliferation pathways and diseases.[4,30,38] Activation of SphK1 is mediated *via* phosphorylation of Ser225 catalyzed by extracellular signal-regulated kinase 1/2 (ERK1/2). In turn, this activation prompts SphK1 to migrate from the cytosol to the plasma membrane where it can acquire nearby Sph to synthesize S1P. Once synthesized, S1P can then be transported outside of the cell by SPNS2 to bind to its native G-protein coupled receptors $S1P_{1\text{-}5}$.[39,40] The $S1P_{1\text{-}5}$ cascade typically results in a flow of downstream signaling events that lead to cell survival and growth effects. The upregulation of SphK1 resulting in elevated pro-survival and growth pathways has been implicated as a contributor to multiple diseases such as cancer and fibrosis.[1,4,13,38]

As opposed to SphK2, the crystal structure of SphK1 as an apoprotein (PDB ID: 3VZB) and as a holoprotein (PDB ID: 3VZC) has been published.[41] Interestingly, the crystal structures portrayed the ligand binding channel of SphK1 as J-shaped and suggest substrates likely enter the binding pocket in a tail-to-head fashion.[41,42] Furthermore, it was observed that aspartic acid residue 81 (Asp81) serves as a catalytic mediator in the activation of Sph *via* deprotonation of the alpha-hydroxy moiety of Sph. This in turn sets up a nucleophilic attack by the Sph anion to the nearby

γ-phosphate of ATP to produce S1P.[41] Utilizing this information, researchers at Pfizer Inc. developed the most potent SphK1-selective inhibitor currently known, compound **1.1** (SphK1 K_i = 3.6 nM) (Figure 1.6).[43] Interestingly, when tested in an animal model of sickle cell disease, inhibitor **1.1** was successful in reducing plasma and blood S1P levels in mice leading to reduced erythrocyte sickling.[11]

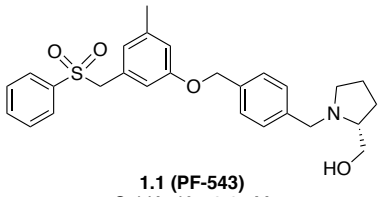

1.1 (PF-543)
SphK1 K_i = 3.6 nM

Figure 1.6. Structure of the SphK1-selective inhibitor **1.1** (PF-543).

1.3.2 Sphingosine Kinase 2

In humans and other mammals, sphingosine kinase 2 exists as two isoforms designated SphK2-S and SphK2-L. Functionally, the two enzymes are identical in that both catalyze the conversion of Sph to S1P. Sequence comparison of the two isoforms reveal that SphK2-S is slightly smaller than SphK2-L (618 versus 654 residues respectively).[36] Interestingly, other than the elongation seen in SphK2-L, the remaining sequence is identical and the biological role of the extra 36 N-terminal amino acid residues remains to be established.[44] Further analysis into the distribution of the two isoforms in the human body found that SphK2-L is the more commonly expressed enzyme except in the brain and kidneys.[44] The significance of this is still under investigation.

1.3.2.1 SphK2 Structure-Function Relationship

Structural comparison of SphK1 and SphK2 revealed a 47% amino acid sequence identity (83% sequence similarity) and five shared conserved domains.[36] However, contributing to its longer sequence, SphK2 also contains multiple unique regions not found in SphK1. In contrast to SphK1 which resides in the cytosol, SphK2 contains a nuclear localization sequence (NLS) to facilitate its occupation inside of the nucleus, although SphK2 can also be found in the mitochondria and endoplasmic reticulum.[45] In addition to the NLS, SphK2 contains a nuclear export sequence (NES) to grant transport out of the nucleus.[46] Selective phosphorylation of serine residues Ser419 and Ser421 in SphK2 grants access for the enzyme to translocate into the cytoplasm, subsequently allowing the synthesis of S1P for receptor signaling.[46] Furthermore, investigation into the proline-rich region of SphK2 found it to play a role in binding cytokine receptor IL-12Rβ1 resulting in the activation of IFN-γ promoted immune responses.[47]

1.3.2.2 SphK2 Localization-Function Relationship

In the cell, SphK2 can be found in the nucleus, endoplasmic reticulum (ER), and mitochondria.[2] Interestingly, the subcellular location of SphK2 can elicit different effects that determine cellular fate. There is evidence that production of S1P in the ER *via* SphK2 leads to an up-regulation of ceramide synthase 2 (CerS2) activity resulting in the production of the pro-apoptotic signaling molecule ceramide.[20] Likewise, mitochondrial SphK2 production of S1P has been shown to be correlated with an increase in Bcl-2 homologous antagonist killer (BAK) protein production resulting in elevated mitochondrial membrane permeabilization.[21] This elevated permeabilization leads to the release of the pro-apoptotic messenger cytochrome *c* into the cytosol thus inducing cell death.[21] Furthermore, S1P synthesized by SphK2 localized in the nucleus has

been shown to inhibit histone deacetylase 1 and 2 (HDAC1/2) activity, thus stimulating gene transcription and expression of p21, a protein associated with cell cycle arrest.[48,49]

On the contrary, investigations into nuclear SphK2 has suggested its activity to be proliferative. Sun *et al.* published findings demonstrating that nuclear S1P produced by SphK2 antagonized the activity of retinoic acid receptor beta (RARβ), a pro-apoptotic protein.[50] Furthermore, nuclear S1P has been shown to stabilize human telomerase reverse transcriptase (hTERT), thus inducing pro-survival effects.[51] Extracellularly, SphK2 has been suggested to possess anti-inflammatory and pro-survival effects as a result of extracellularly synthesized S1P to promote lymphocyte aggregation to damaged cells.[52] Recently, intracellular SphK2 has been implicated as a key mediator in the clearance of S1P from the blood (Figure 1.7).[53] Specifically, Sph formed at the hepatocyte surface *via* extracellular S1P and phospholipid phosphatase 3 (Plpp3) is captured by membrane associated SphK2. Once captured, SphK2 will phosphorylate Sph back to S1P which will then be released into the cytosol to be permanently degraded into hexadecenal and phosphoethanolamine by S1P lyase.[53] These results are in agreement with the well documented phenomenon of SphK2-specific inhibition or genetic deficiency. Curiously, SphK1-specific inhibition in mice or rats reduces blood S1P levels by about 50%, whereas SphK2-specific inhibition results in blood S1P levels to rise nearly 3-fold.[54–56] Regardless, the difference in isoform specific inhibition provides a convenient chemical switch to either increase or decrease blood S1P levels to evoke therapeutic responses towards the diseases discussed herein.

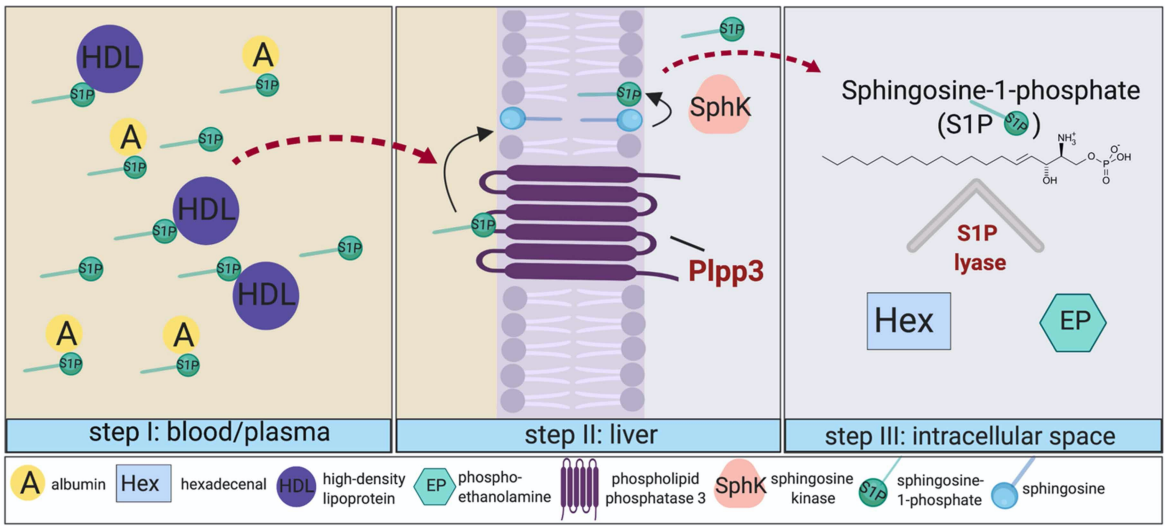

Figure 1.7. Mechanism of S1P clearance from the blood/plasma mediated by SphK2. Reused with permission from reference 53. Copyright 2020 Portland Press.

1.3.2.3 The SphK2 Substrate Binding Pocket

Recently, there have been reports of topographical differences in the Sph binding pocket of SphK1 versus SphK2.[57–59] These differences afford the potential for the development of isoform-selective inhibitors of SphK. In short, these reports present evidence illustrating the substrate binding site of SphK2 to extend deeper into the enzyme while the mid-section of SphK2 is wider due to an isoleucine-to-valine mutation.[57,58] As described by Worrell *et al.*, the SphK substrate binding pocket can be subdivided into 3 distinct regions. Precisely, (1) the head region adjacent to the ATP binding site, (2) the hydrophobic core, and (3) the tail region. Subtle, yet significant differences can be seen with the amino acid make-up in the hydrophobic core, and tail regions that can influence ligand specificity for SphKs. Specifically, an Ile174 (SphK1) to Val304 (SphK2) variation in the hydrophobic core and Phe288 (SphK1) to Cys533 (SphK2) deviation in the tail region. Functionally, with SphK2 possessing the smaller valine residue in the hydrophobic core, the binding pocket has more space to accommodate larger ligands that would not be tolerated

in this region of SphK1. Additionally, incorporation of the smaller cystine residue in SphK2 (phenylalanine in SphK1) permits ligands to migrate deeper into the binding pocket, which would be blocked in SphK1 by Phe288.[59] Taken altogether, these differences in the substrate binding site afford a unique opportunity for the rational design of isoform-specific inhibitors for each kinase.

1.3.2.4 The Role of SphK2 in Disease

Due to its involvement in multiple cellular processes and ability to act as both an intra- and extracellular signaling molecule, it is not surprising that S1P and SphK2 have been implicated in multiple disease states such as fibrosis,[13–15] multiple sclerosis,[9,10] and Alzheimer's disease.[25,26] Interestingly, depending on the disease model taken into consideration, inhibition of SphK2 can result in either therapeutic or harmful consequences.

In humans, the correlation between fibrosis progression and increased SphK2 activity is well documented. In one such study conducted by Xu *et al.*, administration of S1P in a mice model for cystic fibrosis (CF) induced heightened expression of major histocompatibility complex II (MHCII), which is essential for acquired immunity.[29] It was suggested that the observed increase in MHCII expression can potentially be therapeutic and boost immune response against CF. Hypothetically, administration of a SphK2-selective inhibitor, causing in a 3-fold increase in S1P concentrations, could serve as a valuable tool in the fight against CF. In addition to CF, S1P has been implicated in another form of fibrosis, renal fibrosis (RF). Long *et al.* established that elevated concentrations S1P were associated with RF regression.[30] Furthermore, increased levels of S1P were found to inhibit the activity of connective tissue growth factor (CTGF), a vital component for the progression of RF.[30] These results suggest that increasing the concentrations of blood S1P *via* a SphK2-selctive inhibitor could be a viable therapeutic against RF.

The S1P pathway has also been shown to be involved with multiple sclerosis (MS) progression. In 2010, the S1P signaling pathway became a validated druggable target with the FDA approval of the sphingosine analogue **1.2** (Fingolimod, Gilenya®) for the treatment of patients with relapsing remitting multiple sclerosis (rrMS) (Figure 1.8).[60] Mechanistically, **1.2** is a prodrug that is phosphorylated by nuclear SphK2. Phosphorylated **1.2** will travel outside of the cell and act as a functional antagonist causing S1P1/3/4/5 receptor internalization and degradation leading to therapeutic immunosuppression for rrMS patients. More recently, **1.3** (Siponimod, Mayzent®) was granted FDA approval for patients suffering from secondary progressive multiple sclerosis (Figure 1.8).[61] In each of the examples above, it has been shown that elevated levels of S1P are detrimental towards the regression of MS, and especially in the case of **1.2**, application of a SphK2-selective inhibitor would result in the diminished production of active metabolite, phospho-**1.2**.

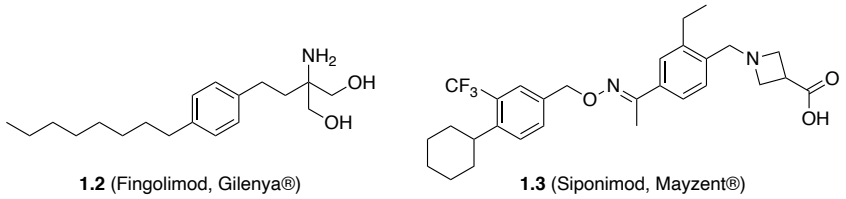

Figure 1.8. Structures of fingolimod and siponimod.

SphK2 may also be involved in the neurodegenerative disorder Alzheimer's disease (AD). Characteristic in the development of AD is the generation of senile plaques due to abundant aggregation of amyloid-β (Aβ) protein. Increased concentrations of S1P have been reported to result in anti-AD effects and could be favorable for AD regression and treatment.[25] Additionally, administration of an S1P analogue in mice expressing high levels of Aβ protein resulted in therapeutic effects.[25] Reasons for this effect have not yet been elucidated; however, based on the phenomenon that SphK2 inhibition results in elevated blood S1P levels, there is sufficient

motivation to develop a SphK2-selective inhibitor. Furthermore, experiments utilizing fluorescently labeled Aβ peptide found that membranes containing higher concentrations of Sph resulted in deeper penetration and binding of Aβ, while membranes with increased S1P levels developed decreased Aβ accumulation.[26] This study hypothesized that higher levels of membrane bound S1P may aid in the formation of an S1P lipid complex that results in an overall tighter packing of the lipid bilayer. This tighter packing ultimately results in the decreased ability of the Aβ peptide to penetrate the lipid membrane theoretically leading to a decrease in senile plaque formation.[26]

1.4 Notable Sphingosine Kinase 2 Selective Inhibitors

As a moderator in the synthesis of S1P and proposed role in numerous diseases, extensive research has been conducted on the development of inhibitors for SphK. As opposed to SphK1-selective, as well as dual SphK1/2 inhibitors, the development of highly potent SphK2-selective inhibitors is limited. Even so, there has been some moderate progress with compounds displaying encouraging results towards inhibiting SphK2 (Figure 1.9).

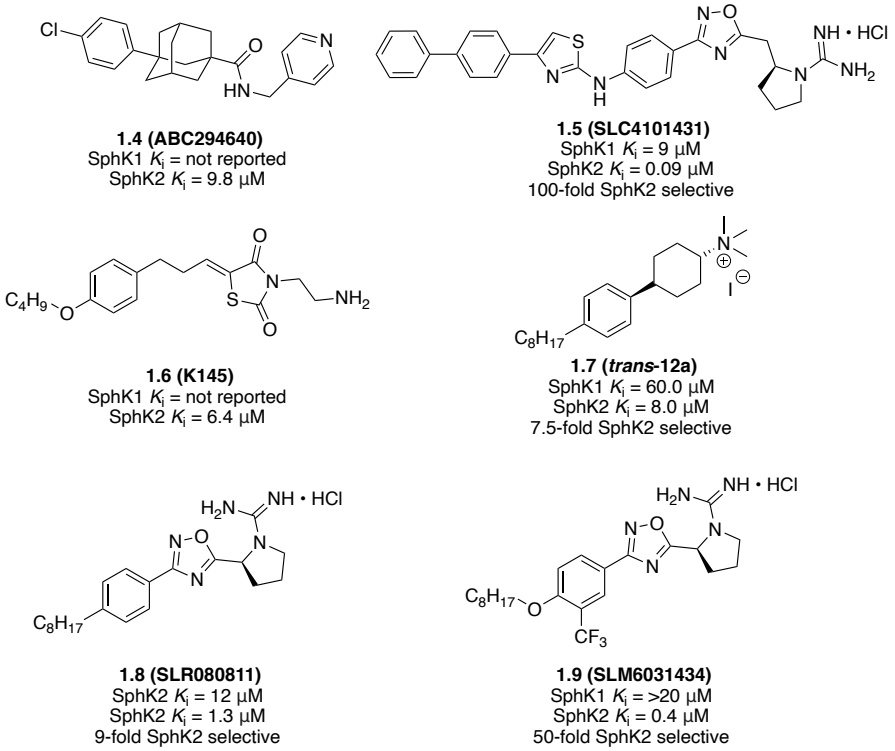

Figure 1.9. Structures of significant SphK2-selective inhibitors.

1.4.1 ABC294640

Perhaps one of the most extensively studied SphK2-selective inhibitors developed is the aryladamantane-based compound **1.4** (ABC294640) (Figure 1.9).[62] Inhibitor **1.4** is reported to be selective for SphK2, displaying moderate potency (K_i = 9.8 μM) and excellent pharmacodynamic properties. When tested with tissue culture, **1.4** was successful in suppressing cellular proliferation and migration in a broad panel of tumor cell lines.[63–66] Furthermore, when dosed in mice, **1.4** displayed excellent oral bioavailability and a half-life of about 4.5 hours. Extensive research efforts have been put forth investigating the therapeutic potential of **1.4** in a variety of disease models including cancer,[63–66] Crohn's disease,[67] rheumatoid arthritis,[68] and colitis.[69] Recently, **1.4** has entered Phase IIA clinical trials for the treatment of cholangiocarcinoma (ClinicalTrials.gov registry identifier NCT03377179). In this trial patients will receive 500 mg of

1.4 administered orally twice per day in 28-day cycles in order to determine the response rate of cholangiocarcinoma. Currently, **1.4** has been approved in Italy as well as Israel for compassionate use to patients displaying life-threatening symptoms of COVID-19. Approximately 160 patients in critical condition were administered **1.4** in three major hospitals located in northern Italy to help fight the COVID-19 virus.[70]

1.4.2 SLC4101431

Compound **1.5** (SLC4101431) was developed through an SAR study focusing on the transformation of SphK1-selective inhibitors into SphK2-selective inhibitors (Figure 1.9).[56] **1.5** is a highly potent aminothiazole-based guanidine containing inhibitor with a measured K_i for SphK2 of 0.9 μM and a 100-fold selectivity for SphK2. Biological assessment of **1.5** with U937 cells showed that it effectively lowered S1P levels, while *in vivo* wild-type mice experiments demonstrated **1.5** administration to cause elevated blood S1P concentrations, a common trait seen with SphK2-selective inhibition.[53,55,71]

1.4.3 K145

Another reported SphK2-selective inhibitor is compound **1.6** (K145) (Figure 1.9).[72] Structurally, **1.6** features a thiazolidine-2,4-dione ring accompanied by a terminal butoxybenzene moiety. Biochemical assessment of **1.6** displayed a K_i for SphK2 of 6.4 μM while showing no inhibition of SphK1 up to 10 μM.[72] Further *in vitro* analysis with U937 cells showed a marginal decrease in S1P levels, as well as increased pro-apoptotic effects.[72] Notably, *in vivo* studies demonstrated that **1.6** is orally bioavailable and was successful in reducing the growth of U937 tumors in nude mice.[72]

1.4.4 trans-12a

The development of **1.7** (*trans*-12a) was the result of an SAR study conducted on an S1P pro-drug agonist (Figure 1.9).[73] Determination of an inhibitory constant for **1.7** revealed a K_i for SphK2 of 8.0 μM and a 7.5-fold selectivity for SphK2. Compound **1.7** is unique in that it is the first reported SphK inhibitor containing a quaternary ammonium salt. It was reported that the charged moiety gave the desired water solubility and potential cell permeability, and established the benefit to having a positive charge on all SphK inhibitors.[73] *In vitro* assessment of **1.7** revealed inhibitory effects towards Akt/ERK phosphorylation suggesting that the compound may inhibit the SphK dependent phosphorylation cascade. However, treatment of U937 cells with **1.7** displayed no change in S1P levels.[73]

1.4.5 SLR080811

Inspired from the success observed with **1.7**, a library of second-generation inhibitors was developed thus yielding compound **1.8** (SLR080811) (Figure 1.9).[55,71] Inhibitor **1.8** replaces the cyclohexyl ring seen in **1.7** with a more ridged 1,2,4-oxadiazole ring, as well as a guanylated pyrrolidine head group. Biochemical characterization of **1.8** displayed improved potency (K_i = 1.3 μM) and selectivity (9-fold) for SphK2. Analysis of **1.8** treatment in leukemia cells displayed an overall decrease in measured S1P levels. Administration in SphK1-null mice resulted in a favorable half-life (~ 5.0 h) and an observed decrease in S1P concentrations. Furthermore, injection of **1.8** into wild-type mice resulted in a rise of blood S1P levels, a common marker of SphK2 inhibition.[53,55,71]

1.4.6 SLM6031434

The development of **1.9** (SLM6031434) was the result of an SAR study focused on improving the observed inhibitory activity of **1.8** (Figure 1.9).[53,55,71] Structurally, **1.9** replaces the octylbenzene moiety seen in **1.8** with a slightly longer octoxybenzene tail. Furthermore, it was observed that the addition of a trifluoromethyl substituent on the internal aryl ring imparted enhanced potency (K_i = 0.4 μM) and selectivity (50-fold) towards SphK2. *In vitro* analysis with cultured cells and **1.9** exhibited a decrease in S1P concentrations in a dose dependent manor. Additionally, administration in mice was successful in recapitulating the inverse relationship of SphK2 inhibition and an increase in blood S1P levels.[53,55,71] More recently, inhibitor **1.9** was utilized in implicating SphK2 as a key player in the mechanism of S1P clearance from blood. Specifically, mice treated with **1.9** displayed significantly diminished clearance of deuterated S1P in blood. [53,55,71]

1.5 Conclusions

The regulation of Sph and S1P levels from the enzymatic action of SphK has shown to be pivotal in various diseases and represents an intriguing target for pharmaceutical intervention. Ideally, the development of selective inhibitors for both SphK1 and SphK2 will be achieved in order to manipulate concentrations of S1P in the body. It is thought that control of S1P levels will aid in the treatment of various disorders such as cancer, Alzheimer's disease, fibrosis, and autoimmunity. To date, investigations focused on the development of SphK1-selective and dual SphK1/2 inhibitors have achieved highly potent compounds with measured K_i values in the nanomolar range. Even so, there remains a considerable amount of research to be conducted in

the field of developing novel and potent SphK2-selective inhibitors. Each year ongoing efforts continue to push forward with more information being disclosed and improved upon.

1.6 Dissertation Overview for the Development of SphK2-selective Inhibitors

Chapter 1 discussed the significance of sphingolipids in cellular signaling and disease, the S1P synthetic pathway, SphK's, and notable SphK2-selective inhibitors. Chapter 2 will discuss an SAR study centered around the SphK2-selective inhibitor **2.10** (SLM6071469). Surprisingly, this study led to the discovery of a small side cavity in the Sph binding site of SphK2. This feature is unique to SphK2 and was exploited in the design of SphK2-selective inhibitors. Chapter 3 will discuss efforts to transform SphK2-selective inhibitors into in an orally bioavailable drug. Excitingly, this work has led to the development of SphK2-selective pro-drugs that are active *in vivo* when administered orally to mice. Chapter 4 presents the supplemental information and experimental details for the compounds synthesized and characterized by the author of this dissertation. NMR spectra for compounds synthesized in Chapter 2 can be found online at https://pubs.acs.org/doi/abs/10.1021/acs.jmedchem.9b01508.

1.7 References

(1) Maceyka, M.; Harikumar, K. B.; Milstien, S.; Spiegel, S. Sphingosine-1-Phosphate Signaling and Its Role in Disease. *Trends Cell Biol*. **2012**, *22*, 50–60.

(2) Santos, W. L.; Lynch, K. R. Drugging Sphingosine Kinases. *ACS Chem. Biol.* **2015**, *10*, 225–233.

(3) Pyne, N. J.; El Buri, A.; Adams, D. R.; Pyne, S. Sphingosine 1-Phosphate and Cancer. *Adv. Biol. Regul.* **2018**, *68*, 97–106.

(4) Geffken, K.; Spiegel, S. Sphingosine Kinase 1 in Breast Cancer. *Adv. Biol. Regul.* **2018**, *67*, 59–65.

(5) Patmanathan, S. N.; Wang, W.; Yap, L. F.; Herr, D. R.; Paterson, I. C. Mechanisms of Sphingosine 1-Phosphate Receptor Signalling in Cancer. *Cell. Signalling.* **2017**, *34*, 66–75.

(6) Yuza, K.; Nakajima, M.; Nagahashi, M.; Tsuchida, J.; Hirose, Y.; Miura, K.; Tajima, Y.; Abe, M.; Sakimura, K.; Takabe, K.; Wakai, T. Different Roles of Sphingosine Kinase 1 and 2 in Pancreatic Cancer Progression. *J. Surg. Res.* **2018**, *232*, 186–194.

(7) LeBlanc, F. R.; Pearson, J. M.; Tan, S.-F.; Cheon, H.; Xing, J. C.; Dunton, W.; Feith, D. J.; Loughran Jr, T. P. Sphingosine Kinase-2 Is Overexpressed in Large Granular Lymphocyte Leukaemia and Promotes Survival through Mcl-1. *Br. J. Haematol.* [Online early access]. DOI: 10.1111/bjh.16530. Published Online: March 2, 2020.

(8) Singh, S. K.; Spiegel, S. Sphingosine-1-Phosphate Signaling: A Novel Target for Simultaneous Adjuvant Treatment of Triple Negative Breast Cancer and Chemotherapy-Induced Neuropathic Pain. *Adv. Biol. Regul.* **2020**, *75*, 100670.

(9) Farez, M. F.; Correale, J. Sphingosine 1-Phosphate Signaling in Astrocytes: Implications

for Progressive Multiple Sclerosis. *J. Neurol. Sci.* **2016**, *361*, 60–65.

(10) Kappos, L.; Bar-Or, A.; Cree, B. A. C.; Fox, R. J.; Giovannoni, G.; Gold, R.; Vermersch, P.; Arnold, D. L.; Arnould, S.; Scherz, T.; Wolf, C.; Wallström, E.; Dahlke, F. Siponimod versus Placebo in Secondary Progressive Multiple Sclerosis (EXPAND): A Double-Blind, Randomised, Phase 3 Study. *Lancet* **2018**, *391*, 1263–1273.

(11) Zhang, Y.; Berka, V.; Song, A.; Sun, K.; Wang, W.; Zhang, W.; Ning, C.; Li, C.; Zhang, Q.; Bogdanov, M.; Alexander, D. C.; Milburn, M. V.; Ahmed, M. H.; Lin, H.; Idowu, M.; Zhang, J.; Kato, G. J.; Abdulmalik, O. Y.; Zhang, W.; Dowhan, W.; Kellems, R. E.; Zhang, P.; Jin, J.; Safo, M.; Tsai, A.; Juneja, H. S.; Xia, Y. Elevated Sphingosine-1-Phosphate Promotes Sickling and Sickle Cell Disease Progression. *J. Clin. Invest.* **2014**, *124*, 2750–2761.

(12) Sun, K.; Zhang, Y.; Bogdanov, M. V; Wu, H.; Song, A.; Li, J.; Dowhan, W.; Idowu, M.; Juneja, H. S.; Molina, J. G.; Blackburn, M. R.; Kellems, R. E.; Xia, Y. Elevate Adenosine Signaling via Adenosine A2B Receptor Induces Normal and Sickle Erythrocyte Sphingosine Kinase 1 Activity. *Blood* **2015**, *125*, 1643–1652.

(13) Huwiler, A.; Pfeilschifter, J. Sphingolipid Signaling in Renal Fibrosis. *Matrix Biol.* **2018**, *68–69*, 230–247.

(14) Schwalm, S.; Beyer, S.; Frey, H.; Haceni, R.; Grammatikos, G.; Thomas, D.; Geisslinger, G.; Schaefer, L.; Huwiler, A.; Pfeilschifter, J. Sphingosine Kinase-2 Deficiency Ameliorates Kidney Fibrosis by Up-Regulating Smad7 in a Mouse Model of Unilateral Ureteral Obstruction. *Am. J. Pathol.* **2017**, *187*, 2413–2429.

(15) Pyne, N. J.; Dubois, G.; Pyne, S. Role of Sphingosine 1-Phosphate and Lysophosphatidic Acid in Fibrosis. *Biochim. Biophys. Acta, Mol. Cell Biol. Lipids* **2013**, *1831*, 228–238.

(16) Pyne, S.; Adams, D. R.; Pyne, N. J. Sphingosine 1-Phosphate and Sphingosine Kinases in Health and Disease: Recent Advances. *Prog. Lipid Res.* **2016**, *62*, 93–106.

(17) Furuya, H.; Shimizu, Y.; Kawamori, T. Sphingolipids in Cancer. *Cancer Metastasis Rev.* **2011**, *30*, 567–576.

(18) Cuvillier, O.; Pirianov, G.; Kleuser, B.; Vanek, P. G.; Coso, O. A.; Gutkind, J. S.; Spiegel, S. Suppression of Ceramide-Mediated Programmed Cell Death by Sphingosine-1-Phosphate. *Nature* **1996**, *381*, 800–803.

(19) Vu, T. M.; Ishizu, A.-N.; Foo, J. C.; Toh, X. R.; Zhang, F.; Whee, D. M.; Torta, F.; Cazenave-Gassiot, A.; Matsumura, T.; Kim, S.; Toh, S.-A. E. S.; Silver, D. L.; Wenk, M. R.; Nguyen, L. N. Mfsd2b Is Essential for the Sphingosine-1-Phosphate Export in Erythrocytes and Platelets. *Nature* **2017**, *550*, 524–528.

(20) Laviad, E. L.; Albee, L.; Pankova-Kholmyansky, I.; Epstein, S.; Park, H.; Merrill, A. H.; Futerman, A. H. Characterization of Ceramide Synthase 2: Tissue Distribution, Substrate Specificity, and Inhibition by Sphingosine 1-Phosphate. *J. Biol. Chem.* **2008**, *283*, 5677–5684.

(21) Chipuk, J. E.; McStay, G. P.; Bharti, A.; Kuwana, T.; Clarke, C. J.; Siskind, L. J.; Obeid, L. M.; Green, D. R. Sphingolipid Metabolism Cooperates with BAK and BAX to Promote the Mitochondrial Pathway of Apoptosis. *Cell* **2012**, *148*, 988–1000.

(22) Alvarez, S. E.; Harikumar, K. B.; Hait, N. C.; Allegood, J.; Strub, G. M.; Kim, E. Y.; Maceyka, M.; Jiang, H.; Luo, C.; Kordula, T.; Milstien, S.; Spiegel, S. Sphingosine-1-Phosphate Is a Missing Cofactor for the E3 Ubiquitin Ligase TRAF2. *Nature* **2010**, *465*, 1084–1088.

(23) Goetzl, E. J.; Wang, W.; McGiffert, C.; Huang, M.-C.; Graler, M. H. Sphingosine 1-

Phosphate and Its G Protein-Coupled Receptors Constitute a Multifunctional Immunoregulatory System. *J. Cell. Biochem.* **2004**, *92*, 1104–1114.

(24) Bruno, G.; Cencetti, F.; Pini, A.; Tondo, A.; Cuzzubbo, D.; Fontani, F.; Strinna, V.; Buccoliero, A. M.; Casazza, G.; Donati, C.; Filippi, L.; Bruni, P.; Favre, C.; Calvani, M. B3-Adrenoreceptor Blockade Reduces Tumor Growth and Increases Neuronal Differentiation in Neuroblastoma via SK2/S1P2 Modulation. *Oncogene* **2020**, *39*, 368–384.

(25) Asle-Rousta, M.; Kolahdooz, Z.; Dargahi, L.; Ahmadiani, A.; Nasoohi, S. Prominence of Central Sphingosine-1-Phosphate Receptor-1 in Attenuating Aβ-Induced Injury by Fingolimod. *J. Mol. Neurosci.* **2014**, *54*, 698–703.

(26) Watanabe, C.; Seigneuret, M.; Staneva, G.; Puff, N.; Angelova, M. I. On the Possible Structural Role of Single Chain Sphingolipids Sphingosine and Sphingosine 1-Phosphate in the Amyloid-β Peptide Interactions with Membranes. Consequences for Alzheimer's Disease Development. *Colloids Surf., A.* **2016**, *510*, 317–327.

(27) Ceccom, J.; Loukh, N.; Lauwers-Cances, V.; Touriol, C.; Nicaise, Y.; Gentil, C.; Uro-Coste, E.; Pitson, S.; Maurage, C. A.; Duyckaerts, C.; Cuvillier, O.; Delisle, M.-B. Reduced Sphingosine Kinase-1 and Enhanced Sphingosine 1-Phosphate Lyase Expression Demonstrate Deregulated Sphingosine 1-Phosphate Signaling in Alzheimer's Disease. *Acta Neuropath. Comm.* **2014**, *2*, 1-12.

(28) Couttas, T. A.; Kain, N.; Daniels, B.; Lim, X. Y.; Shepherd, C.; Kril, J.; Pickford, R.; Li, H.; Garner, B.; Don, A. S. Loss of the Neuroprotective Factor Sphingosine 1-Phosphate Early in Alzheimer's Disease Pathogenesis. *Acta Neuropath. Comm.* **2014**, *2*, 1-9.

(29) Xu, Y.; Krause, A.; Limberis, M.; Worgall, T. S.; Worgall, S. Low Sphingosine-1-

Phosphate Impairs Lung Dendritic Cells in Cystic Fibrosis. *Am. J. Respir. Cell Mol. Biol.* **2013**, *48*, 250–257.

(30) Long, D. A.; Price, K. L. Sphingosine Kinase-1: A Potential Mediator of Renal Fibrosis. *Kidney Int.* **2009**, *76*, 815–817.

(31) Halilbasic, E.; Trauner, M.; Kazemi-Shirazi, L.; Fuerst, E.; Heiden, D.; Untersmayr, E.; Japtok, L.; Kleuser, B.; Diesner, S. C.; Kulu, A.; Jaksch, P.; Hoetzenecker, K.; Kleuser, B.; Kazemi-Shirazi, L.; Untersmayr, E. Plasma Levels of the Bioactive Sphingolipid Metabolite S1P in Adult Cystic Fibrosis Patients: Potential Target for Immunonutrition? *Nutrients* **2020**, *12*, 765.

(32) Wolf, J. J.; Studstill, C. J.; Hahm, B. Emerging Connections of S1P-Metabolizing Enzymes with Host Defense and Immunity During Virus Infections. *Viruses* **2019**, *11*, 1097.

(33) Xia, C.; Seo, Y.-J.; Studstill, C. J.; Vijayan, M.; Wolf, J. J.; Hahm, B. Transient Inhibition of Sphingosine Kinases Confers Protection to Influenza A Virus Infected Mice. *Antiviral Res.* **2018**, *158*, 171–177.

(34) Zemann, B.; Urtz, N.; Reuschel, R.; Mechtcheriakova, D.; Bornancin, F.; Badegruber, R.; Baumruker, T.; Billich, A. Normal Neutrophil Functions in Sphingosine Kinase Type 1 and 2 Knockout Mice. *Immunol. Lett.* **2007**, *109*, 56–63.

(35) Mizugishi, K.; Yamashita, T.; Olivera, A.; Miller, G. F.; Spiegel, S.; Proia, R. L. Essential Role for Sphingosine Kinases in Neural and Vascular Development. *Mol. Cell. Biol.* **2005**, *25*, 11113–11121.

(36) Liu, H.; Sugiura, M.; Nava, V. E.; Edsall, L. C.; Kono, K.; Poulton, S.; Milstien, S.; Kohama, T.; Spiegel, S. Molecular Cloning and Functional Characterization of a Novel

Mammalian Sphingosine Kinase Type 2 Isoform. *J. Biol. Chem.* **2000**, *275*, 19513–19520.

(37) Spiegel, S.; Milstien, S. Sphingosine 1-Phosphate, a Key Cell Signaling Molecule. *J. Biol. Chem.* **2002**, *277*, 25851–25854.

(38) Madhunapantula, S. V; Hengst, J.; Gowda, R.; Fox, T. E.; Yun, J. K.; Robertson, G. P. Targeting Sphingosine Kinase-1 to Inhibit Melanoma. *Pigm. Cell Melanoma Res.* **2012**, *25*, 259–274.

(39) Chan, H.; Pitson, S. M. Post-Translational Regulation of Sphingosine Kinases. *Biochim. Biophys. Acta* **2013**, *1831*, 147–156.

(40) Pitson, S. M.; Moretti, P. A. B.; Zebol, J. R.; Lynn, H. E.; Xia, P.; Vadas, M. A.; Wattenberg, B. W. Activation of Sphingosine Kinase 1 by ERK1/2-Mediated Phosphorylation. *EMBO J.* **2003**, *22*, 5491–5500.

(41) Wang, Z.; Min, X.; Xiao, S.-H.; Johnstone, S.; Romanow, W.; Meininger, D.; Xu, H.; Liu, J.; Dai, J.; An, S.; Thibault, S.; Walker, N. Molecular Basis of Sphingosine Kinase 1 Substrate Recognition and Catalysis. *Structure* **2013**, *21*, 798–809.

(42) Wang, J.; Knapp, S.; Pyne, N. J.; Pyne, S.; Elkins, J. M. Crystal Structure of Sphingosine Kinase 1 with PF-543. *ACS Med. Chem. Lett.* **2014**, *5*, 1329–1333.

(43) Schnute, M. E.; McReynolds, M. D.; Kasten, T.; Yates, M.; Jerome, G.; Rains, J. W.; Hall, T.; Chrencik, J.; Kraus, M.; Cronin, C. N.; Saabye, M.; Highkin, M. K.; Broadus, R.; Ogawa, S.; Cukyne, K.; Zawadzke, L. E.; Peterkin, V.; Iyanar, K.; Scholten, J. A.; Wendling, J.; Fujiwara, H.; Nemirovskiy, O.; Wittwer, A. J.; Nagiec, M. M. Modulation of Cellular S1P Levels with a Novel, Potent and Specific Inhibitor of Sphingosine Kinase-1. *Biochem. J.* **2012**, *444*, 79–88.

(44) Okada, T.; Ding, G.; Sonoda, H.; Kajimoto, T.; Haga, Y.; Khosrowbeygi, A.; Gao, S.;

Miwa, N.; Jahangeer, S.; Nakamura, S.-I. Involvement of N-Terminal-Extended Form of Sphingosine Kinase 2 in Serum-Dependent Regulation of Cell Proliferation and Apoptosis. *J. Biol. Chem.* **2005**, *280*, 36318–36325.

(45) Igarashi, N.; Okada, T.; Hayashi, S.; Fujita, T.; Jahangeer, S.; Nakamura, S. Sphingosine Kinase 2 Is a Nuclear Protein and Inhibits DNA Synthesis. *J. Biol. Chem.* **2003**, *278*, 46832–46839.

(46) Ding, G.; Sonoda, H.; Yu, H.; Kajimoto, T.; Goparaju, S. K.; Jahangeer, S.; Okada, T.; Nakamura, S. Protein Kinase D-Mediated Phosphorylation and Nuclear Export of Sphingosine Kinase 2. *J. Biol. Chem.* **2007**, *282*, 27493–27502.

(47) Yoshimoto, T.; Furuhata, M.; Kamiya, S.; Hisada, M.; Miyaji, H.; Magami, Y.; Yamamoto, K.; Fujiwara, H.; Mizuguchi, J. Positive Modulation of IL-12 Signaling by Sphingosine Kinase 2 Associating with the IL-12 Receptor Beta 1 Cytoplasmic Region. *J. Immunol.* **2003**, *171*, 1352–1359.

(48) Hait, N. C.; Allegood, J.; Maceyka, M.; Strub, G. M.; Harikumar, K. B.; Singh, S. K.; Luo, C.; Marmorstein, R.; Kordula, T.; Milstien, S.; Spiegel, S. Regulation of Histone Acetylation in the Nucleus by Sphingosine-1-Phosphate. *Science* **2009**, *325*, 1254–1257.

(49) Sankala, H. M.; Hait, N. C.; Paugh, S. W.; Shida, D.; Lepine, S.; Elmore, L. W.; Dent, P.; Milstien, S.; Spiegel, S. Involvement of Sphingosine Kinase 2 in P53-Independent Induction of P21 by the Chemotherapeutic Drug Doxorubicin. *Cancer Res.* **2007**, *67*, 10466–10474.

(50) Sun, D.-F.; Gao, Z.-H.; Liu, H.-P.; Yuan, Y.; Qu, X.-J. Sphingosine 1-Phosphate Antagonizes the Effect of All-Trans Retinoic Acid (ATRA) in a Human Colon Cancer Cell Line by Modulation of RARbeta Expression. *Cancer Lett.* **2012**, *319*, 182–189.

(51) Panneer Selvam, S.; De Palma, R. M.; Oaks, J. J.; Oleinik, N.; Peterson, Y. K.; Stahelin, R. V; Skordalakes, E.; Ponnusamy, S.; Garrett-Mayer, E.; Smith, C. D.; Ogretmen, B. Binding of the Sphingolipid S1P to HTERT Stabilizes Telomerase at the Nuclear Periphery by Allosterically Mimicking Protein Phosphorylation. *Science Signal.* **2015**, *8*, 1–13.

(52) Weigert, A.; Cremer, S.; Schmidt, M. V.; von Knethen, A.; Angioni, C.; Geisslinger, G.; Brune, B. Cleavage of Sphingosine Kinase 2 by Caspase-1 Provokes Its Release from Apoptotic Cells. *Blood* **2010**, *115*, 3531–3540.

(53) Kharel, Y.; Huang, T.; Salamon, A.; Harris, T. E.; Santos, W. L.; Lynch, K. R. Mechanism of Sphingosine 1-Phosphate Clearance from Blood. *Biochem. J.* **2020**, *477*, 925–935.

(54) Kharel, Y.; Raje, M.; Gao, M.; Gellett, A. M.; Tomsig, J. L.; Lynch, K. R.; Santos, W. L. Sphingosine Kinase Type 2 Inhibition Elevates Circulating Sphingosine 1-Phosphate. *Biochem. J.* **2012**, *447*, 149–157.

(55) Kharel, Y.; Morris, E. A.; Congdon, M. D.; Thorpe, S. B.; Tomsig, J. L.; Santos, W. L.; Lynch, K. R. Sphingosine Kinase 2 Inhibition and Blood Sphingosine 1-Phosphate Levels. *J. Pharmacol. Exp. Ther.* **2015**, *355*, 23–31.

(56) Childress, E. S.; Kharel, Y.; Brown, A. M.; Bevan, D. R.; Lynch, K. R.; Santos, W. L. Transforming Sphingosine Kinase 1 Inhibitors into Dual and Sphingosine Kinase 2 Selective Inhibitors: Design, Synthesis, and in Vivo Activity. *J. Med. Chem.* **2017**, *60*, 3933–3957.

(57) Adams, D. R.; Tawati, S.; Berretta, G.; Rivas, P. L.; Baiget, J.; Jiang, Z.; Alsfouk, A.; Mackay, S. P.; Pyne, N. J.; Pyne, S. Topographical Mapping of Isoform-Selectivity

Determinants for J-Channel-Binding Inhibitors of Sphingosine Kinases 1 and 2. *J. Med. Chem.* **2019**, *62*, 3658–3676.

(58) Congdon, M. D.; Childress, E. S.; Patwardhan, N. N.; Gumkowski, J.; Morris, E. A.; Kharel, Y.; Lynch, K. R.; Santos, W. L. Structure-Activity Relationship Studies of the Lipophilic Tail Region of Sphingosine Kinase 2 Inhibitors. *Bioorg. Med. Chem. Lett.* **2015**, *25*, 4956–4960.

(59) Worrell, B. L.; Brown, A. M.; Santos, W. L.; Bevan, D. R. In Silico Characterization of Structural Distinctions between Isoforms of Human and Mouse Sphingosine Kinases for Accelerating Drug Discovery. *J. Chem. Inf. Model.* **2019**, *59*, 2339-2351.

(60) Novartis, *Novartis Gains FDA Approval for Gilenya ™, a Novel First-Line Multiple Sclerosis Treatment Shown to Significantly Reduce Relapses and Delay Disability Progression*; http://iomsn.org/wp-content/uploads/2016/07/Gilenya-FDA-Approval-US-PressRelease.pdf (accessed Apr 18, 2020).

(61) Novartis, *Novartis Receives FDA Approval for Mayzent ® (Siponimod), the First Oral Drug to Treat Secondary Progressive MS with Active Disease*; https://www.novartis.com/news/media-releases/novartis-receives-fda-approval-mayzent-siponimod-first-oral-drug-treat-secondary-progressive-ms-active-disease (accessed Apr 18, 2020).

(62) French, K. J.; Zhuang, Y.; Maines, L. W.; Gao, P.; Wang, W.; Beljanski, V.; Upson, J. J.; Green, C. L.; Keller, S. N.; Smith, C. D. Pharmacology and Antitumor Activity of ABC294640, a Selective Inhibitor of Sphingosine Kinase-2. *J. Pharmacol. Exp. Ther.* **2010**, *333*, 129-139.

(63) Song, K.; Dai, L.; Long, X.; Cui, X.; Liu, Y.; Di, W. Sphingosine Kinase 2 Inhibitor

ABC294640 Displays Anti-Epithelial Ovarian Cancer Activities in Vitro and in Vivo. *OncoTargets and Therapy* **2019**, *12*, 4437–4449.

(64) Lewis, C. S.; Voelkel-Johnson, C.; Smith, C. D. Suppression of C-MYC and RRM2 Expression in Pancreatic Cancer Cells by the Sphingosine Kinase-2 Inhibitor ABC294640. *Oncotarget* **2016**, *7*, 60181–60192.

(65) Xun, C.; Chen, M.-B.; Qi, L.; Tie-Ning, Z.; Peng, X.; Ning, L.; Zhi-Xiao, C.; Li-Wei, W. Targeting Sphingosine Kinase 2 (SphK2) by ABC294640 Inhibits Colorectal Cancer Cell Growth in Vitro and in Vivo. *J. Exp. Clin. Cancer Res.* **2015**, *34*, 94/91-94/99.

(66) Beljanski, V.; Lewis, C. S.; Smith, C. D. Antitumor Activity of Sphingosine Kinase 2 Inhibitor ABC294640 and Sorafenib in Hepatocellular Carcinoma Xenografts. *Cancer Biol. Ther.* **2011**, *11*, 524–534.

(67) Maines, L. W.; Fitzpatrick, L. R.; Green, C. L.; Zhuang, Y.; Smith, C. D. Efficacy of a Novel Sphingosine Kinase Inhibitor in Experimental Crohn's Disease. *Inflammopharmacology* **2010**, *18*, 73–85.

(68) Fitzpatrick, L. R.; Green, C.; Frauenhoffer, E. E.; French, K. J.; Zhuang, Y.; Maines, L. W.; Upson, J. J.; Paul, E.; Donahue, H.; Mosher, T. J.; Smith, C. D. Attenuation of Arthritis in Rodents by a Novel Orally-Available Inhibitor of Sphingosine Kinase. *Inflammopharmacology* **2011**, *19*, 75–87.

(69) Maines, L. W.; Fitzpatrick, L. R.; French, K. J.; Zhuang, Y.; Xia, Z.; Keller, S. N.; Upson, J. J.; Smith, C. D. Suppression of Ulcerative Colitis in Mice by Orally Available Inhibitors of Sphingosine Kinase. *Dig. Dis. Sci.* **2008**, *53*, 997–1012.

(70) RedHill Biopharma, *RedHill Biopharma Announces Approval of Compassionate Use of Opaganib for COVID-19 in Italy*; https://www.biospace.com/article/releases/redhill-

biopharma-announces-approval-of-compassionate-use-of-opaganib-for-covid-19-in-italy/ (accessed May 12, 2020).

(71) Kharel, Y.; Raje, M.; Gao, M.; Gellett, A. M.; Tomsig, J. L.; Lynch, K. R.; Santos, W. L. Sphingosine Kinase Type 2 Inhibition Elevates Circulating Sphingosine 1-Phosphate. *Biochem. J.* **2012**, *447*, 149–157.

(72) Liu, K.; Guo, T. L.; Hait, N. C.; Allegood, J.; Parikh, H. I.; Xu, W.; Kellogg, G. E.; Grant, S.; Spiegel, S.; Zhang, S. Biological Characterization of 3-(2-Amino-Ethyl)-5-[3-(4-Butoxyl-Phenyl)-Propylidene]-Thiazolidine-2,4-Dione (K145) as a Selective Sphingosine Kinase-2 Inhibitor and Anticancer Agent. *PLoS One* **2013**, *8*, e56471.

(73) Raje, M. R.; Knott, K.; Kharel, Y.; Bissel, P.; Lynch, K. R.; Santos, W. L. Design, Synthesis and Biological Activity of Sphingosine Kinase 2 Selective Inhibitors. *Bioorg. Med. Chem.* **2012**, *20*, 183–194.

2 Discovery of a Small Side Cavity in Sphingosine Kinase 2 that Enhances Inhibitor Potency and Selectivity

2.1 Contributions

The work in this chapter was done primarily by the author. The author synthesized and characterized all final compounds and their corresponding intermediates. Dr. Yugesh Kharel of the University of Virginia Department of Pharmacology conducted biological analyses of the reported compounds. Dr. Tao Huang purified compounds for animal studies and conducted LC/MS analysis of biological samples. Dr. Anne M. Brown conducted the molecular modeling experiments. The final manuscript was written by the author and Dr. Webster Santos. This chapter is a reprint with permission from the *Journal of Medicinal Chemistry* [Sibley, C. D.; Morris, E. A.; Kharel, Y.; Brown, A. M.; Huang, T.; Bevan, D. R.; Lynch, K. R.; Santos, W. L. Discovery of a Small Side Cavity in Sphingosine Kinase 2 That Enhances Inhibitor Potency and Selectivity. *J. Med. Chem.* **2020**, *63* (3), 1178–1198, © 2020 American Chemical Society].

2.2 Abstract

The sphingosine-1-phosphate (S1P) signaling pathway is an attractive drug target due to its involvement in immune cell chemotaxis and vascular integrity. The formation of S1P is catalyzed by sphingosine kinase 1 or 2 (SphK1 or SphK2) from sphingosine (Sph) and ATP. Inhibition of SphK1 and 2 to attenuate levels of S1P has been reported to be efficacious in animal models of diseases such as cancer, sickle cell disease and renal fibrosis. While inhibitors of both SphKs have been reported, improvements in potency and selectivity are still needed. Towards that end, we performed a structure-activity relationship profiling of **2.8** (SLM6031434) and discovered a heretofore unrecognized side cavity that increased inhibitor potency toward SphK2. Interrogating this region revealed that relatively small hydrophobic moieties are preferred with **2.10** being the

most potent SphK2 selective inhibitor (K_i = 89 nM, 73-fold SphK2 selective) with validated *in vivo* activity.

2.3 Introduction

Over the last two decades, sphingolipid signaling has emerged as an attractive candidate for drug development due to its involvement in a wide range of cellular processes. One sphingolipid in particular, sphingosine 1-phosphate (S1P), has garnered attention due to its implication in pathologic processes including cancer,[1–4] sickle cell disease,[5,6] renal fibrosis,[7–9] and autoimmunity.[10,11] S1P circulates at low micromolar concentrations in the blood of mammals and perhaps all vertebrates.[12] S1P is produced solely *via* ATP-dependent phosphorylation of sphingosine (Sph) by sphingosine kinases (SphK1 and SphK2) (Figure 2.1). The biologic roles of both enzymes are, to a certain extent, redundant in that mice lacking either isoform are viable, fertile and phenotypically unremarkable. However, elimination of both SphK1 and 2 is embryonically lethal at about day E13.5.[13,14] While both isoforms catalyze the conversion of Sph to S1P, the two enzymes differ in cellular localization and degree of substrate selectivity. SphK1 is predominantly located in the cytosol while SphK2 is found in the nucleus, mitochondria, and endoplasmic reticulum. The association of S1P with a wide array of cellular processes and diseases is, in part, due to its acting as both an intra- and extra-cellular signaling molecule. Extracellularly, S1P is a high affinity ligand for five G-protein coupled receptors ($S1P_{1-5}$) resulting in a downstream signaling cascade leading to cellular migration and survival.[3,15,16] In contrast, intracellular S1P is reported to interact with pathways influencing cellular functions ranging from cell arrest and apoptosis to proliferation and survival.[17] In one such example, Laviad *et al.* reported findings of intracellular S1P acting as a noncompetitive inhibitor towards the pro-apoptotic protein ceramide synthase 2 (CerS2), thus conferring pro-survival effects.[18] Conversely, studies reported by Chipuk

et al. demonstrated that mitochondrial S1P can interact with Bcl-2 homologous antagonist killer (BAK) protein, resulting in an increase in mitochondrial membrane permeabilization. Subsequent elevated permeabilization leads to the release of the pro-apoptotic messenger cytochrome c into the cytosol inducing apoptosis.[19] From a pharmaceutical viewpoint, S1P signaling and synthesis represent interesting targets to manipulate and evoke a broad range of cellular responses.

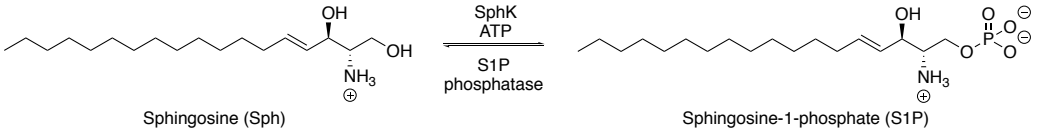

Figure 2.1. The Sph/S1P equilibrium. Interconversion of Sph to S1P is catalyzed by SphK while the reverse is achieved by S1P phosphatase.

Recently, our laboratories as well as Pyne *et al*. disclosed findings on topographical differences between the two isoform ligand binding pockets.[20,21] The studies indicate that compared to SphK1, the Sph binding pocket of SphK2 extends deeper into the enzyme while the mid-section is narrower due to a isoleucine to valine substitution. Such differences afford the potential for ligand selectivity. A curious difference between the two isoforms is the change of blood S1P levels in response to isoform inhibition or genetic deficiency. Specifically, inhibition of SphK1 in mice or rats reduces blood S1P levels by >50%, while inhibition of SphK2 increases blood S1P concentrations by roughly 3-fold.[22–24] The rise in S1P in response to SphK2 deficiency has been ascribed to a cascade wherein Sph, which is formed at the hepatocyte surface by dephosphorylation of blood S1P, is captured by SphK2-mediated phosphorylation.[25] Thus isoform-selective inhibition provides a method to either raise or lower blood S1P levels.

Since 2010, the S1P pathway has become a validated, druggable target with the FDA approval of compound **2.1** (fingolimod), a Sph analogue, for the treatment of relapsing remitting multiple sclerosis (rrMS) (Figure 2.2). Mechanistically, **2.1** is a prodrug that is phosphorylated by

SphK2. Phosphorylated **2.1** ((*S*)-phospho-fingolimod) is then transported outside of cells *via* the S1P exporter, SPNS2[26], to act as a functional antagonist at the S1P1/3/4/5 receptors, triggering S1P receptor internalization and degradation. Specifically, the absence of the cell surface S1P1 receptor hinders the ability of naïve and central memory T lymphocytes to follow the lymph S1P concentration gradient out of secondary lymphoid tissues into the lymph and thence to the blood, ultimately resulting in therapeutic immunosuppression for patients with rrMS. More recently, the FDA granted marketing approval for **2.2** (siponimod) for the treatment of secondary progressive multiple sclerosis.[27]

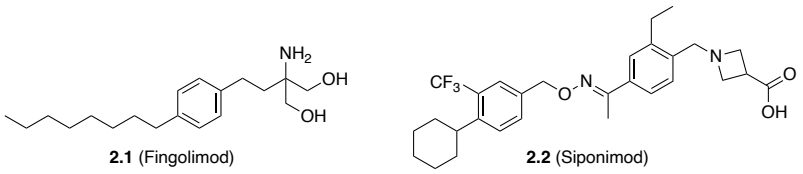

Figure 2.2. Chemical structures of Fingolimod and Siponimod.

In addition to acting on the S1P receptors, targeting other portions of the S1P pathway such as SphK are also promising. To date, there are examples of SphK1 selective as well as SphK1/2 dual inhibitors. Compounds **2.3a** (PF-543), **2.3b** (Amgen 23), and **2.4** (SLP7111228) are three of the most potent SphK1 selective inhibitors reported and have served as valuable molecular tools to probe the S1P pathway for better understanding (Figure 2.3).[28-29] In an animal model for sickle cell disease (SCD), mice treated with **2.3a** exhibited reduced blood and plasma S1P levels resulting in decreased erythrocyte sickling.[5] In a separate study, rats dosed with 10 mg/kg of **2.4** displayed decreased blood S1P levels by about 80%. Further evaluation of **2.4** exhibited favorable *in vivo* stability, low nanomolar potency, and high (>200 fold) selectivity for SphK1. As is the case for SphK1 selective inhibitors, progress has been made to develop SphK1/2 dual inhibitors. A strategy employed by Pitson *et al.* utilizes both the substrate and ATP binding sites to afford compound **2.5** (MP-A08) with measured human SphK1 and SphK2 K_i values of 27 ± 3 μM and 6.9 ± 0.8 μM,

respectively.[30] Another dual inhibitor is compound **2.6** (27a) developed by Schnute and coworkers at Pfizer (Figure 2.3).[31] Inhibitor **2.6** exhibits an IC_{50} of <1.7 nM for both kinase isoforms. Further computational docking revealed the phenyl ether moiety in **2.6** potentially allows for favorable rotation inside the enzyme binding pocket. In this manner, **2.6** avoids the deep hydrophobic pocket found in the Sph active site and instead participates in strong π–hydrophobic or π–π interactions between the phenyl substituent and F259.

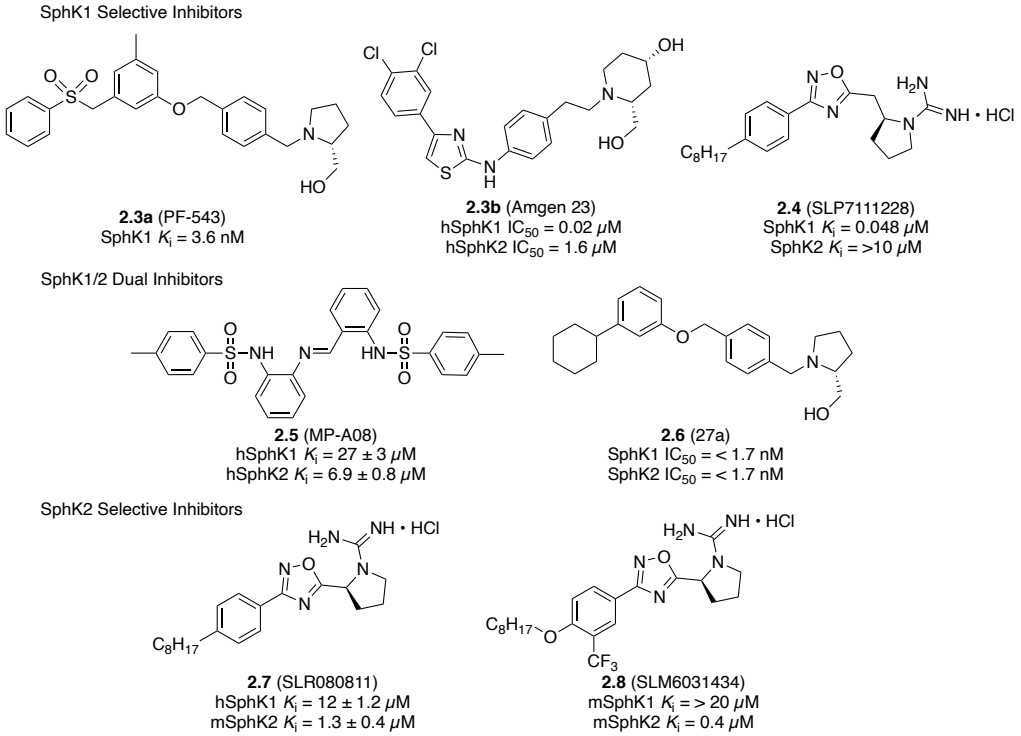

Figure 2.3. Select structures of SphK1, dual SphK1/2, and SphK2 inhibitors.

In contrast, highly potent (<100 nM) and selective (>100-fold) SphK2 inhibitors are scarce, thus prompting our interest in expanding the known chemical toolkit. Two early generation compounds designed by our group are **2.7** (SLR080811) and **2.8** (SLM6031434) (Figure 2.3).[23,22] Both of these guanidine-based inhibitors possess moderate selectivity, low micromolar SphK2 potency, and ability to lower cellular S1P levels *in vitro* with measured mouse SphK2 K_i values of

1.3 μM and 0.4 μM, respectively.[22] Additionally, compound **2.8** treatment in mice was successful in recapitulating the inverse relationship observed with SphK2 inhibition or genetic deficiency and an increase in blood S1P concentration. Herein we report the development, synthesis, and biological evaluation of, to the best of our knowledge, the most potent SphK2 selective inhibitor with in vivo activity described to date.

2.4 Results and Discussion

2.4.1 Inhibitor Design

Previous work in our group was committed to the development of novel and potent SphK2 selective inhibitors, leading to the discovery of **2.7**, a second generation SphK2 inhibitor. Evaluation of **2.7** revealed a 9-fold selectivity for the SphK2 over SphK1 with a SphK2 K_i value of 1.3 μM (12 μM for SphK1). Structurally, inhibitor **2.7** possesses an octylphenyl "tail" attached to a 1,2,4-oxadiazole linker, followed by a guanylated pyrrolidine head group. Molecular modeling studies conducted with similar SphK inhibitors possessing a guanidine head group predict that the guanidine moiety in our scaffold hydrogen bonds to catalytic amino acid residue Asp211 flanking the ATP active site when docked in the Sph binding pocket of SphK2.[32,33] Structure-activity relationship (SAR) studies conducted by Congdon *et al.* on the scaffold of **2.7** established that deletion of the aryl portion of the octylbenzene tail resulted in a significantly diminished inhibition towards SphK2, demonstrating that the aryl ring is essential for inhibitor efficacy.[21] Further SAR experiments focused on the tail portion led to the development of inhibitors **2.8** and **2.9** (SLM6031422) (Table 2.1). Both analogues retain the 1,2,4-oxadiazole linker and guanylated pyrrolidine head group but with an additional ether linkage to the octylbenzene tail. In addition, **2.8** possesses a trifluoromethyl moiety at the 3-position of the internal aryl ring. Surprisingly, the trifluoromethyl addition in compound **2.8** imparted improved selectivity (50-fold) and potency

(0.4 μM) for SphK2. In contrast, compound **2.9** exhibited reduced potency towards both SphK1 and SphK2 compared to **2.7**. These results highlight the significance of the trifluoromethyl group in SphK2 selective binding.

The Sph binding site of SphKs can be divided up into three regions as defined by Worrell *et al.* They are as follows: (1) the head region adjacent to the ATP binding site, (2) the hydrophobic core region, and (3) the tail region.[33] Molecular docking of **2.8** and **2.9** demonstrate different ligand orientations in the Sph binding site of SphK2, giving insight into the role and influence the trifluoromethyl group has in regard to SphK2 selectivity (Figure 2.4). Compound **2.8** docks in the Sph binding pocket of SphK2 in a position that indicates more interactions in the tail region of the binding site, as influenced by the hydrophobic core of the pocket, in particular, the space for the trifluoromethyl group to sit between hydrophobic residues Phe548, Leu544, and Leu547 (Figure 2.4A, B). This positioning and space at helix α8 can be accommodated in SphK2, whereas in docked poses of **2.9** (Figure 2.4C, D) in SphK2, or docked poses of **2.8** in SphK1 (see supporting information), this is not observed. In comparison, compound **2.9** is positioned in the Sph binding site of SphK2 in the traditional "J-shape" conformation that has been observed in SphK1 structures crystallized with various inhibitors.[34,35] Additionally, interactions of **2.9** with residues in the head region near the ATP binding site are observed. These interactions are at the threshold for hydrogen bonding and strong electrostatic interactions, indicating a potentially weak and non-selective inhibitor based on previous docking studies.[32,33] The unique binding mode of **2.8** maximizes interactions in the hydrophobic core and tail regions within the Sph binding site of SphK2, a phenomenon not observed in SphK1 (see supporting information). There are small but significant differences between the Sph binding site residues of SphK1 versus SphK2 with variations Ile174 to Val304 in the hydrophobic core region and Phe288 to Cys533 in the tail region, respectively.[33]

With SphK2 having the smaller amino acid, valine, in the hydrophobic core of the binding site, the trifluoromethyl group can favorably interact with the residues (Phe548, Leu544, and Leu547) that form a side cavity within the Sph binding pocket of SphK2. This interaction in the side cavity is not tolerated in SphK1 with the presence of the larger isoleucine residue. Additionally, the presence of the smaller cysteine residue in the tail region of SphK2 grants access for our inhibitors to migrate deeper towards the tail of the binding pocket which, in comparison, is blocked by Phe288 in SphK1, resulting in restricted inhibitor docking (see supporting information).

Further SAR experiments conducted in our group with the scaffold of **2.8** led to the development of molecule **2.10** (SLM6071469) (Table 2.1). This inhibitor replaces the octyloxy benzene moiety for a shorter, less flexible 4-trifluoromethyl benzyl tail that, when assessed *in vitro,* exhibited comparable activity to **2.8**. Molecular docking of **2.10** in the Sph binding site of SphK2 demonstrates a similar pose as **2.8** (Figure 2.4E, F). These results highlight the superiority of the 4-trifluoromethylbenzyl tail with significantly reduced rotatable bonds, which allows favorable hydrophobic interactions at key residues in the tail region of the binding site. These presumably lead to the observed comparable inhibition towards SphK2. Further evaluation with SphK2 illustrated that 1 μM of **2.10** was successful in inhibiting SphK2 activity by roughly 77%, albeit with decreased SphK2 selectivity, and was more potent than **2.8** at lower (0.3 μM) concentrations (Table 2.1). In this study, we probed the importance of substituents spanning the internal phenyl ring and the potential presence of an unexplored side cavity within the Sph binding pocket of SphK2. A wide range of alkyl and aryl substituents were attached and examined for their effect on SphK2 inhibition.

Table 2.1. Inhibitory activity of select compounds represented as % inhibition of SphK1 and SphK2[a]

Compound	Structure	% hSphK1 inhibition (1.0 μM)	% hSphK2 inhibition (1.0 μM)	% hSphK2 inhibition (0.3 μM)
2.8	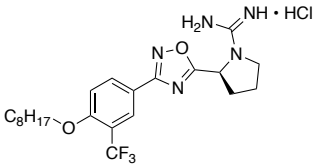	6 ± 5	80 ± 2	51 ± 4
2.9	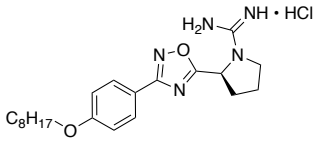	11 ± 3	8 ± 2	3 ± 1
2.10	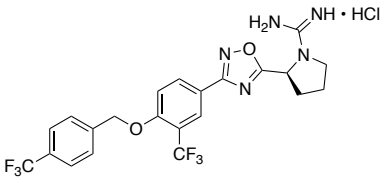	20 ± 1	77 ± 3	65 ± 3

[a]SphK inhibition is presented as % control (no inhibitor added). Recombinant human SphK1 or SphK2 were isolated from cell lysates. Enzyme inhibition was measured with 5 μM (SphK1) or 10 μM (SphK2) sphingosine and 250 μM γ-[^{32}P] ATP. Compounds were assayed at 1.0 and 0.3 μM in triplicate.

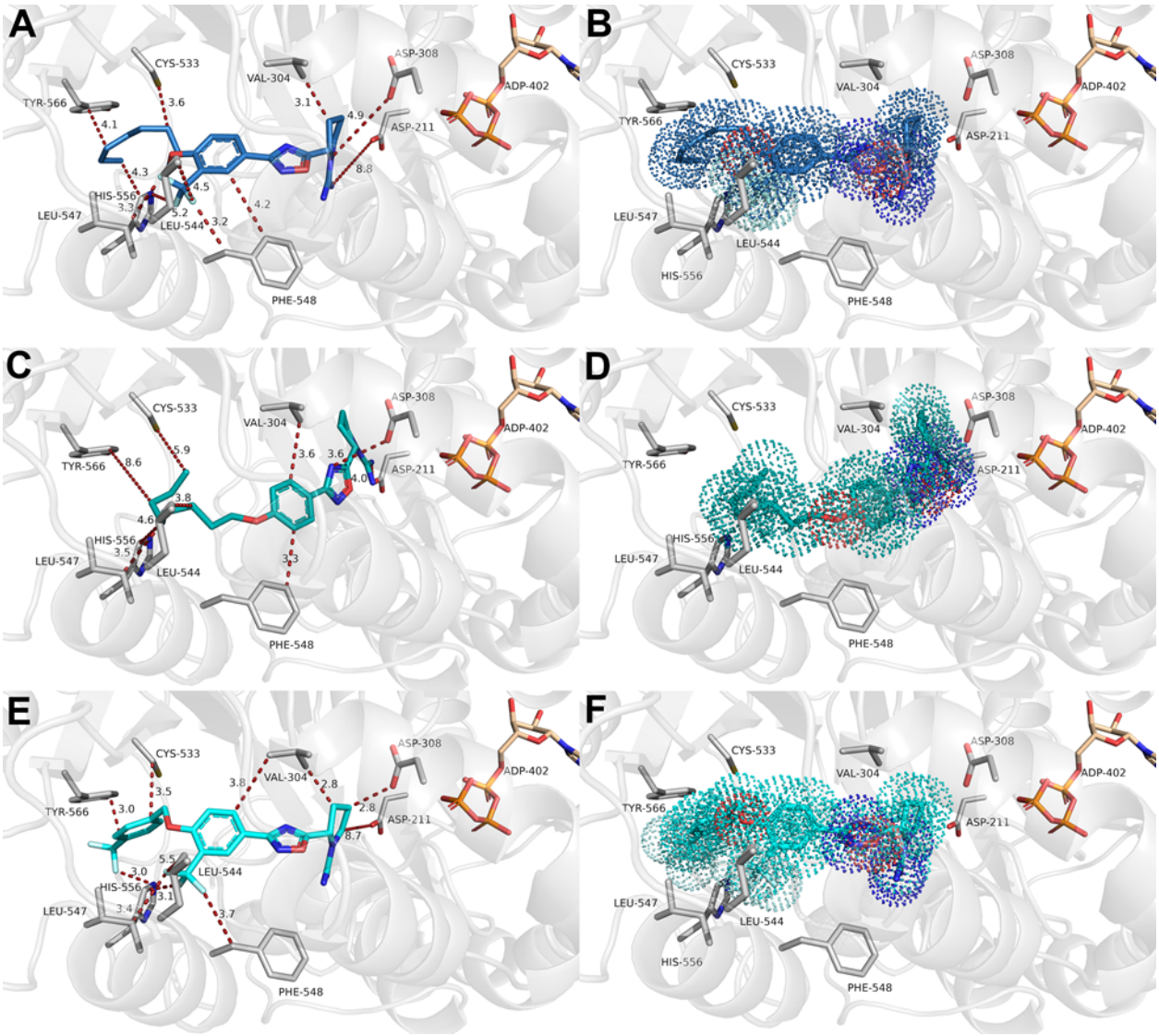

Figure 2.4. Comparison of the docked poses of **2.8** (A, B), **2.9** (C, D), and **2.10** (E, F) in a homology model of hSphK2 (PDB ID: 3VZB used as a starting template). Key residues in the binding pocket are represented by grey sticks and are labeled, ATP is shown in orange and colored by element. The SphK2 protein structure is depicted in grey cartoon. Distances between interacting atoms are shown as dashed lines. Inhibitors are shown as stick and colored by element, with the carbon atom indicating inhibitor (**2.8** – blue, **2.9** – teal, **2.10** – cyan). Panels B, D, and F show the inhibitor as Van der Waals radii in dots to represent volume occupancy of the inhibitors.

2.4.2 Chemistry

To investigate substitutions on the internal aryl ring of the **2.10** scaffold, analogues **2.15a-q**, and **2.15s** were synthesized containing various alkyl and aryl moieties at the 2- and 3-positions

as shown in Scheme 2.1. Intermediates **2.11a-e** were synthesized in a microwave reactor *via* two different Suzuki-Miyaura coupling conditions using 3-bromo-4-hydroxybenzonitrile (**2.11g**) and various boronic acids. Compounds **2.11f-o** are available for purchase from commercial sources. Allylation of 4-hydroxybenzonitrile (**2.11f**) with allyl bromide and potassium carbonate was performed followed by microwave-assisted Claisen rearrangement to afford compound **2.11p**. Subsequent hydrogenation of the allyl group with Pd/C in the presence of tetrahydroxydiboron afforded the propyl analog **2.11q**.[36] Compound **2.11r** is available for purchase from commercial sources. With the requisite materials in hand, derivatives **2.11a-r** were reacted with 4-(trifluoromethyl)benzyl bromide and potassium carbonate at 80 ºC in acetonitrile to afford intermediates **2.12a-r**. Subsequently, a mixture of hydroxylamine hydrochloride, triethylamine (TEA) and **2.12a-r** were refluxed in ethanol to generate amidoxime intermediates **2.13a-r**. Afterwards, **2.13a-r** were dissolved in DMF and heated to 100 ºC in the presence of Boc-L-proline, HCTU and Hünig's base to afford 1,2,4-oxadiazole intermediates **2.14a-r**. Synthesis of **2.14s** was performed *via* a Sonogashira coupling reaction with **2.14g** and TMS-acetylene, followed by removal of the TMS group using TBAF and subsequent hydrogenation. Lastly, Boc deprotection of compounds **2.14a-s** was completed using trifluoroacetic acid (TFA), which was followed by reaction with N,N'-*di*-Boc-1H-pyrazole-1-carboxamidine and Hünig's base to install the guanidine moiety. Removal of the Boc protecting groups was performed with HCl in methanol to provide the desired analogues **2.15a-q**, **2.15s**, and **2.10** as HCl salts (see Table 2.2 for structures).

Scheme 2.1. Synthesis of Analogues **2.15a–q**, **2.15s**, and **2.10** [a]

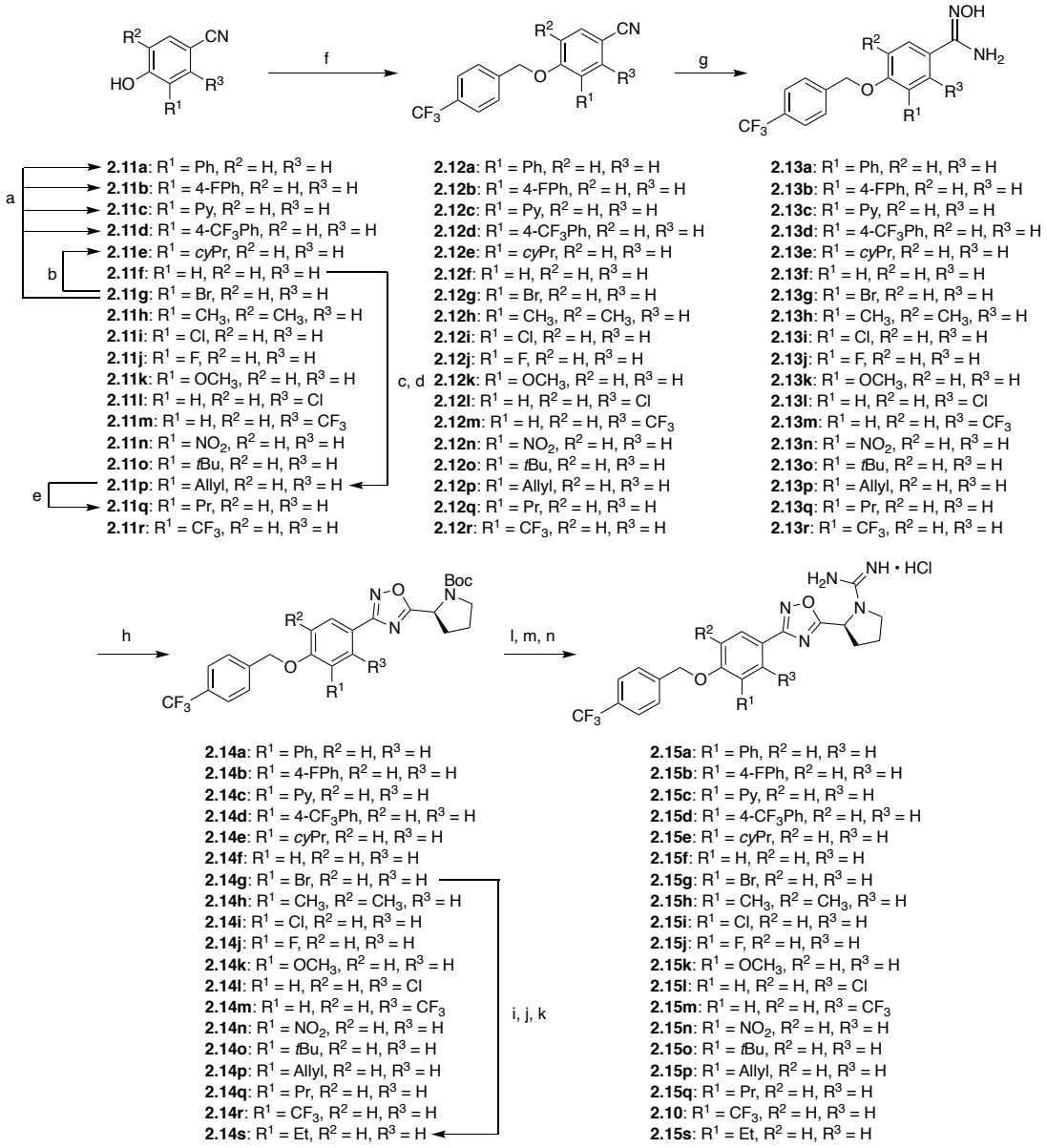

[a]Reagents and conditions: (a) boronic acid derivative, Cs_2CO_3, $PdCl_2$(dppf), DMF, 100 ºC, microwave, 60 min, 52-57%; (b) boronic acid derivative, K_2PO_4H, $Pd(OAc)_2$, $P(Cy)_3$, tol/H_2O, 100 ºC, 72 h, 50%; (c) allyl bromide, K_2CO_3, CH_3CN, 80 ºC, 4-6 h, 92%; (d) neat, 200 ºC, microwave, 20 min, 76%; (e) Pd/C, $B_2(OH)_4$, H_2O, CH_2Cl_2, rt, 18 h, 85%; (f) 4-(trifluoromethyl)benzyl bromide, K_2CO_3, CH_3CN, 80 ºC, 4-6 h, 48-99%; (g) NH_2OH•HCl, Et_3N, EtOH, reflux, 3 h, 47-96%; (h) Boc-L-proline, DIEA, HCTU•PF_6, DMF, 100-110 ºC, 18 h, 27-65%; (i) Et_3N, CuI, TMS-acetylene, $Pd(PPh)_2Cl_2$, THF, reflux, 48 h, 74%; (j) TBAF, THF, rt, 3 h, 100%; (k) H_2 (g), Pd/C, EtOH, rt, 18 h, 45%. (l) TFA, CH_2Cl_2, 3-12 h, 90-99%; (m) N,N'-*di*-Boc-1H-pyrazole-1-carboxamidine, DIEA, CH_3CN, 50 ºC, microwave, 3 h, 47-96%; (n) HCl (g), MeOH, rt, 15 min, 90-99%.

Synthesis of methyl analogue **2.20** is outlined as shown in Scheme 2.2. Execution of a nucleophilic aromatic substitution reaction of 4-(trifluoromethyl)benzyl alcohol with commercially available 4-fluoro-3-methylbenzonitrile (**2.16**) and sodium hydride afforded benzonitrile intermediate **2.17**. Next, a mixture of **2.17**, hydroxylamine hydrochloride, and TEA in ethanol was heated to generate compound **2.18**. Afterwards, HCTU coupling with Boc-L-proline, Boc deprotection, installation of the guanidine group and final deprotection yielded the desired analogue **2.20** as an HCl salt.

Scheme 2.2. Synthesis of Analogue **2.20**[a]

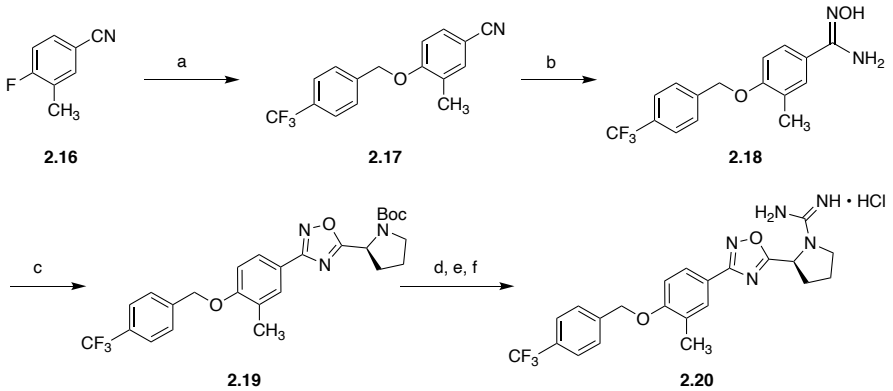

[a]Reagents and conditions: (a) 4-(trifluoromethyl)benzyl alcohol, NaH, DMF, 0 ºC-rt, 18 h, 54%; (b) NH_2OH•HCl, Et_3N, EtOH, reflux, 3 h, 89%; (c) Boc-L-proline, DIEA, HCTU•PF_6, DMF, 100 ºC, 18 h, 36%; (d) TFA, CH_2Cl_2, 12 h, 90%; (e) N,N'-*di*-Boc-1H-pyrazole-1-carboxamidine, DIEA, CH_3CN, 50 ºC, microwave, 3 h, 86%; (f) HCl (g), MeOH, rt, 15 min, 90%.

Synthesis of isopropyl analogue **2.27** is shown in Scheme 2.3. Intermediate **2.22** was produced *via* the nucleophilic substitution of commercially available 3-acetyl-4-hydroxybenzonitrile (**2.21**) using 4-(trifluoromethyl)benzyl bromide and potassium carbonate. Next, reduction of the acetyl moiety was completed through a Wittig reaction using *n*-butyl lithium and methyltriphenylphosphonium bromide dissolved in THF and cooled to 0 ºC for eighteen hours to generate compound **2.23**. Next, refluxing **2.23** in ethanol for three hours in the presence of

hydroxylamine hydrochloride and TEA generated amidoxime intermediate **2.24**. Following the sequence of oxadiazole formation, hydrogenation, Boc deprotection, installation of guanidine and final removal of Boc groups produced derivative **2.27**.

Scheme 2.3. Synthesis of Analogue **2.27**[a]

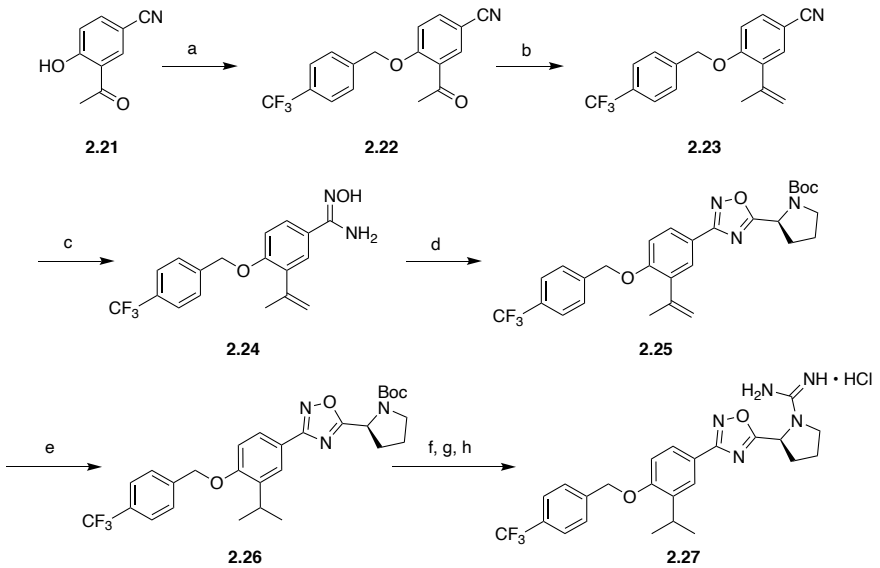

[a]Reagents and conditions: (a) 4-(trifluoromethyl)benzyl bromide, K_2CO_3, CH_3CN, 80 ºC, 6 h, 97%; (b) *n*-BuLi, $CH_3P(Ph)_3Br$, THF, 0 ºC-rt, 18 h, 59%; (c) NH_2OH•HCl, Et_3N, EtOH, reflux, 3 h, 90%; (d) Boc-L-proline, DIEA, HCTU•PF_6, DMF, 100 ºC, 18 h, 67%; (e) H_2 (g), Pd/C, EtOH, rt, 18 h, 72%; (f) TFA, CH_2Cl_2, 12 h, 90%; (g) N,N'-*di*-Boc-1H-pyrazole-1-carboxamidine, DIEA, CH_3CN, 50 ºC, microwave, 3 h, 62%; (h) HCl (g), MeOH, rt, 15 min, 90%.

2.4.3 Structure-Activity Relationship Studies and Biological Evaluation of Derivatives

The goal of this SAR was to improve SphK2 inhibition observed with **2.10** and probe the significance of substitutions on the internal phenyl ring with respect to SphK2 inhibition and selectivity. A library of compounds with various substituents spanning the 2-, 3- and 5-positions of the internal phenyl ring were synthesized and assayed according to a previously described protocol.[29,37] This assay, which utilizes recombinant SphKs and γ-[^{32}P]ATP, was used as a

preliminary screen to identify inhibitors suitable for further evaluation. The compounds were assayed at 0.3 μM. To confirm the advantage of substituents attached to the 3-position of the internal phenyl ring, **2.15f** was synthesized to represent the minimal scaffold with no substituents attached (Table 2.2). As expected, removal of the CF_3 group resulted in little to no inhibitory activity towards SphK2. Compounds **2.15a-d** were designed to replace the relatively small CF_3 moiety with a much bulkier aryl substituent to probe the size of any potential docking space, as well as potential π-π stacking or hydrophobic interactions with nearby residues Phe-548 and His-556. Substitution with a phenyl ring (**2.15a**) resulted in poor SphK2 inhibition. Likewise, decoration of the phenyl substituent (**2.15b-c**) to exploit potential hydrophobic interactions, also led to poor inhibition of SphK2. Compound **2.15d** was synthesized to mimic **2.10**, but with an additional phenyl ring in between the scaffold backbone and CF_3. Our rationale was that the added phenyl linker could potentially extend the CF_3 moiety deeper into the previously unexplored side cavity leading to increased ligand affinity. However, this increase in steric bulk resulted in a significant loss of efficacy compared to **2.10**. These results suggest that larger substituents sterically clashed inside that portion of the active site, directing us towards smaller moieties. Thus, halogen substituents at the 3-carbon were explored with compounds **2.15g** and **2.15i-j**. The identity of the halogen seemed to be important with the most successful being the chloro variant (**2.15i**), inhibiting normal SphK2 activity by about 33%. Compared to inhibitor **2.15i**, it was observed that the fluoro (**2.15j**) and bromo (**2.15g**) derivatives did not have as large of an inhibitory impact towards SphK2. We next investigated the effect of migrating substituents over to the 2-position of the internal phenyl ring. However, compared to **2.10**, both the 2-chloro (**2.15l**) and 2-CF_3 (**2.15m**) moieties had minimal impact on SphK2 inhibition. We also examined the effect of the electronics on the phenyl ring with electron withdrawing (**2.15n**) or donating (**2.15k**) groups. While the nitro

derivative **2.15n** was roughly twice as effective as methoxy variant **2.15k** with inhibiting SphK2, neither was improved compared to **2.10**. Next, the impact of 3,5-disubstitution was determined with compound **2.15h**. Unfortunately, addition of a second moiety on our scaffold resulted in poor inhibition of SphK2. Taken together, our data indicate that monosubstitution at the 3-position of the aryl ring is conducive to further structure-activity relationship profiling. Thus, alkyl substituents were synthesized to probe the size of this potential side cavity within the binding site. Replacing the trifluoromethyl group with a smaller methyl (**2.20**) led to a significant decrease in potency while the slightly larger ethyl (**2.15s**) substituent had modest SphK2 inhibitory activity. To fine-tune the size of the side cavity, we synthesized compounds containing propyl (**2.15q**), allyl (**2.15p**), isopropyl (**2.27**), cyclopropyl (**2.15e**), and *tert*-butyl (**2.15o**) groups. Collectively, these moieties had similar inhibitory activity against SphK2 along with **2.10**. Nonetheless, our studies indicate that there is a *bona fide* side binding cavity around the central phenyl ring that can accommodate a substituent larger than a methyl group, but smaller than a phenyl ring.

Table 2.2. Activity of SphK2 inhibitors represented as % inhibition of the enzyme.[a]

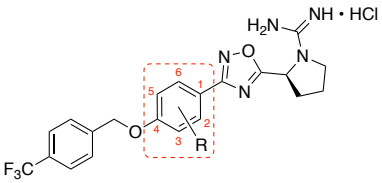

Cmpd	R	% SphK2 inhibition (0.3 μM)	Cmpd	R	% SphK2 inhibition (0.3 μM)
2.10	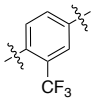	65 ± 3	**2.15n**	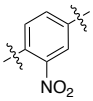	33 ± 4
2.15f		2 ± 0.2	**2.15k**	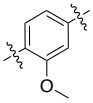	15 ± 1
2.15a	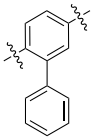	28 ± 1	**2.15h**	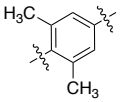	23 ± 2
2.15b	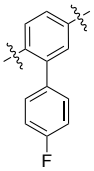	31 ± 1.9	**2.20**	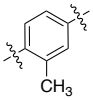	3 ± 0.4
2.15c	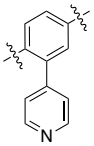	8 ± 0.8	**2.15s**	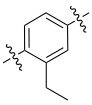	42 ± 4
2.15d	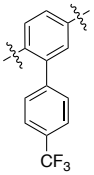	12 ± 1	**2.15q**	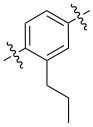	60 ± 4
2.15g		24 ± 3	**2.15p**	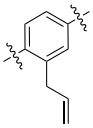	59 ± 4
2.15i		33 ± 2	**2.27**	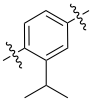	67 ± 5
2.15j		23 ± 2	**2.15e**	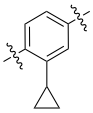	52 ± 6

2.15l	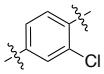	40 ± 4	**2.15o**	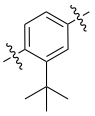	66 ± 7
2.15m	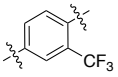	35 ± 3			

[a]SphK inhibition is presented as % control (no inhibitor added). Recombinant human SphK2 was isolated from a cell lysate. Enzyme activity was measured with 10 μM (SphK2), sphingosine and 250 μM γ-[^{32}P] ATP. Compounds were assayed at 0.3 μM in triplicate.

Considering our observations summarized in Table 2.2, select inhibitors that displayed moderate (>42%) or greater SphK2 inhibitory activity were carried forward for further evaluation. Thus, inhibitors were subjected to an *in vitro* assay that utilizes the budding yeast *Saccharomyces cerevisiae* as a platform for assessing inhibitors of human SphK1 and 2 (hSphK1 and 2).[38] In short, this assay takes advantage of the observed toxicity of excessive levels of phosphorylated long chain bases, such as S1P, towards *S. cerevisiae*. Rescue of a modified yeast cell line (KYA1) designed to harbor plasmids expressing either hSphK1 or 2 in the presence of select inhibitors can be accomplished in a dose dependent fashion by measuring the growth of yeast culture. In this manner, dose-response curves with our lead compound **2.10** demonstrated hSphK2 inhibition with an EC_{50} of 59 nM, while also displaying a 16-fold selectivity for hSphK2 over hSphK1 (Figure 2.6). As shown in Table 2.3, the *n*-propyl (**2.15q**) and isopropyl (**2.27**) derivatives were the most potent inhibitors with measured EC_{50} values of 37 nM and 32 nM respectively. Interestingly, the trifluoromethyl (**2.10**), allyl (**2.15p**), cyclopropyl (**2.15e**) and *tert*-butyl (**2.15o**) analogs were

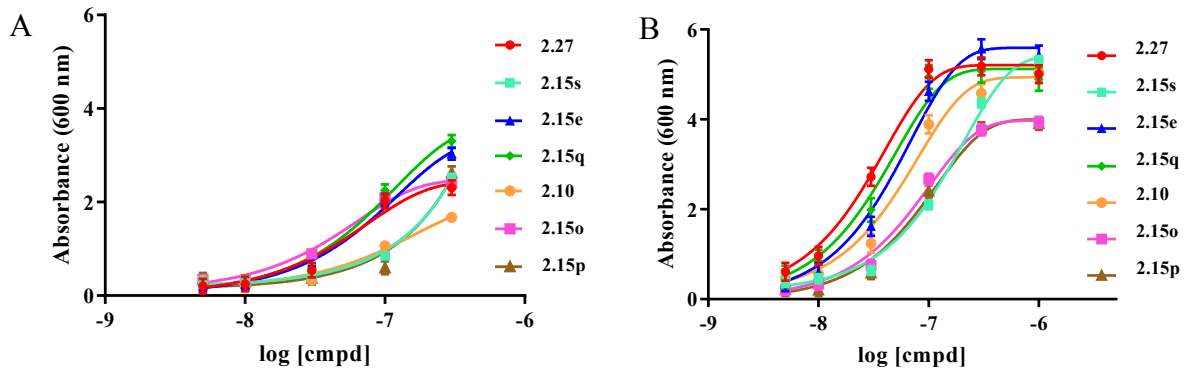

Figure 2.6. Rescue of growth of yeast strain KYA1 expressing hSphK1 (A) or hSphK2 (B) in the presence of inhibitor over 24 hours.

slightly less potent with EC_{50} values ranging from 50 nM to 84 nM, while the ethyl derivative (**2.15s**) was the least potent (EC_{50} = 146 nM). From our experience, there are some nuances in using the yeast cells as a secondary screening tool. For example, inhibitor concentrations higher than 3 μM result in cell death; fortunately, our compounds are effective at much lower concentrations. Furthermore, guanidine containing compounds accumulate inside the yeast cells at varying degrees, thus, generating apparent improved efficacy. Nonetheless, this assay affords a rapid and simple process for validating SphK inhibition *in vitro*.

The inhibitory constant (K_i) was determined for the most potent derivatives in this library.[23] As shown in Table 2.4, evaluation of the propyl derivative (**2.15q**) displayed good SphK2 inhibition with a K_i of 201 nM whereas the *tert*-butyl (**2.15o**), isopropyl (**2.27**), and cyclopropyl (**2.15e**) substituents exhibited similar K_i's ranging from 197-186 nM. Interestingly, the trifluoromethyl analogue (**2.10**) proved to be the most potent SphK2 inhibitor in the series with a K_i of 89 nM. This result is consistent with our molecular modeling studies that indicate a side cavity within the Sph binding pocket comprised of Phe548, Leu544, and Leu547. That is, the side cavity is relatively small, hydrophobic, and can best accommodate a trifluoromethyl

group due to its optimal size and hydrophobic nature. Furthermore, the selectivity of the compounds between SphK2 vs. SphK1 follows the trend of increasing size leading to poor SphK2 selectivity attributing to the fact that SphK2 has an overall smaller binding pocket than SphK1. Specifically, SphK2 selectivity decreases from CF_3 > cyclopropyl ~ isopropyl > propyl > *tert*-butyl. One of the key residues that lines the SphK2 substrate binding site is Val304, which is Ile174 in SphK1. It is predicted that Ile174 of SphK1 causes a steric clash with the trifluoromethyl group forcing the molecule to shift upwards and away from the ATP binding site, and as a result, the inhibitor migrates away from the side cavity (see supporting information). However, the variation of Ile174 → Val304 in SphK2 does not cause this steric clash, thus allowing the molecule to slide deeper into the binding site permitting the trifluoromethyl group to lock into the side cavity leading to improved SphK2 selectivity. Likewise, when the phenyl substituent is a *tert*-butyl group, the steric clash with Ile174 in SphK1 becomes even greater, sending the inhibitor towards the head of the binding pocket. However, unlike **2.10**, the increased steric clash orients the molecule towards the ATP binding site, leading to marginal SphK1 inhibition (see supporting information).

Table 2.3. EC_{50} Values of Select SphK2 Inhibitors.[a]

Compound	Structure	hSphK1 EC_{50} (nM)	hSphK2 EC_{50} (nM)
2.27	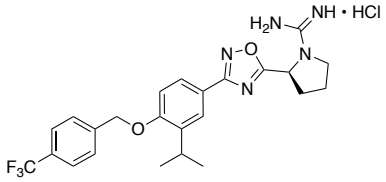	>550 ± 85	32 ± 6
2.15s	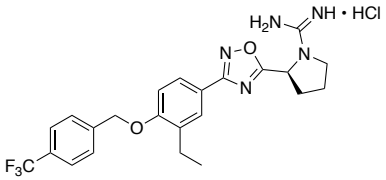	>1000 ± 160	146 ± 15
2.15e	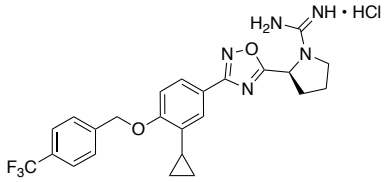	>800 ± 100	50 ± 11
2.15q	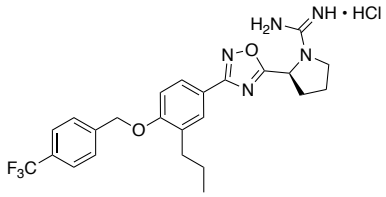	>800 ± 105	37 ± 10
2.10	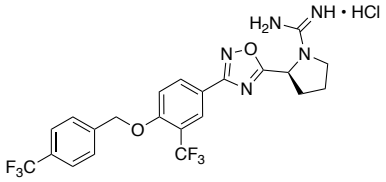	>950 ± 65	59 ± 12
2.15o	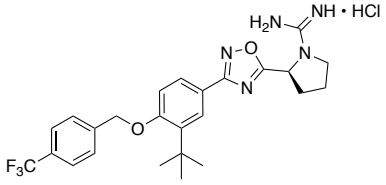	>500± 45	73 ± 9
2.15p	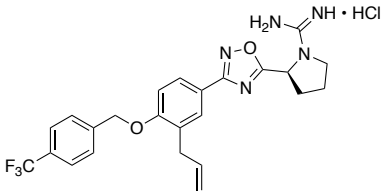	>1000 ± 135	84 ± 11

[a]EC_{50} values of various compounds were calculated from the growth curves of yeast strain KYA1 encoding either hSphK1 or hSphK2 in the presence of inhibitor over 24 hours. For detailed assay conditions, see the experimental section.

To assess inhibition of SphK2 *in vivo*, we administered C57BL/6 male mice with a single 10 mg/kg intraperitoneal (i.p.) dose of **2.10** and measured blood S1P levels. S1P level has proven to be an excellent pharmacodynamic marker for SphK2 inhibition.[22-24] Thus, blood S1P levels were measured at the indicated time points up to 8 hours post administration of **2.10** *via* LC-MS/MS. As shown in Figure 2.7, the levels of **2.10** in blood peaked at ~8 μM, which increased blood S1P levels by nearly two-fold after 4 hours and remained elevated for up to 6 hours. The elevation of S1P levels indicates blockade of SphK2 activity *in vivo* and recapitulate the inverse relationship between blood S1P levels and SphK2 inhibition. Taken together, our investigations suggest that **2.10** not only inhibits SphK2 *in vitro* using recombinant protein and in yeast, but also *in vivo* using C57BL/6 mice.

Table 2.4. K_i Values of Select SphK2 Inhibitors.[a]

Cmpd	Structure	hSphK1 K_i (nM)	hSphK2 K_i (nM)	hSphK2 selectivity
2.15q	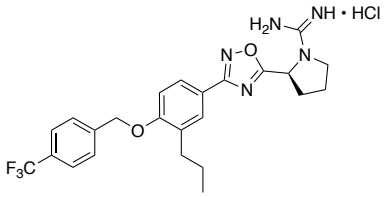	9600 ± 2100	201 ± 11	48
2.15o	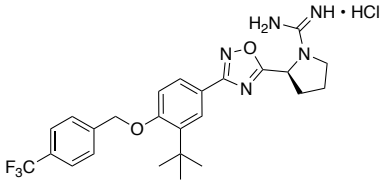	6100 ± 1700	197 ± 76	31
2.27	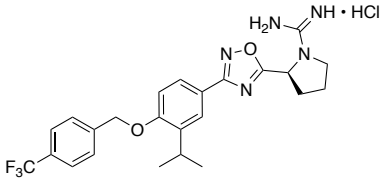	3500 ± 800	192 ± 39	18
2.15e	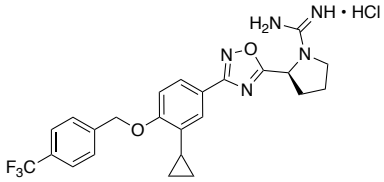	5300 ± 1700	186 ± 12	28
2.10	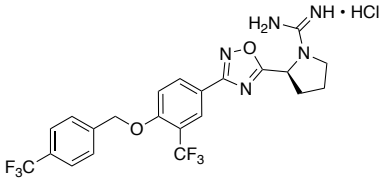	6500 ± 1500	89 ± 8	73

[a]Inhibitory constants for recombinant enzymes were obtained by kinetic analysis of S1P production using variable concentration of sphingosine and a fixed concentration of ATP in the presence or absence of compounds. Selectivity for each compound was determined by dividing the K_m SphK2 by the K_m of SphK1.

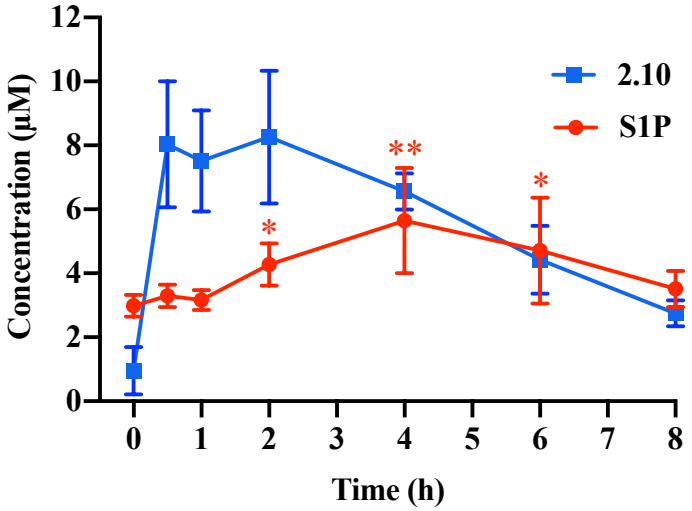

Figure 2.7. Blood concentrations of S1P and **2.10** in C57BL/6 male mice after IP administration with 10 mg/kg of **2.10**. The level of significance is indicated for S1P concentrations (*$P < 0.05$ and **$P < 0.01$) using an unpaired *t*-test (compared to vehicle injected control).

2.5 Conclusions

Modulating S1P signaling at the level of S1P receptors represents a clinically validated approach for managing relapsing remitting multiple sclerosis. This fact encourages investigations as to whether other nodes in the S1P signaling cascades are also drug targets. Inhibition of the S1P generative enzymes SphK1 and 2 can facilitate the decrease or increase in blood S1P levels, respectively, which may have the potential for treating other diseases such as sickle cell disease, renal fibrosis and cancer. As a result of SphK1 and its inhibitors being a subject of intense investigation, potent and SphK1 selective compounds have been developed. However, potent and SphK2 selective inhibitors are lacking. In this report, we discovered a heretofore undisclosed side cavity within the Sph binding site. Interrogating this cavity with various functional groups revealed that relatively small hydrophobic moieties (i.e., trifluoromethyl) are best accommodated. Indeed, characterization of inhibitor **2.10** revealed the most potent SphK2 selective inhibitor to date (K_i 89 nM, 73-fold SphK2 selective). Molecular modeling studies suggest that the trifluoromethyl group fits securely into the side cavity generated by residues Phe548, Leu544, and Leu547 imparting

increased potency towards SphK2, whereas the Val304 to Ile174 variation in SphK1 causes a steric clash that forces the CF_3 group out of the side cavity. Collectively, these phenomena increase SphK2 inhibitor potency and selectivity. Overall, our investigations provide a platform for developing SphK inhibitors that may lead to compounds useful for treating diseases where sphingosine mediated signaling events have gone awry.

2.6 Funding Sources

This work was supported by the NIH (grants R01 GM104366 and R01 GM121075) and Commonwealth of Virginia's Alzheimer's and Related Diseases Research Award Fund.

2.7 References

(1) Pyne, N. J.; El Buri, A.; Adams, D. R.; Pyne, S. Sphingosine 1-Phosphate and Cancer. *Adv. Biol. Regul.* **2018**, *68*, 97–106.

(2) Geffken, K.; Spiegel, S. Sphingosine Kinase 1 in Breast Cancer. *Adv. Biol. Regul.* **2018**, *67*, 59–65.

(3) Patmanathan, S. N.; Wang, W.; Yap, L. F.; Herr, D. R.; Paterson, I. C. Mechanisms of Sphingosine 1-Phosphate Receptor Signalling in Cancer. *Cell. Signal.* **2017**, *34*, 66–75.

(4) Yuza, K.; Nakajima, M.; Nagahashi, M.; Tsuchida, J.; Hirose, Y.; Miura, K.; Tajima, Y.; Abe, M.; Sakimura, K.; Takabe, K.; Wakai, T. Different Roles of Sphingosine Kinase 1 and 2 in Pancreatic Cancer Progression. *J. Surg. Res.* **2018**, *232*, 186–194.

(5) Zhang, Y.; Berka, V.; Song, A.; Sun, K.; Wang, W.; Zhang, W.; Ning, C.; Li, C.; Zhang, Q.; Bogdanov, M.; Alexander, D. C.; Milburn, M. V.; Ahmed, M. H.; Lin, H.; Idowu, M.; Zhang, J.; Kato, G. J.; Abdulmalik, O. Y.; Zhang, W.; Dowhan, W.; Kellems, R. E.; Zhang, P.; Jin, J.; Safo, M.; Tsai, A.; Juneja, H. S.; Xia, Y. Elevated Sphingosine-1-Phosphate Promotes Sickling and Sickle Cell Disease Progression. *J. Clin. Invest.* **2014**, *124*, 2750–2761.

(6) Sun, K.; Zhang, Y.; Bogdanov, M. V; Wu, H.; Song, A.; Li, J.; Dowhan, W.; Idowu, M.; Juneja, H. S.; Molina, J. G.; Blackburn, M. R.; Kellems, R. E.; Xia, Y. Elevate Adenosine Signaling via Adenosine A2B Receptor Induces Normal and Sickle Erythrocyte Sphingosine Kinase 1 Activity. *Blood* **2015**, *125*, 1643–1652.

(7) Huwiler, A.; Pfeilschifter, J. Sphingolipid Signaling in Renal Fibrosis. *Matrix Biol.* **2018**, *68–69*, 230–247.

(8) Schwalm, S.; Beyer, S.; Frey, H.; Haceni, R.; Grammatikos, G.; Thomas, D.; Geisslinger,

G.; Schaefer, L.; Huwiler, A.; Pfeilschifter, J. Sphingosine Kinase-2 Deficiency Ameliorates Kidney Fibrosis by Up-Regulating Smad7 in a Mouse Model of Unilateral Ureteral Obstruction. *Am. J. Pathol.* **2017**, *187*, 2413–2429.

(9) Pyne, N. J.; Dubois, G.; Pyne, S. Role of Sphingosine 1-Phosphate and Lysophosphatidic Acid in Fibrosis. *Biochim. Biophys. Acta, Mol. Cell Biol. Lipids* **2013**, *1831*, 228–238.

(10) Farez, M. F.; Correale, J. Sphingosine 1-Phosphate Signaling in Astrocytes: Implications for Progressive Multiple Sclerosis. *J. Neurol. Sci.* **2016**, *361*, 60–65.

(11) Kappos, L.; Bar-Or, A.; Cree, B. A. C.; Fox, R. J.; Giovannoni, G.; Gold, R.; Vermersch, P.; Arnold, D. L.; Arnould, S.; Scherz, T.; Wolf, C.; Wallström, E.; Dahlke, F. Siponimod versus Placebo in Secondary Progressive Multiple Sclerosis (EXPAND): A Double-Blind, Randomised, Phase 3 Study. *Lancet* **2018**, *391*, 1263–1273.

(12) Yatomi, Y.; Igarashi, Y.; Yang, L.; Hisano, N.; Qi, R.; Asazuma, N.; Satoh, K.; Ozaki, Y.; Kume, S. Sphingosine 1-Phosphate, a Bioactive Sphingolipid Abundantly Stored in Platelets, Is a Normal Constituent of Human Plasma and Serum. *J. Biochem.* **1997**, *121*, 969–973.

(13) Zemann, B.; Urtz, N.; Reuschel, R.; Mechtcheriakova, D.; Bornancin, F.; Badegruber, R.; Baumruker, T.; Billich, A. Normal Neutrophil Functions in Sphingosine Kinase Type 1 and 2 Knockout Mice. *Immunol. Lett.* **2007**, *109*, 56–63.

(14) Mizugishi, K.; Yamashita, T.; Olivera, A.; Miller, G. F.; Spiegel, S.; Proia, R. L. Essential Role for Sphingosine Kinases in Neural and Vascular Development. *Mol. Cell. Biol.* **2005**, *25*, 11113–11121.

(15) Rosen, H.; Gonzalez-Cabrera, P. J.; Sanna, M. G.; Brown, S. Sphingosine 1-Phosphate Receptor Signaling. *Annu. Rev. Biochem.* **2009**, *78*, 743–768.

(16) Pyne, S.; Adams, D. R.; Pyne, N. J. Sphingosine 1-Phosphate and Sphingosine Kinases in Health and Disease: Recent Advances. *Prog. Lipid Res.* **2016**, *62*, 93–106.

(17) Mendelson, K.; Evans, T.; Hla, T. Sphingosine 1-Phosphate Signalling. *Development* **2014**, *141*, 5–9.

(18) Laviad, E. L.; Albee, L.; Pankova-Kholmyansky, I.; Epstein, S.; Park, H.; Merrill, A. H.; Futerman, A. H. Characterization of Ceramide Synthase 2: Tissue Distribution, Substrate Specificity, and Inhibition by Sphingosine 1-Phosphate. *J. Biol. Chem.* **2008**, *283*, 5677–5684.

(19) Chipuk, J. E.; McStay, G. P.; Bharti, A.; Kuwana, T.; Clarke, C. J.; Siskind, L. J.; Obeid, L. M.; Green, D. R. Sphingolipid Metabolism Cooperates with BAK and BAX to Promote the Mitochondrial Pathway of Apoptosis. *Cell* **2012**, *148*, 988–1000.

(20) Adams, D. R.; Tawati, S.; Berretta, G.; Rivas, P. L.; Baiget, J.; Jiang, Z.; Alsfouk, A.; Mackay, S. P.; Pyne, N. J.; Pyne, S. Topographical Mapping of Isoform-Selectivity Determinants for J-Channel-Binding Inhibitors of Sphingosine Kinases 1 and 2. *J. Med. Chem.* **2019**, *62*, 3658–3676.

(21) Congdon, M. D.; Childress, E. S.; Patwardhan, N. N.; Gumkowski, J.; Morris, E. A.; Kharel, Y.; Lynch, K. R.; Santos, W. L. Structure-Activity Relationship Studies of the Lipophilic Tail Region of Sphingosine Kinase 2 Inhibitors. *Bioorg. Med. Chem. Lett.* **2015**, *25*, 4956–4960.

(22) Kharel, Y.; Morris, E. A.; Congdon, M. D.; Thorpe, S. B.; Tomsig, J. L.; Santos, W. L.; Lynch, K. R. Sphingosine Kinase 2 Inhibition and Blood Sphingosine 1-Phosphate Levels. *J. Pharmacol. Exp. Ther.* **2015**, *355*, 23–31.

(23) Kharel, Y.; Raje, M.; Gao, M.; Gellett, A. M.; Tomsig, J. L.; Lynch, K. R.; Santos, W. L.

Sphingosine Kinase Type 2 Inhibition Elevates Circulating Sphingosine 1-Phosphate. *Biochem. J.* **2012**, *447*, 149–157.

(24) Childress, E. S.; Kharel, Y.; Brown, A. M.; Bevan, D. R.; Lynch, K. R.; Santos, W. L. Transforming Sphingosine Kinase 1 Inhibitors into Dual and Sphingosine Kinase 2 Selective Inhibitors: Design, Synthesis, and in Vivo Activity. *J. Med. Chem.* **2017**, *60*, 3933–3957.

(25) Kharel, Y.; Huang, T.; Salamon, A.; Harris, T. E.; Santos, W. L.; Lynch, K. R. Mechanism of Sphingosine 1-Phosphate Clearance from Blood. *Biochem. J.* **2020**, *477*, 925–935.

(26) Mendoza, A.; Bréart, B.; Ramos-Perez, W. D.; Pitt, L. A.; Gobert, M.; Sunkara, M.; Lafaille, J. J.; Morris, A. J.; Schwab, S. R. The Transporter Spns2 Is Required for Secretion of Lymph but Not Plasma Sphingosine-1-Phosphate. *Cell Rep.* **2012**, *2*, 1104–1110.

(27) Novartis, *Novartis Receives FDA Approval for Mayzent ® (Siponimod), the First Oral Drug to Treat Secondary Progressive MS with Active Disease*; https://www.novartis.com/news/media-releases/novartis-receives-fda-approval-mayzent-siponimod-first-oral-drug-treat-secondary-progressive-ms-active-disease (accessed Apr 18, 2020).

(28) Schnute, M. E.; McReynolds, M. D.; Kasten, T.; Yates, M.; Jerome, G.; Rains, J. W.; Hall, T.; Chrencik, J.; Kraus, M.; Cronin, C. N.; Saabye, M.; Highkin, M. K.; Broadus, R.; Ogawa, S.; Cukyne, K.; Zawadzke, L. E.; Peterkin, V.; Iyanar, K.; Scholten, J. A.; Wendling, J.; Fujiwara, H.; Nemirovskiy, O.; Wittwer, A. J.; Nagiec, M. M. Modulation of Cellular S1P Levels with a Novel, Potent and Specific Inhibitor of Sphingosine Kinase-

1. *Biochem. J.* **2012**, *444*, 79–88.

(29) Patwardhan, N. N.; Morris, E. A.; Kharel, Y.; Raje, M. R.; Gao, M.; Tomsig, J. L.; Lynch, K. R.; Santos, W. L. Structure-Activity Relationship Studies and in Vivo Activity of Guanidine-Based Sphingosine Kinase Inhibitors: Discovery of SphK1- and SphK2-Selective Inhibitors. *J. Med. Chem.* **2015**, *58*, 1879–1899.

(30) Pitman, M. R.; Powell, J. A.; Coolen, C.; Moretti, P. A. B.; Zebol, J. R.; Pham, D. H.; Finnie, J. W.; Don, A. S.; Ebert, L. M.; Bonder, C. S.; Gliddon, B. L.; Pitson, S. M. A Selective ATP-Competitive Sphingosine Kinase Inhibitor Demonstrates Anti-Cancer Properties. *Oncotarget* **2015**, *6*, 7065–7083.

(31) Schnute, M. E.; McReynolds, M. D.; Carroll, J.; Chrencik, J.; Highkin, M. K.; Iyanar, K.; Jerome, G.; Rains, J. W.; Saabye, M.; Scholten, J. A.; Yates, M.; Nagiec, M. M. Discovery of a Potent and Selective Sphingosine Kinase 1 Inhibitor through the Molecular Combination of Chemotype-Distinct Screening Hits. *J. Med. Chem.* **2017**, *60*, 2562–2572.

(32) Congdon, M. D.; Kharel, Y.; Brown, A. M.; Lewis, S. N.; Bevan, D. R.; Lynch, K. R.; Santos, W. L. Structure-Activity Relationship Studies and Molecular Modeling of Naphthalene-Based Sphingosine Kinase 2 Inhibitors. *ACS Med. Chem. Lett.* **2016**, *7*, 229–234.

(33) Worrell, B. L.; Brown, A. M.; Santos, W. L.; Bevan, D. R. In Silico Characterization of Structural Distinctions between Isoforms of Human and Mouse Sphingosine Kinases for Accelerating Drug Discovery. *J. Chem. Inf. Model.* **2019**, *59*, 2339-2351.

(34) Wang, Z.; Min, X.; Xiao, S.-H.; Johnstone, S.; Romanow, W.; Meininger, D.; Xu, H.; Liu, J.; Dai, J.; An, S.; Thibault, S.; Walker, N. Molecular Basis of Sphingosine Kinase 1 Substrate Recognition and Catalysis. *Structure* **2013**, *21*, 798–809.

(35) Wang, J.; Knapp, S.; Pyne, N. J.; Pyne, S.; Elkins, J. M. Crystal Structure of Sphingosine Kinase 1 with PF-543. *ACS Med. Chem. Lett.* **2014**, *5*, 1329–1333.

(36) Cummings, S. P.; Le, T.-N.; Fernandez, G. E.; Quiambao, L. G.; Stokes, B. J. Tetrahydroxydiboron-Mediated Palladium-Catalyzed Transfer Hydrogenation and Deuteriation of Alkenes and Alkynes Using Water as the Stoichiometric H or D Atom Donor. *J. Am. Chem. Soc.* **2016**, *138*, 6107–6110.

(37) Kharel, Y.; Mathews, T. P.; Kennedy, A. J.; Houck, J. D.; Macdonald, T. L.; Lynch, K. R. A Rapid Assay for Assessment of Sphingosine Kinase Inhibitors and Substrates. *Anal. Biochem.* **2011**, *411*, 230–235.

(38) Kharel, Y.; Agah, S.; Huang, T.; Mendelson, A. J.; Eletu, O. T.; Barkey-Bircann, P.; Gesualdi, J.; Smith, J. S.; Santos, W. L.; Lynch, K. R. Saccharomyces Cerevisiae as a Platform for Assessing Sphingolipid Lipid Kinase Inhibitors. *PLoS One* **2018**, *13*, e0192179.

(39) Morris, G. M.; Huey, R.; Lindstrom, W.; Sanner, M. F.; Belew, R. K.; Goodsell, D. S.; Olson, A. J. AutoDock4 and AutoDockTools4: Automated Docking with Selective Receptor Flexibility. *J. Comput. Chem.* **2009**, *30*, 2785–2791.

(40) Trott, O.; Olson, A. J. AutoDock Vina: Improving the Speed and Accuracy of Docking with a New Scoring Function, Efficient Optimization and Multithreading. *J. Comput. Chem.* **2010**, *31*, 455–461.

3 Enhancing the Oral Bioavailability of Guanidine-Containing Drug Leads: An Investigation into Sphingosine Kinase 2

3.1 Contributions

The work in this chapter was done primarily by the author. The author synthesized and characterized all final compounds and their corresponding intermediates with the exception of compound **3.20u** which was synthesized by Christopher Shrader, and compound **3.20t** which was synthesized by Kyle Dunnavant. Dr. Yugesh Kharel of the University of Virginia Department of Pharmacology conducted biological analyses of the reported compounds. Dr. Tao Huang purified compounds for animal studies and LC/MS analysis of biological samples. This chapter is an adaption of a manuscript currently being written by the author and Dr. Webster L. Santos for publication in a peer-reviewed journal.

3.2 Abstract

The goal for most drug discovery campaigns is to develop a medication that can be administered to patients orally, *i.e.*, per oral (p.o.). Unfortunately, drugs administered p.o. face the greatest challenges associated with reaching the intended biological target, while also displaying the largest variability in overall bioavailability. Drug absorption is, in part, dependent on the intrinsic physical and chemical properties of the drug. Guanidine-containing compounds have been extensively utilized in the rational design of various medications and are commonly observed in nature. Unfortunately, due to their inherent polarity and basicity, guanidine-based drugs are frequently associated with poor oral bioavailability. While there are reported examples of orally bioavailable guanidine-containing drugs, improvements in adsorption are still needed. Toward that end, we performed structure-activity relationship profiling of the guanidine-based inhibitor **3.14** (SLS1081832), our most potent SphK2-selective inhibitor (K_i = 82 nM, 122-fold SphK2 selective)

with validated *in vivo* activity. Unfortunately, **3.14** suffers from poor oral bioavailability. Modifications to the guanidine head of **3.14** revealed attachment of β-alkoxy acetamide moieties to be the most effective in alleviating the observed poor oral bioavailability. Specifically, biological assessment of compounds **3.20t** and **3.20u** displayed significantly improved oral bioavailability, and prodrug activity to deliver active metabolite **3.14** *in vivo*.

3.3 Introduction

In order for a drug to be efficacious *in vivo*, it is essential for the compound to reach the intended molecular target. Depending on the physiological location of the target, some routes of drug administration may be advantageous for reasons such as mechanism of action, metabolism, drug distribution, and other pharmacokinetic properties. The goal for most drug discovery campaigns is to develop a medication that can be administered to patients orally, *i.e.*, per oral (p.o.). Compared to other methods of drug delivery, oral administration is by far the most convenient route for individuals undergoing chronic treatment and ensures the greatest patient compliance for doctors prescribing these medications. Furthermore, orally bioavailable drugs provide the greatest cost-effectiveness in large scale manufacturing, fewest constraints on the sterility of the drug, and greatest flexibility in terms of the prescribed dose.[1,2] Unfortunately, drugs administered p.o. suffer the greatest challenges associated with achieving the maximum delivered payload to the preferred target *in vivo*, and as such display the greatest variability in terms of overall bioavailability.[3]

For a drug to be considered bioavailable, it must be present in the bloodstream.[3] As opposed to other routes of administration, such as intraperitoneal (IP) or intramuscular (IM) where access into systemic circulation is accomplished with relative ease, medications introduced p.o. are required to navigate and survive a myriad of barriers before entering into circulation. For a drug

to be orally bioavailable, it must survive passage through the acidic stomach content and travel to the small intestine (SI). Next, the drug will need to diffuse across the lumen of the SI to reach the hepatic portal system leading to the liver before reaching systemic circulation. This process is often accompanied by a dramatic reduction in the concentration of active drug and is known as first pass metabolism.[4] Unfortunately, drug absorption in the gastrointestinal (GI) tract is greatly dependent on the intrinsic physical and chemical properties of the drug as well as the physiological aspects of the SI. Various factors that can affect adsorption and must be taken into consideration during a drug discovery campaign include local pH, inherent drug basicity or acidity, microbial colonization, and Lipinski's rule of five.[1,4,5]

Guanidine-containing compounds have been extensively utilized in the rational drug design of various medications and are commonly observed in nature. As shown in Figure 3.1, synthetic examples include compound **3.1** (zanamivir), an effective neuraminidase inhibitor approved by the FDA for the treatment of influenza type A and B, as well as FDA approved bi-guanidine medications **3.2** (metformin) and **3.3** (proguanil) for the treatment of Type 2 diabetes and malaria, respectively. The guanidine functionality is also found in many important naturally occurring compounds such as **3.4** (creatine), **3.5** (L-arginine), and **3.6** (streptomycin) (Figure 3.1). Unfortunately, the high basicity of the guanidine functional group ($pK_a = 13.6$) causes protonation upon entering the acidic environment in the SI (pH = 6.0 – 7.4), leading to a condition known as ion trapping.[3] Once in the GI tract, this positive charge prevents the drug from progressing toward the hepatic portal system leading to systemic circulation. This is due to the resulting high desolvation cost during passive diffusion and subsequent poor absorption across the lumen of the SI.[6] Taken together, guanidine-containing compounds are very frequently associated with poor oral bioavailability.[7]

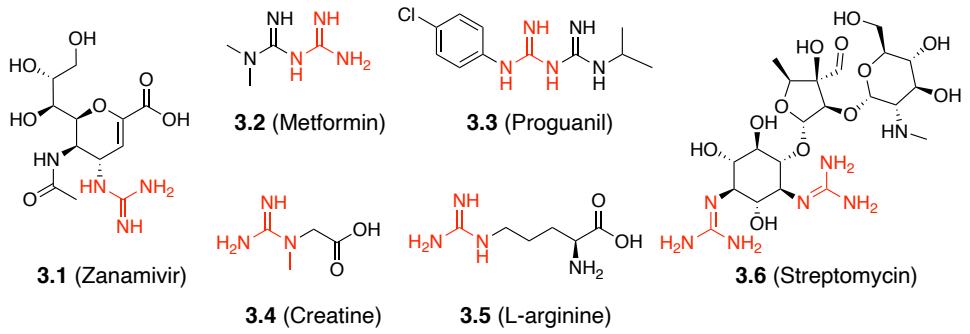

Figure 3.1. Chemical structures of synthetic and natural guanidine containing compounds.

Several strategies have been proposed to improve the oral bioavailability of guanidine containing drugs. Potential solutions range from chemical attachment of an acidic moiety such as a carboxylic acid to create an ion pair and an overall neutral drug,[8,9] and selective targeting of membrane transporters in the SI to facilitate transport across the epithelial cell wall.[10,11] Perhaps the most extensively utilized approach is the chemical modification of the guanidine moiety with metabolically labile hydrophobic alkyl and aryl substituents to increase compound lipophilicity and serve as a platform for bioactivation. This strategy has shown moderate success in developing prodrugs that effectively hide the positively charged guanidine in order to promote passive diffusion across the SI lumen and subsequent metabolic activation once in the liver.[12–15] For example, Huttunen and coworkers reported the benefit of increasing the lipophilicity of **3.2** to improve oral bioavailability. Impressively, they successfully developed prodrug **3.7** (2a). Through *in vivo* rat studies, **3.7** displayed quantitative bioconversion to active metabolite **3.2** when administered IV, as well as a 22% increase in bioavailability upon oral administration.[12] In another report, Hsu *et al.* disclosed that the synthesis of the acylguanidine derivative of **3.9** (guanidino-oseltamivir carboxylic acid: GOC), a potent therapeutic against influenza type A and B, improved cell permeability and overall bioavailability. The production of acylguanidine derivatives represents an interesting prodrug strategy. It has been documented that acylguanidine moieties are

susceptible to hydrolysis *in vivo* and could potentially serve as platforms for bioactivation.[16] Satisfyingly, Hsu *et al.* demonstrated that guanidino *N*-acylation of **3.9** with *n*-octanoic acid to produce prodrug **3.8** (8a) resulted in a 28-fold increase in cellular uptake when administered to MDCK cells and roughly 10% of **3.8** being hydrolyzed to form active metabolite **3.9** *in vitro* (Figure 3.2).[13] Another promising prodrug strategy is the synthesis of *N*-hydroxyguanidine derivatives.[17–19] Investigations have shown these moieties to aid in the smuggling of poorly adsorbed substrates into the liver while also being susceptible to metabolic reduction to form their corresponding guanidine derivatives.[18, 20–22] However, the mechanism by which this bio-reduction takes place is still debated. One proposed metabolic route is due to the action of liver homogenates and hepatocytes catalyzed by a microsomal NADH-dependent system.[23] Regardless, the production of *N*-hydroxyguanidine derivatives presents another possible method to enhance the oral bioavailability of guanidine containing drugs.

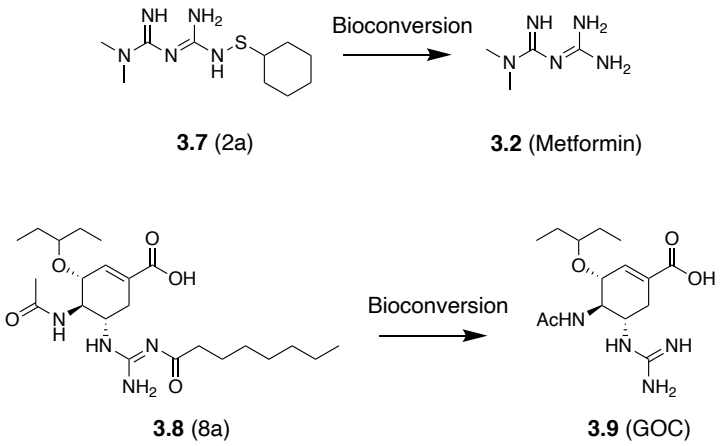

Figure 3.2. Chemical structures of prodrugs **3.7** and **3.8** with bioconversion into their active metabolites.

Recently, our laboratory reported the discovery of a small side cavity in the active site of sphingosine kinase 2 (SphK2).[24] In mammals and perhaps all vertebrates, sphingosine 1-phosphate

(S1P) is produced exclusively from the ATP-dependent phosphorylation of sphingosine (Sph) by sphingosine kinases (SphK1 and SphK2) (Figure 3.3). It is well documented that S1P is implicated in various animal models of diseases such as renal fibrosis,[25,26] cancer,[27–29] and multiple sclerosis.[30,31] Furthermore, multiple studies have demonstrated that inhibition of SphK1 or SphK2 has therapeutic potential in these disease models.[32,33] Significant efforts by our group have focused on the development of SphK1-selective, dual SphK1/2, and SphK2-selective inhibitors. Recently, Sibley *et al.* reported the guanidine-based inhibitor **3.10** (SLM6071469) which is the most potent SphK2-selective inhibitor published in the literature to date (Table 3.1). Additional findings included molecular modeling studies that showed that the internal trifluoromethyl substituent likely interacts with a previously unrecognized side cavity resulting in enhanced inhibitor potency toward SphK2. Moreover, it was shown that the guanidine moiety in **3.10** forms a salt-bridge with the carboxylate of Asp211, which flanks the ATP active site when docked in the Sph binding pocket of SphK2. Further experiments were conducted assessing the *in vivo* properties of inhibitor **3.10**. Measured blood S1P concentrations have proven to be an exceptional pharmacodynamic marker for SphK2 inhibition in mice. Curiously, SphK2 specific inhibition results in blood S1P concentrations to rise nearly 3-fold.[34,35] Kharel *et al.* proposed that this phenomenon is the result of a cascade wherein Sph, formed at the hepatocyte surface *via* dephosphorylation of blood S1P, is captured and phosphorylated by SphK2 and in turn degraded by intracellular S1P lyase. Small molecule inhibition of SphK2 causes the recently formed Sph to then in turn be captured and phosphorylated by SphK1 resulting in an overall increase in S1P concentrations.[36] Administration of a single 10 mg/kg dose of **3.10** in C57BL/6 mice *via* IP injection displayed a 2-fold increase in blood S1P concentrations after 4 hours post injection and remained elevated for up to 6 hours. The observed rise in blood S1P levels is strong evidence that **3.10** is inhibiting SphK2 in an isoform

selective manner when administered *in vivo*. However, as stated earlier, our goal is to develop an orally bioavailable SphK2-selective inhibitor. Unfortunately, as with other guanidine containing drugs, oral administration of **3.10** is ineffective. Therefore, we sought to design a guanidine prodrug that would improve the poor oral bioavailability of **3.10**. Herein, we report the development, synthesis, and evaluation of orally bioavailable prodrugs of guanidine-based SphK2-selective inhibitors.

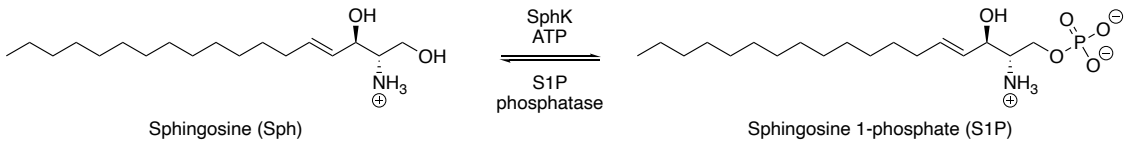

Figure 3.3. The Sph/S1P equilibrium *in vivo*.

3.4 Results and Discussion

3.4.1 Prodrug Design

Previous work in our group has been focused on the design and synthesis of highly potent and selective inhibitors of SphK2. Early experiments conducted examined whether there was a benefit of having a positively charged moiety on our inhibitor scaffold. It was rationalized that when docked in the active site of SphK2, a positively charged amine within our molecule could mimic the electrostatic interactions observed between Sph and catalytic amino acid Asp211.[37] A series of first-generation inhibitors designed utilized various terminal amine functionalities leading to the development of compounds **3.11** (*trans*-11a) and **3.12** (*trans*-12a) (Table 3.1).[38] Investigation into the effect of a positively charged species with regards to SphK2 inhibition revealed that compared to neutral inhibitor **3.11**, charged derivative **3.12** displayed increased potency (K_i = 8.0 μM) and selectivity (8-fold) for SphK2 thus validating our theory that a positive charge is beneficial for kinase inhibition. Inspired from these results, as well as known amidine-

based inhibitors of sphingosine kinases,[39,40] a library of second-generation inhibitors was synthesized that replaced the quaternary ammonium salt moiety with a guanidine functionality. This strategy led to the development of compound **3.13** (SLR080811) (Table 3.1).[35,41] When tested for enzyme inhibition, **3.13** displayed improved potency (K_i = 1.3 μM) and selectivity (9-fold) for SphK2. Encouraged from these results, we next focused on fine-tuning the remaining portions of our scaffold, eventually leading to the discovery of **3.10**.[24] Inhibitor **3.10** contains a shorter, less flexible 4-trifluoromethyl benzyl ether tail in place of the *n*-octyl moiety in **3.11-3.13**, as well as the addition of a trifluoromethyl substituent on the internal aryl ring. Biologic evaluation of **3.10** revealed it to be the most potent (89 nM) SphK2-selective (73-fold) inhibitor known at the time. Further structure-activity relationship (SAR) studies conducted with inhibitor **3.10** led to the synthesis of compound **3.14** (SLS1081832) (Table 3.1). It was observed that replacement of the 4-trifluoromethyl benzyl ether moiety for a 2-cyclohexylethoxy substituent imparted improved potency (82 nM) and selectivity (122-fold) for SphK2, thus making it the most potent SphK2-selective inhibitor currently known.

Table 3.1. K_i Values of Select SphK2 Inhibitors.[a]

Cmpd	Structure	SphK1 K_i (μM)	SphK2 K_i (μM)	SphK2 selectivity
3.10 (SLM6071469)	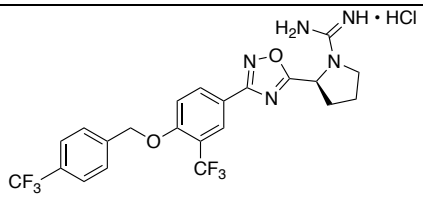	6.5 ± 1.5	0.089 ± 0.008	73
3.11 *(trans*-11a)	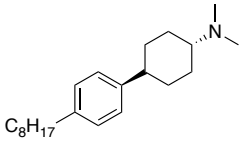	40 ± 7	27 ± 5	1
3.12 *(trans*-12a)	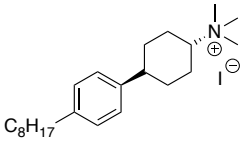	60 ± 6	8 ± 2	8
3.13 (SLR080811)	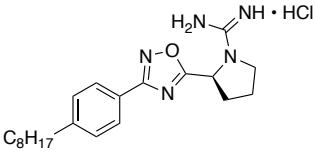	12 ± 1	1.3 ± 0.4	9
3.14 (SLS1081832)	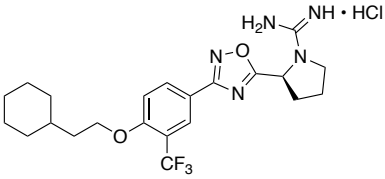	>10	0.082 ± 0.015	122

[a]Inhibitory constants for recombinant enzymes were obtained by kinetic analysis of S1P production using variable concentration of sphingosine and a fixed concentration of ATP in the presence or absence of compounds. Selectivity for each compound was determined by dividing the K_m SphK2 by the K_m of SphK1.

Unfortunately, as with the other guanidine containing inhibitors developed in our group, **3.14** suffers the same deficiency of poor oral bioavailability. In this study, we examined the effect of guanidino *N*-substitutions on guanidine-based SphK2-selective inhibitors in regards to oral bioavailability and prodrug activity. A wide range of substituents were attached to parent compound **3.14** and examined for their effect on oral bioavailability and subsequent metabolism, resulting in improved SphK2 inhibition.

3.4.2 Chemistry

To investigate the effect of *N*-substitution on the oral bioavailability of guanidine-based SphK2-selective inhibitors, a series of derivatives was synthesized. The synthesis started with preparation of the common intermediate **3.14** (Scheme 3.1). Compound **3.15** (4-fluoro-3-(trifluoromethyl)benzonitrile) is available for purchase from commercial sources. Completion of a nucleophilic aromatic substitution reaction of **3.15** with 2-cyclohexylethanol and sodium hydride was performed to generate benzonitrile intermediate **3.16**. Next, intermediate **3.16** was treated with hydroxylamine hydrochloride and triethylamine (TEA) while refluxing in ethanol to produce amidoxime intermediate **3.17**. Following amidoxime production, **3.17** was dissolved in DMF and heated to 100 ºC in the presence of Boc-L-Proline, HCTU, and Hünig's base to afford 1,2,4-oxadiazole intermediate **3.18**. Next, installation of the guanidine moiety was completed by removing the Boc protecting group with a mixture of trifluoroacetic acid **(**TFA), **3.18** and CH_2Cl_2 followed by reaction with *N*,*N*'-*di*-Boc-1*H*-pyrazole-1-carboxamidine and Hünig's base to afford the *bis*-Boc-protected intermediate. Subsequent removal of the Boc protecting groups was achieved with HCl in dioxane (4.0 M) to yield the desired common intermediate **3.14** as an HCl salt. Similarly, production of pyrrolidinium analogue **3.19** was carried out with a mixture of intermediate **3.18** and HCl in dioxane (4.0 M) to yield the desired secondary amine HCl salt.

Scheme 3.1. Synthesis of Common Intermediate **3.14** and Analogue **3.19** [a]

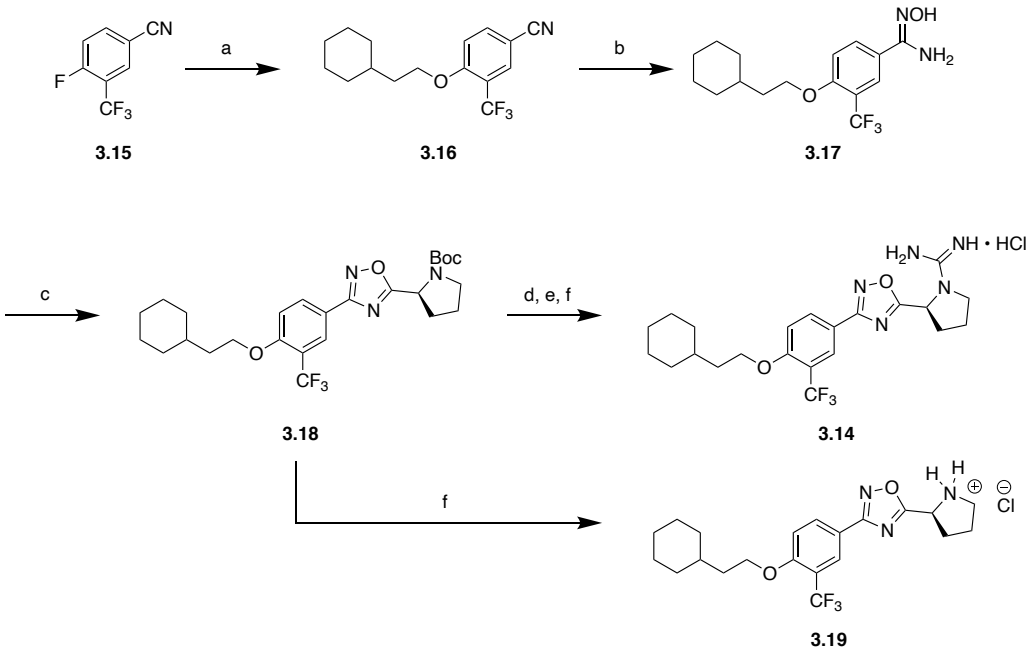

[a]Reagents and conditions: (a) 2-cyclohexylethanol, NaH, THF, 0 ºC-rt, 18 h, 87%; (b) NH_2OH•HCl, Et_3N, EtOH, reflux, 3 h, 96%; (c) Boc-L-proline, DIEA, HCTU•PF_6, DMF, 100 ºC, 18 h, 84%; (d) TFA, CH_2Cl_2, 3-12 h, 87%; (e) N,N'-*di*-Boc-1H-pyrazole-1-carboxamidine, DIEA, CH_3CN, rt, 18 h, 86%; (f) HCl, Dioxane, rt, 18 h, 89-91%.

Synthesis of *N*-substituted guanidine analogues **3.20a**–**u** was performed as shown in Scheme 3.2. Analogues **3.20a**–**c** were prepared through a nucleophilic substitution reaction of **3.14**, Hünig's base and various carbamoyl chlorides dissolved in CH_2Cl_2. Likewise, carbamate analogues **3.20d**–**i** were synthesized *via* nucleophilic substitution reaction of intermediate **3.14** with various chloroformates and Hünig's base. Reaction of **3.14** with cyanogen bromide and Hünig's base in CH_2Cl_2 resulted in the formation of cyanoguanidine analogue **3.20j**. Sulfonamide analogues **3.20k**–**m** were generated through nucleophilic substitution reaction of **3.14**, Hünig's base, and various sulfonyl chlorides. Formation of benzamide derivative **3.20n** was completed with a mixture of **3.14**, benzoic acid, carbonyldiimidazole (CDI), 4-dimethylaminopyridine

(DMAP), and TEA while stirring in CH_2Cl_2. Synthesis of trifluoroacetamide analogue **3.20p** was performed *via* a nucleophilic substitution reaction with **3.14**, trifluoroacetic anhydride, and Hünig's base. A mixture of **3.14**, Hünig's base and various acyl chlorides were stirred in CH_2Cl_2 at room temperature to generate acylguanidine derivatives **3.20o**, and **3.20q–u**.

Scheme 3.2. Synthesis of Analogues **3.20a–u** [a]

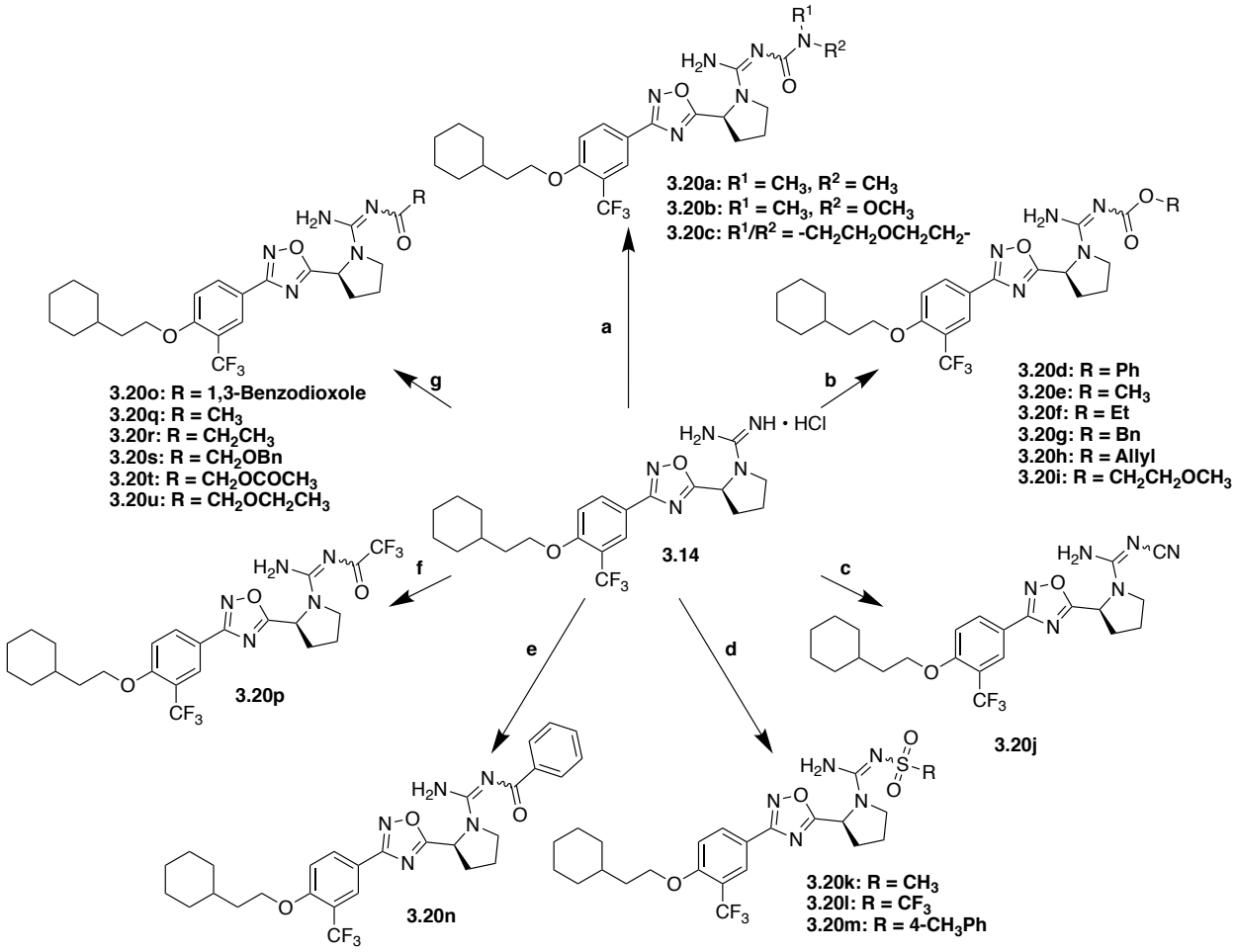

[a]Reagents and conditions: (a) carbamoyl chloride derivative, DIEA, CH_2Cl_2, 10 min, 38-79%; (b) chloroformate derivative, DIEA, CH_2Cl_2, 10 min, 66-94%; (c) BrCN, DIEA, CH_2Cl_2, 40 ºC, 2 h, 30%; (d) sulfonyl chloride derivative, DIEA, CH_2Cl_2, 10 min, 30-66%; (e) benzoic acid, CDI, TEA, DMAP, CH_2Cl_2, 18 h, 84%; (f) 2,2,2-trifluoroacetic anhydride, DIEA, CH_2Cl_2, 10 min, 71%; (g) acyl chloride derivative, DIEA, CH_2Cl_2, 10 min, 30-79%.

The synthesis of analogues **3.20v** and **3.20w** are shown in Scheme 3.3. Intermediate **3.18** was added to a mixture of TFA and CH_2Cl_2 to promote the removal of the Boc protecting group resulting in the production of intermediate **3.21** as a TFA salt. Following Boc removal, cyanamide formation was accomplished by the reaction of **3.21** with Hünig's base and cyanogen bromide while refluxing in acetonitrile to produce intermediate **3.22**. Synthesis of amino guanidine analogue **3.20v** was performed *via* a reaction with **3.22** in the presence of hydrazine hydrate and cesium carbonate while heating in THF. Similarly, production of hydroxy guanidine derivative **3.20w** was accomplished *via* a reaction with **3.22** in the presence of hydroxylamine hydrochloride and cesium carbonate refluxed in ethanol.

Scheme 3.3. Synthesis of Analogues **3.20v** and **3.20w** [a]

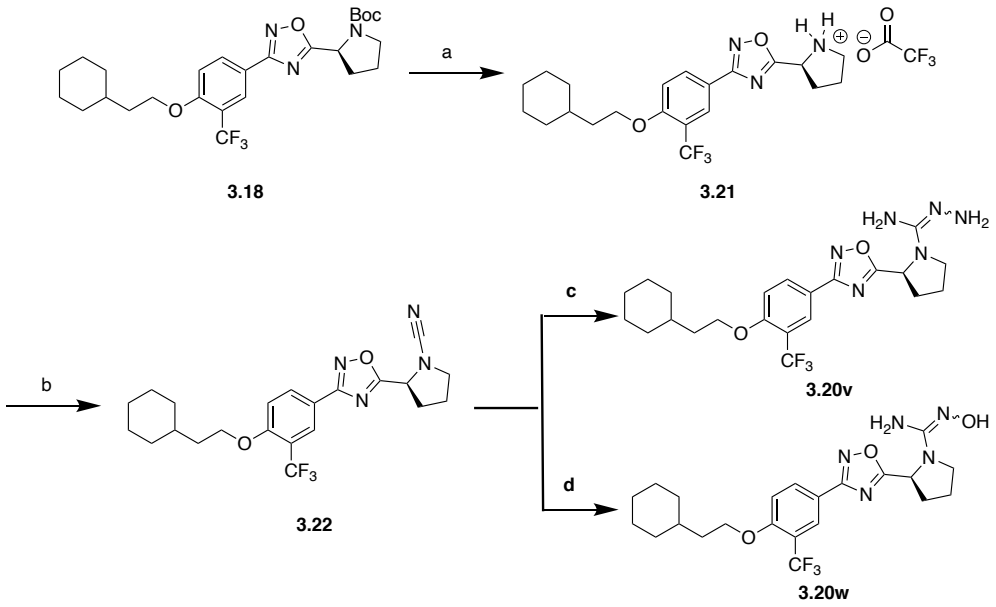

[a]Reagents and conditions: (a) TFA, CH_2Cl_2, 3-12 h, 87%; (b) BrCN, DIEA, CH_3CN, 80 ºC, 2 h, 87%; (c) NH_2NH_2•H_2O, Cs_2CO_3, THF, 65 ºC, 18 h, 33%; (d) NH_2OH•HCl, Cs_2CO_3, EtOH, 85 ºC, 18 h, 40%.

3.4.3 Biological Evaluation of Prodrug Derivatives.

The goal of this SAR was to improve the observed poor oral bioavailability of the highly potent guanidine based SphK2-selective inhibitor **3.14**. Specifically, we aimed to probe the benefit of guanidino *N*-substitutions with respect to oral bioavailability, *in vivo* metabolism to active compound **3.14**, and thereby subsequent SphK2 inhibition. A library of compounds with various substituents spanning the terminal guanidine head of the **3.14** scaffold was synthesized and assessed for improved oral bioavailability and SphK2 specific inhibitory activity, i.e. increased blood S1P levels. To assess improved oral bioavailability *in vivo*, we administered C57BL/6 mice with a single bolus 30 mg/kg p.o. dose of test prodrug and measured blood S1P levels. When considering *in vivo* investigations, an observed rise in blood S1P concentrations has been proven to be an exceptional pharmacodynamic marker for SphK2 specific inhibition.[34–36] As shown in Figures 3.4A-H, blood S1P levels were measured at 6 h post administration of test compound *via* liquid chromatography-tandem MS. To determine the amount of innate oral bioavailability, we first administered parent compound **3.14** into mice (Table 3.2). Comparison of vehicle (no treatment) versus **3.14** displayed an 18% increase in blood S1P levels, indicating that inhibitor **3.14** is somewhat, albeit not significantly, orally bioavailable and is selective for SphK2 *in vivo*. Thus, any tested prodrug that is successful in inducing blood S1P concentrations to rise ≥18% would be considered significant. Next, to confirm the advantage of the guanidine head with respect to SphK2 inhibition, **3.19** was synthesized to represent the minimal scaffold without the guanidine functionality (Table 3.2). As expected, removal of the guanidine head resulted in a small 10% increase of blood S1P, thus validating our use of the guanidine moiety to achieve maximum SphK2 inhibition. Compounds **3.20a-c** were designed to transform the guanidine into a urea-like derivative to probe any potential for improved adsorption and

subsequent urea metabolism once in the liver. Conversion to a dimethyl urea moiety (**3.20a**) resulted in only a slight increase of blood S1P levels, indicating poor compound adsorption or metabolism. Likewise, Weinreb amide (**3.20b**) and acyl morpholine (**3.20c**) derivatives were unsuccessful with increasing blood S1P levels more than **3.14**, thus indicating the use of urea moieties as a poor prodrug strategy. Accordingly, carbamate analogues were explored with compounds **3.20d-i**. Transformation of the guanidine head to a carbamate moiety potentially allows for prodrug metabolism *via* hydrolysis and carbon dioxide release, thus exposing active metabolite **3.14**. Utilization of aryl carbamates did not favor oral bioavailability as phenyl carbamate (**3.20d**) and benzyl carbamate (**3.20g**) derivatives resulted in a 10% and 11% rise in blood S1P levels, respectively. Interestingly, extension of the alkyl carbamate carbon chain had a positive impact on oral bioavailability, as indicated by ethyl carbamate variant **3.20f** increasing blood S1P levels by nearly twice as much as methyl carbamate (**3.20e**). Encouraged from this observation, we synthesized allyl (**3.20h**) and 2-methoxyethyl (**3.20i**) analogues. However, compared to compound **3.20f**, this resulted in a decrease in measured blood S1P levels. Thereafter, we explored the benefit of a cyanoguanidine (**3.20j**) moiety for improved oral bioavailability. Excitingly, **3.20j** was successful in increasing blood S1P concentrations by 30%; nearly 1.7-fold greater than **3.14**. Next, inspired from the potential leaving group ability of sulfonamide functional groups, mesyl (**3.20k**), triflyl (**3.20l**), and tosyl (**3.20m**) sulfonamides were synthesized. Collectively, these derivatives had an overall poor effect on oral bioavailability as indicated by marginal increases in blood S1P. We next investigated the potential of benzamide (**3.20n**) and 1,3-benzodioxole-5-carboxamide (**3.20o**) functionalities towards improved oral bioavailability. Unfortunately, this resulted in poor SphK2 inhibition as indicated by minimal increases in blood S1P. Thereafter, the effect of trifluoroacetamide (**3.20p**),

acetamide (**3.20q**), and propionamide (**3.20r**) variants was examined. Comparison of measured blood S1P levels revealed that **3.20q** was nearly twice as effective as **3.20p** and **3.20r** in terms of SphK2 inhibition. Inspired by these results, decoration of the guanidine head with β-alkoxy acetamides was explored with compounds **3.20s-u**. Fortunately, these derivatives proved to be the most effective in terms of improved oral bioavailability and SphK2 inhibition. All three analogues displayed significant increases in blood S1P levels compared to **3.14**, with β-benzyloxyacetamide (**3.20s**) and β-ethoxyacetamide (**3.20u**) demonstrating to be more effective than β-acetoxyacetamide (**3.20t**). Furthermore, comparison of **3.20u** with parent compound **3.14** displayed a considerable 4-fold improvement with increasing blood S1P levels *in vivo*. Lastly, the effect of heteroatom substitution was explored with aminoguanidine (**3.20v**) and hydroxyguanidine (**3.20w**) derivatives. Measurement of blood S1P revealed that **3.20v** was ineffective while **3.20w** displayed significant increases in blood S1P by 35% compared to vehicle. It should be noted that **3.20v** and **3.20w** were assessed at a reduced concentration of 20 mg/kg.

Considering our observations summarized in Table 3.2, we next wanted to measure blood concentrations of active metabolite **3.14** after treatment of test compound *in vivo*. Collectively, this would help determine whether our modified compounds were behaving as prodrugs and regenerating significant concentrations of the active metabolite. As shown in Figure 3.5, comparison of blood **3.14** levels for vehicle (no treatment control) versus **3.14** administered p.o. displayed a detected concentration of 0.028 μM, thus indicating marginal innate oral bioavailability. Next, to serve as a control, administration of pyrrolidine derivative **3.19** was assessed and as expected, did not register any detectable levels of **3.14**. After, methyl (**3.20e**) and ethyl (**3.20f**) carbamates were examined, and surprisingly neither yielded significant

concentrations of parent compound **3.14**. Considering the observed significant rise in blood S1P levels with **3.20f**, these results suggest these compounds possibly possess inherent SphK2 inhibitory activity, although this remains to be further investigated. Examination of cyanoguanidine (**3.20j**) revealed detected parent compound levels that were similar to that of direct **3.14** p.o. administration. Given these results combined with **3.20j** inducing only moderate increases in blood S1P, cyanoguanidines do not seem to be a viable prodrug strategy. Moving forward, compounds **3.20k** and **3.20o** were analyzed and registered no detected **3.14** levels in blood. These results are consistent with the observed poor SphK2 inhibitory activity of **3.20k** and **3.20o**. Administration of trifluoroacetamide (**3.20p**) analogue resulted in a 2.5-fold increase of detected **3.14**, while the propionamide (**3.20r**) derivative displayed no prodrug activity. Excitingly, oral administration of all three β-alkoxy acetamides (**3.20s-u**) resulted in significant detected levels of active metabolite **3.14**. When compared to **3.14** oral administration, **3.20t** and **3.20u** were successful in increasing active metabolite levels by 25-fold and 11-fold respectively. Furthermore, these results are consistent with the observed excellent SphK2 inhibitory activity, i.e. rise in blood S1P, observed for these compounds *in vivo*. Taken altogether, these results suggest that decoration of a guanidine functional group with β-alkoxy acetamide moeities are a viable prodrug strategy in order to alleviate poor oral bioavailability. Currently, investigations are still ongoing, and measurements for all tested compounds ($t_{1/2}$, C_{max}, T_{max}, %F) are still being obtained.

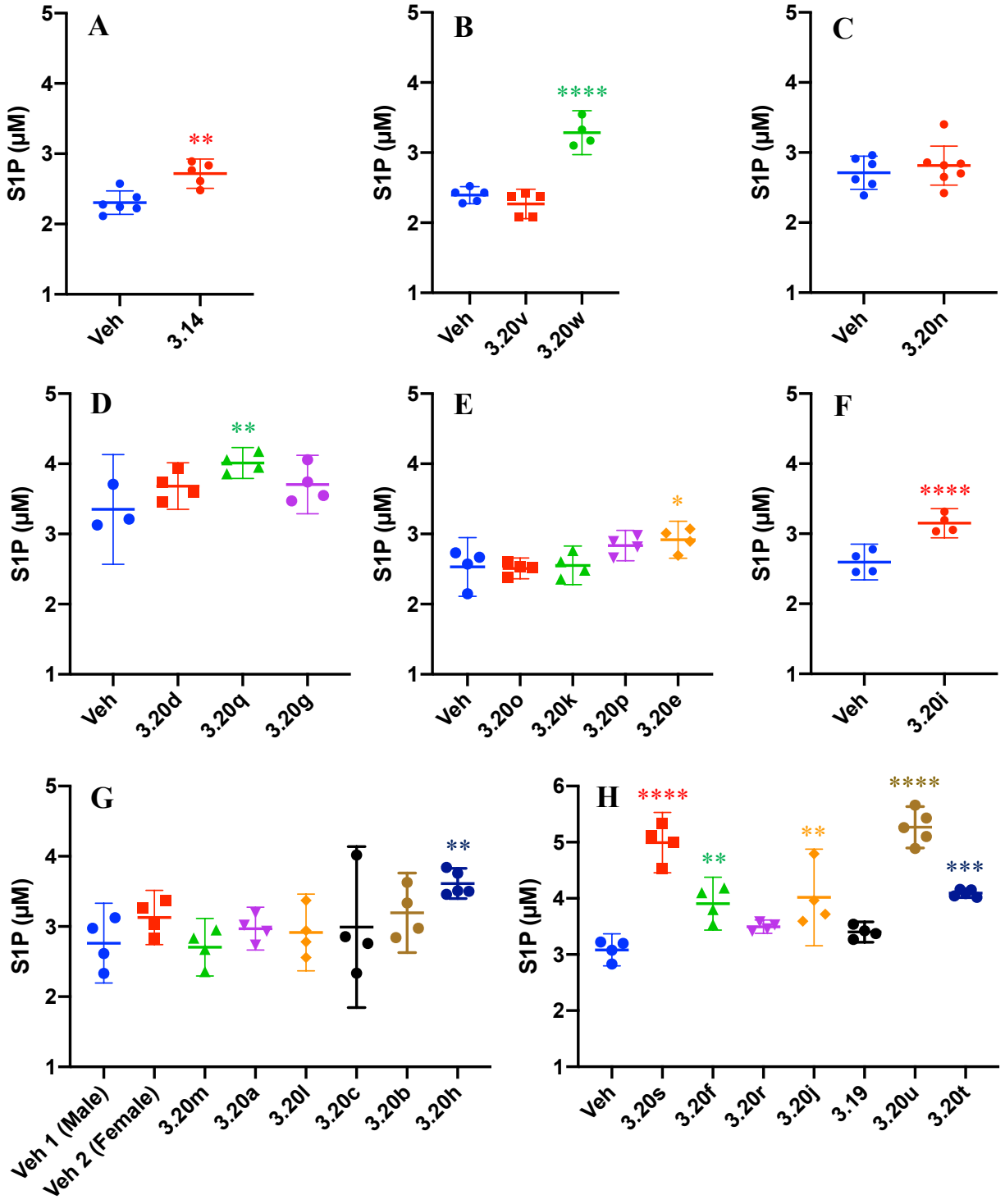

Figure 3.4. Blood concentrations of S1P in C57BL/6 mice after 6 h post PO administration with 30 mg/kg test compound. The level of significance is indicated for S1P concentrations (*P < 0.05, **P < 0.01, ***P < 0.001, and ****P < 0.0001) using an unpaired *t*-test (compared to vehicle administered control).

Table 3.2. Activity of SphK2 Inhibitors Represented as % Increase of Blood S1P Levels versus Vehicle. [a]

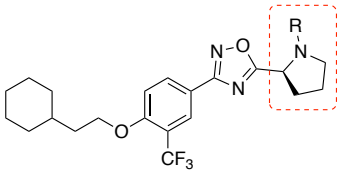

Cmpd	R	% Inc. Blood [S1P]	Cmpd	R	% Inc. Blood [S1P]
3.14	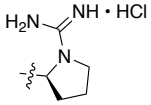	18 ± 4	**3.20i**	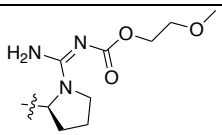	21 ± 3
3.19	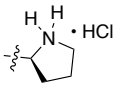	10 ± 3	**3.20j**	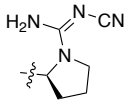	30 ± 10
3.20a	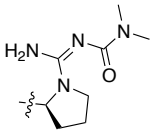	8 ± 5	**3.20k**	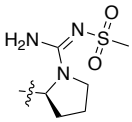	1 ± 3
3.20b	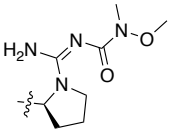	2 ± 9	**3.20l**	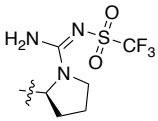	5 ± 9
3.20c	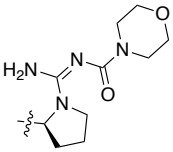	8 ± 16	**3.20m**	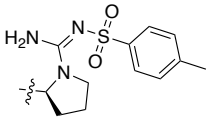	0 ± 7
3.20d	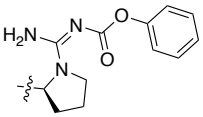	10 ± 4	**3.20n**	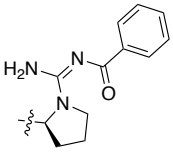	4 ± 3
3.20e	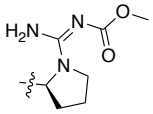	15 ± 4	**3.20o**	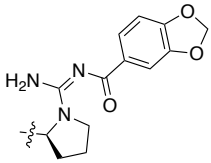	0 ± 1
3.20f	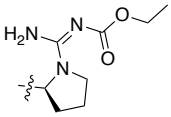	27 ± 5	**3.20p**	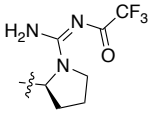	12 ± 3
3.20g	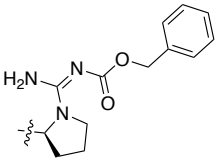	11 ± 5	**3.20q**	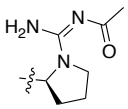	20 ± 3
3.20h	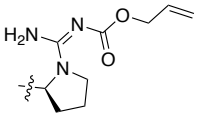	16 ± 4	**3.20r**	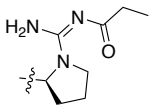	13 ± 1

3.20s	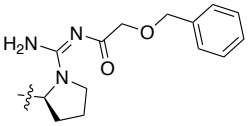	62 ± 5	**3.20v**	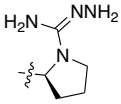	0 ± 3*
3.20t	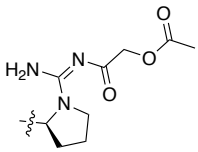	33 ± 1	**3.20w**	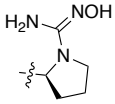	35 ± 4*
3.20u	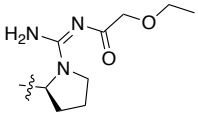	71 ± 4			

[a] Percent increase of blood S1P for various compounds was calculated from comparison of vehicle (no compound administered as control) versus administered test compound in C57BL/6 mice after PO administration with 30 mg/kg test compound after 6 h. % values with * indicate test compound was administered at 20 mg/kg. For detailed assay conditions, see Experimental Section.

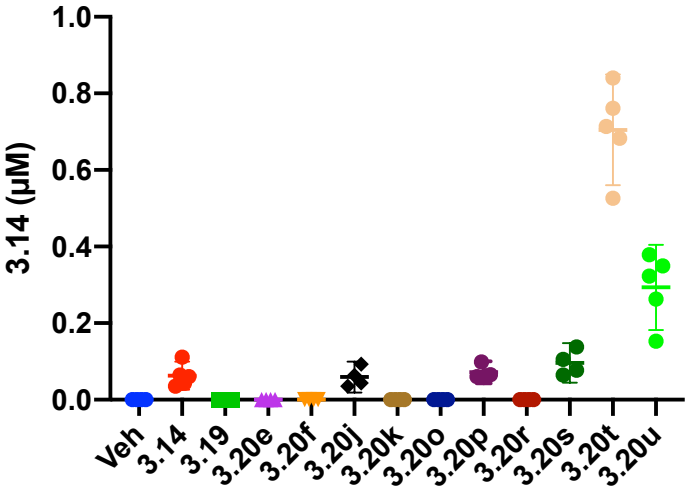

Figure 3.5. Blood concentrations of active metabolite **3.14** in C57BL/6 mice after 6 h post PO administration with 30 mg/kg test compound.

3.5 Current Efforts and Future Directions

From the data presented in Table 3.2, eight prodrugs displayed significant (>18%) increases in blood S1P levels compared to oral treatment of parent compound **3.14**. However, as shown in Figure 3.5, we have only obtained blood measurements of **3.14** for five of the eight leads. Current efforts involve measuring blood **3.14** levels for all remaining compounds. This will allow us to identify if any other derivatives are behaving as prodrugs and facilitating the release of active metabolite **3.14** *in vivo*. Additionally, we are also in the process of analyzing all compounds *in vitro*. We hope to illustrate that removing the ability for all tested compounds to be metabolized will lead to a complete loss of SphK2 inhibition. We aim to show that any inhibitory activity observed in Table 3.2 was the result of prodrug metabolism releasing parent compound **3.14**. Positive results from these studies will provide a strong foundation for the development of future guanidine containing SphK2 inhibitors that display enhanced activity when administered p.o.

3.6 Conclusions

When considering prescribed medications in humans and animals, it has been shown that in order to achieve maximum patient compliance and ensure the greatest ease of treatment, orally administered drugs are unsurpassed. Unfortunately, drugs that are administered orally face the greatest barriers *in vivo* on route to their intended biological target. Towards that end, it has been shown that certain functionalities that comprise the drug can also be problematic once administered orally into humans leading to poor oral bioavailability. Numerous investigations have revealed various strategies to alleviate this problem *via* chemical modification, thus effectively hiding the troublesome functionality. This in turn has been demonstrated to promote enhanced drug adsorption *in vivo* and subsequent metabolism to reveal the active parent compound. In this study,

we aimed to develop a prodrug of the highly potent, guanidine-based SphK2 inhibitor **3.14** (K_i = 82 nM, 122-fold SphK2 selective). SphK2 has proven to be implicated in a wide variety of disease states, and chemical inhibition has been demonstrated to be therapeutic. Structurally, the guanidine functionality on **3.14** has been shown to be crucial for the observed pharmacodynamic effect; unfortunately, it also diminished oral bioavailability. As such, guanidine containing drugs are frequently associated with poor oral bioavailability. Chemical modification of the guanidine head resulted in the synthesis of two highly effective prodrugs, **3.20t** and **3.20u**. Biological assessment demonstrated that these two compounds were successful in enhancing oral adsorption in mice and increased active metabolite **3.14** levels by up to 25-fold greater than previously observed. Additionally, measurement of potential SphK2 inhibitory activity revealed significant increases in blood S1P levels up to 71% compared to **3.14** treatment alone. Collectively, this data demonstrates that these modifications unquestionably enhance inhibitor oral bioavailability and magnify the delivered payload into systemic circulation *in vivo*. Overall, these investigations provide a strong foundation for the development of future guanidine containing prodrugs, and may lead to the clinical advancement of future medications where oral bioavailability is lacking.

3.7 Funding Sources

This work was supported by the NIH (grants R01 GM104366 and R01 GM121075).

3.8 References

(1) Viswanathan, P.; Muralidaran, Y.; Ragavan, G. Chapter 7 - Challenges in Oral Drug Delivery: A Nano-Based Strategy to Overcome. In *Nanostructures for Oral Medicine*, 1st ed.; Andronescu, E., Grumezescu, A. M., Eds.; 2017; pp 173–201.

(2) Tetteh, E.; Morris, S. Systematic Review of Drug Administration Costs and Implications for Biopharmaceutical Manufacturing. *Appl. Health Econ. and Health Policy*. **2013**, *11*, 445–456.

(3) Bardal, S. K.; Waechter, J. E.; Martin, D. S. Chapter 2 - Pharmacokinetics. In *Applied Pharmacology*, 1st ed.; Bardal, S. K., Waechter, J. E., Martin, D. S., Eds.; Saunders: Philadelphia, 2011; pp 17–34.

(4) Zhu, L.; Lu, L.; Wang, S.; Wu, J.; Shi, J.; Yan, T.; Xie, C.; Li, Q.; Hu, M.; Liu, Z. Chapter 11 - Oral Absorption Basics: Pathways and Physicochemical and Biological Factors Affecting Absorption. In *Developing Solid Oral Dosage Forms Pharmaceutical Theory and Practice*, 2nd ed.; Qiu, Y., Chen, Y., Zhang, G. G. Z., Yu, L., Mantri, R. V., Second E. Eds.; Academic Press: Boston, 2017; pp 297–329.

(5) Lipinski, C. A.; Lombardo, F.; Dominy, B. W.; Feeney, P. J. Experimental and Computational Approaches to Estimate Solubility and Permeability in Drug Discovery and Development Settings. *Adv. Drug Deliv. Rev.* **1997**, *23*, 3–25.

(6) Lam, P. Y. S.; Clark, C. G.; Li, R.; Pinto, D. J. P.; Orwat, M. J.; Galemmo, R. A.; Fevig, J. M.; Teleha, C. A.; Alexander, R. S.; Smallwood, A. M.; Rossi, K. A.; Wright, M. R.; Bai, S. A.; Luettgen, J. M.; Wong, P. C.; Knabb, R. M.; Wexler, R. R. Structure-Based Design of Novel Guanidine/Benzamidine Mimics: Potent and Orally Bioavailable Factor Xa Inhibitors as Novel Anticoagulants. *J. Med. Chem.* **2003**, *46*, 4405–4418.

(7) Sun, J.; Miller, J. M.; Beig, A.; Rozen, L.; Amidon, G. L.; Dahan, A. Mechanistic Enhancement of the Intestinal Absorption of Drugs Containing the Polar Guanidino Functionality. *Expert Opin. Drug Metab. Toxicol.* **2011**, *7*, 313–323.

(8) Miller, J. M.; Dahan, A.; Gupta, D.; Varghese, S.; Amidon, G. L. Enabling the Intestinal Absorption of Highly Polar Antiviral Agents: Ion-Pair Facilitated Membrane Permeation of Zanamivir Heptyl Ester and Guanidino Oseltamivir. *Mol. Pharmaceutics.* **2010**, *7*, 1223–1234.

(9) Liu, K.-C.; Lee, P.-S.; Wang, S.-Y.; Cheng, Y.-S. E.; Fang, J.-M.; Wong, C.-H. Intramolecular Ion-Pair Prodrugs of Zanamivir and Guanidino-Oseltamivir. *Bioorg. Med. Chem.* **2011**, *19*, 4796–4802.

(10) Sun, J.; Dahan, A.; Amidon, G. L. Enhancing the Intestinal Absorption of Molecules Containing the Polar Guanidino Functionality: A Double-Targeted Prodrug Approach. *J. Med. Chem.* **2010**, *53*, 624–632.

(11) Sun, J.; Dahan, A.; Walls, Z. F.; Lai, L.; Lee, K.-D.; Amidon, G. L. Specificity of a Prodrug-Activating Enzyme hVACVase: The Leaving Group Effect. *Mol. Pharmaceutics.* **2010**, *7*, 2362–2368.

(12) Huttunen, K. M.; Mannila, A.; Laine, K.; Kemppainen, E.; Leppänen, J.; Vepsäläinen, J.; Järvinen, T.; Rautio, J. The First Bioreversible Prodrug of Metformin with Improved Lipophilicity and Enhanced Intestinal Absorption. *J. Med. Chem.* **2009**, *52*, 4142–4148.

(13) Hsu, P.-H.; Chiu, D.-C.; Wu, K.-L.; Lee, P.-S.; Jan, J.-T.; Cheng, Y.-S. E.; Tsai, K.-C.; Cheng, T.-J.; Fang, J.-M. Acylguanidine Derivatives of Zanamivir and Oseltamivir: Potential Orally Available Prodrugs Against Influenza Viruses. *Eur. J. Med. Chem.* **2018**, *154*, 314–323.

(14) Saulnier, M. G.; Frennesson, D. B.; Deshpande, M. S.; Hansel, S. B.; Vyas, D. M. An Efficient Method for the Synthesis of Guanidino Prodrugs. *Bioorg. Med. Chem. Lett.* **1994**, *4*, 1985–1990.

(15) Arafa, R. K.; Ismail, M. A.; Munde, M.; Wilson, W. D.; Wenzler, T.; Brun, R.; Boykin, D. W. Novel Linear Triaryl Guanidines, *N*-Substituted Guanidines and Potential Prodrugs as Antiprotozoal Agents. *Eur. J. Med. Chem.* **2008**, *43*, 2901–2908.

(16) Humphreys, W. G.; Obermeier, M. T.; Chong, S.; Kimball, S. D.; Das, J.; Chen, P.; Moquin, R.; Han, W.-C.; Gedamke, R.; White, R. E.; Morrison, R. A. Oxidative Activation of Acylguanidine Prodrugs: Intestinal Presystemic Activation in Rats Limits Absorption and Can Be Inhibited by Co-Administration of Ketoconazole. *Xenobiotica* **2003**, *33*, 93–106.

(17) Schade, D.; Kotthaus, J.; Riebling, L.; Kotthaus, J.; Muller-Fielitz, H.; Raasch, W.; Hoffmann, A.; Schmidtke, M.; Clement, B. Zanamivir Amidoxime- and N-Hydroxyguanidine-Based Prodrug Approaches to Tackle Poor Oral Bioavailability. *J. Pharm. Sci.* **2015**, *104*, 3208–3219.

(18) Schade, D.; Kotthaus, J.; Klein, N.; Kotthaus, J.; Clement, B. Prodrug Design for the Potent Cardiovascular Agent Nω-Hydroxy-l-Arginine (NOHA): Synthetic Approaches and Physicochemical Characterization. *Org. Biomol. Chem.* **2011**, *9*, 5249–5259.

(19) Maryanoff, B. E.; McComsey, D. F.; Costanzo, M. J.; Yabut, S. C.; Lu, T.; Player, M. R.; Giardino, E. C.; Damiano, B. P. Exploration of Potential Prodrugs of RWJ-445167, an Oxyguanidine-Based Dual Inhibitor of Thrombin and Factor Xa. *Chem. Biol. Drug Des.* **2006**, *68*, 29–36.

(20) Kotthaus, J.; Wahl, B.; Havemeyer, A.; Kotthaus, J.; Schade, D.; Garbe-Schönberg, D.;

Mendel, R.; Bittner, F.; Clement, B. Reduction of Nω-Hydroxy-L-Arginine by the Mitochondrial Amidoxime Reducing Component (mARC). *Biochem. J.* **2010**, *433*, 383–391.

(21) Clement, B.; Demesmaeker, M.; Linne, S. Microsomal Catalyzed N-Hydroxylation of Guanabenz and Reduction of the N-Hydroxylated Metabolite: Characterization of the Two Reactions and Genotoxic Potential of Guanoxabenz1. *Chem. Res. Toxicol.* **1996**, *9*, 682–688.

(22) Froehlich, A. K.; Girreser, U.; Clement, B. Metabolism of N-Hydroxyguanidines (N-Hydroxydebrisoquine) In Human and Porcine Hepatocytes: Reduction and Formation of Glucuronides. *Drug Metab. Dispos.* **2005**, *33*, 1532–1537.

(23) Clement, B.; Schultze-Mosgau, M. H.; Wohlers, H. Cytochrome P450 Dependent N-Hydroxylation of a Guanidine (Debrisoquine), Microsomal Catalysed Reduction and Further Oxidation of the N-Hydroxy-Guanidine Metabolite to the Urea Derivative. Similarity with the Oxidation of Arginine to Citrulline and Nitric Oxide. *Biochem. Pharmacol.* **1993**, *46*, 2249–2267.

(24) Sibley, C. D.; Morris, E. A.; Kharel, Y.; Brown, A. M.; Huang, T.; Bevan, D. R.; Lynch, K. R.; Santos, W. L. Discovery of a Small Side Cavity in Sphingosine Kinase 2 That Enhances Inhibitor Potency and Selectivity. *J. Med. Chem.* **2020**, *63*, 1178–1198.

(25) Huwiler, A.; Pfeilschifter, J. Sphingolipid Signaling in Renal Fibrosis. *Matrix Biol.* **2018**, *68–69*, 230–247.

(26) Schwalm, S.; Beyer, S.; Frey, H.; Haceni, R.; Grammatikos, G.; Thomas, D.; Geisslinger, G.; Schaefer, L.; Huwiler, A.; Pfeilschifter, J. Sphingosine Kinase-2 Deficiency Ameliorates Kidney Fibrosis by Up-Regulating Smad7 in a Mouse Model of Unilateral

Ureteral Obstruction. *Am. J. Pathol.* **2017**, *187*, 2413–2429.

(27) Pyne, N. J.; El Buri, A.; Adams, D. R.; Pyne, S. Sphingosine 1-Phosphate and Cancer. *Adv. Biol. Regul.* **2018**, *68*, 97–106.

(28) Yuza, K.; Nakajima, M.; Nagahashi, M.; Tsuchida, J.; Hirose, Y.; Miura, K.; Tajima, Y.; Abe, M.; Sakimura, K.; Takabe, K.; Wakai, T. Different Roles of Sphingosine Kinase 1 and 2 in Pancreatic Cancer Progression. *J. Surg. Res.* **2018**, *232*, 186–194.

(29) LeBlanc, F. R.; Pearson, J. M.; Tan, S.-F.; Cheon, H.; Xing, J. C.; Dunton, W.; Feith, D. J.; Loughran Jr, T. P. Sphingosine Kinase-2 Is Overexpressed in Large Granular Lymphocyte Leukaemia and Promotes Survival through Mcl-1. *Br. J. Haematol.* [Online early access]. DOI: 10.1111/bjh.16530. Published Online: March 2, 2020.

(30) Farez, M. F.; Correale, J. Sphingosine 1-Phosphate Signaling in Astrocytes: Implications for Progressive Multiple Sclerosis. *J. Neurol. Sci.* **2016**, *361*, 60–65.

(31) Kappos, L.; Bar-Or, A.; Cree, B. A. C.; Fox, R. J.; Giovannoni, G.; Gold, R.; Vermersch, P.; Arnold, D. L.; Arnould, S.; Scherz, T.; Wolf, C.; Wallström, E.; Dahlke, F. Siponimod versus Placebo in Secondary Progressive Multiple Sclerosis (EXPAND): A Double-Blind, Randomised, Phase 3 Study. *Lancet* **2018**, *391*, 1263–1273.

(32) Santos, W. L.; Lynch, K. R. Drugging Sphingosine Kinases. *ACS Chem. Biol.* **2015**, *10*, 225–233.

(33) Pyne, S.; Adams, D. R.; Pyne, N. J. Sphingosine 1-Phosphate and Sphingosine Kinases in Health and Disease: Recent Advances. *Prog. Lipid Res.* **2016**, *62*, 93–106.

(34) Kharel, Y.; Morris, E. A.; Congdon, M. D.; Thorpe, S. B.; Tomsig, J. L.; Santos, W. L.; Lynch, K. R. Sphingosine Kinase 2 Inhibition and Blood Sphingosine 1-Phosphate Levels. *J. Pharmacol. Exp. Ther.* **2015**, *355*, 23–31.

(35) Kharel, Y.; Raje, M.; Gao, M.; Gellett, A. M.; Tomsig, J. L.; Lynch, K. R.; Santos, W. L. Sphingosine Kinase Type 2 Inhibition Elevates Circulating Sphingosine 1-Phosphate. *Biochem. J.* **2012**, *447*, 149–157.

(36) Kharel, Y.; Huang, T.; Salamon, A.; Harris, T. E.; Santos, W. L.; Lynch, K. R. Mechanism of Sphingosine 1-Phosphate Clearance from Blood. *Biochem. J.* **2020**, *477*, 925–935.

(37) Worrell, B. L.; Brown, A. M.; Santos, W. L.; Bevan, D. R. In Silico Characterization of Structural Distinctions between Isoforms of Human and Mouse Sphingosine Kinases for Accelerating Drug Discovery. *J. Chem. Inf. Model.* **2019**, *59*, 2339-2351.

(38) Raje, M. R.; Knott, K.; Kharel, Y.; Bissel, P.; Lynch, K. R.; Santos, W. L. Design, Synthesis and Biological Activity of Sphingosine Kinase 2 Selective Inhibitors. *Bioorg. Med. Chem.* **2012**, *20*, 183–194.

(39) Mathews, T. P.; Kennedy, A. J.; Kharel, Y.; Kennedy, P. C.; Nicoara, O.; Sunkara, M.; Morris, A. J.; Wamhoff, B. R.; Lynch, K. R.; Macdonald, T. L. Discovery, Biological Evaluation, and Structure−Activity Relationship of Amidine Based Sphingosine Kinase Inhibitors. *J. Med. Chem.* **2010**, *53*, 2766–2778.

(40) Kennedy, A. J.; Mathews, T. P.; Kharel, Y.; Field, S. D.; Moyer, M. L.; East, J. E.; Houck, J. D.; Lynch, K. R.; Macdonald, T. L. Development of Amidine-Based Sphingosine Kinase 1 Nanomolar Inhibitors and Reduction of Sphingosine 1-Phosphate in Human Leukemia Cells. *J. Med. Chem.* **2011**, *54*, 3524–3548.

(41) Patwardhan, N. N.; Morris, E. A.; Kharel, Y.; Raje, M. R.; Gao, M.; Tomsig, J. L.; Lynch, K. R.; Santos, W. L. Structure-Activity Relationship Studies and In Vivo Activity of Guanidine-Based Sphingosine Kinase Inhibitors: Discovery of SphK1- and SphK2-

Selective Inhibitors. *J. Med. Chem.* **2015**, *58*, 1879–1899.

4 Experimental Section

4.1 Discovery of a Small Side Cavity in Sphingosine Kinase 2 that Enhances Inhibitor Potency and Selectivity

4.1.1 Sphingosine Kinase Biological Assays

The percent inhibition of SphK2 from synthesized compounds was performed using a previously described protocol.[1,2] Recombinant human SphK2 (10 μM) was isolated from a cell lysate and incubated with (0.3 μM) or without compound, sphingosine, and 250 μM γ-[^{32}P] ATP *via* scintillation counting. Compounds were assayed in triplicate.

The growth of recombinant yeast (*Saccharomyces cerevisiae*) cells encoding either hSphK1 or hSphK2 was performed according to our previously described protocol.[3] Briefly, yeast strain KYA1 harboring a plasmid encoding either hSphK1 or hSphK2 was selected, maintained and grown in SC-URA media with 2% glucose overnight at 30 ºC. Following overnight growth media was diluted 1:100 into SC-URA media supplemented with 2% galactose and various concentrations of test inhibitor. After another incubation period of 24 - 48 hours at 30 ºC, cellular growth was quantified by measuring absorbance at 600 nm.

In vivo mouse studies were conducted as follows. Groups of 8 to 10 week old male C57BL/6 mice were injected intraperitoneally (i.p.) with either vehicle or indicated dose of test compounds (2% solution of hydroxypropyl-β-cyclodextrin, Cargill Cavitron 82004). After 0.5, 1, 2, 4, 6, and 8 hours of injection, whole blood was collected from the retro-orbital sinus and 10 μL of blood was processed for LC/MS analysis as described previously.[4] The use of mice for these studies was approved by the University of Virginia's School of Medicine Animal Care and Use Committee prior to experimentation.

4.1.2 Molecular Docking

To visualize and rationalize differences in efficacy of **2.8**, **2.9**, **2.10**, and **2.15o** molecular docking was utilized to predict position and ligand-protein interactions of the inhibitors in the sphingosine binding pocket of SphK2. The SphK2 model, with ATP and Mg^{2+} bound, was generated with Molecular Operating Environment (MOE) and energy minimized as previously described.[5,6] In order to draw, display, and characterize chemical structures, substructures, and reactions for preparation in docking programs, Marvin 17.3.13, 2017 was used (ChemAxon; http://www.chemaxon.com) to create structure files that were cleaned in 3D . AutoDock Tools was used to prepare the protein and ligand files.[7] In order to perform the docking, AutoDock Vina was utilized to dock the inhibitors to SphK2, with 9 poses being created for each inhibitor.[8] The grid box was set to 20 X 20 X 28 $Å^3$ with grid spacing of 1.000 Å. To include all known key residues in the sphingosine binding cavity, the grid box was positioned at the approximate center of the ligand-binding cavity based on the position of sphingosine in the crystal structure (PDB ID: 3VZB).[5,9] The lowest energy docked pose for each molecule was then used to compare potential differences in ligand docking position inside the SphK2 active site.

4.1.3 General Material and Synthetic Procedures

Where indicated, reactions utilizing a microwave reactor were performed with a Discover SP microwave synthesizer (CEM Corporation). All solvents used were dried using a PureSolv solvent system and all chemical reagents were purchased from commercial sources without further purification. Aluminum-backed silica gel, 200 μm, F254 plates were utilized for all thin-layer chromatography (TLC) experiments. A Combiflash Rf purification system with flash grade silica gel, 40−63 μm was used for all column chromatography. All reported ^{1}H NMR spectra were measured at 400 MHz and the complementary ^{13}C NMR frequency was 101 MHz.

Reported ^{1}H NMR chemical shifts are in ppm with the solvent resonance as an internal standard ($CDCl_3$: 7.26 ppm; CD_3OD: 3.31 ppm; $(CD_3)_2CO$: 2.05 ppm). Reported ^{13}C NMR chemical shifts are in ppm with the solvent resonance as the internal standard ($CDCl_3$: 77.16 ppm; CD_3OD: 49.00 ppm; $(CD_3)_2CO$: 206.26 ppm). Reported ^{19}F NMR chemical shifts are referenced to trifluoroacetic acid (-76.55 ppm) as an external standard. NMR spectra for all reported intermediates and final compounds can be found online (https://pubs.acs.org/doi/10.1021/acs.jmedchem.9b01508). High-resolution mass spectrometry (HRMS) data was obtained using an Agilent 6220 Accurate-MS TOF LC-MS by electrospray ionization (ESI). All compounds tested in biological assays possess ≥95% purity, as determined by HPLC analyses. HPLC was performed using a Thermo Electron TSQ triple quadrupole mass spectrometer fitted with an ESI source.

General Procedure 2A: Suzuki-Miyaura Coupling of Aryl Bromides with Phenyl Boronic Acids. 3-bromo-4-hydroxybenzonitrile (**2.11g**) (1.0 equiv) was dissolved in DMF (0.2 M solution) and put under a nitrogen gas atmosphere. The appropriate phenyl boronic acid (3.0 equiv) was then added followed by Cs_2CO_3 (2.0 equiv). The resulting mixture was degassed for 15 min by bubbling N_2 through solution. Next, $Pd(dppf)Cl_2$ (0.03 equiv) was added and the resulting mixture was heated in a microwave reactor at 100 ºC for 60 min. Next, the solution was partitioned between EtOAc and LiBr aqueous solution. Using additional EtOAc, the aqueous LiBr solution was washed three times and the combined organic layers were dried over Na_2SO_4, filtered, and concentrated *via* vacuum. The resulting concentrate was then purified by silica gel chromatography to yield a mixture of the major product detected by TLC as well as a minor impurity. Isolated fractions were then carried forward crude without further characterization.

General Procedure 2B: Williamson Ether Synthesis of Hydroxybenzonitrile Derivatives. K_2CO_3 (4 equiv) was added to a solution of the CH_3CN (0.2 M solution) and the appropriate hydroxybenzonitrile derivative (1.0 equiv). 4-(trifluoromethyl)benzyl bromide (1.2 equiv) was then added followed by flushing the reaction container with nitrogen gas. The reaction mixture was refluxed at 80 ºC for 4 – 6 hours. Afterward, the reaction was concentrated *via* vacuum and then purified by silica gel chromatography to yield the desired product.

General Procedure 2C: Synthesis of Amide-Oxime Analogs. To a solution of ethanol (0.2 M) and the appropriate benzonitrile (1.0 equiv), hydroxylamine hydrochloride (2.0 equiv) was added followed by TEA (3.0 equiv). The reaction mixture was heated to 85 ºC for 4 hours. The resulting mixture was then concentrated *via* vacuum and then purified by silica gel chromatography to yield the desired product.

General Procedure 2D: Coupling of Amide-Oxime Analogs with Boc-L-Proline. The appropriate amide-oxime derivative (1.0 equiv) was dissolved in DMF (0.2 M solution) and put under an N_2 blanket. Boc-L-Proline (1.2 equiv) followed by Hünig's base (1.8 equiv) and HCTU (1.2 equiv) were then added and stirred vigorously at 100 ºC for 18 hours. The reaction progress was monitored by TLC. Subsequently, the resulting solution was partitioned between EtOAc and LiBr aqueous solution. Using additional EtOAc, the aqueous LiBr solution was washed three times and the combined organic layers were dried over Na_2SO_4, filtered, and concentrated *via* vacuum. The resulting concentrate was purified by silica gel chromatography.

General Procedure 2E: Boc Deprotection of Pyrrolidine Intermediates With TFA, Guanylation of Deprotected Amines and Subsequent Boc Deprotection of Guanyl Groups with HCl (g). To a solution of dichloromethane (0.2 M) and the appropriate Boc protected pyrrolidine (1.0 equiv), 1.0 M TFA (10 equiv) was added and allowed to stir at room temperature for 3 – 12

hours. The reaction progress was monitored by TLC. Next, the dichloromethane was removed *via* vacuum and replaced with diethyl ether to promote TFA salt precipitation. Once the desired product was precipitated, the diethyl ether was removed *via* vacuum and the resulting Boc deprotected product was carried forward crude. Thereafter, the resulting Boc deprotected product was dissolved in CH_3CN (0.2 M) and put under an N_2 atmosphere. To the reaction mixture, Hünig's base (10 equiv) followed by N,N'-*di*-Boc-1H-pyrazole-1-carboxamidine (1.2 equiv) were added and the reaction mixture was heated to 50 ºC inside a microwave reactor for 3 hours. The reaction mixture was then concentrated *via* vacuum, and the resulting concentrate was then purified by silica gel chromatography to afford bis-Boc-protected intermediates. Following silica gel chromatography, bis-Boc-protected intermediates were then dissolved in methanol (0.2 M) and bubbled with HCl gas for 2 – 5 minutes to yield the desired Boc deprotected moiety. Lastly, the organic mixture was concentrated *via* vacuum and triturated with diethyl ether to afford the corresponding analogue as an HCl salt.

4.1.4 Characterization

(S)-2-(3-(3-(trifluoromethyl)-4-((4-(trifluoromethyl)benzyl)oxy)phenyl)-1,2,4-oxadiazol-5-yl)pyrrolidine-1-carboximidamide (**2.10**). Synthesized by General Procedure 2E: 58 mg, 59%, white solid. ^{1}H NMR (400 MHz, CD_3OD) δ 8.28 – 8.26 (m, 2H), 7.70 (q, J = 8.3 Hz, 4H), 7.44 (d, J = 9.2 Hz, 1H), 5.45 (dd, J = 8.0, 1.8 Hz, 1H), 5.42 (s, 2H), 3.78 (t, J = 9.4 Hz, 1H), 3.62 (q, J = 9.6 Hz, 1H), 2.61 – 2.44 (m, 2H), 2.28 – 2.19 (m, 1H), 2.13 – 2.02 (m, 1H); ^{13}C NMR (101 MHz, CD_3OD) δ 179.28, 168.45, 159.92, 157.11, 141.91, 134.01, 131.26 (q, $^2J_{CF}$ = 32.5 Hz), 128.54, 127.25 (q, $^3J_{CF}$ = 5.0 Hz), 126.53 (q, $^3J_{CF}$ = 3.6 Hz), 125.53 (q, $^1J_{CF}$ = 272.9 Hz), 124.63 (q, $^1J_{CF}$ = 271.9 Hz), 120.61 (q, $^2J_{CF}$ = 30.4 Hz), 120.24, 115.48, 70.89, 56.48, 32.72, 24.32; ^{19}F

NMR (376 MHz, CD_3OD) δ -63.61 (s, 3F), -63.63 (s, 3F); HRMS (ESI+): calcd for $C_{22}H_{20}F_6N_5O_2$ $[M]^+$ 500.1521; found, 500.1518.

6-((4-(trifluoromethyl)benzyl)oxy)-[1,1'-biphenyl]-3-carbonitrile (**2.12a**). Synthesized by General Procedure 2B: 165 mg, 91%, white solid. ^{1}H NMR (400 MHz, $(CD_3)_2CO$) δ 7.75-7.67 (m, 4H), 7.61 (d, J = 7.7 Hz, 4H), 7.45 (t, J = 7.3 Hz, 2H), 7.41 – 7.32 (m, 2H), 5.36 (s, 2H); ^{13}C NMR (101 MHz, $(CD_3)_2CO$) 159.46, 141.93 (d, $^4J_{CF_3}$ = 1.3 Hz), 137.23, 135.08, 134.09, 132.98, 130.34, 130.23 (q, $^2J_{CF_3}$ = 32.3 Hz), 129.01, 128.66, 128.37, 126.15 (q, $^3J_{CF_3}$ = 3.7 Hz), 125.16 (q, $^1J_{CF_3}$ = 271.1 Hz), 119.42, 114.47, 105.58, 70.28; HRMS (ESI+): calcd for $C_{21}H_{15}F_3NO$ $[M+H]^+$ 354.1100; found, 354.1104.

4'-fluoro-6-((4-(trifluoromethyl)benzyl)oxy)-[1,1'-biphenyl]-3-carbonitrile (**2.12b**). Synthesized by General Procedure 2B: 151 mg, 87%, white solid. ^{1}H NMR (400 MHz, $(CD_3)_2CO$) δ 7.81-7.62 (m, 8H), 7.40 (d, J = 8.4 Hz, 1H), 7.23 (t, J = 8.7 Hz, 2H), 5.43 (s, 2H); ^{13}C NMR (101 MHz, $(CD_3)_2CO$) 163.37 (d, $^1J_{CF}$ = 245.8 Hz), 159.52, 142.03 (d, $^4J_{CF_3}$ = 1.2 Hz), 135.12, 134.30, 133.51 (d, $^4J_{CF}$ = 3.4 Hz), 132.45 (d, $^3J_{CF}$ = 8.3 Hz), 131.97, 130.29 (q, $^2J_{CF_3}$ = 32.0 Hz), 128.51, 126.27 (q, $^3J_{CF_3}$ = 3.8 Hz), 125.17 (q, $^1J_{CF_3}$ = 271.0 Hz), 119.34, 115.84 (d, $^2J_{CF}$ = 21.5 Hz), 114.61, 105.63, 70.41; HRMS (ESI+): calcd for $C_{21}H_{17}F_4N_2O$ $[M+NH_4]^+$ 389.1272; found, 389.1269.

3-(pyridin-4-yl)-4-((4-(trifluoromethyl)benzyl)oxy)benzonitrile (**2.12c**). Synthesized by General Procedure 2B: 87 mg, 48%, yellow solid. ^{1}H NMR (400 MHz, $CDCl_3$) δ 8.68 (s, 2H), 7.72-7.57 (m, 4H), 7.48-7.36 (m, 4H), 7.10 (d, J = 8.4 Hz, 1H), 5.24 (s, 2H); ^{13}C NMR (101 MHz $CDCl_3$) 158.43, 149.97, 143.95, 139.38 (d, $^4J_{CF_3}$ = 1.2 Hz), 134.51, 134.47, 130.65 (q, $^2J_{CF_3}$ = 32.6 Hz), 129.68, 127.02, 125.86 (q, $^3J_{CF_3}$ = 3.7 Hz), 124.15, 123.97 (q, $^1J_{CF_3}$ = 271.1 Hz), 118.52, 113.36, 105.50, 69.98; HRMS (ESI+): calcd for $C_{20}H_{14}F_3N_2O$ $[M+H]^+$ 355.1053; found, 355.1083.

4'-(trifluoromethyl)-6-((4-(trifluoromethyl)benzyl)oxy)-[1,1'-biphenyl]-3-carbonitrile (**2.12d**). Synthesized by General Procedure 2B: 361 mg, 78%, white solid. ^{1}H NMR (400 MHz, $CDCl_3$) δ 7.74-7.59 (m, 8H), 7.41 (d, J = 8.0 Hz, 2H), 7.11 (d, J = 8.6 Hz, 1H), 5.25 (s, 2H); ^{13}C NMR (101 MHz $CDCl_3$) 158.46, 139.84 (q, $^{4}J_{CF_3}$ = 1.3 Hz), 139.62 (q, $^{4}J_{CF_3}$ = 1.3 Hz), 134.72, 133.99, 131.11, 130.55 (q, $^{2}J_{CF_3}$ = 32.7 Hz), 130.20 (q, $^{2}J_{CF_3}$ = 32.6 Hz), 129.88, 127.00, 125.82 (q, $^{3}J_{CF_3}$ = 3.7 Hz), 125.34 (q, $^{3}J_{CF_3}$ = 3.8 Hz), 124.20 (q, $^{1}J_{CF_3}$ = 272.0 Hz), 124.13 (q, $^{1}J_{CF_3}$ = 272.0 Hz), 118.73, 113.36, 105.35, 69.93; HRMS (ESI-): calcd for $C_{22}H_{12}F_6NO$ $[M - H]^-$ 420.0829; found, 420.0807.

3-cyclopropyl-4-((4-(trifluoromethyl)benzyl)oxy)benzonitrile (**2.12e**). Synthesized by General Procedure 2B: 83 mg, 49%, off-white solid. ^{1}H NMR (400 MHz, $CDCl_3$) δ 7.63 (dd, J = 38.7, 8.0 Hz, 4H), 7.43 (d, J = 8.5 Hz, 1H), 7.15 (s, 1H), 6.90 (d, J = 8.5 Hz, 1H), 5.23 (s, 2H), 2.25-2.15 (m, 1H), 1.01 (q, J = 5.7 Hz, 2H), 0.69 (q, J = 5.4 Hz, 2H); ^{13}C NMR (101 MHz $CDCl_3$) 160.45, 140.31 (d, $^{4}J_{CF_3}$ = 1.3 Hz), 134.29, 131.30, 130.50 (d, $^{2}J_{CF_3}$ = 33.0 Hz), 129.39, 127.27, 125.80 (q, $^{3}J_{CF_3}$ = 3.8 Hz), 124.12 (q, $^{1}J_{CF_3}$ = 271.5 Hz), 119.45, 111.64, 104.56, 69.49, 9.69, 8.01; HRMS (ESI+): calcd for $C_{18}H_{15}F_3NO$ $[M+H]^+$ 318.1100; found, 318.1091.

4-((4-(trifluoromethyl)benzyl)oxy)benzonitrile (**2.12f**). Synthesized by General Procedure 2B: 270 mg, 97%, white solid. ^{1}H NMR (400 MHz, $CDCl_3$) δ 7.65 (d, J = 8.0 Hz, 2H), 7.56 (dd, J = 8.8, 12.2 Hz, 4H), 7.02 (d, J = 8.8 Hz, 2H), 5.18 (s, 2H); ^{13}C NMR (101 MHz $CDCl_3$) 161.59, 139.87 (d, $^{4}J_{CF_3}$ = 1.4 Hz), 134.10, 130.47 (q, $^{2}J_{CF_3}$ = 32.8 Hz), 127.48, 125.70 (q, $^{3}J_{CF_3}$ = 3.8 Hz), 124.01 (d, $^{1}J_{CF_3}$ = 272.3 Hz), 119.08, 115.58, 104.62, 69.32; HRMS (ESI+): calcd for $C_{15}H_{10}F_3NO$ $[M+H]^+$ 278.0787; found, 278.0769.

3-bromo-4-((4-(trifluoromethyl)benzyl)oxy)benzonitrile (**2.12g**). Synthesized by General Procedure 2B: 372 mg, 98%, off-white solid. ^{1}H NMR (400 MHz, $CDCl_3$) δ 7.87 (d, J = 2.0 Hz, 1H), 7.72–7.55 (m, 5H), 6.96 (d, J = 8.6 Hz, 1H), 5.27 (s, 2H); ^{13}C NMR (101 MHz $CDCl_3$) 158.25, 139.28 (d, $^{4}J_{CF_3}$ = 1.4 Hz), 137.07, 133.21, 130.77 (q, $^{2}J_{CF_3}$ = 32.6 Hz), 127.16, 125.93 (q, $^{3}J_{CF_3}$ = 3.9 Hz), 124.08 (q, $^{1}J_{CF_3}$ = 271.2 Hz), 117.68, 113.32, 113.10, 106.09, 70.24; HRMS (ESI+): calcd for $C_{15}H_{13}BrF_3N_2O$ $[M+NH_4]^+$ 373.0158; found, 373.0162.

3,5-dimethyl-4-((4-(trifluoromethyl)benzyl)oxy)benzonitrile (**2.12h**). Synthesized by General Procedure 2B: 209 mg, 92%, off-white solid. ^{1}H NMR (400 MHz, $CDCl_3$) δ 7.63 (dd, J = 8.1, 39.0 Hz, 4H), 7.36 (s, 2H), 4.91 (s, 2H); ^{13}C NMR (101 MHz $CDCl_3$) 159.40, 140.84 (d, $^{4}J_{CF_3}$ = 1.2 Hz), 133. 05, 132.81, 130.56 (q, $^{2}J_{CF_3}$ = 32.6 Hz), 127.64, 125.73 (q, $^{3}J_{CF_3}$ = 3.8 Hz), 124.15 (q, $^{1}J_{CF_3}$ = 272.3 Hz), 119.01, 108.05, 73.26, 16.45; HRMS (ESI+): calcd for $C_{17}H_{14}F_3NNaO$ $[M+Na]^+$ 328.0920; found, 328.0944.

3-chloro-4-((4-(trifluoromethyl)benzyl)oxy)benzonitrile (**2.12i**). Synthesized by General Procedure 2B: 197 mg, 99%, off-white solid. ^{1}H NMR (400 MHz, $CDCl_3$) δ 7.69-7.54 (m, 5H), 7.50 (dd, J = 2.0, 8.6 Hz, 1H), 7.01 (d, J = 8.7 Hz, 1H), 5.25 (s, 2H); ^{13}C NMR (101 MHz $CDCl_3$) 157.32, 139.28 (d, $^{4}J_{CF_3}$ = 1.2 Hz), 133.76, 132.41, 130.50 (q, $^{2}J_{CF_3}$ = 32.6 Hz), 127.14, 125.73 (q, $^{3}J_{CF_3}$ = 3.8 Hz), 124.13, 124.00 (q, $^{1}J_{CF_3}$ = 272.8 Hz), 117.76, 113.56, 105.34, 70.01; HRMS (ESI-): calcd for $C_{15}H_8ClF_3NO$ $[M - H]^-$ 310.0252; found, 310.0232.

3-fluoro-4-((4-(trifluoromethyl)benzyl)oxy)benzonitrile (**2.12j**). Synthesized by General Procedure 2B: 236 mg, 99%, off-white solid. ^{1}H NMR (400 MHz, $CDCl_3$) δ 7.60 (dd, J = 8.1, 38.4 Hz, 4H), 7.38 (t, J = 7.7 Hz, 2H), 7.05 (t, 8.70 Hz, 1H), 5.25 (s, 2H); ^{13}C NMR (101 MHz $CDCl_3$) 151.98 (d, $^{1}J_{CF}$ = 250.8 Hz), 150.54 (d, $^{2}J_{CF}$ = 10.3 Hz), 139.29, 130.67 (q, $^{2}J_{CF_3}$ = 32.6 Hz),

129.67 (d, $^4J_{CF}$ = 4.0 Hz), 127.47, 125.79 (q, $^3J_{CF_3}$ = 3.8 Hz), 123.91 (q, $^1J_{CF_3}$ = 272.5 Hz), 119.93 (d, $^2J_{CF}$ = 21.2 Hz), 117.88 (d, $^3J_{CF}$ = 2.5 Hz), 115.23 (d, $^3J_{CF}$ = 2.2 Hz), 104.77 (d, $^4J_{CF}$ = 8.2 Hz), 70.30; HRMS (ESI+): calcd for $C_{15}H_{10}F_4NO$ $[M + H]^+$ 296.0693; found, 296.0687.

3-methoxy-4-((4-(trifluoromethyl)benzyl)oxy)benzonitrile (**2.12k**). Synthesized by General Procedure 2B: 229 mg, 99%, off-white solid. ^{1}H NMR (400 MHz, $CDCl_3$) δ 7.58 (dd, *J* = 8.3, 36.7 Hz, 4H), 7.20 (dd, *J* = 1.9, 8.4 Hz, 1H), 7.10 (d, *J* = 1.8 Hz, 1H), 6.88 (d, *J* = 8.4 Hz, 1H), 5.22 (s, 2H), 3.89 (s, 3H); ^{13}C NMR (101 MHz $CDCl_3$) 151.60, 149.74, 139.98 (d, $^4J_{CF_3}$ = 1.4 Hz), 130.41 (q, $^2J_{CF_3}$ = 32.1 Hz), 127.33, 126.22, 125.72 (q, $^3J_{CF_3}$ = 3.8 Hz), 124.05 (q, $^1J_{CF_3}$ = 272.2 Hz), 119.10, 114.49, 113.32, 104.70, 70.00, 56.19; HRMS (ESI+): calcd for $C_{16}H_{13}F_3NO_2$ $[M + H]^+$ 308.0893; found, 308.0897.

2-chloro-4-((4-(trifluoromethyl)benzyl)oxy)benzonitrile (**2.12l**). Synthesized by General Procedure 2B: 221 mg, 99%, off-white solid. ^{1}H NMR (400 MHz, $CDCl_3$) δ 7.60 (dd, *J* = 7.9, 42.7 Hz, 5H), 7.09 (s, 1H), 6.95 (d, , *J* = 8.3 Hz, 1H), 5.18 (s, 2H); ^{13}C NMR (101 MHz $CDCl_3$) 162.10, 139.28 (d, $^4J_{CF_3}$ = 1.3 Hz), 138.28, 135.15, 130.58 (q, $^2J_{CF_3}$ = 32.6 Hz), 127.55, 125.73 (q, $^3J_{CF_3}$ = 3.8 Hz), 124.03 (q, $^1J_{CF_3}$ = 272.3 Hz), 116.52, 116.28, 114.10, 105.55, 69.74; HRMS (ESI+): calcd for $C_{15}H_{10}ClF_3NO$ $[M + H]^+$ 312.0398; found, 312.0386.

2-(trifluoromethyl)-4-((4-(trifluoromethyl)benzyl)oxy)benzonitrile (**2.12m**). Synthesized by General Procedure 2B: 270 mg, 98%, white solid. ^{1}H NMR (400 MHz, $CDCl_3$) δ 7.75 (d, *J* = 8.7 Hz, 1H), 7.62 (dd, *J* = 8.1, 36.6 Hz, 4H), 7.39 (d, *J* = 2.4 Hz, 1H), 7.22 (dd, *J* = 2.4, 8.6 Hz, 1H), 5.26 (s, 2H); ^{13}C NMR (101 MHz $CDCl_3$) 161.51, 139.14 (q, $^4J_{CF_3}$ = 1.4 Hz), 136.77, 134.67 (q, $^2J_{CF_3}$ = 32.1 Hz), 130.72 (q, $^2J_{CF_3}$ = 32.1 Hz), 127.67, 125.80 (q, $^3J_{CF_3}$ = 3.5 Hz), 124.07 (q, $^1J_{CF_3}$ = 271.7 Hz), 122.19 (q, $^1J_{CF_3}$ = 272.9 Hz), 117.51, 115.82, 114.46 (q, $^3J_{CF_3}$ = 4.9 Hz), 101.82

(q, $^{3}J_{CF_3}$ = 2.0 Hz), 69.92; HRMS (ESI+): calcd for $C_{16}H_{10}F_6NO$ [M + H]$^+$ 346.0661; found, 346.0670.

3-nitro-4-((4-(trifluoromethyl)benzyl)oxy)benzonitrile (**2.12n**). Synthesized by General Procedure 2B: 270 mg, 98%, white solid. ^{1}H NMR (400 MHz, $CDCl_3$) δ 8.19 (s, 1H), 7.81 (d, *J* = 8.4 Hz, 1H), 7.63 (dd, *J* = 7.8, 44.1 Hz, 4H), 7.21 (d, *J* = 8.8 Hz, 1H), 5.36 (s, 2H); ^{13}C NMR (101 MHz $CDCl_3$) 154.62, 138.24, 137.75, 131.95, 130.03, 127.19, 126.11 (q, $^{3}J_{CF_3}$ = 3.6 Hz), 125.15 (q, $^{1}J_{CF_3}$ = 272.2 Hz), 116.72, 115.64, 110.15, 105.17, 70.85; HRMS (ESI+): calcd for $C_{15}H_{13}F_3N_3O_3$ [M + NH_4]$^+$ 340.0904; found, 312.0916.

3-(tert-butyl)-4-((4-(trifluoromethyl)benzyl)oxy)benzonitrile (**2.12o**). Synthesized by General Procedure 2B: 277 mg, 97%, white solid. ^{1}H NMR (400 MHz, $CDCl_3$) δ 7.71 - 7.56 (m, 5H), 7.47 (dd, *J* = 2.1, 8.5 Hz, 1H), 6.96 (d, *J* = 8.5 Hz, 1H), 5.25 (s, 2H), 1.40 (s, 9H); ^{13}C NMR (101 MHz $CDCl_3$) 160.47, 140.06 (q, $^{4}J_{CF_3}$ = 1.2 Hz), 139.74, 131.95, 131.01, 130.40 (q, $^{2}J_{CF_3}$ = 32.3 Hz), 127.55, 125.77 (q, $^{3}J_{CF_3}$ = 3.8 Hz), 124.07 (q, $^{1}J_{CF_3}$ = 272.3 Hz), 119.68, 112.71, 104.22, 69.68, 35.15, 29.39; HRMS (ESI+): calcd for $C_{19}H_{19}F_3NO$ [M + H]$^+$ 334.1413; found, 334.1412.

3-allyl-4-((4-(trifluoromethyl)benzyl)oxy)benzonitrile (**2.12p**). Synthesized by General Procedure 2B: 277 mg, 97%, white solid. ^{1}H NMR (400 MHz, $CDCl_3$) δ 7.61 (dd, *J* = 8.2, 35.4 Hz, 4H), 7.48 - 7.41 (m, 2H), 6.95 (d, *J* = 8.8 Hz, 1H), 6.03 - 5.91 (m, 1H), 5.20 (s, 2H), 5.16 – 5.06 (m, 2H), 3.45 (d, *J* = 6.3 Hz, 2H); ^{13}C NMR (101 MHz $CDCl_3$) 159.21, 140.10 (q, $^{4}J_{CF_3}$ = 1.2 Hz), 134.99, 133.35, 132.20, 130.38, 130.14 (q, $^{2}J_{CF_3}$ = 32.4 Hz), 127.16, 125.52 (q, $^{3}J_{CF_3}$ = 3.8 Hz), 124.02 (q, $^{1}J_{CF_3}$ = 272.0 Hz), 119.16, 116.83, 111.71, 104.20, 69.17, 33.82; HRMS (ESI+): calcd for $C_{18}H_{15}F_3NO$ [M + H]$^+$ 318.1100; found, 318.1121.

3-propyl-4-((4-(trifluoromethyl)benzyl)oxy)benzonitrile (**2.12q**). Synthesized by General Procedure 2B: 525mg, 78%, white solid. ^{1}H NMR (400 MHz, $CDCl_3$) δ 7.61 (dd, *J* = 8.1, 43.9 Hz, 4H), 7.48 – 7.39 (m, 2H), 6.92 (d, *J* = 8.4 Hz, 1H), 5.20 (s, 2H), 2.67 (t, *J* = 7.4 Hz, 2H), 1.70 – 1.60 (m, 2H), 0.96 (t, *J* = 7.3 Hz, 2H); ^{13}C NMR (101 MHz $CDCl_3$) 159.49, 140.30 (d, $^4J_{CF_3}$ = 1.3 Hz), 133.48, 132.77, 131.84, 130.23 (q, $^2J_{CF_3}$ = 32.5 Hz), 127. 08, 125.64 (q, $^3J_{CF_3}$ = 3.7 Hz), 124.1 (q, $^1J_{CF_3}$ = 272.0 Hz), 119.40, 111.68, 104.10, 69.13, 31.92, 22.45, 13.84; HRMS (ESI+): calcd for $C_{18}H_{17}F_3NO$ $[M + H]^+$ 320.1257; found, 320.1259.

3-(trifluoromethyl)-4-((4-(trifluoromethyl)benzyl)oxy)benzonitrile (**2.12r**). Synthesized by General Procedure 2B: 200 mg, 98%, white solid. ^{1}H NMR (400 MHz, $CDCl_3$) δ 7.90 (d, *J* = 1.8 Hz, 1H), 7.79 (dd, *J* = 8.7, 2.1 Hz, 1H), 7.67 (d, *J*=8.4 Hz, 2H), 7.55 (d, *J*=8.7 Hz, 2H), 7.12 (d, *J*=8.7 Hz, 1H), 5.32 (s, 2H); ^{13}C NMR (101 MHz, $CDCl_3$) δ 159.23, 138.96, 137.72, 131.70 ($^3J_{CF}$ = 5.3 Hz), 130.80 ($^2J_{CF}$ = 30.2 Hz), 127.05, 125.95 ($^3J_{CF}$ = 3.8 Hz), 123.90 ($^1J_{CF}$ = 274.7 Hz), 122.26 ($^1J_{CF}$ = 274.3 Hz), 120.66 (q,$^2J_{CF}$ = 33.4 Hz), 117.72, 113.91, 104.80, 70.07; HRMS (ESI+): calcd for $C_{16}H_{10}F_6NO$ $[M + H]^+$ 346.0661; found, 346.0666.

N'-hydroxy-6-((4-(trifluoromethyl)benzyl)oxy)-[1,1'-biphenyl]-3-carboximidamide (**2.13a**). Synthesized by General Procedure 2C: 56 mg, 51%, white solid. ^{1}H NMR (400 MHz, $(CD_3)_2CO$) δ 7.75 – 7.59 (m, 8H), 7.43 (t, *J* = 7.4 Hz, 2H), 7.34 (t, *J* = 7.2 Hz, 1H), 7.18 (d, *J* = 8.5, 1H), 5.55 (s, 2H), 5.29 (s, 2H); ^{13}C NMR (101 MHz $(CD_3)_2CO$) 156.83, 151.90, 142.91 (d, $^4J_{CF_3}$ = 1.3 Hz), 139.14, 131.56, 130.42, 129.98 (d, $^2J_{CF_3}$ = 32.0 Hz), 128.98, 128.82, 128.33, 127.93, 127.74, 126.91, 126.07 (q, $^3J_{CF_3}$ = 3.9 Hz), 125.25 (d, $^1J_{CF_3}$ = 271.7 Hz), 113.65, 70.11; HRMS (ESI+): calcd for $C_{21}H_{18}F_3N_2O_2$ $[M+H]^+$ 387.1315; found, 387.1321.

4'-fluoro-N'-hydroxy-6-((4-(trifluoromethyl)benzyl)oxy)-[1,1'-biphenyl]-3-carboximidamide (**2.13b**). Synthesized by General Procedure 2C: 70 mg, 64%, white solid. ^{1}H NMR (400 MHz,

CD_3OD) δ 7.91 – 7.80 (m, 1H), 7.66 – 7.41 (m, 7H), 7.18 – 7.03 (m, 3H), 5.15 (d, J = 18.6, 2H); ^{13}C NMR (101 MHz CD_3OD) 171.72, 163.52 (d, $^1J_{CF}$ = 245.2 Hz), 159.33, 157.62, 155.13, 142.80 (d, $^4J_{CF_3}$ = 1.3 Hz), 135.38 (d, $^4J_{CF}$ = 3.4 Hz), 132.50 (d, $^3J_{CF}$ = 8.1 Hz), 131.52, 129.93, 128.38, 127.88, 126.31 (q, $^3J_{CF_3}$ = 3.9 Hz), 125.60 (q, $^1J_{CF_3}$ = 271.0 Hz), 115.78 (d, $^2J_{CF}$ = 21.8 Hz), 114.03, 70.54; HRMS (ESI+): calcd for $C_{21}H_{17}F_4N_2O_2$ $[M+H]^+$ 405.1221; found, 405.1206.

N'-hydroxy-3-(pyridin-4-yl)-4-((4-(trifluoromethyl)benzyl)oxy)benzimidamide (**2.13c**). Synthesized by General Procedure 2C: 75 mg, 79%, white solid. ^1H NMR (400 MHz, $(CD_3)_2CO$) δ 8.95 (br s, 1H), 8.62 (d, J = 5.4 Hz, 2H), 7.82 – 7.60 (m, 8H), 7.25 (d, J = 8.3 Hz, 1H), 5.56 (s, 2H), 5.35 (s, 2H); ^{13}C NMR (101 MHz $(CD_3)_2CO$) 156.86, 151.51, 150.44, 146.57, 142.63 (d, $^4J_{CF_3}$ = 1.4 Hz), 130.15 (d, $^2J_{CF_3}$ = 32.1 Hz), 128.67, 128.62, 128.49, 128.22, 128.03, 126.21 (q, $^3J_{CF_3}$ = 3.8 Hz), 125.2 (d, $^1J_{CF_3}$ = 271.5 Hz), 125.10, 113.77, 70.26; HRMS (ESI+): calcd for $C_{20}H_{16}F_3N_3O_2$ $[M]^+$ 387.1195; found, 387.1225.

N'-hydroxy-4'-(trifluoromethyl)-6-((4-(trifluoromethyl)benzyl)oxy)-[1,1'-biphenyl]-3-carboximidamide (**2.13d**). Synthesized by General Procedure 2C: 290 mg, 74%, white solid. ^1H NMR (400 MHz, CD_3OD) δ 7.95 – 7.59 (m, 8H), 7.50 (t, J = 7.3 Hz, 2H), 7.26 – 7.17 (m, 1H), 5.26 (d, J = 18.4 Hz, 2H); ^{13}C NMR (101 MHz CD_3OD) 159.40, 157.69, 155.01, 143.41 (d, $^4J_{CF_3}$ = 1.4 Hz), 142.75 (d, $^4J_{CF_3}$ = 1.4 Hz), 131.30, 130.91 (q, $^2J_{CF_3}$ = 32.2 Hz), 130.87, 130.22 (q, $^2J_{CF_3}$ = 32.4 Hz), 129.93, 128.55, 127.53, 126.36 (q, $^3J_{CF_3}$ = 3.8 Hz), 125.87 (q, $^3J_{CF_3}$ = 3.8 Hz), 125.83 (d, $^1J_{CF_3}$ = 271.3 Hz), 125.63 (d, $^1J_{CF_3}$ = 271.1 Hz), 114.28, 70.77; HRMS (ESI+): calcd for $C_{22}H_{17}F_6N_2O_2$ $[M+H]^+$ 455.1189; found, 455.1184.

3-cyclopropyl-N'-hydroxy-4-((4-(trifluoromethyl)benzyl)oxy)benzimidamide (**2.13e**). Synthesized by General Procedure 2C: 73 mg, 80%, white solid. ^1H NMR (400 MHz, $CDCl_3$) δ 7.62 (dd, J =

8.0, 30.6 Hz, 4H), 7.37 (d, J = 8.4 Hz, 1H), 7.17 (s, 1H), 6.86 (d, J = 8.4 Hz, 1H), 5.20 (s, 2H), 4.83 (s, 2H), 2.26 – 2.19 (m, 1H), 0.96 (q, J = 5.3 Hz, 2H), 0.72 (q, J = 5.1 Hz, 2H); ^{13}C NMR (101 MHz $CDCl_3$) 158.61, 141.23 (d, $^4J_{CF_3}$ = 1.3 Hz), 133.06, 130.23 (d, $^2J_{CF_3}$ = 32.5 Hz), 127.25, 125.70 (q, $^3J_{CF_3}$ = 3.8 Hz), 125.57, 125.47, 124.17, 123.28, 111.50, 69.47, 29.85, 9.85, 7.94; HRMS (ESI+): calcd for $C_{18}H_{18}F_3N_2O_2$ [M + H]$^+$ 351.1315; found, 351.1309.

N'-hydroxy-4-((4-(trifluoromethyl)benzyl)oxy)benzimidamide (**2.13f**). Synthesized by General Procedure 2C: 73 mg, 80%, white solid. ^{1}H NMR (400 MHz, $CDCl_3$) δ 7.83 – 7.53 (m, 6H), 6.99 (t, J = 11.3 Hz, 2H), 5.90 (br s, 1H), 5.15 (s, 2H) 4.84 (s, 2H); ^{13}C NMR (101 MHz $CDCl_3$) 168.89, 161.44, 159.85, 152.56, 140.79, 129.54, 127.50, 125.73, 115.02, 114.79, 69.29; HRMS (ESI+): calcd for $C_{15}H_{14}F_3N_2O_2$ [M + H]$^+$ 311.1002; found, 311.1006.

3-bromo-N'-hydroxy-4-((4-(trifluoromethyl)benzyl)oxy)benzimidamide (**2.13g**). Synthesized by General Procedure 2C: 250 mg, 62%, white solid. ^{1}H NMR (400 MHz, $CDCl_3$) δ 8.07 – 7.86 (m, 1H), 7.77 – 7.51 (m, 5H), 6.97 – 6.89 (m, 1H), 5.85 (br s, 1H), 5.25 (d, J = 13.3 Hz, 2H), 4.81 (s, 2H); ^{13}C NMR (101 MHz $CDCl_3$) 156.04, 151.52, 140.21, 139.89, 133.07, 131.24, 128.41, 127.15, 126.26, 125.82, 113.34, 112.86, 70.10; HRMS (ESI+): calcd for $C_{15}H_{13}BrF_3N_2O_2$ [M + H]$^+$ 389.0107; found, 389.0112.

N'-hydroxy-3,5-dimethyl-4-((4-(trifluoromethyl)benzyl)oxy)benzimidamide (**2.13h**). Synthesized by General Procedure 2C: 201 mg, 88%, white solid. ^{1}H NMR (400 MHz, CD_3OD) δ 7.71 – 7.63 (m, 4H), 7.59 (s, 1H), 7.34 (s, 1H), 4.92 (d, J = 11.4 Hz, 2H), 2.28 (d, J = 9.0 Hz, 6H); ^{13}C NMR (101 MHz CD_3OD) 172.09, 158.08, 143.41, 132.25, 131.03 (d, $^2J_{CF_3}$ = 32.4 Hz), 129.67, 129.10, 127.95, 126.36,_125.63 (d, $^1J_{CF_3}$ = 272.6 Hz), 74.02, 16.62; HRMS (ESI+): calcd for $C_{17}H_{18}F_3N_2O_2$ [M + H]$^+$ 339.1315; found, 339.1314.

3-chloro-N'-hydroxy-4-((4-(trifluoromethyl)benzyl)oxy)benzimidamide (**2.13i**). Synthesized by General Procedure 2C: 193 mg, 89%, white solid. ^{1}H NMR (400 MHz, CD_3OD) δ 7.98 – 7.62 (m, 5H), 7.52 (d, J = 8.3 Hz, 1H), 7.18 – 7.07 (m, 1H), 5.27 (d, J = 15.7 Hz, 2H); ^{13}C NMR (101 MHz CD_3OD) 170.45, 157.90, 156.16, 154.02, 142.43, 130.90, 129.13, 128.54, 126.96, 126.42, 123.96, 114.66, 70.77; HRMS (ESI+): calcd for $C_{15}H_{13}ClF_3N_2O_2$ $[M + H]^+$ 345.0612; found, 345.0610.

3-fluoro-N'-hydroxy-4-((4-(trifluoromethyl)benzyl)oxy)benzimidamide (**2.13j**). Synthesized by General Procedure 2C: 243 mg, 93%, white solid. ^{1}H NMR (400 MHz, CD_3OD) δ 7.65 (q, J = 7.6 Hz, 4H), 7.40 (q, J = 12.1 Hz, 2H), 7.22 – 7.10 (m, 1H), 5.24 (s, 1H); ^{13}C NMR (101 MHz CD_3OD) 154.13 (d, $^{4}J_{CF}$ = 2.3 Hz), 153.47 (d, $^{1}J_{CF}$ = 245.1 Hz), 148.83 (d, $^{2}J_{CF}$ = 11.0 Hz), 142.47 (q, $^{4}J_{CF_3}$ = 1.3 Hz), 131.10 (q, $^{2}J_{CF_3}$ = 32.8 Hz), 128.80, 127.89 (d, $^{3}J_{CF}$ = 6.9 Hz), 126.43 (q, $^{3}J_{CF_3}$ = 3.8 Hz), 125.45 (q, $^{1}J_{CF_3}$ = 271.1 Hz), 123.43 (d, $^{4}J_{CF}$ = 3.5 Hz), 116.18 (d, $^{3}J_{CF}$ = 2.0 Hz), 115.14 (d, $^{2}J_{CF}$ = 20.3 Hz), 71.10; HRMS (ESI+): calcd for $C_{15}H_{13}F_4N_2O_2$ $[M + H]^+$ 329.0908; found, 329.0890.

N'-hydroxy-3-methoxy-4-((4-(trifluoromethyl)benzyl)oxy)benzimidamide (**2.13k**). Synthesized by General Procedure 2C: 243 mg, 93%, white solid. ^{1}H NMR (400 MHz, CD_3OD) δ 7.64 (q, 4.6 Hz, 4H), 7.27 (s, 1H), 7.17 (d, J = 8.4 Hz, 1H), 6.98 (d, J = 8.3 Hz, 1H), 5.19 (s, 2H), 3.88 (s, 3H); ^{13}C NMR (101 MHz CD_3OD) 155.36, 150.89, 150.50, 143.11, 130.92 (d, $^{2}J_{CF_3}$ = 32.6 Hz), 128.85, 127.69, 126.33 (d, $^{3}J_{CF_3}$ = 3.4 Hz), 122.17, 120.02, 114.97, 111.33, 71.03, 56.44; HRMS (ESI+): calcd for $C_{16}H_{16}F_3N_2O_3$ $[M + H]^+$ 341.1108; found, 341.1109.

2-chloro-N'-hydroxy-4-((4-(trifluoromethyl)benzyl)oxy)benzimidamide (**2.13l**). Synthesized by General Procedure 2C: 220 mg, 90%, white solid. ^{1}H NMR (400 MHz, CD_3OD) δ 7.64 (d, J = 19.8 Hz, 4H), 7.44 (dd, J = 8.2, 61.5 Hz, 1H), 7.11 (s, 1H), 6.99 (s, 1H), 5.19 (s, 2H); ^{13}C NMR (101 MHz CD_3OD) 171.81, 161.03, 154.08, 142.40, 135.14, 133.05, 131.66, 131.04 (d, $^{2}J_{CF_3}$ =

32.5 Hz), 126.40 (d, $^{3}J_{CF_3}$ = 3.8 Hz), 125.50 (q, $^{1}J_{CF_3}$ = 271.4 Hz), 117.30, 114.46, 70.26; HRMS (ESI+): calcd for $C_{15}H_{13}ClF_3N_2O_2$ [M + H]$^+$ 345.0612; found, 341.0600.

N'-hydroxy-2-(trifluoromethyl)-4-((4-(trifluoromethyl)benzyl)oxy)benzimidamide (**2.13m**). Synthesized by General Procedure 2C: 139 mg, 47%, white solid. ^{1}H NMR (400 MHz, CD_3OD) δ 7.66 (q, *J* = 7.9 Hz, 4H), 7.51 (dd, *J* = 8.5, 22.5 Hz, 1H), 7.36 (s, 1H), 7.28 (d, *J* = 8.8 Hz, 1H), 5.27 (s, 2H); ^{13}C NMR (101 MHz CD_3OD) 173.08, 160.42, 154.00, 142.33 (q, $^{4}J_{CF_3}$ = 1.2 Hz), 134.20, 131.64 (q, $^{2}J_{CF_3}$ = 31.6 Hz), 131.45, 128.90, 126.47 (q, $^{3}J_{CF_3}$ = 3.8 Hz), 125.54 (q, $^{1}J_{CF_3}$ = 271.0 Hz), 124.93 (q, $^{1}J_{CF_3}$ = 272.9 Hz), 118.61 (q, $^{4}J_{CF_3}$ = 1.2 Hz), 114.63 (q, $^{3}J_{CF_3}$ = 5.3 Hz), 70.42; HRMS (ESI+): calcd for $C_{16}H_{13}F_6N_2O_2$ [M + H]$^+$ 379.0876; found, 379.0866.

N'-hydroxy-3-nitro-4-((4-(trifluoromethyl)benzyl)oxy)benzimidamide (**2.13n**). Synthesized by General Procedure 2C: 220 mg, 85%, yellow solid. ^{1}H NMR (400 MHz, CD_3OD) δ 8.13 (s, 1H), 7.83 (d, *J* = 8.4 Hz, 1H), 7.64 (s, 4H), 7.29 (d, *J* = 8.8 Hz, 1H), 5.32 (s, 2H); ^{13}C NMR (101 MHz CD_3OD) 169.28, 153.32, 141.66, 140.95, 132.65, 131.10 (d, $^{2}J_{CF_3}$ = 32.3 Hz), 128.45, 127.24, 125.34 (q, $^{1}J_{CF_3}$ = 271.80 Hz), 126.41 (q, $^{3}J_{CF_3}$ = 3.8 Hz), 124.16, 116.13, 71.20; HRMS (ESI+): calcd for $C_{15}H_{13}F_3N_3O_4$ [M + H]$^+$ 356.0853; found, 356.0864.

3-(tert-butyl)-N'-hydroxy-4-((4-(trifluoromethyl)benzyl)oxy)benzimidamide (**2.13o**). Synthesized by General Procedure 2C: 268 mg, 88%, white solid. ^{1}H NMR (400 MHz, $CDCl_3$) δ 7.85 – 7.64 (m, 3H), 7.79 – 7.40 (m, 3H), 6.90 (t, *J* = 7.60 Hz, 1H), 6.12 (s, 1H), 5.21 (d, *J* = 11.6 Hz, 2H), 4.87 (br s, 2H), 1.42 (s, 9H); ^{13}C NMR (101 MHz $CDCl_3$) 169.82, 160.22, 158.63, 152.92, 141.05, 138.76, 127.45, 126.86, 125.78, 124.96, 112.37, 111.98, 69.56, 35.18, 29.77; HRMS (ESI+): calcd for $C_{19}H_{22}F_3N_2O_2$ [M + H]$^+$ 367.1628; found, 367.1647.

3-allyl-N'-hydroxy-4-((4-(trifluoromethyl)benzyl)oxy)benzimidamide (**2.13p**). Synthesized by General Procedure 2C: 504 mg, 96%, white solid. ^{1}H NMR (400 MHz, CD_3OD) δ 7.63 (q, *J* = 8.4

Hz, 4H), 7.49 – 7.44 (m, 2H), 6.97 (d, J = 9.2 Hz, 1H), 6.05 – 5.94 (m, 1H), 5.17 (s, 2H), 5.06 – 5.00 (m, 2H), 3.44 (d, J = 6.5 Hz, 2H); ^{13}C NMR (101 MHz CD_3OD) 172.05, 158.60, 155.44, 143.13 (d, $^4J_{CF_3}$ = 1.2 Hz), 137.73, 130.89 (q, $^2J_{CF_3}$ = 32.3 Hz), 130.06, 129.12, 128.56, 126.98, 126.70, 126.36 (q, $^3J_{CF_3}$ = 3.9 Hz), 125.62 (q, $^1J_{CF_3}$ = 271.7 Hz), 112.58, 70.04, 35.51; HRMS (ESI+): calcd for $C_{18}H_{18}F_3N_2O_2$ [M + H]$^+$ 351.1315; found, 351.1340.

N'-hydroxy-3-propyl-4-((4-(trifluoromethyl)benzyl)oxy)benzimidamide (**2.13q**). Synthesized by General Procedure 2C: 504 mg, 96%, white solid. ^{1}H NMR (400 MHz, CD_3OD) δ 7.75 – 7.58 (m, 5H), 7.47 – 7.44 (m ,1H), 7.02 – 6.94 (m, 1H), 5.18 (s, 2H), 2.67 (t, J = 7.3 Hz, 2H), 1.64 (q, J = 7.5 Hz, 2H), 0.94 (t, J = 7.3 Hz, 3H); ^{13}C NMR (101 MHz CD_3OD) 172.20, 158.82, 155.58, 143.30 (d, $^4J_{CF_3}$ = 1.3 Hz), 132.39, 130.86 (q, $^2J_{CF_3}$ = 32.3 Hz), 129.14, 128.50, 126.40 (q, $^3J_{CF_3}$ = 3.9 Hz), 126.26, 125.59 (q, $^1J_{CF_3}$ = 271.5 Hz), 112.51, 69.99, 33.52, 24.15, 14.38; HRMS (ESI+): calcd for $C_{18}H_{20}F_3N_2O_2$ [M + H]$^+$ 353.1471; found, 353.1479.

N'-hydroxy-3-(trifluoromethyl)-4-((4-(trifluoromethyl)benzyl)oxy)benzimidamide (**2.13r**). Synthesized by General Procedure 2C: 304 mg, 96%, white solid. ^{1}H NMR (400 MHz, CD_3OD) δ 7.93 (d, J = 2.1 Hz, 1H), 7.83 (dd, J = 8.7, 2.2 Hz, 1H), 7.69 (d, J = 8.3 Hz, 2H), 7.65 (d, J = 8.3 Hz, 2H), 7.25 (d, J = 8.7 Hz, 1H), 5.34 (s, 2H); ^{13}C NMR (101 MHz, CD_3OD) δ 158.37, 154.01, 142.26, 132.55, 131.13 (q, $^2J_{CF}$ = 32.3 Hz), 128.44, 126.97, 126.46 (q, $^3J_{CF}$ = 3.8 Hz), 126.17 (q, $^3J_{CF}$ = 5.4 Hz), 125.49 (q, $^1J_{CF}$ = 264 Hz), 125.02 (q, $^1J_{CF}$ = 277 Hz), 119.92 (q,$^2J_{CF}$ = 30.9 Hz), 114.61, 70.61; HRMS (ESI+): calcd for $C_{16}H_{13}F_6N_2O_2$ [M + H]$^+$ 379.0876; found 379.0879.

tert-butyl (S)-2-(3-(6-((4-(trifluoromethyl)benzyl)oxy)-[1,1'-biphenyl]-3-yl)-1,2,4-oxadiazol-5-yl)pyrrolidine-1-carboxylate (**2.14a**). Synthesized by General Procedure 2D: 33 mg, 40%, yellow oil. ^{1}H NMR (400 MHz, $CDCl_3$) δ 8.10 (s, 1H), 8.02 (d, J = 8.9 Hz, 1H), 7.63 – 7.56 (m, 4H), 7.48 – 7.34 (m, 5H), 7.11 – 7.05 (m, 1H), 5.21 (s, 2H), 5.09 – 5.02 (m, 1H), 3.76 – 3.63 (m, 1H), 3.61

– 3.45 (m, 1H), 2.46 – 2.30 (m, 1H), 2.21 – 2.09 (m, 2H), 2.04 – 1.95 (m, 1H), 1.46 (s, 1H), 1.31 (s, 6H); ^{13}C NMR (101 MHz $CDCl_3$) 180.63, 168.05, 157.58, 153.80, 140.74, 137.46, 132.08, 130.41, 129.72, 128.21, 127.65, 126.91, 125.61 (q, $^3J_{CF_3}$ = 3.7 Hz), 124.44 (q, $^1J_{CF_3}$ = 272.6 Hz), 120.21, 113.15, 80.71, 69.70, 53.95, 46.50, 32.52, 31.61, 28.52, 28.30, 23.82; HRMS (ESI+): calcd for $C_{31}H_{31}F_3N_3O_4$ [M + H]$^+$ 566.2261; found, 566.2291.

tert-butyl (S)-2-(3-(4'-fluoro-6-((4-(trifluoromethyl)benzyl)oxy)-[1,1'-biphenyl]-3-yl)-1,2,4-oxadiazol-5-yl)pyrrolidine-1-carboxylate (**2.14b**). Synthesized by General Procedure 2D: 43 mg, 43%, yellow oil. ^{1}H NMR (400 MHz, $CDCl_3$) δ 8.08 – 7.99 (m, 2H), 7.65 – 7.51 (m, 4H), 7.42 (d, *J* = 8.1 Hz, 2H), 7.17 – 7.04 (m, 3H), 5.21 (s, 2H), 5.10 – 5.02 (m, 1H), 3.76 – 3.63 (m, 1H), 3.61 – 3.45 (m, 1H), 2.47 – 2.29 (m, 1H), 2.21 – 2.09 (m, 2H), 2.06 – 1.95 (m, 1H), 1.46 (s, 3H), 1.30 (s, 6H); ^{13}C NMR (101 MHz $CDCl_3$) 180.73, 167.97, 162.38 (d, $^1J_{CF}$ = 245.4 Hz), 157.50, 153.69, 140.59 (d, $^4J_{CF_3}$ = 1.5 Hz), 133.39 (d, $^4J_{CF}$ = 2.9 Hz), 131.37 (d, $^3J_{CF}$ = 8.0 Hz), 130.26, 128.34, 126.94, 125.69 (q, $^3J_{CF_3}$ = 3.8 Hz), 124.20 (d, $^1J_{CF_3}$ = 271.8 Hz), 120.30, 115.14 (d, $^2J_{CF}$ = 20.9 Hz), 113.14, 80.60, 69.77, 53.96, 46.50, 32.56, 31.66, 29.85, 28.32, 23.86; HRMS (ESI+): calcd for $C_{31}H_{30}F_4N_3O_4$ [M + H]$^+$ 584.2167; found, 584.2175.

tert-butyl (S)-2-(3-(3-(pyridin-4-yl)-4-((4-(trifluoromethyl)benzyl)oxy)phenyl)-1,2,4-oxadiazol-5-yl)pyrrolidine-1-carboxylate (**2.14c**). Synthesized by General Procedure 2D: 65 mg, 59%, yellow oil. ^{1}H NMR (400 MHz, $CDCl_3$) δ 8.66 (s, 2H), 8.10 (s, 2H), 7.61 (d, *J* = 8.1 Hz, 2H), 7.56 – 7.49 (m, 2H), 7.42 (d, *J* = 8.0 Hz, 2H), 7.16 – 7.08 (m, 1H), 5.23 (s, 2H), 5.09 – 5.02 (m, 1H), 3.76 – 3.62 (m, 1H), 3.59 – 3.44 (m, 1H), 2.45 – 2.33 (m, 1H), 2.20 – 2.09 (m, 2H), 2.05 – 1.96 (m, 1H), 1.45 (s, 3H), 1.30 (s, 6H); ^{13}C NMR (101 MHz $CDCl_3$) 180.89, 167.68, 157.51, 153.64, 149.70, 145.38, 140.15, 130.00, 129.80,125.76 (d, $^3J_{CF_3}$ = 3.2 Hz) 124.12 (d, $^1J_{CF_3}$ = 272.0 Hz), 120.51,

113.19, 80.58, 69.85, 53.92, 46.47, 32.53, 31.63, 29.82, 28.50, 28.28, 24.52, 23.84; HRMS (ESI+): calcd for $C_{30}H_{30}F_3N_4O_4$ $[M + H]^+$ 567.2214; found, 567.2244.

tert-butyl (S)-2-(3-(4'-(trifluoromethyl)-6-((4-(trifluoromethyl)benzyl)oxy)-[1,1'-biphenyl]-3-yl)-1,2,4-oxadiazol-5-yl)pyrrolidine-1-carboxylate (**2.14d**). Synthesized by General Procedure 2D: 206 mg, 51%, yellow oil. ^{1}H NMR (400 MHz, $CDCl_3$) δ 8.12 – 8.01 (m, 2H), 7.73 – 7.67 (m, 4H), 7.60 (d, *J* = 8.3 Hz, 2H), 7.41 (d, *J* = 7.7 Hz, 2H), 7.15 – 7.06 (m, 1H), 5.23 (s, 2H), 5.12 – 5.02 (m, 1H), 3.77 – 3.63 (m, 1H), 3.62 – 3.46 (m, 1H), 2.47 – 2.32 (m, 1H), 2.20 – 2.10 (m, 2H), 2.04 – 1.95 (m, 1H), 1.47 (s, 3H), 1.31 (s, 6H); ^{13}C NMR (101 MHz $CDCl_3$) 180.81, 167.82, 157.48, 153.74, 141.17, 140.36, 130.51, 130.31, 130.03, 129.00, 125.70 (q, $^3J_{CF_3}$ = 3.8 Hz), 125.12 (q, $^3J_{CF_3}$ = 3.6 Hz), 124.40 (d, $^1J_{CF_3}$ = 272.2 Hz), 124.19 (q, $^1J_{CF_3}$ = 272.4 Hz), 120.41, 113.23, 80.66, 69.83, 53.94, 46.49, 32.50, 31.60, 28.49, 28.27, 24.49, 23.81; HRMS (ESI+): calcd for $C_{32}H_{30}F_6N_3O_4$ $[M + H]^+$ 634.2135; found, 634.2105.

tert-butyl (S)-2-(3-(3-cyclopropyl-4-((4-(trifluoromethyl)benzyl)oxy)phenyl)-1,2,4-oxadiazol-5-yl)pyrrolidine-1-carboxylate (**2.14e**). Synthesized by General Procedure 2D: 15 mg, 27%, yellow oil. ^{1}H NMR (400 MHz, $CDCl_3$) δ 7.85 (d, *J* = 7.5 Hz, 1H), 7.67 (d, *J* = 7.5 Hz, 1H), 7.60 (d, *J* = 6.4 Hz, 2H), 7.27 (q, *J* = 8.0 Hz, 2H), 6.99 – 6.90 (m, 1H), 5.29 – 4.99 (m, 3H), 3.78 – 3.63 (m, 1H), 3.61 – 3.40 (m, 1H), 2.44 – 2.30 (m, 1H), 2.29 – 2.22 (m, 1H), 2.21 – 2.07 (m, 2H), 2.05 – 1.96 (m, 1H), 1.46 (s, 3H), 1.30 (s, 6H), 1.04 – 0.95 (m, 2H), 0.82 – 0.72 (m, 2H); ^{13}C NMR (101 MHz $CDCl_3$) 180.46, 168.26, 159.53, 153.73, 141.06, 134.06, 133.60, 132.44, 130.30 (d, $^2J_{CF_3}$ = 32.7 Hz), 129.62, 127.28, 126.25, 125.72 (q, $^3J_{CF_3}$ = 3.7 Hz), 124.68, 124.19 (q, $^1J_{CF_3}$ = 272.1 Hz), 119.71, 111.58, 80.59, 69.43, 53.96, 46.49, 28.30, 7.99; HRMS (ESI+): calcd for $C_{28}H_{31}F_3N_3O_4$ $[M + H]^+$ 530.2261; found, 530.2242.

tert-butyl (S)-2-(3-(4-((4-(trifluoromethyl)benzyl)oxy)phenyl)-1,2,4-oxadiazol-5-yl)pyrrolidine-1-carboxylate (**2.14f**). Synthesized by General Procedure 2D: 148 mg, 63%, yellow oil. ^{1}H NMR (400 MHz, $CDCl_3$) δ 8.05 – 7.97 (m, 2H), 7.58 (dd, *J* = 7.8, 36.4 Hz, 4H), 7.07 – 6.97 (m, 2H), 5.15 (s, 2H), 5.07 – 5.01 (1H), 3.74 – 3.60 (m, 1H), 3.58 – 3.43 (m, 1H), 2.43 – 2.26 (m, 1H), 2.17 – 2.06 (m, 2H), 2.03 – 1.91 (m, 1H), 1.44 (s, 3H), 1.28 (s, 6H); ^{13}C NMR (101 MHz $CDCl_3$) 180.52, 167.94, 160.71, 153.57, 140.59, 130.23 (q, $^{2}J_{CF_3}$ = 32.7 Hz), 129.18, 127.43, 125.59 (q, $^{3}J_{CF_3}$ = 3.2 Hz), 124.07 (d, $^{1}J_{CF_3}$ = 272.0 Hz), 119.87, 115.13, 80.40, 69.13, 46.37, 32.38, 28.40, 28.16, 23.71; HRMS (ESI+): calcd for $C_{25}H_{26}F_3N_3NaO_4$ $[M+Na]^+$ 512.1768; found, 512.1773.

tert-butyl (S)-2-(3-(3-bromo-4-((4-(trifluoromethyl)benzyl)oxy)phenyl)-1,2,4-oxadiazol-5-yl)pyrrolidine-1-carboxylate (**2.14g**). Synthesized by General Procedure 2D: 172 mg, 47%, yellow oil. ^{1}H NMR (400 MHz, $CDCl_3$) δ 8.30 (s, 1H), 8.00 – 7.91 (m, 1H), 7.62 (dd, *J* = 7.8, 21.5 Hz, 4H), 7.01 – 6.92 (m, 1H), 5.24 (s, 2H), 5.07 – 5.00 (m, 1H), 3.74 – 3.62 (m, 1H), 3.57 – 3.44 (m, 1H), 2.43 – 2.30 (m, 1H), 2.17 – 2.07 (m, 2H), 2.03 – 1.95 (m, 1H), 1.44 (s, 3H), 1.28 (s, 6H); ^{13}C NMR (101 MHz $CDCl_3$) 180.88, 166.98, 156.87, 153.54, 140.03, 132.62, 130.30 (q, $^{2}J_{CF_3}$ = 31.4 Hz), 127.98, 127.07, 125.66 (d, $^{3}J_{CF_3}$ = 3.1 Hz),, 124.12 (q, $^{1}J_{CF_3}$ = 271.8 Hz), 121.14, 113.30, 80.49, 69.94, 53.83, 46.41, 32.43, 29.75, 28.19, 23.75; HRMS (ESI+): calcd for $C_{25}H_{25}BrF_3N_3NaO_4$ $[M+Na]^+$ 590.0873; found, 590.0877.

tert-butyl (S)-2-(3-(3,5-dimethyl-4-((4-(trifluoromethyl)benzyl)oxy)phenyl)-1,2,4-oxadiazol-5-yl)pyrrolidine-1-carboxylate (**2.14h**). Synthesized by General Procedure 2D: 190 mg, 62%, yellow oil. ^{1}H NMR (400 MHz, $CDCl_3$) δ 7.76 (s, 2H), 7.61 (dd, *J* = 8.2, 26.3 Hz, 4H), 5.08 – 5.00 (m, 1H), 4.89 (s, 2H), 3.72 – 3.65 (m, 1H), 3.57 – 3.47 (m, 1H), 2.32 (s, 6H), 2.17 – 2.08 (m, 2H), 2.04 – 1.87 (m, 2H), 1.44 (s, 3H), 1.28 (s, 6H); ^{13}C NMR (101 MHz $CDCl_3$) 180.62, 168.07, 158.10, 153.56, 141.36, 131.84, 130.16 (q, $^{2}J_{CF_3}$ = 32.3 Hz), 128.23, 127.56, 125.51 (d, $^{3}J_{CF_3}$ = 3.6 Hz),

122.79, 122.53, 80.42, 73.00, 53.86, 46.40, 32.46, 28.17, 23.74, 16.42; HRMS (ESI+): calcd for $C_{27}H_{31}F_3N_3O_4$ $[M+H]^+$ 518.2261; found, 518.2267.

tert-butyl (S)-2-(3-(3-chloro-4-((4-(trifluoromethyl)benzyl)oxy)phenyl)-1,2,4-oxadiazol-5-yl)pyrrolidine-1-carboxylate (**2.14i**). Synthesized by General Procedure 2D: 190 mg, 62%, yellow oil. ^{1}H NMR (400 MHz, $CDCl_3$) δ 8.17 – 8.05 (m, 1H), 7.95 – 7.83 (m, 1H), 7.60 (dd, J = 8.1, 25.0 Hz, 4H), 7.05 – 6.94 (m, 1H), 5.23 (s, 2H), 5.07 – 5.01 (m,1H), 3.76 – 3.62 (m, 1H), 3.60 – 3.44 (m, 1H), 2.46 – 2.28 (m, 1H), 2.18 – 2.07 (m, 2H), 2.04 – 1.93 (m, 1H), 1.45 (s, 3H), 1.28 (s, 6H); ^{13}C NMR (101 MHz $CDCl_3$) 180.84, 167.12, 156.04, 153.65, 140.03, 130.33 (q, $^2J_{CF_3}$ = 32.5 Hz), 129.55, 127.13, 125.67 (q, $^3J_{CF_3}$ = 3.8 Hz), 124.13 (q, $^1J_{CF_3}$ = 272.5 Hz), 123.86, 120.69, 113.57, 80.61, 69.90, 53.85, 46.43, 32.41, 28.42, 28.19, 23.74; HRMS (ESI+): calcd for $C_{25}H_{25}ClF_3N_3NaO_4$ $[M+Na]^+$ 546.1378; found, 546.1384.

tert-butyl (S)-2-(3-(3-fluoro-4-((4-(trifluoromethyl)benzyl)oxy)phenyl)-1,2,4-oxadiazol-5-yl)pyrrolidine-1-carboxylate (**2.14j**). Synthesized by General Procedure 2D: 217 mg, 58%, yellow oil. ^{1}H NMR (400 MHz, $CDCl_3$) δ 7.83 – 7.70 (m, 2H), 7.57 (dd, J = 7.9, 21.3 Hz, 4H), 7.08 – 6.97 (m, 1H), 5.26 – 4.99 (m, 3H), 3.74 – 3.60 (m, 1H), 3.58 – 3.42 (m, 1H), 2.43 – 2.25 (m, 1H), 2.17 – 2.04 (m, 2H), 1.99 – 1.91 (m, 1H), 1.43 (s, 3H), 1.27 (s, 6H); ^{13}C NMR (101 MHz $CDCl_3$) 180.81, 167.23 (d, $^4J_{CF}$ = 2.2 Hz), 153.61, 152.63 (d, $^1J_{CF}$ = 247.4 Hz), 148.84 (d, $^2J_{CF}$ = 10.9 Hz), 140.05, 130.38 (q, $^2J_{CF_3}$ = 32.2 Hz), 127.41, 125.63 (q, $^3J_{CF_3}$ = 3.8 Hz), 124.00 (q, $^1J_{CF_3}$ = 272.3 Hz), 123.97 (d, $^4J_{CF}$ = 3.7 Hz), 120.43 (d, $^3J_{CF}$ = 7.2 Hz), 115.56 (d, $^2J_{CF}$ = 20.7 Hz), 115.20, 80.55, 70.24, 53.81, 46.40, 32.35, 28.14, 23.69; HRMS (ESI+): calcd for $C_{25}H_{25}F_4N_3NaO_4$ $[M+Na]^+$ 530.1673; found, 530.1679.

tert-butyl (S)-2-(3-(3-methoxy-4-((4-(trifluoromethyl)benzyl)oxy)phenyl)-1,2,4-oxadiazol-5-yl)pyrrolidine-1-carboxylate (**2.14k**). Synthesized by General Procedure 2D: 175 mg, 65%, yellow

oil. ^{1}H NMR (400 MHz, $CDCl_3$) δ 7.80 – 7.51 (m, 6H), 6.95 – 6.82 (m, 1H), 5.25 – 5.02 (m, 3H), 3.94 (s, 2H), 3.89 (s, 1H), 3.77 – 3.63 (m, 1H), 3.59 – 3.45 (m, 1H), 2.43 – 2.30 (m, 1H), 2.18 – 2.06 (m, 2H), 2.02 – 1.93 (m, 1H), 1.45 (s, 3H), 1.29 (s, 6H); ^{13}C NMR (101 MHz $CDCl_3$) 180.43, 168.04, 153.81, 150.26, 149.77, 140.62, 130.15 (q, $^{2}J_{CF_3}$ = 33.0 Hz), 127.33, 125.55 (d, $^{3}J_{CF_3}$ = 3.8 Hz), 124.14 (q, $^{1}J_{CF_3}$ = 272.0 Hz), 120.77, 120.11, 113.48, 110.41, 80.72, 70.02, 56.11, 53.87, 46.45, 32.37, 28.17, 23.71; HRMS (ESI+): calcd for $C_{26}H_{29}F_3N_3O_5$ $[M+H]^+$ 520.2054; found, 520.2032.

tert-butyl (S)-2-(3-(2-chloro-4-((4-(trifluoromethyl)benzyl)oxy)phenyl)-1,2,4-oxadiazol-5-yl)pyrrolidine-1-carboxylate (**2.14l**). Synthesized by General Procedure 2D: 110 mg, 33%, yellow oil. ^{1}H NMR (400 MHz, $CDCl_3$) δ 7.91 – 7.83 (m, 1H), 7.58 (dd, *J* = 7.5, 35.9 Hz, 4H), 7.14 – 7.07 (m, 1H), 6.98 – 6.89 (m, 1H), 5.22 – 5.00 (m, 3H), 3.73 – 3.60 (m, 1H), 3.57 – 3.42 (m, 1H), 2.43 – 2.29 (m, 1H), 2.18 – 2.07 (m, 2H), 2.02 – 1.93 (1H), 1.44 (s, 3H), 1.29 (s, 6H); ^{13}C NMR (101 MHz $CDCl_3$) 180.08, 166.85, 160.44, 153.53, 139.97, 134.56, 132.83, 130.45 (q, $^{2}J_{CF_3}$ = 31.6 Hz), 127.48, 125.70 (d, $^{3}J_{CF_3}$ = 3.6 Hz), 124.08 (q, $^{1}J_{CF_3}$ = 272.5 Hz), 119.03, 117.22, 113.73, 80.49, 69.46, 53.79, 46.40, 32.47, 28.20, 23.73; HRMS (ESI+): calcd for $C_{25}H_{26}ClF_3N_3O_4$ $[M+H]^+$ 524.1558; found, 524.1574.

tert-butyl (S)-2-(3-(2-(trifluoromethyl)-4-((4-(trifluoromethyl)benzyl)oxy)phenyl)-1,2,4-oxadiazol-5-yl)pyrrolidine-1-carboxylate (**2.14m**). Synthesized by General Procedure 2D: 68 mg, 33%, yellow oil. ^{1}H NMR (400 MHz, $CDCl_3$) δ 7.72 (d, *J* = 8.5 Hz, 1H), 7.58 (dd, *J* = 7.9, 29.1 Hz, 4H), 7.42 – 7.36 (m, 1H), 7.19 – 7.11 (m, 1H), 5.22 – 5.02 (m, 3H), 3.70 – 3.58 (m, 1H), 3.56 – 3.40 (m, 1H), 2.43 – 2.27 (m, 1H), 2.16 – 2.05 (m, 2H), 2.00 – 1.92 (m, 1H), 1.42 (s, 3H), 1.30 (s, 6H); ^{13}C NMR (101 MHz $CDCl_3$) 180.63, 167.20, 159.90, 153.46, 139.81, 133.58, 130.82 (q, $^{2}J_{CF_3}$ = 32.3 Hz), 130.47 (q, $^{2}J_{CF_3}$ = 32.4 Hz), 127.50, 125.67 (q, $^{3}J_{CF_3}$ = 3.7 Hz), 124.05 (q, ^{1}J

$_{CF_3}$ = 272.3 Hz), 123.07 (q, $^1J_{CF_3}$ = 273.3 Hz), 117.24, 114.20 (q, $^3J_{CF_3}$ = 5.6 Hz), 80.47, 69.49, 53.72, 46.35, 32.47, 28.31, 28.06, 23.60; HRMS (ESI+): calcd for $C_{26}H_{25}F_6N_3NaO_4$ [M + Na]$^+$ 580.1641; found, 580.1637.

tert-butyl (S)-2-(3-(3-nitro-4-((4-(trifluoromethyl)benzyl)oxy)phenyl)-1,2,4-oxadiazol-5-yl)pyrrolidine-1-carboxylate (**2.14n**). Synthesized by General Procedure 2D: 149 mg, 39%, yellow oil. ^{1}H NMR (400 MHz, $CDCl_3$) δ 8.58 – 8.49 (m, 1H), 8.23 – 8.13 (m, 1H), 7.59 (q, *J* = 7.1 Hz, 4H), 7.24 – 7.14 (m, 1H), 5.32 (s, 2H), 5.20 – 5.00 (m, 1H), 3.72 – 3.61 (m, 1H), 3.57 – 3.45 (m, 1H), 2.44 – 2.30 (m, 1H), 2.18 – 2.06 (m, 2H), 2.04 – 1.94 (m, 1H), 1.43 (s, 3H), 1.26 (s, 6H); ^{13}C NMR (101 MHz $CDCl_3$) 181.36, 166.39, 153.33, 139.10, 132.86, 130.45 (q, $^2J_{CF_3}$ = 32.8 Hz), 127.05, 125.72 (d, $^3J_{CF_3}$ = 3.7 Hz), 124.97, 123.99 (q, $^1J_{CF_3}$ = 271.3 Hz), 120.05, 115.16, 80.50, 70.36, 53.78, 46.39, 32.39, 31.47, 28.36, 28.15, 23.72; HRMS (ESI+): calcd for $C_{25}H_{25}F_3N_4NaO_6$ [M + Na]$^+$ 557.1618; found, 524.1588.

tert-butyl (S)-2-(3-(3-(tert-butyl)-4-((4-(trifluoromethyl)benzyl)oxy)phenyl)-1,2,4-oxadiazol-5-yl)pyrrolidine-1-carboxylate (**2.14o**). Synthesized by General Procedure 2D: 210 mg, 53%, yellow oil. ^{1}H NMR (400 MHz, $CDCl_3$) δ 8.07 – 8.01 (m, 1H), 7.92 – 7.84 (m, 1H), 7.61 (dd, *J* = 8.8, 31.7 Hz, 4H), 6.99 – 6.91 (m, 1H), 5.23 – 5.01 (m, 3H), 3.73 – 3.62 (m, 1H), 3.58 – 3.45 (m, 1H), 2.41 – 2.30 (m, 1H), 2.16 – 2.06 (m, 2H), 2.00 – 1.93 (m, 1H), 1.43 (s, 12H), 1.30 (s, 6H); ^{13}C NMR (101 MHz $CDCl_3$) 180.32, 168.35, 159.51, 153.58, 140.79, 138.98, 130.09 (q, $^2J_{CF_3}$ = 33.2 Hz), 127.44, 126.89, 126.27, 125.62 (d, $^3J_{CF_3}$ = 3.7 Hz), 124.12 (q, $^1J_{CF_3}$ = 271.7 Hz), 119.30, 112.48, 80.33, 69.44, 53.82, 46.33, 35.06, 32.36, 29.68, 28.13, 23.68; HRMS (ESI+): calcd for $C_{29}H_{35}F_3N_3O_4$ [M + H]$^+$ 546.2574; found, 546.2576.

tert-butyl (S)-2-(3-(3-allyl-4-((4-(trifluoromethyl)benzyl)oxy)phenyl)-1,2,4-oxadiazol-5-yl)pyrrolidine-1-carboxylate (**2.14p**). Synthesized by General Procedure 2D: 444 mg, 58%, yellow

oil. ^{1}H NMR (400 MHz, $CDCl_3$) δ 7.89 (s, 2H), 7.56 (dd, *J* = 7.6, 35.7 Hz, 4H), 6.94 – 6.86 (m, 1H), 6.05 – 5.92 (m, 1H), 5.19 – 4.99 (m, 5H), 3.70 – 3.60 (m, 1H), 3.54 – 3.41 (m, 3H), 2.39 – 2.27 (m, 1H), 2.14 – 2.03 (m, 2H), 1.98 – 1.90 (m, 1H), 1.42 (s, 3H), 1.27 (s, 6H); ^{13}C NMR (101 MHz $CDCl_3$) 180.38, 167.96, 158.28, 153.48, 140.77, 135.94, 129.98 (q, $^{2}J_{CF_3}$ = 33.3 Hz), 129.60, 129.13, 127.09, 125.45 (d, $^{3}J_{CF_3}$ = 3.3 Hz), 124.22 (q, $^{1}J_{CF_3}$ = 272.0 Hz), 119.50, 116.11, 111.50, 80.25, 68.99, 53.75, 46.28, 34.37, 32.28, 28.26, 28.03, 23.61; HRMS (ESI+): calcd for $C_{28}H_{31}F_3N_3O_4$ $[M + H]^+$ 530.2261; found, 530.2274.

tert-butyl (S)-2-(3-(3-propyl-4-((4-(trifluoromethyl)benzyl)oxy)phenyl)-1,2,4-oxadiazol-5-yl)pyrrolidine-1-carboxylate (**2.14q**). Synthesized by General Procedure 2D: 480 mg, 58%, yellow oil. ^{1}H NMR (400 MHz, $CDCl_3$) δ 7.91 – 7.82 (m, 2H), 7.58 (dd, *J* = 7.4, 38.8 Hz, 4H), 6.94 – 6.86 (m, 1H), 5.20 – 5.01 (m, 3H), 3.74 – 3.62 (m, 1H), 3.57 – 3.42 (m, 1H), 2.73 – 2.64 (m, 2H), 2.41 – 2.28 (m, 1H), 2.16 – 2.05 (m, 2H), 1.99 – 1.90 (m, 1H), 1.72 – 1.61 (m, 2H), 1.43 (s, 3H), 1.28 (s, 6H), 1.00 – 0.88 (m, 3H); ^{13}C NMR (101 MHz $CDCl_3$) 180.37, 168.12, 158.55, 153.55, 141.00, 132.05, 130.00 (q, $^{2}J_{CF_3}$ = 32.2 Hz), 129.24, 127.00, 126.65, 125.52 (d, $^{3}J_{CF_3}$ = 3.8 Hz), 124.14 (q, $^{1}J_{CF_3}$ = 271.1 Hz), 119.31, 111.46, 80.33, 68.94, 53.81, 46.33, 32.34, 28.32, 28.09, 23.66, 22.88, 14.00; HRMS (ESI+): calcd for $C_{28}H_{33}F_3N_3O_4$ $[M + H]^+$ 532.2418; found, 532.2397.

tert-butyl (S)-2-(3-(3-(trifluoromethyl)-4-((4-(trifluoromethyl)benzyl)oxy)phenyl)-1,2,4-oxadiazol-5-yl)pyrrolidine-1-carboxylate (**2.14r**). Synthesized by General Procedure 2D: 146 mg, 64%, yellow oil. ^{1}H NMR (400 MHz, $CDCl_3$) δ 8.34 (s, 1H), 8.20 (d, *J* = 8.6 Hz, 1H), 7.67 (d, *J* = 8.2 Hz, 2H), 7.57 (d, *J* = 8.1 Hz, 2H), 7.11 (t, *J* = 8.7 Hz, 1H), 5.31 (s, 2H), 5.20 – 5.05 (m, 1H), 3.75 – 3.63 (m, 1H), 3.62 – 3.42 (m, 1H), 2.49 – 2.31 (m, 1H), 2.22 – 1.96 (m, 3H), 1.46 (s, 3H), 1.30 (s, 6H); ^{13}C NMR (101 MHz, $CDCl_3$) δ 181.13, 167.22, 158.21, 153.63, 139.76, 132.66, 130.48 (q, $^{2}J_{CF}$ = 30.3 Hz), 127.00, 125.82 (t, $^{3}J_{CF}$ = 3.8 Hz), 123.99 (q, $^{1}J_{CF}$ = 272.8 Hz), 123.17

(q, $^{1}J_{CF}$ = 273.1 Hz), 119.69, 113.45, 80.64, 69.73, 53.92, 46.49, 32.53, 31.60, 28.50, 28.28, 23.85; HRMS (ESI+): calcd for $C_{26}H_{26}F_6N_3O_4Na$ $[M + Na]^+$ 580.1641; found, 580.1652.

tert-butyl (S)-2-(3-(3-ethyl-4-((4-(trifluoromethyl)benzyl)oxy)phenyl)-1,2,4-oxadiazol-5-yl)pyrrolidine-1-carboxylate (**2.14s**). Synthesis was carried forward *via* a three step process according to the following protocol: To a solution of THF (0.2 M) under an atmosphere of argon gas, 370 mg (1 equiv) of tert-butyl (S)-2-(3-(3-bromo-4-((4-(trifluoromethyl)benzyl)oxy)phenyl)-1,2,4-oxadiazol-5-yl)pyrrolidine-1-carboxylate (compound 2.14g), 197 mg (3 equiv) of triethylamine, and 77 mg (1.2 equiv) of trimethylsilylacetylene were sequentially added to reaction vessel. Reaction solution was then degassed for 30 minutes by bubbling argon gas through solution while stirring. Next, 46 mg (0.1 equiv) of bis(triphenylphosphine) palladium(II) dichloride was added followed by 6 mg (0.05 equiv) copper(I) iodide. Reaction mixture was refluxed at 60 ºC for 48 hours. The reaction progress was monitored by TLC. Subsequently, the resulting solution was partitioned between EtOAc and brine solution. Using additional EtOAc, the brine solution was washed three times and the combined organic layers were dried over Na_2SO_4, filtered, and concentrated *via* vacuum. The resulting concentrate was purified by silica gel chromatography to yield 280 mg (74% yield) of intermediate product. Next, purified intermediate was then dissolved in a solution of THF (0.2 M) containing 250 mg (2 equiv) of tetra-n-butylammonium fluoride (TBAF) and stirred at room temperature for 3 hours. The reaction progress was monitored by TLC and concentrated *via* vacuum. The resulting concentrate was purified by silica gel chromatography to yield 245 mg (100% yield) of intermediate product. Finally, the resulting intermediate was hydrogenated by dissolving in ethanol (190 proof, 0.2 M) followed by addition of 10% palladium on carbon (0.1 equiv). Reaction mixture was then put under light vacuum followed by purge of hydrogen gas. Vacuum followed by addition of hydrogen gas was repeated three times. The

resulting mixture was stirred at room temperature for 18 hours followed by concentration *via* vacuum and purification by silica gel chromatography to yield final product: 114 mg, 45%, yellow oil. ^{1}H NMR (400 MHz, $CDCl_3$) δ 8.05 – 7.86 (m, 2H), 7.61(dd, *J* = 7.8, 39.3 Hz, 4H), 7.06 – 6.91 (m, 1H), 5.22 – 5.01 (m, 3H), 3.76 – 3.64 (m, 1H), 3.59 – 3.46 (m, 1H), 2.83 – 2.70 (m, 2H), 2.45 – 2.32 (m, 1H), 2.19 – 2.10 (m, 2H), 2.04 – 1.95 (m, 1H), 1.46 (s, 3H), 1.30 (s, 9H); ^{13}C NMR (101 MHz $CDCl_3$) 180.46, 168.25, 158.55, 153.70, 141.01, 133.71, 130.23 (q, $^2J_{CF_3}$ = 32.2 Hz), 128.47, 127.19, 126.75, 125.71 (d, $^3J_{CF_3}$ = 3.3 Hz), 124.21 (q, $^1J_{CF_3}$ = 272.6 Hz), 119.55, 115.21, 111.44, 80.54, 69.12, 53.94, 46.46, 32.52, 28.26, 23.53, 14.13; HRMS (ESI+): calcd for $C_{27}H_{31}F_3N_3O_4$ [M + H]$^+$ 518.2261; found, 518.2259.

(S)-2-(3-(6-((4-(trifluoromethyl)benzyl)oxy)-[1,1'-biphenyl]-3-yl)-1,2,4-oxadiazol-5-yl)pyrrolidine-1-carboximidamide (**2.15a**). Synthesized by General Procedure 2E: 15 mg, 90%, white solid. ^{1}H NMR (400 MHz, CD_3OD) δ 8.06 – 7.97 (m, 2H), 7.62 (d, *J* = 8.2 Hz, 2H), 7.54 (dd, *J* = 7.5, 12.4 Hz, 4H), 7.47 – 7.35 (m, 3H), 7.30 (d, *J* = 8.6 Hz, 1H), 5.44 (d, *J* = 7.8 Hz, 1H), 5.29 (s, 2H), 3.81 – 3.74 (m, 1H), 3.61 (q, *J* = 9.31 Hz, 1H), 2.62 – 2.52 (m, 1H), 2.52 – 2.43 (m, 1H), 2.28 – 2.18 (m, 1H), 2.16 – 2.02 (m, 1H); ^{13}C NMR (101 MHz CD_3OD) 178.87, 169.28, 159.27, 157.07, 142.73, 138.86, 133.38, 130.90, 130.88 (q, $^2J_{CF_3}$ = 31.9 Hz), 130.58, 129.27, 129.17, 128.60, 128.44, 126.34 (q, $^3J_{CF_3}$ = 3.7 Hz), 125.56 (q, $^1J_{CF_3}$ = 271.8 Hz), 120.60, 114.58, 70.65, 56.47, 32.72, 24.34; HRMS (ESI+): calcd for $C_{27}H_{25}F_3N_5O_2$ [M + H]$^+$ 508.1955; found, 508.1963.

(S)-2-(3-(4'-fluoro-6-((4-(trifluoromethyl)benzyl)oxy)-[1,1'-biphenyl]-3-yl)-1,2,4-oxadiazol-5-yl)pyrrolidine-1-carboximidamide (**2.15b**). Synthesized by General Procedure 2E: 112 mg, 63%, white solid. ^{1}H NMR (400 MHz, CD_3OD) δ 7.99 (d, *J* = 8.3 Hz, 1H), 7.94 (s, 1H), 6.60 – 7.45 (m, 6H), 7.24 (d, *J* = 8.3 Hz, 1H), 7.12 (t, *J* = 8.7 Hz, 2H), 5.49 (d, *J* = 7.1 Hz, 1H), 5.22 (s, 2H), 3.79

(t, J = 8.4 Hz, 1H), 3.63 (q, J = 9.3 Hz, 1H), 2.61 – 2.50 (m, 1H), 2.48 – 2.42 (m, 1H), 2.27 – 2.18 (m, 1H), 2.13 – 2.03 (m, 1H); ^{13}C NMR (101 MHz CD_3OD) 178.86, 169.13, 163.60 (d, $^1J_{CF}$ = 245.4 Hz), 159.05, 157.03, 142.48 (d, $^2J_{CF_3}$ = 1.2 Hz), 134.83 (d, $^4J_{CF}$ = 3.3 Hz), 132.45 (d, $^3J_{CF}$ = 8.2 Hz), 131.97, 130.83 (q, $^2J_{CF_3}$ = 32.5 Hz), 130.72, 129.45, 128.42, 126.32 (q, $^3J_{CF_3}$ = 3.8 Hz), 125.49 (q, $^1J_{CF_3}$ = 271.2 Hz), 120.57, 115.87 (d, $^2J_{CF}$ = 21.5 Hz), 114.48, 70.63, 56.43, 32.69, 24.34; HRMS (ESI+): calcd for $C_{27}H_{24}F_4N_5O_2$ [M + H]$^+$ 526.1861; found, 526.1863.

(S)-2-(3-(3-(pyridin-4-yl)-4-((4-(trifluoromethyl)benzyl)oxy)phenyl)-1,2,4-oxadiazol-5-yl)pyrrolidine-1-carboximidamide (**2.15c**). Synthesized by General Procedure 2E: 20 mg, 93%, white solid. ^{1}H NMR (400 MHz, CD_3OD) δ 8.89 (s, 2H), 8.33 (d, J = 36.0 Hz, 4H), 7.66 (dd, J = 7.8, 28.2 Hz, 4H), 7.54 – 7.43 (m, 1H), 5.54 – 5.38 (m, 3H), 3.82 – 3.73 (m, 1H), 3.68 – 3.60 (m, 1H), 2.63 – 2.54 (m, 1H), 2.53 – 2.45 (m, 1H), 2.29 – 2.20 (m, 1H), 2.15 – 2.04 (m, 1H); ^{13}C NMR (101 MHz CD_3OD) 179.29, 168.66, 159.51, 157.07, 156.93, 142.70, 141.73, 133.22, 131.35 (q, $^2J_{CF_3}$ = 32.1 Hz), 131.06, 129.25, 128.82, 126.88, 126.64 (q, $^3J_{CF_3}$ = 3.7 Hz), 124.19, 121.51, 115.34, 71.44, 56.50, 32.79, 24.35; HRMS (ESI+): calcd for $C_{26}H_{24}F_3N_6O_2$ [M + H]$^+$ 509.1907; found, 509.1919.

(S)-2-(3-(4'-(trifluoromethyl)-6-((4-(trifluoromethyl)benzyl)oxy)-[1,1'-biphenyl]-3-yl)-1,2,4-oxadiazol-5-yl)pyrrolidine-1-carboximidamide (**2.15d**). Synthesized by General Procedure 2E: 102 mg, 86%, white solid. ^{1}H NMR (400 MHz, CD_3OD) δ 8.11 – 8.02 (m, 2H), 7.77 – 7.71 (m, 4H), 7.58 (dd, J = 7.7, 44.6 Hz, 4H), 7.34 (d, J = 9.2 Hz, 1H), 5.45 (d, J = 7.2 Hz, 1H), 5.32 (s, 2H), 3.81 – 3.74 (m, 1H), 3.67 – 3.58 (m, 1H), 2.63 – 2.43 (m, 2H), 2.28 – 2.19 (m, 1H), 2.15 – 2.01 (m, 1H); ^{13}C NMR (101 MHz CD_3OD) 178.97, 169.10, 159.19, 157.07, 142.86 (q, $^4J_{CF_3}$ = 1.4 Hz), 142.44 (q, $^4J_{CF_3}$ = 1.4 Hz), 131.67, 131.26, 131.06 (d, $^2J_{CF_3}$ = 32.3 Hz), 130.84, 130.56 (d, $^2J_{CF_3}$ = 32.3 Hz), 130.15, 128.60, 126.42 (q, $^3J_{CF_3}$ = 3.8 Hz), 126.04 (q, $^3J_{CF_3}$ = 3.9 Hz), 125.73

(d, $^{1}J_{CF_3}$ = 271.5 Hz), 125.55 (d, $^{1}J_{CF_3}$ = 271.1 Hz), 120.81, 114.76, 70.84, 56.48, 32.73, 24.34; HRMS (ESI+): calcd for $C_{28}H_{24}F_6N_5O_2$ $[M]^+$ 576.1829; found, 576.1838.

(S)-2-(3-(3-cyclopropyl-4-((4-(trifluoromethyl)benzyl)oxy)phenyl)-1,2,4-oxadiazol-5-yl)pyrrolidine-1-carboximidamide (**2.15e**). Synthesized by General Procedure 2E: 102 mg, 86%, white solid. ^{1}H NMR (400 MHz, CD_3OD) δ 7.84 (dd, *J* = 2.1, 8.5 Hz, 1H), 7.71 (s, 4H), 7.58 (d, *J* = 2.1 Hz, 1H), 5.42 (d, *J* = 7.9 Hz, 1H), 5.32 (s, 2H), 3.82 – 3.74 (m, 1H), 3.66 – 3.57 (m, 1H), 2.61 – 2.44 (m, 2H), 2.31 – 2.19 (m, 2H), 2.14 – 2.03 (m, 1H), 1.01 (q, *J* = 5.7 Hz, 2H), 0.70 (q, *J* = 5.2 Hz, 2H); ^{13}C NMR (101 MHz CD_3OD) 178.70, 169.51, 161.25, 157.08, 143.06, 134.59, 131.02 (d, $^{2}J_{CF_3}$ = 32.2 Hz), 128.69, 127.34, 126.48 (q, $^{3}J_{CF_3}$ = 3.8 Hz), 125.37, 122.60, 120.09, 113.01, 70.38, 56.47, 32.73, 28.12, 24.35, 10.66, 8.11; HRMS (ESI+): calcd for $C_{24}H_{25}F_3N_5O_2$ $[M + H]^+$ 472.1955; found, 472.1980.

(S)-2-(3-(4-((4-(trifluoromethyl)benzyl)oxy)phenyl)-1,2,4-oxadiazol-5-yl)pyrrolidine-1-carboximidamide (**2.15f**). Synthesized by General Procedure 2E: 68 mg, 38%, white solid. ^{1}H NMR (400 MHz, CD_3OD) δ 8.01 (d, *J* = 8.9 Hz, 2H), 7.69 (q, *J* = 8.2 Hz, 4H), 7.17 (d, *J* = 8.2 Hz, 2H), 5.43 (d, *J* = 8.2 Hz, 1H), 5.28 (s, 2H), 3.77 (t, *J* = 9.3 Hz, 1H), 3.62 (q, *J* = 9.1 Hz, 1H), 2.62 – 2.44 (m, 2H), 2.29 – 2.19 (m, 1H), 2.16 – 2.03 (m, 1H); ^{13}C NMR (101 MHz CD_3OD) 178.74, 169.34, 162.61, 157.07, 142.79 (d, $^{4}J_{CF_3}$ = 1.3 Hz), 130.17, 128.85, 126.47 (q, $^{3}J_{CF_3}$ = 3.7 Hz), 124.30, 120.37, 116.43, 70.17, 56.46, 32.70, 24.32; HRMS (ESI+): calcd for $C_{21}H_{21}F_3N_5O_2$ $[M + H]^+$ 432.1642; found, 432.1643.

(S)-2-(3-(3-bromo-4-((4-(trifluoromethyl)benzyl)oxy)phenyl)-1,2,4-oxadiazol-5-yl)pyrrolidine-1-carboximidamide (**2.15g**). Synthesized by General Procedure 2E: 42 mg, 80%, white solid. ^{1}H NMR (400 MHz, CD_3OD) δ 8.23 (d, *J* = 2.0 Hz, 1H), 8.00 (dd, *J* = 2.1, 8.6 Hz, 1H), 7.74 – 7.67 (m, 4H), 7.26 (d, *J* = 8.5 Hz, 1H), 5.46 (d, *J* = 8.0 Hz, 1H), 5.35 (s, 2H), 3.78 (t, *J* = 9.5 Hz, 1H),

3.63 (q, J = 9.1 Hz, 1H), 2.62 – 2.43 (m, 2H), 2.28 – 2.18 (m, 1H), 2.15 – 2.02 (m, 1H); ^{13}C NMR (101 MHz CD_3OD) 179.09, 168.27, 158.64, 157.05, 142.20 (d, $^4J_{CF_3}$ = 1.2 Hz), 133.25, 131.13 (q, $^2J_{CF_3}$ = 32.4 Hz), 129.21, 128.60, 126.48 (q, $^3J_{CF_3}$ = 3.7 Hz), 125.58 (q, $^1J_{CF_3}$ = 271.5 Hz), 121.67, 114.99, 113.49, 71.02, 56.45, 32.69, 24.31; HRMS (ESI+): calcd for $C_{21}H_{20}BrF_3N_5O_2$ [M + H]$^+$ 510.0747; found, 510.0750.

(S)-2-(3-(3,5-dimethyl-4-((4-(trifluoromethyl)benzyl)oxy)phenyl)-1,2,4-oxadiazol-5-yl)pyrrolidine-1-carboximidamide (**2.15h**). Synthesized by General Procedure 2E: 67 mg, 91%, white solid. ^{1}H NMR (400 MHz, CD_3OD) δ 7.75 (s, 2H), 7.70 (t, J = 9.6 Hz, 4H), 5.46 (d, J = 7.9 Hz, 1H), 4.98 (s, 2H), 3.78 (t, J = 9.6 Hz, 1H), 3.63 (q, J = 8.9 Hz, 1H), 2.62 – 2.51 (m, 1H), 2.51 – 2.43 (m, 1H), 2.33 (s, 6H), 2.28 – 2.19 (m, 1H), 2.15 – 2.02 (m, 1H); ^{13}C NMR (101 MHz CD_3OD) 178.83, 169.32, 159.69, 157.06, 143.26 (d, $^4J_{CF_3}$ = 1.2 Hz), 133.32, 131.12 (q, $^2J_{CF_3}$ = 32.4 Hz), 129.18, 129.15, 126.41 (q, $^3J_{CF_3}$ = 3.7 Hz), 125.55 (q, $^1J_{CF_3}$ = 272.1 Hz), 123.30, 74.12, 56.45, 32.71, 24.32, 16.62; HRMS (ESI+): calcd for $C_{23}H_{25}F_3N_5O_2$ [M + H]$^+$ 460.1955; found, 460.1969.

(S)-2-(3-(3-chloro-4-((4-(trifluoromethyl)benzyl)oxy)phenyl)-1,2,4-oxadiazol-5-yl)pyrrolidine-1-carboximidamide (**2.15i**). Synthesized by General Procedure 2E: 62 mg, 88%, white solid. ^{1}H NMR (400 MHz, CD_3OD) δ 8.03 (d, J = 2.1 Hz, 1H), 7.94 (dd, J = 2.1, 8.5 Hz, 1H), 7.69 (s, 4H), 7.27 (d, J = 8.7 Hz, 1H), 5.47 (d, J = 8.0 Hz, 1H), 5.33 (s, 2H), 3.79 (t, J = 9.4 Hz, 1H), 3.63 (q, J = 9.1 Hz, 1H), 2.63 – 2.51 (m, 1H), 2.50 – 2.42 (m, 1H), 2.29 – 2.18 (m, 1H), 2.16 – 2.02 (m, 1H); ^{13}C NMR (101 MHz CD_3OD) 179.06, 168.37, 157.68, 157.04, 142.16 (d, $^4J_{CF_3}$ = 1.3 Hz), 131.10 (q, $^2J_{CF_3}$ = 32.5 Hz), 130.95, 128.61, 128.50, 126.46 (q, $^3J_{CF_3}$ = 3.8 Hz), 125.53 (q, $^1J_{CF_3}$ = 271.4 Hz), 124.57, 121.20, 115.20, 70.93, 56.42, 32.67, 24.31; HRMS (ESI+): calcd for $C_{21}H_{20}ClF_3N_5O_2$ [M]$^+$ 466.1252; found, 466.1235.

(S)-2-(3-(3-fluoro-4-((4-(trifluoromethyl)benzyl)oxy)phenyl)-1,2,4-oxadiazol-5-yl)pyrrolidine-1-carboximidamide (**2.15j**). Synthesized by General Procedure 2E: 132 mg, 96%, white solid. ^{1}H NMR (400 MHz, CD_3OD) δ 7.82 – 7.72 (m, 2H), 7.67 (dd, *J* = 8.8, 12.8 Hz, 4H), 7.29 (t, *J* = 8.5 Hz, 1H), 5.48 (d, *J* = 7.8 Hz, 1H), 5.31 (s, 2H), 3.78 (t, *J* = 9.4 Hz, 1H), 3.63 (q, *J* = 8.2 Hz, 1H), 2.62 – 2.51 (m, 1H), 2.48 – 2.42 (m, 1H), 2.27 – 2.19 (m, 1H), 2.14 – 2.02 (m, 1H); ^{13}C NMR (101 MHz CD_3OD) 179.06, 168.55 (d, $^{4}J_{CF}$ = 2.6 Hz), 157.04, 153.72 (d, $^{1}J_{CF}$ = 246.4 Hz), 150.52 (d, $^{2}J_{CF}$ = 10.8 Hz), 142.16 (q, $^{4}J_{CF_3}$ = 1.2 Hz), 131.17 (q, $^{2}J_{CF_3}$ = 32.0 Hz), 128.87, 126.47 (q, $^{3}J_{CF_3}$ = 3.8 Hz), 125.47 (q, $^{1}J_{CF_3}$ = 271.0 Hz), 125.28 (d, $^{4}J_{CF}$ = 3.6 Hz), 120.84 (d, $^{3}J_{CF}$ = 7.1 Hz), 116.57 (d, $^{3}J_{CF}$ = 1.6 Hz), 115.98 (d, $^{2}J_{CF}$ = 20.8 Hz), 71.10, 56.41, 32.65, 24.30; HRMS (ESI+): calcd for $C_{21}H_{20}F_4N_5O_2$ $[M + H]^+$ 450.1548; found, 450.1555.

(S)-2-(3-(3-methoxy-4-((4-(trifluoromethyl)benzyl)oxy)phenyl)-1,2,4-oxadiazol-5-yl)pyrrolidine-1-carboximidamide (**2.15k**). Synthesized by General Procedure 2E: 132 mg, 96%, white solid. ^{1}H NMR (400 MHz, CD_3OD) δ 7.72 – 7.60 (m, 6H), 7.14 (d, *J* = 8.1 Hz, 1H), 5.44 (d, *J* = 7.7 Hz, 1H), 5.27 (s, 2H), 3.93 (s, 3H), 3.77 (t, *J* = 9.4 Hz, 1H), 3.62 (q, *J* = 8.0 Hz, 1H), 2.62 – 2.43 (m, 2H), 2.28 – 2.18 (m, 1H), 2.16 – 2.02 (m, 1H); ^{13}C NMR (101 MHz CD_3OD) 178.79, 169.43, 157.07, 152.23, 151.39, 142.83 (d, $^{4}J_{CF_3}$ = 1.3 Hz), 131.06 (d, $^{2}J_{CF_3}$ = 32.9 Hz), 128.88, 126.41 (q, $^{3}J_{CF_3}$ = 3.8 Hz), 125.61 (d, $^{1}J_{CF_3}$ = 271.9 Hz), 122.05, 120.75, 115.06, 111.66, 70.96, 56.60, 56.47, 32.74, 24.34; HRMS (ESI+): calcd for $C_{22}H_{23}F_3N_5O_3$ $[M + H]^+$ 462.1748; found, 462.1757.

(S)-2-(3-(2-chloro-4-((4-(trifluoromethyl)benzyl)oxy)phenyl)-1,2,4-oxadiazol-5-yl)pyrrolidine-1-carboximidamide (**2.15l**). Synthesized by General Procedure 2E: 28 mg, 59%, white solid. ^{1}H NMR (400 MHz, CD_3OD) δ 7.89 (d, *J* = 8.4 Hz, 1H), 7.68 (q, *J* = 8.7 Hz, 4H), 7.27 (s, 1H), 7.13 (d, *J* = 8.1 Hz, 1H), 5.46 (d, *J* = 7.0 Hz, 1H), 5.28 (s, 2H), 3.76 (t, *J* = 8.7 Hz, 1H), 3.62 (q, *J* = 8.4 Hz, 1H), 2.63 – 2.43 (m, 2H), 2.28 – 2.19 (m, 1H), 2.14 – 2.02 (m, 1H); ^{13}C NMR (101 MHz

CD_3OD) 178.23, 168.14, 162.38, 157.04, 142.22 135.51, 134.01, 131.18 (q, $^2J_{CF_3}$ = 32.2 Hz), 128.95, 126.50 (q, $^3J_{CF_3}$ = 3.7 Hz), 125.55 (q, $^1J_{CF_3}$ = 271.4 Hz), 119.37, 118.37, 115.04, 70.57, 56.43, 32.71, 24.32; HRMS (ESI+): calcd for $C_{21}H_{19}ClF_3N_5O_2$ [M + H]$^+$ 466.1252; found, 466.1241.

(S)-2-(3-(2-(trifluoromethyl)-4-((4-(trifluoromethyl)benzyl)oxy)phenyl)-1,2,4-oxadiazol-5-yl)pyrrolidine-1-carboximidamide (**2.15m**). Synthesized by General Procedure 2E: 100 mg, 63%, white solid. ^{1}H NMR (400 MHz, CD_3OD) δ 7.82 (d, *J* = 8.6 Hz, 1H), 7.69 (dd, *J* = 8.5, 13.8 Hz, 4H), 7.50 (d, *J* = 2.4 Hz, 1H), 7.40 (d, *J* = 9.0 Hz, 1H), 5.51 (d, *J* = 7.9 Hz, 1H), 5.34 (s, 2H), 3.75 (t, *J* = 9.4 Hz, 1H), 3.62 (q, *J* = 8.9 Hz, 1H), 2.63 – 2.52 (m, 1H), 2.48 – 2.41 (m, 1H), 2.28 – 2.20 (m, 1H), 2.12 – 1.99 (m, 1H); ^{13}C NMR (101 MHz CD_3OD) 178.73, 168.57, 161.81, 157.04, 142.09 (q, $^4J_{CF_3}$ = 1.3 Hz), 134.93, 131.70 (q, $^2J_{CF_3}$ = 32.1 Hz), 131.22 (q, $^2J_{CF_3}$ = 32.1 Hz), 128.97, 126.52 (q, $^3J_{CF_3}$ = 3.9 Hz), 125.58 (q, $^1J_{CF_3}$ = 271.4 Hz), 124.53 (q, $^1J_{CF_3}$ = 272.3 Hz), 118.70, 118.34 (q, $^3J_{CF_3}$ = 2.0 Hz), 115.51 (q, $^3J_{CF_3}$ = 5.6 Hz), 70.63, 56.30, 32.65, 24.18; HRMS (ESI+): calcd for $C_{22}H_{20}F_6N_5O_2$ [M + H]$^+$ 500.1516; found, 500.1516.

(S)-2-(3-(3-nitro-4-((4-(trifluoromethyl)benzyl)oxy)phenyl)-1,2,4-oxadiazol-5-yl)pyrrolidine-1-carboximidamide (**2.15n**). Synthesized by General Procedure 2E: 100 mg, 63%, white solid. ^{1}H NMR (400 MHz, CD_3OD) δ 8.41 (s, 1H), 8.21 (br s, 1H), 7.67 (s, 4H), 7.54 – 7.45 (m, 1H), 5.52 (s, 1H), 5.42 (s, 2H), 3.85 – 3.77 (m, 1H), 3.65 (br s, 1H), 2.52 (d, *J* = 43.2 Hz, 2H), 2.18 (d, *J* = 51.4 Hz, 2H); ^{13}C NMR (101 MHz CD_3OD) 179.42, 167.73, 156.98, 154.78, 141.38 (d, $^4J_{CF_3}$ = 1.3 Hz), 141.13, 134.00, 131.13 (q, $^2J_{CF_3}$ = 31.8 Hz), 128.58, 126.45 (q, $^3J_{CF_3}$ = 3.7 Hz), 125.42, 125.39 (q, $^1J_{CF_3}$ = 271.5 Hz), 120.35, 117.17, 71.61, 56.45, 32.72, 24.36; HRMS (ESI+): calcd for $C_{21}H_{20}F_3N_6O_4$ [M + H]$^+$ 477.1493; found, 477.1493.

(S)-2-(3-(3-(tert-butyl)-4-((4-(trifluoromethyl)benzyl)oxy)phenyl)-1,2,4-oxadiazol-5-yl)pyrrolidine-1-carboximidamide (**2.15o**). Synthesized by General Procedure 2E: 25 mg, 58%, white solid. ^{1}H NMR (400 MHz, CD_3OD) δ 8.02 (d, *J* = 2.1 Hz, 1H), 7.89 (dd, *J* = 2.2, 8.6 Hz, 1H), 7.72 (dd, *J* = 9.0, 13.0 Hz, 4H), 7.17 (d, *J* = 9.0 Hz, 1H), 5.44 (d, *J* = 8.1 Hz, 1H), 5.32 (s, 2H), 3.78 (t, *J* = 9.5 Hz, 1H), 3.62 (q, *J* = 8.9 Hz, 1H), 2.62 – 2.51 (m, 1H), 2.51 – 2.44 (m, 1H), 2.28 – 2.20 (m, 1H), 2.16 – 2.04 (m, 1H), 1.44 (s, 9H); ^{13}C NMR (101 MHz CD_3OD) 178.67, 169.75, 161.33, 157.13, 142.77 (d, $^4J_{CF_3}$ = 1.3 Hz), 140.19, 131.20 (q, $^2J_{CF_3}$ = 32.3 Hz), 129.20, 128.12, 127.03, 126.57 (q, $^3J_{CF_3}$ = 3.8 Hz), 125.67 (q, $^1J_{CF_3}$ = 272.7 Hz), 119.84, 114.11, 70.70, 56.47, 35.95, 32.71, 30.12, 24.36; HRMS (ESI+): calcd for $C_{25}H_{29}F_3N_5O_2$ $[M + H]^+$ 488.2268; found, 488.2293.

(S)-2-(3-(3-allyl-4-((4-(trifluoromethyl)benzyl)oxy)phenyl)-1,2,4-oxadiazol-5-yl)pyrrolidine-1-carboximidamide (**2.15p**). Synthesized by General Procedure 2E: 24 mg, 79%, white solid. ^{1}H NMR (400 MHz, CD_3OD) δ 7.91 (d, *J* = 8.6 Hz, 1H), 7.86 (s, 1H), 7.69 (dd, *J* = 8.2, 15.5 Hz, 4H), 7.15 (d, *J* = 8.6 Hz, 1H), 6.09 – 5.96 (m, 1H), 5.44 (d, *J* = 7.5 Hz, 1H), 5.29 (s, 2H), 5.11 – 5.03 (m, 2H), 3.78 (t, *J* = 9.2 Hz, 1H), 3.62 (q, *J* = 10.1 Hz, 1H), 3.50 (d, *J* = 6.4 Hz, 2H), 2.61 – 2.51 (m, 1H), 2.50 – 2.42 (m, 1H), 2.27 – 2.18 (m, 1H), 2.14 – 2.02 (m, 1H); ^{13}C NMR (101 MHz CD_3OD) 178.71, 169.45, 160.17, 157.13, 142.91, 137.49, 131.09 (q, $^2J_{CF_3}$ = 32.4 Hz), 131.01, 130.12, 128.71, 128.38, 126.46 (q, $^3J_{CF_3}$ = 3.7 Hz), 125.58 (q, $^1J_{CF_3}$ = 271.3 Hz), 120.16, 116.35, 113.23, 70.32, 56.44, 35.34, 32.69, 24.34; HRMS (ESI+): calcd for $C_{24}H_{25}F_3N_5O_2$ $[M + H]^+$ 472.1955; found, 472.1947.

(S)-2-(3-(3-propyl-4-((4-(trifluoromethyl)benzyl)oxy)phenyl)-1,2,4-oxadiazol-5-yl)pyrrolidine-1-carboximidamide (**2.15q**). Synthesized by General Procedure 2E: 218 mg, 77%, white solid. ^{1}H NMR (400 MHz, CD_3OD) δ 7.84 (d, *J* = 8.3 Hz, 1H), 7.79 (s, 1H), 7.62 (q, *J* = 8.3 Hz, 4H), 7.05

(d, J = 8.0 Hz, 1H), 5.53 (d, J = 7.5 Hz, 1H), 5.18 (s, 2H), 3.80 (t, J = 9.1 Hz, 1H), 3.64 (q, J = 8.5 Hz, 1H), 2.64 (t, J = 7.5 Hz, 2H), 2.59 – 2.50 (m, 1H), 2.46 – 2.39 (m, 1H), 2.25 – 2.17 (m, 1H), 2.11 – 2.00 (m, 1H), 1.61 (sx, J = 7.1 Hz, 2H), 0.91 (t, J = 7.2 Hz, 3H); ^{13}C NMR (101 MHz CD_3OD) 178.58, 169.33, 160.10, 156.96, 142.81 (d, $^4J_{CF_3}$ = 1.3 Hz), 132.99, 130.77 (q, $^2J_{CF_3}$ = 32.4 Hz), 129.96, 128.44, 127.94, 126.36 (q, $^3J_{CF_3}$ = 3.8 Hz), 125.56 (q, $^2J_{CF_3}$ = 271.5 Hz), 119.80, 112.93, 70.02, 56.35, 33.33, 32.61, 24.31, 23.90, 14.33; HRMS (ESI+): calcd for $C_{24}H_{27}F_3N_5O_2$ $[M + H]^+$ 474.2111; found, 474.2112.

(S)-2-(3-(3-ethyl-4-((4-(trifluoromethyl)benzyl)oxy)phenyl)-1,2,4-oxadiazol-5-yl)pyrrolidine-1-carboximidamide (**2.15s**). Synthesized by General Procedure 2E: 32 mg, 77%, white solid. ^{1}H NMR (400 MHz, CD_3OD) δ 7.89 – 7.84 (m, 2H), 7.68 (q, J = 6.9 Hz, 4H), 7.11 (q, J = 8.3 Hz, 1H), 5.45 (d, J = 7.0 Hz, 1H), 5.27 (s, 2H), 3.78 (t, J = 8.7 Hz, 1H), 3.62 (q, J = 8.7 Hz, 1H), 2.76 (q, J = 7.7 Hz, 2H), 2.61 – 2.51 (m, 1H), 2.49 – 2.43 (m, 1H), 2.27 – 2.19 (m, 1H), 2.14 – 2.04 (m, 1H), 1.24 (m, J = 7.4 Hz, 3H); ^{13}C NMR (101 MHz CD_3OD) 178.66, 169.45, 160.16, 157.03, 142.97 (d, $^4J_{CF_3}$ = 1.4 Hz), 134.76, 130.98 (q, $^2J_{CF_3}$ = 32.0 Hz), 129.17, 128.64, 127.92, 126.47 (q, $^3J_{CF_3}$ = 3.8 Hz), 125.63 (q, $^1J_{CF_3}$ = 271.1 Hz), 120.03, 112.95, 70.15, 56.45, 32.71, 24.48, 24.34, 14.55; HRMS (ESI+): calcd for $C_{23}H_{25}F_3N_5O_2$ $[M]^+$ 460.1955; found, 460.1955.

3-methyl-4-((4-(trifluoromethyl)benzyl)oxy)benzonitrile (**2.17**). Synthesized according to the following protocol: To a solution of THF (0.2 M), 4-(trifluoromethyl)benzyl alcohol (1.2 equiv) was added followed by blanking with nitrogen gas and chilled to 0 ºC. Next, sodium hydride (1.1 equiv) was added and stirred for 5 minutes. 4-fluoro-3-methylbenzonitrile was then added and the reaction was allowed to warm to room temperature and stirred for 16 hours. Subsequently, the resulting solution was partitioned between EtOAc and brine solution. Using additional EtOAc, the brine solution was washed three times and the combined organic layers were dried over Na_2SO_4,

filtered, and concentrated *via* vacuum. The resulting concentrate was purified by silica gel chromatography to yield the final product; 234 mg, 54%, white solid. ^{1}H NMR (400 MHz, $CDCl_3$) δ 7.61 (dd, J = 8.1, 49.1 Hz, 4H), 7.50 – 7.43 (m, 2H), 6.89 (d, J = 8.6 Hz, 1H), 5.19 (s, 2H), 2.30 (s, 3H); ^{13}C NMR (101 MHz CD_3OD) 159.87, 140.23 (d, $^{4}J_{CF_3}$ = 1.4 Hz), 134.34, 132.03, 130.54 (q, $^{2}J_{CF_3}$ = 32.4 Hz), 128.67, 127.25, 125.82 (q, $^{3}J_{CF_3}$ = 3.8 Hz), 124.12 (q, $^{1}J_{CF_3}$ = 271.7 Hz), 119.38, 111.47, 104.30, 69.31, 16.33; HRMS (ESI+): calcd for $C_{16}H_{13}F_3NO$ $[M + H]^+$ 292.0944; found, 292.0924.

N'-hydroxy-3-methyl-4-((4-(trifluoromethyl)benzyl)oxy)benzimidamide (**2.18**). Synthesized by General Procedure 2C: 183 mg, 70%, white solid. ^{1}H NMR (400 MHz, CD_3OD) δ 7.65 (q, J = 9.3 Hz, 4H), 7.47 – 7.41 (m, 2H), 6.95 (d, J = 8.5 Hz, 1H), 5.20 (s, 2H), 2.29 (s, 3H); ^{13}C NMR (101 MHz CD_3OD) 159.10, 155.59, 143.29 (d, $^{4}J_{CF_3}$ = 1.3 Hz), 130.88 (q, $^{2}J_{CF_3}$ = 32.3 Hz), 129.70, 128.55, 127.96, 126.47, 126.39 (q, $^{3}J_{CF_3}$ = 3.9 Hz), 126.20, 125.58 (d, $^{1}J_{CF_3}$ = 272.5 Hz), 112.25, 69.99, 16.53; HRMS (ESI+): calcd for $C_{16}H_{16}F_3N_2O_2$ $[M + H]^+$ 325.1158; found, 325.1125.

tert-butyl (S)-2-(3-(3-methyl-4-((4-(trifluoromethyl)benzyl)oxy)phenyl)-1,2,4-oxadiazol-5-yl)pyrrolidine-1-carboxylate (**2.19**). Synthesized by General Procedure 2D: 47 mg, 32%, yellow oil. ^{1}H NMR (400 MHz, $CDCl_3$) δ 7.94 – 7.83 (m, 2H), 7.60 (dd, J = 7.9, 37.2 Hz, 4H), 6.95 – 6.87 (m, 1H), 5.22 – 5.02 (m, 3H), 3.76 – 3.62 (m, 1H), 3.60 – 3.46 (m, 1H), 2.46 – 2.29 (m, 4H), 2.19 – 2.08 (m, 2H), 2.04 – 1.95 (m, 1H), 1.46 (s, 3H), 1.29 (s, 6H); ^{13}C NMR (101 MHz $CDCl_3$) 180.49, 168.18, 158.92, 153.68, 140.98, 130.00, 127.84, 127.21, 126.74, 125.67 (d, $^{3}J_{CF_3}$ = 3.7 Hz), 124.16 (d, $^{1}J_{CF_3}$ = 272.4 Hz), 119.38, 111.29, 80.52, 69.12, 53.93, 46.46, 32.51, 28.49, 28.25, 23.82, 16.44; HRMS (ESI+): calcd for $C_{26}H_{28}F_3N_3NaO_4$ $[M + Na]^+$ 526.1924; found, 526.1935.

(S)-2-(3-(3-methyl-4-((4-(trifluoromethyl)benzyl)oxy)phenyl)-1,2,4-oxadiazol-5-yl)pyrrolidine-1-carboximidamide (**2.20**). Synthesized by General Procedure 2E: 75 mg, 65%, white solid. ^{1}H NMR

(400 MHz, CD_3OD) δ 7.88 – 7.84 (m, 2H), 7.68 (dd, *J* = 8.7, 14.6 Hz, 4H), 7.09 (d, *J* = 9.3 Hz, 1H), 5.45 (d, *J* = 7.8 Hz, 1H), 5.27 (s, 2H), 3.78 (t, *J* = 9.6 Hz, 1H), 3.62 (q, *J* = 8.6 Hz, 1H), 2.61 – 2.51 (m, 1H), 2.49 – 2.42 (m, 1H), 2.33 (s, 3H), 2.27 – 2.19 (m, 1H), 2.14 – 2.03 (m, 1H); ^{13}C NMR (101 MHz $CDCl_3$) 178.65, 169.42, 160.57, 157.05, 142.99 (d, $^4J_{CF_3}$ = 1.3 Hz), 130.98 (q, $^2J_{CF_3}$ = 32.5 Hz), 130.63, 128.84, 128.63, 127.88, 126.46 (q, $^3J_{CF_3}$ = 3.9 Hz), 125.59 (q, $^1J_{CF_3}$ =271.2 Hz), 119.87, 112.71, 70.12, 56.43, 32.68, 24.32, 16.50; HRMS (ESI+): calcd for $C_{22}H_{23}F_3N_5O_2$ $[M + H]^+$ 446.1798; found, 446.1800.

3-acetyl-4-((4-(trifluoromethyl)benzyl)oxy)benzonitrile (**2.22**). Synthesized by General Procedure 2B: 219 mg, 92%, white solid. ^1H NMR (400 MHz, $CDCl_3$) δ 7.92 (s, 1H), 7.69 – 7.50 (m, 5H), 7.11 (d, *J* = 8.3 Hz, 1H), 5.29 (s, 2H), 2.55 (s, 3H); ^{13}C NMR (101 MHz $CDCl_3$) 197.12, 160.21, 138.93 (d, $^4J_{CF_3}$ = 1.2 Hz), 136.97, 134.67, 130.54 (q, $^2J_{CF_3}$ = 32.4 Hz), 129.12, 127.77, 125.72 (q, $^3J_{CF_3}$ = 3.7 Hz), 123.82 (q, $^1J_{CF_3}$ = 272.7 Hz), 118.05, 113.67, 104.71, 70.25, 31.69; HRMS (ESI+): calcd for $C_{17}H_{13}F_3NO_2$ $[M + H]^+$ 320.0893; found, 320.0896.

3-(prop-1-en-2-yl)-4-((4-(trifluoromethyl)benzyl)oxy)benzonitrile (**2.23**). Synthesized according to the following protocol: To a solution of THF (0.2 M) methyltriphenylphosphonium bromide (2 equiv) was added followed by cooling reaction to 0 ºC and put under an N_2 atmosphere. Next, *n*-BuLi (2.0 equiv) was added to reaction mixture dropwise and allowed to stir for 10 minutes. 1 equivalent of 3-acetyl-4-((4-(trifluoromethyl)benzyl)oxy)benzonitrile (compound 2.22) was added portion wise, and the resulting reaction mixture was allowed to warm to room temperature and stir for 18 hours. Subsequently, the resulting solution was partitioned between EtOAc and brine solution. Using additional EtOAc, the brine solution was washed three times and the combined organic layers were dried over Na_2SO_4, filtered, and concentrated *via* vacuum. The resulting concentrate was purified by silica gel chromatography to yield the final product; 60 mg, 61%,

white solid. ^{1}H NMR (400 MHz, $CDCl_3$) δ 7.68 – 7.48 (m, 6H), 6.94 (d, J = 8.4 Hz, 1H), 5.25 – 5.20 (m, 3H), 5.11 (s, 1H), 2.12 (s, 3H); ^{13}C NMR (101 MHz $CDCl_3$) 158.70, 142.04, 139.98 (d, $^4J_{CF_3}$ = 1.3 Hz), 134.52, 133.42, 133.01, 130.47 (q, $^2J_{CF_3}$ = 32.5 Hz), 127.27, 125.80 (q, $^3J_{CF_3}$ = 3.8 Hz), 124.08 (q, $^1J_{CF_3}$ = 272.4 Hz), 119.13, 117.19, 112.47, 104.62, 69.63, 22.95; HRMS (ESI+): calcd for $C_{18}H_{15}F_3NO$ $[M + H]^+$ 318.1100; found, 318.1091.

N'-hydroxy-3-(prop-1-en-2-yl)-4-((4-(trifluoromethyl)benzyl)oxy)benzimidamide (**2.24**). Synthesized by General Procedure 2C: 556 mg, 90%, white solid. ^{1}H NMR (400 MHz, $CDCl_3$) δ 7.68 – 7.47 (m, 6H), 6.98 (d, J = 9.0 Hz, 1H), 5.19 – 5.07 (m, 4H), 2.10 (s, 3H); ^{13}C NMR (101 MHz $CDCl_3$) 157.86, 155.21, 145.03, 142.90 (d, $^4J_{CF_3}$ = 1.4 Hz), 134.31, 130.83 (q, $^2J_{CF_3}$ = 32.0 Hz), 128.63, 128.51, 127.51, 126.75, 126.33 (q, $^3J_{CF_3}$ = 3.8 Hz), 125.54 (d, $^1J_{CF_3}$ = 271.4 Hz), 116.19, 113.28, 70.33, 23.51; HRMS (ESI+): calcd for $C_{18}H_{18}F_3N_2O_2$ $[M + H]^+$ 351.1315; found, 351.1295.

tert-butyl(S)-2-(3-(3-(prop-1-en-2-yl)-4-((4-(trifluoromethyl)benzyl)oxy)phenyl)-1,2,4-oxadiazol-5-yl)pyrrolidine-1-carboxylate (**2.25**). Synthesized by General Procedure 2D: 420 mg, 50%, yellow oil. ^{1}H NMR (400 MHz, $CDCl_3$) δ 7.99 – 7.87 (m, 2H), 7.56 (dd, J = 8.1, 37.8 Hz, 4H), 6.99 – 6.90 (m, 1H), 5.22 – 5.00 (m, 5H), 3.73 – 3.61 (m, 1H), 3.56 – 3.43 (m, 1H), 2.41 – 2.28 (m, 1H), 2.16 – 2.04 (m, 5H), 2.00 – 1.91 (m, 1H), 1.43 (s, 3H), 1.28 (s, 6H); ^{13}C NMR (101 MHz $CDCl_3$) 180.46, 167.91, 157.63, 153.53, 142.94, 140.68, 133.80, 130.02 (q, $^2J_{CF_3}$ = 32.4 Hz), 128.76, 127.85, 127.16, 125.52 (d, $^3J_{CF_3}$ = 3.7 Hz), 124.09 (q, $^1J_{CF_3}$ = 271.9 Hz), 119.61, 116.22, 112.24, 80.35. 69.37, 53.79, 46.33, 32.35, 28.10, 23.67, 23.11; HRMS (ESI+): calcd for $C_{28}H_{31}F_3N_3O_4$ $[M + H]^+$ 530.2261; found, 530.2231.

tert-butyl (S)-2-(3-(3-isopropyl-4-((4-(trifluoromethyl)benzyl)oxy)phenyl)-1,2,4-oxadiazol-5-yl)pyrrolidine-1-carboxylate (**2.26**). Synthesized according to the following protocol: To a

solution of ethanol (190 proof, 0.2 M) addition of *tert*-butyl(S)-2-(3-(3-(prop-1-en-2-yl)-4-((4-(trifluoromethyl)benzyl)oxy)phenyl)-1,2,4-oxadiazol-5-yl)pyrrolidine-1-carboxylate (1 equiv, compound 2.25) followed by 10% palladium on carbon (0.1 equiv) was performed and stirred. Reaction mixture was then put under light vacuum followed by purge of hydrogen gas. Vacuum followed by addition of hydrogen gas was repeated three times. The resulting mixture was stirred at room temperature for 18 hours followed by concentration *via* vacuum and purification by silica gel chromatography to yield final product; 178 mg, 72%, yellow oil. ^{1}H NMR (400 MHz, $CDCl_3$) δ 7.96 (s, 1H), 7.90 – 7.84 (m, 1H), 7.59 (dd, J = 7.9, 36.9 Hz, 4H), 6.98 – 6.88 (m, 1H), 5.21 – 5.01 (m, 3H), 3.74 – 3.63 (m, 1H), 3.57 – 3.38 (m, 2H), 2.41 – 2.29 (m, 1H), 2.17 – 2.05 (m, 2H), 1.99 – 1.91 (m, 1H), 1.44 (s, 3H), 1.35 – 1.22 (m, 12H); ^{13}C NMR (101 MHz $CDCl_3$) 180.34, 168.26, 157.88, 153.58, 140.96, 137.93, 130.06 (q, $^{2}J_{CF_3}$ = 32.1 Hz), 127.14, 126.49, 125.56 (q, $^{3}J_{CF_3}$ = 3.6 Hz), 124.18 (q, $^{1}J_{CF_3}$ = 272.2 Hz), 119.62, 111.52, 80.35, 69.11, 53.83, 46.35, 32.37, 28.35, 28.13, 27.08, 23.69, 22.49; HRMS (ESI+): calcd for $C_{28}H_{33}F_3N_3O_4$ $[M + H]^+$ 532.2418; found, 532.2408.

(S)-2-(3-(3-isopropyl-4-((4-(trifluoromethyl)benzyl)oxy)phenyl)-1,2,4-oxadiazol-5-yl)pyrrolidine-1-carboximidamide (**2.27**). Synthesized by General Procedure 2E: 24 mg, 55%, white solid. ^{1}H NMR (400 MHz, $CDCl_3$) δ 7.92 (s, 1H), 7.88 (d, J = 8.5 Hz, 1H), 7.70 (q, J = 7.2 Hz, 4H), 7.14 (d, J = 8.5 Hz, 1H), 5.44 (d, J = 7.6 Hz, 1H), 5.29 (s, 2H), 3.79 (t, J = 9.4 Hz, 1H), 3.62 (q, J = 9.0 Hz, 1H), 3.45 (p, J = 6.6 Hz, 1H), 2.62 – 2.53 (m, 1H), 2.51 – 2.43 (m, 1H), 2.28 – 2.20 (m, 1H), 2.14 – 2.05 (m, 1H), 1.28 (d, J = 7.1 Hz, 6H); ^{13}C NMR (101 MHz $CDCl_3$) 178.70, 169.60, 159.65, 157.07, 142.98 (d, $^{4}J_{CF_3}$ = 1.4 Hz), 139.09, 131.04 (q, $^{2}J_{CF_3}$ = 32.2 Hz), 128.73, 127.73, 126.51 (q, $^{3}J_{CF_3}$ = 3.8 Hz), 126.34, 125.61 (q, $^{1}J_{CF_3}$ = 271.6 Hz), 120.16, 113.18, 70.32,

56.47, 32.74, 28.28, 24.36, 22.88; HRMS (ESI+): calcd for $C_{24}H_{27}F_3N_5O_2$ $[M]^+$ 474.2111; found, 474.2115.

4.2 Enhancing the Oral Bioavailability of Guanidine Containing Drug Leads: An Investigation into Sphingosine Kinase 2

4.2.1 Sphingosine Kinase Biological Assays

Biological assessment of synthesized compounds *via in vivo* mouse studies were conducted as follows. Groups of 8 to 10 week old C57BL/6 mice were orally gavaged (p.o.) with either vehicle or 30 mg/kg test compound (2% solution of hydroxypropyl-β-cyclodextrin, Cargill Cavitron 82004). After 6 hours of administration, whole blood was collected from the retro-orbital sinus and 10 μL of blood was processed for LC/MS analysis as described previously. The use of mice for these studies was approved by the University of Virginia's School of Medicine Animal Care and Use Committee prior to experimentation.

4.2.2 General Material and Synthetic Procedures

All solvents used were dried using a PureSolv solvent system and all chemical reagents were purchased from commercial sources without further purification. Aluminum-backed silica gel, 200 μm, F254 plates were utilized for all thin-layer chromatography (TLC) experiments. A Combiflash Rf purification system with flash grade silica gel, 40−63 μm was used for all column chromatography. All reported ^{1}H NMR spectra were measured at 400 MHz and the complementary ^{13}C NMR frequency was 101 MHz. Reported ^{1}H NMR chemical shifts are in ppm with the solvent resonance as an internal standard ($CDCl_3$: 7.26 ppm; CD_3OD: 3.31 ppm). Reported ^{13}C NMR chemical shifts are in ppm with the solvent resonance as the internal standard ($CDCl_3$: 77.16 ppm; CD_3OD: 49.00 ppm). Reported ^{19}F NMR chemical shifts are referenced to trifluoroacetic acid (-76.55 ppm) as an external standard. High-resolution mass spectrometry (HRMS) data was obtained using an Agilent 6220 Accurate-MS TOF LC-MS electrospray ionization (ESI). All compounds tested in biological assays possess ≥95% purity, as determined

by HPLC analyses. HPLC was performed using a Thermo Electron TSQ triple quadrupole mass spectrometer fitted with an ESI source.

General Procedure 3A: Nucleophilic Substitution of Guanidine Derivatives with Acyl Chlorides. (S)-2-(3-(4-(2-cyclohexylethoxy)-3-(trifluoromethyl)phenyl)-1,2,4-oxadiazol-5-yl)pyrrolidine-1-carboximidamide hydrochloride (**3.14**) (1.0 equiv) was dissolved in CH_2Cl_2 (0.2 M solution) and put under a argon gas atmosphere. Next *N*,*N*-diisopropylethylamine (2.0 equiv) was added followed by dropwise addition of the appropriate acyl chloride (1.1 equiv). The reaction mixture was stirred at room temperature for 10 minutes. The reaction progress was monitored by TLC. Afterward, the reaction was concentrated *via* vacuum and then purified by silica gel chromatography to yield the desired product.

General Procedure 3B: Nucleophilic Substitution of Guanidine Derivatives with Sulfonyl Chlorides. (S)-2-(3-(4-(2-cyclohexylethoxy)-3-(trifluoromethyl)phenyl)-1,2,4-oxadiazol-5-yl)pyrrolidine-1-carboximidamide hydrochloride (**3.14**) (1.0 equiv) was dissolved in CH_2Cl_2 (0.2 M solution) and put under a argon gas atmosphere. Next *N*,*N*-diisopropylethylamine (2.0 equiv) was added followed by dropwise addition of the appropriate sulfonyl chloride (1.1 equiv). The reaction mixture was stirred at room temperature for 10 minutes. The reaction progress was monitored by TLC. Afterward, the reaction was concentrated *via* vacuum and then purified by silica gel chromatography to yield the desired product.

4.2.3 Characterization

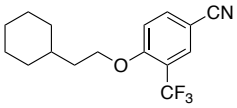

4-(2-cyclohexylethoxy)-3-(trifluoromethyl)benzonitrile (**3.16**). Synthesized according to the following protocol: To a solution of THF (0.2 M), 2-cyclohexylethan-1-ol (1.0 equiv) was added followed by purging with argon gas then cooling to 0 ºC with a brine/ice bath. Next, sodium hydride (1.1 equiv) was added and the reaction stirred for 5 minutes. 4-fluoro-3-(trifluoromethyl)benzonitrile (**3.15**) was then added and the reaction was allowed to warm to room temperature and stir for 18 hours. The reaction progress was monitored by TLC. After, the resulting solution was slowly quenched with methanol, and concentrated *via* vacuum. The resulting concentrate was purified by silica gel chromatography to yield the final product; 1.374 g, 87%, yellow solid. ^{1}H NMR (400 MHz, $CDCl_3$) δ 7.78-7.71 (m, 2H), 7.07 (d, J = 8.6 Hz, 1H), 4.12 (t, J = 6.6 Hz, 2H), 1.73-1.56 (m, 7H), 1.54-1.43 (m, 1H), 1.26-1.05 (m, 3H), 0.98-0.86 (m, 2H); ^{13}C NMR (101 MHz, $CDCl_3$) δ 160.1, 137.4, 131.1 (q, $^{3}J_{CF_3}$ = 5.3 Hz), 122.3 (q, $^{1}J_{CF_3}$ = 273.8 Hz), 119.8 (q, $^{2}J_{CF_3}$ = 31.2 Hz), 117.8, 113.4, 103.3, 67.5, 35.8, 34.2, 32.9, 26.3, 26.0; HRMS (ESI+): calcd for $C_{16}H_{19}F_3NO$ $[M+H]^+$, 298.1413; found, 298.1426.

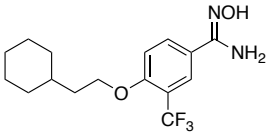

*4-(2-cyclohexylethoxy)-*N*′-hydroxy-3-(trifluoromethyl)benzimidamide* (**3.17**). Synthesized according to the following protocol: To a solution of 200 proof ethanol (0.2 M) and 4-(2-cyclohexylethoxy)-3-(trifluoromethyl)benzonitrile (**3.16**) (1.0 equiv), hydroxylamine hydrochloride (2.0 equiv) was added followed by TEA (3.0 equiv). Next, the reaction mixture was refluxed at 85 ºC for 3 hours. The reaction progress was monitored by TLC. The resulting mixture was concentrated *in vacuo*, followed by addition of ethyl acetate to yield a white precipitate. The white precipitate was filtered off and the resulting filtrate was concentrated *in vacuo* and purified by silica gel chromatography to yield the desired

product; 1.464 g, 96%, yellow solid. ^{1}H NMR (400 MHz, CD_3OD) δ 8.18-7.74 (m, 2H), 7.35-7.02 (m, 1H), 4.17-4.02 (m, 2H), 1.80-1.59 (m, 7H), 1.58-1.48 (m, 1H), 1.31-1.11 (m, 3H), 1.02-0.87 (m, 2H); ^{13}C NMR (101 MHz, CD_3OD) δ 159.2, 153.9, 132.2, 125.8 (q, $^{3}J_{CF_3}$ = 5.4 Hz), 125.5, 124.8 (q, $^{1}J_{CF_3}$ = 273.1 Hz), 119.4 (q, $^{2}J_{CF_3}$ = 32.2 Hz), 113.7, 67.7, 37.2, 35.4, 34.1, 27.5, 27.2; HRMS (ESI+): calcd for $C_{16}H_{22}F_3N_2O_2$ $[M+H]^+$, 331.1628; found, 331.1642.

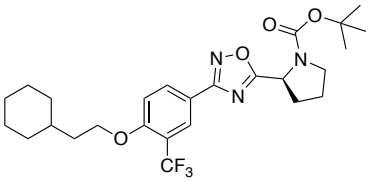

*tert-butyl (*S*)-2-(3-(4-(2-cyclohexylethoxy)-3-(trifluoromethyl)phenyl)-1,2,4-oxadiazol-5-yl)pyrrolidine-1-carboxylate* (**3.18**). Synthesized according to the following protocol: 4-(2-cyclohexylethoxy)-*N*'-hydroxy-3-(trifluoromethyl)benzimidamide (**3.17**) (1.0 equiv) was dissolved in DMF (0.2 M solution) and purged with Ar. Next, Boc-L-Proline (1.2 equiv) was added to the reaction mixture followed by Hünig's base (1.8 equiv) and then HCTU (1.2 equiv) and stirred vigorously at 100 ºC for 18 hours. The reaction progress was monitored by TLC. After completion of reaction, the resulting solution was partitioned between EtOAc and aqueous LiBr solution. Using additional EtOAc, the aqueous LiBr solution was washed three times and the combined organic layers were dried over Na_2SO_4, filtered, and concentrated *in vacuo*. The resulting concentrate was purified by silica gel chromatography; 1.453 g, 84%, yellow oil. ^{1}H NMR (400 MHz, $CDCl_3$) δ 8.26 (s, 1H), 8.17 (d, *J* = 8.7 Hz, 1H), 7.05 (t, *J* = 8.7 Hz, 1H), 5.20-5.02 (m, 1H), 4.13 (t, *J* = 6.3 Hz, 2H), 3.69 (m, 1H), 3.75-3.63 (m, 1H), 3.59-3.43 (m, 1H), 2.45-2.31 (m, 1H), 2.19-2.08 (m, 2H), 2.04-1.96 (m, 1H), 1.78-1.61 (m, 7H), 1.57-1.49 (m, 1H), 1.44 (s, 3H), 1.28 (s, 6H), 1.26-1.09 (m, 3H), 1.01-0.90 (m, 2H); ^{13}C NMR (101 MHz, $CDCl_3$) δ 180.9, 167.4, 159.3, 153.6, 132.5, 126.7 (q, $^{3}J_{CF_3}$ = 5.3 Hz), 123.3 (q, $^{1}J_{CF_3}$ = 273.0 Hz), 119.5 (q, $^{2}J_{CF_3}$ = 32.8 Hz), 118.6, 113.0, 80.6, 67.2, 53.9, 46.5, 36.2, 34.4, 33.2, 32.5, 28.2,

26.6, 26.3, 23.8; HRMS (ESI+): calcd for $C_{26}H_{34}F_3N_3NaO_4$ $[M+Na]^+$, 532.2394; found, 532.2392.

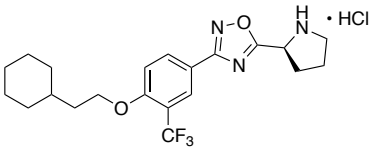

*(*S*)-2-(3-(4-(2-cyclohexylethoxy)-3-(trifluoromethyl)phenyl)-1,2,4-oxadiazol-5-yl)pyrrolidin-1-ium chloride* (**3.19**). Synthesized according to the following protocol: To a solution of HCl and 1,4-dioxane (4.0 M), (*S*)-2-(3-(4-(2-cyclohexylethoxy)-3-(trifluoromethyl)phenyl)-1,2,4-oxadiazol-5-yl)pyrrolidine-1-carboxylate (**3.18**) (1.0 equiv) was added and then allowed to stir at room temperature for 18 hours. The reaction progress was monitored by TLC. Next, the reaction was concentrated *in vacuo* followed by addition of diethyl ether to promote HCl salt precipitation. Once the desired product was precipitated as a white solid, the diethyl ether was removed *via* vacuum to afford the corresponding product as a HCl salt; 123 mg, 89%, white solid. ^{1}H NMR (400 MHz, CD_3OD) δ 8.31-8.26 (m, 2H), 7.36 (d, J = 8.5 Hz, 1H), 5.18 (t, J = 7.8 Hz, 1H), 4.23 (t, J = 6.4 Hz, 2H), 3.63-3.48 (m, 2H), 2.72-2.62 (m, 1H), 2.47-2.37 (m, 1H), 2.34-2.19 (m, 2H), 1.83-1.65 (m, 7H), 1.64-1.53 (m, 1H), 1.35-1.15 (m, 3H), 1.07-0.96 (m, 2H); ^{13}C NMR (101 MHz, CD_3OD) δ 176.3, 168.7, 161.0, 134.0, 127.3 (q, $^3J_{CF_3}$ = 5.5 Hz), 124.7 (q, $^1J_{CF_3}$ = 272.0 Hz), 120.3 (q, $^2J_{CF_3}$ = 31.4 Hz), 119.0, 115.0, 68.3, 55.6, 47.4, 37.4, 35.6, 34.3, 30.2, 27.6, 27.4, 24.5; HRMS (ESI+): calcd for $C_{21}H_{27}F_3N_3O_2$ $[M+H]^+$, 410.2050; found, 410.2056.

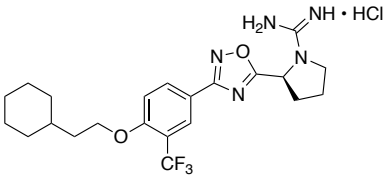

*(*S*)-2-(3-(4-(2-cyclohexylethoxy)-3-(trifluoromethyl)phenyl)-1,2,4-oxadiazol-5-yl)pyrrolidine-1-carboximidamide hydrochloride* (**3.14**). Synthesized according to the following protocol: To a solution of CH_3CN (0.2 M) and (*S*)-2-(3-(4-(2-cyclohexylethoxy)-3-(trifluoromethyl)phenyl)-1,2,4-oxadiazol-5-yl)pyrrolidin-1-ium 2,2,2-trifluoroacetate (**3.21**)

purged with argon, Hünig's base (10 equiv) was added followed by *N,N'-di*-Boc-1*H*-pyrazole-1-carboxamidine (1.2 equiv) and the reaction mixture was allowed to stir at room temperature for 18 hours. The reaction progress was monitored by TLC. Next, the reaction mixture was then concentrated *via* vacuum, and the resulting concentrate was purified by silica gel chromatography to afford the *bis*-Boc-protected intermediate. Following silica gel chromatography, the *bis*-Boc-protected intermediate was then dissolved in a 4.0 M HCl/dioxane solution (8.0 equiv) and stirred for 18 hours to yield the desired Boc deprotected final product. Lastly, the organic mixture was concentrated *via* vacuum and triturated with diethyl ether to afford the corresponding product as an HCl salt; 303 mg, 91%, white solid. ^{1}H NMR (400 MHz, CD_3OD) δ 8.27-8.19 (m, 2H), 7.33 (d, J = 8.8 Hz, 1H), 5.50-5.45 (m, 1H), 4.21 (t, J = 6.5 Hz, 2H), 3.83-3.76 (m, 1H), 3.67-3.59 (m, 1H), 2.63-2.53 (m, 1H), 2.51-2.45 (m, 1H), 2.28-2.21 (m, 1H), 2.14-2.04 (m, 1H), 1.82-1.64 (m, 7H), 1.63-1.54 (m, 1H), 1.33-1.16 (m, 3H), 1.05-0.95 (m, 2H); ^{13}C NMR (101 MHz, CD_3OD) δ 179.2, 168.5, 160.7, 157.0, 134.0, 127.0 (q, $^{3}J_{CF_3}$ = 5.4 Hz), 124.6 (q, $^{1}J_{CF_3}$ = 271.6 Hz), 120.1 (q, $^{2}J_{CF_3}$ = 31.4 Hz), 119.3, 114.8, 68.3, 56.4, 37.3, 35.5, 34.2, 32.7, 27.6, 27.3, 24.3; HRMS (ESI+): calcd for $C_{22}H_{29}F_3N_5O_2$ $[M+H]^+$, 452.2268; found, 452.2276.

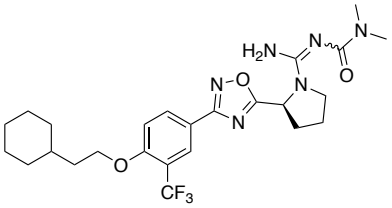

*(S)-2-(3-(4-(2-cyclohexylethoxy)-3-(trifluoromethyl)phenyl)-1,2,4-oxadiazol-5-yl)-*N*′-(dimethylcarbamoyl)pyrrolidine-1-carboximidamide* (**3.20a**). Synthesized by General Procedure 3A: 82 mg, 38%, white solid. ^{1}H NMR (400 MHz, CD_3OD) δ 8.21-8.15 (m, 2H), 7.26 (d, J = 9.7 Hz, 1H), 5.40-5.32 (m, 1H), 4.18 (t, J = 6.5 Hz, 2H), 3.76-3.67 (m, 1H), 3.57-3.49 (m, 1H), 2.75 (s, 6H), 2.50-2.38 (m, 1H), 2.34-2.23 (m, 1H), 2.20-2.05 (m, 2H), 1.82-1.63 (m, 7H), 1.62-1.50 (m, 1H), 1.33-1.14 (m, 3H), 1.05-0.92 (m, 2H); ^{13}C NMR (101 MHz, CD_3OD) δ 183.1, 168.3,

166.3, 160.6, 159.0, 133.8, 126.9 (q, $^{3}J_{CF_3}$ = 5.5 Hz), 124.7 (q, $^{1}J_{CF_3}$ = 271.9 Hz), 120.2 (q, $^{2}J_{CF_3}$ = 31.8 Hz), 119.8, 114.7, 68.2, 55.8, 46.8, 37.4, 35.6, 34.2, 32.1, 27.6, 27.4, 25.3; HRMS (ESI+): calcd for $C_{25}H_{34}F_3N_6O_3$ $[M+H]^+$, 523.2639; found, 523.2631.

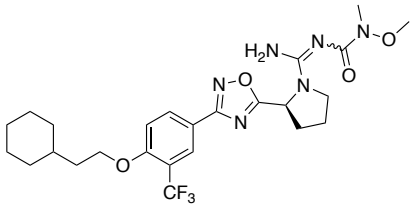

*(*S*)-2-(3-(4-(2-cyclohexylethoxy)-3-(trifluoromethyl)phenyl)-1,2,4-oxadiazol-5-yl)-*N*′-(methoxy(methyl)carbamoyl)pyrrolidine-1-carboximidamide* (**3.20b**). Synthesized by General Procedure 3A: 174 mg, 79%, white solid. ^{1}H NMR (400 MHz, CD_3OD) δ 8.19-8.12 (m, 2H), 7.22 (d, *J* = 9.5 Hz, 1H), 5.42-5.32 (m, 1H), 4.15 (t, *J* = 6.4 Hz, 2H), 3.76-3.68 (m, 1H), 3.57-3.45 (m, 4H), 2.96 (s, 3H), 2.48-2.37 (m, 1H), 2.33-2.22 (m, 1H), 2.20-2.05 (m, 2H), 1.80-1.61 (m, 7H), 1.60-1.49 (m, 1H), 1.32-1.11 (m, 3H), 1.02-0.90 (m, 2H); ^{13}C NMR (101 MHz, CD_3OD) δ 182.7, 168.3, 166.8, 160.6, 159.7, 133.7, 126.9 (q, $^{3}J_{CF_3}$ = 5.5 Hz), 124.7 (q, $^{1}J_{CF_3}$ = 272.0 Hz), 120.14 (q, $^{2}J_{CF_3}$ = 31.2 Hz), 119.7, 114.7, 68.2, 61.2, 55.9, 46.9, 37.3, 35.9, 35.6, 34.2, 32.1, 27.6, 27.3, 25.2; HRMS (ESI+): calcd for $C_{25}H_{33}F_3N_6NaO_4$ $[M+Na]^+$, 561.2408; found, 561.2391.

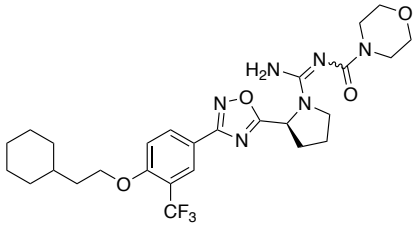

*(*S*)-*N*-(amino(2-(3-(4-(2-cyclohexylethoxy)-3-(trifluoromethyl)phenyl)-1,2,4 oxadiazol-5-yl)pyrrolidin-1-yl)methylene)morpholine-4-carboxamide* (**3.20c**). Synthesized by General Procedure 3A: 145 mg, 63%, white solid. ^{1}H NMR (400 MHz, $CDCl_3$) δ 8.30-8.05 (m, 2H), 7.04 (d, *J* = 9.1 Hz, 1H), 5.38-5.27 (m, 1H), 4.12 (t, *J* = 6.2 Hz, 2H), 3.70-3.22 (m, 10H), 2.43-2.25 (m, 2H), 2.20-2.03 (m, 2H), 1.84-1.57 (m, 7H), 1.57-1.45 (m, 1H), 1.30-1.07 (m, 3H), 1.03-0.80 (m, 2H); ^{13}C NMR (101 MHz, CD_3OD) δ 182.9, 168.2, 164.4, 160.6, 159.4, 133.7, 126.9 (q, $^{3}J_{CF_3}$ = 5.3 Hz), 124.6 (q, $^{1}J_{CF_3}$ = 271.4 Hz), 120.2

(q, $^2J_{CF_3}$ = 32.0 Hz), 119.7, 114.7, 68.2, 67.8, 67.5, 55.8, 46.9, 37.3, 35.6, 34.2, 32.0, 27.6, 27.3, 25.3; HRMS (ESI+): calcd for $C_{25}H_{33}F_3N_6NaO_4$ $[M+Na]^+$, 561.2408; found, 561.2391.

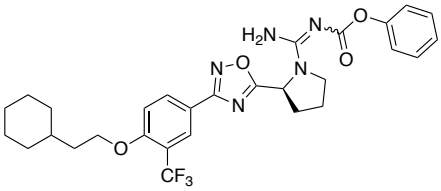

*phenyl (*S*)-(amino(2-(3-(4-(2-cyclohexylethoxy)-3-(trifluoromethyl)phenyl)-1,2,4-oxadiazol-5-yl)pyrrolidin-1-yl)methylene)carbamate* (**3.20d**). Synthesized by General Procedure 3A: 70 mg, 66%, tan solid. ^{1}H NMR (400 MHz, CD_3OD) δ 8.23-8.14 (m, 2H), 7.32-7.00 (m, 4H), 6.94-6.73 (m, 2H), 5.52-5.31 (m, 1H), 4.21-4.13 (m, 2H), 3.77-3.68 (m, 1H), 3.58-3.48 (m, 1H), 2.45-2.31 (m, 1H), 2.22-2.05 (m, 3H), 1.81-1.63 (m, 7H), 1.62-1.51 (m, 1H), 1.32-1.16 (m, 3H), 1.04-0.93 (m, 2H); ^{13}C NMR (101 MHz, CD_3OD) δ 181.6, 168.3, 163.5, 160.6, 153.7, 133.9, 130.4, 130.0, 127.1 (q, $^3J_{CF_3}$ = 5.6 Hz), 125.6, 124.7 (q, $^1J_{CF_3}$ = 272.5 Hz), 122.8, 120.2 (q, $^2J_{CF_3}$ = 31.6 Hz), 119.8, 116.2, 114.7, 68.2, 47.2, 37.3, 35.6, 34.2, 32.2, 27.6, 27.3, 24.8; HRMS (ESI+): calcd for $C_{29}H_{33}F_3N_5O_4$ $[M+H]^+$, 572.2479; found, 572.2472.

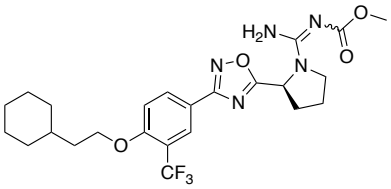

*methyl (*S*)-(amino(2-(3-(4-(2-cyclohexylethoxy)-3-(trifluoromethyl)phenyl)-1,2,4-oxadiazol-5-yl)pyrrolidin-1-yl)methylene)carbamate* (**3.20e**). Synthesized by General Procedure 3A: 197 mg, 94%, white solid. ^{1}H NMR (400 MHz, CD_3OD) δ 8.19-8.09 (m, 2H), 7.20 (d, J = 9.5 Hz, 1H), 5.48 (d, J = 8.5 Hz, 1H), 4.13 (t, J = 6.1 Hz, 2H), 3.79-3.69 (m, 1H), 3.60-3.45 (m, 4H), 2.49-2.35 (m, 1H), 2.26-2.09 (m, 3H), 1.79-1.60 (m, 7H), 1.58-1.48 (m, 1H), 1.32-1.11 (m, 3H), 1.02-0.89 (m, 2H); ^{13}C NMR (101 MHz, CD_3OD) δ 182.0, 168.3, 165.4, 160.9, 160.5, 133.8, 127.0 (q, $^3J_{CF_3}$ = 5.4 Hz), 124.6 (q, $^1J_{CF_3}$ = 272.6 Hz), 120.1 (q, $^2J_{CF_3}$ = 31.4 Hz), 119.7, 114.6, 68.2, 55.8, 53.2, 47.2, 37.3, 35.5, 34.2, 32.2, 27.6, 27.3, 24.8; HRMS (ESI+): calcd for $C_{24}H_{31}F_3N_5O_4$ $[M+H]^+$, 510.2323; found, 510.2304.

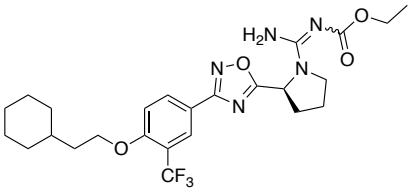

*ethyl (*S*)-(amino(2-(3-(4-(2-cyclohexylethoxy)-3-(trifluoromethyl)phenyl)-1,2,4-oxadiazol-5-yl)pyrrolidin-1-yl)methylene)carbamate* (**3.20f**). Synthesized by General Procedure 3A: 188 mg, 88%, white solid. ^{1}H NMR (400 MHz, CD_3OD) δ 8.19-8.11 (m, 2H), 7.21 (d, J = 8.9 Hz, 1H), 5.49 (d, J = 8.3 Hz, 1H), 4.14 (t, J = 6.7 Hz, 2H), 3.99-3.84 (m, 2H), 3.79-3.69 (m, 1H), 3.60-3.49 (m, 1H), 2.50-2.36 (m, 1H), 2.28-2.11 (m, 3H), 1.81-1.61 (m, 7H), 1.61-1.48 (m, 1H), 1.32-1.14 (m, 3H), 1.09 (t, J = 7.1 Hz, 3H), 1.03-0.90 (m, 2H); ^{13}C NMR (101 MHz, CD_3OD) δ 182.0, 168.3, 164.9, 161.0, 160.6, 133.8, 127.0 (q, $^{3}J_{CF_3}$ = 5.4 Hz), 124.7 (q, $^{1}J_{CF_3}$ = 272.0 Hz), 120.1 (q, $^{2}J_{CF_3}$ = 30.9 Hz), 119.7, 114.6, 68.2, 62.3, 55.8, 47.2, 37.3, 35.6, 34.2, 32.2, 27.6, 27.3, 24.8, 15.0; HRMS (ESI+): calcd for $C_{25}H_{33}F_3N_5O_4$ $[M+H]^+$, 524.2479; found, 524.2466.

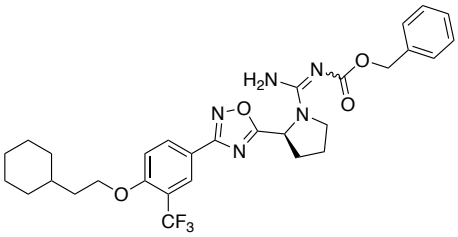

*benzyl (*S*)-(amino(2-(3-(4-(2-cyclohexylethoxy)-3-(trifluoromethyl)phenyl)-1,2,4-oxadiazol-5-yl)pyrrolidin-1-yl)methylene)carbamate* (**3.20g**). Synthesized by General Procedure 3A: 225 mg, 94%, yellow solid. ^{1}H NMR (400 MHz, CD_3OD) δ 8.14-8.03 (m, 2H), 7.22-7.05 (m, 6H), 5.44 (d, J = 7.3 Hz, 1H), 4.97-4.85 (m, 2H), 4.07 (t, J = 6.4 Hz, 2H), 3.74-3.63 (m, 1H), 3.54-3.44 (m, 1H), 2.41-2.29 (m, 1H), 2.20-2.04 (m, 3H), 1.77-1.59 (m, 7H), 1.56-1.46 (m, 1H), 1.29-1.09 (m, 3H), 0.99-0.86 (m, 2H); ^{13}C NMR (101 MHz, CD_3OD) δ 181.9, 168.2, 164.4, 160.8, 160.5, 138.7, 133.8, 129.2, 128.5, 128.3, 127.0 (q, $^{3}J_{CF_3}$ = 5.2 Hz), 124.6 (q, $^{1}J_{CF_3}$ = 272.3 Hz), 120.0 (q, $^{2}J_{CF_3}$ = 31.7 Hz), 119.6, 114.5, 68.3, 68.1, 55.9, 47.2, 37.2, 35.5, 34.1, 32.1, 27.5, 27.3, 24.8; HRMS (ESI+): calcd for $C_{30}H_{35}F_3N_5O_4$ $[M+H]^+$, 586.2636; found, 586.2618.

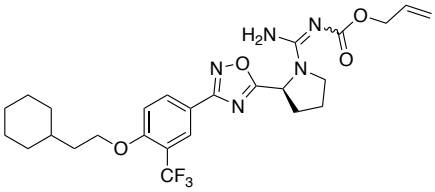

*allyl (*S*)-(amino(2-(3-(4-(2-cyclohexylethoxy)-3-(trifluoromethyl)phenyl)-1,2,4-oxadiazol-5-yl)pyrrolidin-1-yl)methylene)carbamate* (**3.20h**). Synthesized by General Procedure 3A: 170 mg, 77%, white solid. ^{1}H NMR (400 MHz, CD_3OD) δ 8.19-8.12 (m, 2H), 7.21 (d, J = 9.3 Hz, 1H), 5.87-5.72 (m, 1H), 5.48 (d, J = 7.8 Hz, 1H), 5.13 (d, J = 17.3 Hz, 1H), 5.00 (d, J = 10.6 Hz, 1H), 4.45-4.31 (m, 2H), 4.14 (t, J = 6.9 Hz, 2H), 3.77-3.69 (m, 1H), 3.60-3.51 (m, 1H), 2.50-2.37 (m, 1H), 2.26-2.11 (m, 3H), 1.79-1.61 (m, 7H), 1.59-1.48 (m, 1H), 1.32-1.12 (m, 3H), 1.02-0.90 (m, 2H); ^{13}C NMR (101 MHz, CD_3OD) δ 182.0, 168.3, 164.5, 161.0, 160.5, 134.9, 133.8, 127.0 (q, $^{3}J_{CF_3}$ = 5.3 Hz), 124.6 (q, $^{1}J_{CF_3}$ = 272.2 Hz), 120.1 (q, $^{2}J_{CF_3}$ = 31.8 Hz), 119.7, 116.9, 114.6, 68.2, 67.3, 55.9, 47.2, 37.3, 35.5, 34.2, 32.2, 27.6, 27.3, 24.9; HRMS (ESI+): calcd for $C_{26}H_{33}F_3N_5O_4$ $[M+H]^+$, 536.2479; found, 536.2469.

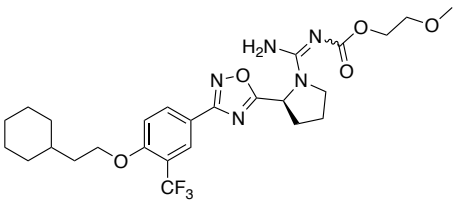

*2-methoxyethyl (*S*)-(amino(2-(3-(4-(2-cyclohexylethoxy)-3-(trifluoromethyl)phenyl)-1,2,4-oxadiazol-5-yl)pyrrolidin-1-yl)methylene)carbamate* (**3.20i**). Synthesized by General Procedure 3A: 197 mg, 87%, white solid. ^{1}H NMR (400 MHz, CD_3OD) δ 8.19-8.12 (m, 2H), 7.23 (d, J = 9.4 Hz, 1H), 5.49 (d, J = 8.0 Hz, 1H), 4.15 (t, J = 6.2 Hz, 2H), 4.07-3.92 (m, 1H), 3.78-3.69 (m, 1H), 3.60-3.50 (m, 1H), 3.47-3.37 (m, 2H), 3.21 (s, 3H), 2.50-2.37 (m, 1H), 2.27-2.11 (m, 3H), 1.80-1.61 (m, 7H), 1.61-1.48 (m, 1H), 1.32-1.11 (m, 3H), 1.04-0.90 (m, 2H); ^{13}C NMR (101 MHz, CD_3OD) δ 182.0, 168.3, 164.6, 160.9, 160.6, 133.8, 127.0 (q, $^{3}J_{CF_3}$ = 5.4 Hz), 124.6 (q, $^{1}J_{CF_3}$ = 271.8 Hz), 120.1 (q, $^{2}J_{CF_3}$ = 31.8 Hz), 119.7, 114.7, 72.0, 68.2, 65.8, 59.0, 55.8, 47.2, 37.3, 35.6, 34.2, 32.2, 27.6, 27.3, 24.8; HRMS (ESI+): calcd for $C_{26}H_{35}F_3N_5O_5$ $[M+H]^+$, 554.2585; found, 554.2562.

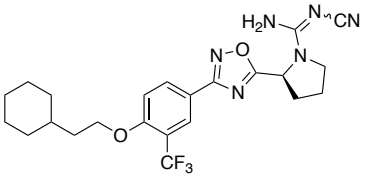

*(*S*)-*N*′-cyano-2-(3-(4-(2-cyclohexylethoxy)-3-(trifluoromethyl)phenyl)-1,2,4-oxadiazol-5-yl)pyrrolidine-1-carboximidamide* (**3.20j**). Synthesized according to the following protocol: (*S*)-2-(3-(4-(2-cyclohexylethoxy)-3-(trifluoromethyl)phenyl)-1,2,4-oxadiazol-5-yl)pyrrolidine-1-carboximidamide hydrochloride (**3.14**) (1.0 equiv) was dissolved in CH_2Cl_2 (0.2 M solution) and put under an argon gas atmosphere. Next *N*,*N*-diisopropylethylamine (2.0 equiv) was added followed by addition of cyanic bromide (1.1 equiv). The reaction mixture was then stirred at 40 ºC for 2 hours. The reaction progress was monitored by TLC. Afterward, the reaction was concentrated *via* vacuum and then purified by silica gel chromatography to yield the desired product; 61 mg, 30%, yellow solid. ^{1}H NMR (400 MHz, CD_3OD) δ 8.26-8.14 (m, 2H), 7.28 (d, J = 8.5 Hz, 1H), 5.38-5.29 (m, 1H), 4.19 (t, J = 6.3 Hz, 2H), 3.79-3.68 (m, 1H), 3.61-3.50 (m, 1H), 2.51-2.38 (m, 1H), 2.27-2.10 (m, 3H), 1.84-1.63 (m, 7H), 1.62-1.52 (m, 1H), 1.35-1.15 (m, 3H), 1.05-0.93 (m, 2H); ^{13}C NMR (101 MHz, CD_3OD) δ 181.6, 168.4, 161.0, 160.7, 133.9, 127.0 (q, $^3J_{CF_3}$ = 5.4 Hz), 124.8 (q, $^1J_{CF_3}$ = 273.0 Hz), 120.2 (q, $^2J_{CF_3}$ = 31.4 Hz), 119.6, 119.1, 114.7, 68.2, 56.3, 48.2, 37.4, 35.6, 34.2, 32.4, 27.6, 27.4, 25.1; HRMS (ESI+): calcd for $C_{23}H_{28}F_3N_6O_2$ $[M+H]^+$, 477.2220; found, 477.2215.

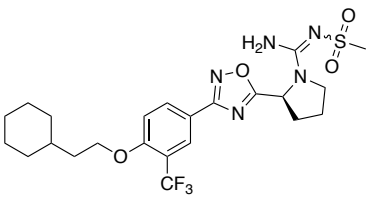

*(*S*)-2-(3-(4-(2-cyclohexylethoxy)-3-(trifluoromethyl)phenyl)-1,2,4-oxadiazol-5-yl)-*N*′-(methylsulfonyl)pyrrolidine-1-carboximidamide* (**3.20k**). Synthesized by General Procedure 3B: 144 mg, 66%, white solid. ^{1}H NMR (400 MHz, CD_3OD) δ 8.24-8.14 (m, 2H), 7.28 (d, J = 8.5 Hz, 1H), 5.41-5.34 (m, 1H), 4.18 (t, J = 6.5 Hz, 2H), 3.77-3.69 (m, 1H), 3.61-3.52 (m, 1H), 2.66 (s, 3H), 2.53-2.41 (m, 1H), 2.28-2.12 (m, 3H), 1.81-1.64 (m, 7H), 1.62-1.52 (m, 1H), 1.34-1.15 (m, 3H), 1.05-0.93 (m, 2H); ^{13}C NMR (101 MHz, CD_3OD) δ 181.9, 168.4, 160.6, 156.4, 133.9,

127.0 (q, $^{3}J_{CF_3}$ = 5.4 Hz), 124.7 (q, $^{1}J_{CF_3}$ = 272.1 Hz), 120.2 (q, $^{2}J_{CF_3}$ = 31.1 Hz), 119.6, 114.8, 68.2, 56.2, 47.6, 41.1, 37.3, 35.6, 34.2, 32.1, 27.6, 27.3, 25.1; HRMS (ESI+): calcd for $C_{23}H_{31}F_3N_5O_4S$ $[M+H]^+$, 530.2043; found, 530.2027.

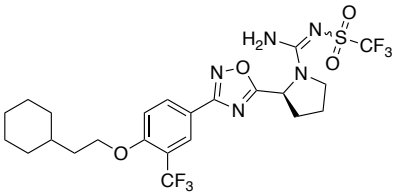

*(S)-2-(3-(4-(2-cyclohexylethoxy)-3-(trifluoromethyl)phenyl)-1,2,4-oxadiazol-5-yl)-*N′*-((trifluoromethyl)sulfonyl)pyrrolidine-1-carboximidamide* (**3.20l**). Synthesized by General Procedure 3B: 71 mg, 30%, white solid. ^{1}H NMR (400 MHz, CD_3OD) δ 8.23-8.13 (m, 2H), 7.30 (d, *J* = 8.4 Hz, 1H), 5.50-5.37 (m, 1H), 4.20 (t, *J* = 6.4 Hz, 2H), 3.82-3.72 (m, 1H), 3.64-3.55 (m, 1H), 2.55-2.41 (m, 1H), 2.31-2.12 (m, 3H), 1.84-1.63 (m, 7H), 1.63-1.52 (m, 1H), 1.35-1.15 (m, 3H), 1.07-0.93 (m, 2H); ^{13}C NMR (101 MHz, CD_3OD) δ 181.1, 168.4, 160.7, 157.2, 133.8, 127.1 (q, $^{3}J_{CF_3}$ = 5.4 Hz), 124.7 (q, $^{1}J_{CF_3}$ = 272.8 Hz), 120.2 (q, $^{2}J_{CF_3}$ = 31.1 Hz), 119.7, 114.7, 68.2, 56.7, 48.0, 37.4, 35.6, 34.2, 32.0, 27.6, 27.4, 25.0; HRMS (ESI+): calcd for $C_{23}H_{28}F_6N_5O_4S$ $[M+H]^+$, 584.1761; found, 584.1753.

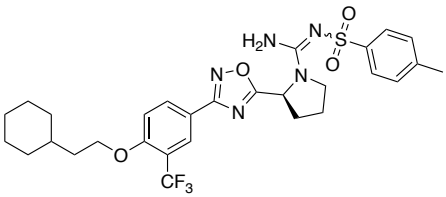

*(S)-2-(3-(4-(2-cyclohexylethoxy)-3-(trifluoromethyl)phenyl)-1,2,4-oxadiazol-5-yl)-*N′*-tosylpyrrolidine-1-carboximidamide* (**3.20m**). Synthesized by General Procedure 3B: 133 mg, 54%, white solid. ^{1}H NMR (400 MHz, $CDCl_3$) δ 8.12-8.00 (m, 2H), 7.44 (d, *J* = 7.4 Hz, 2H), 7.06 (d, *J* = 8.6 Hz, 1H), 6.87 (d, *J* = 6.9 Hz, 2H), 6.59 (br s, 2H), 5.39 (d, *J* = 6.8 Hz, 1H), 4.15 (t, *J* = 6.6 Hz, 2H), 3.69-3.60 (m, 1H), 3.57-3.47 (m, 1H), 2.43-2.31 (m, 1H), 2.23-2.00 (m, 6H), 1.80-1.62 (m, 7H), 1.60-1.49 (m, 1H), 1.31-1.10 (m, 3H), 1.05-0.90 (m, 2H); ^{13}C NMR (101 MHz, $CDCl_3$) δ 179.8, 167.0, 159.2, 154.2, 141.7, 139.7, 132.1, 129.0, 126.6 (q, $^{3}J_{CF_3}$ = 5.4 Hz), 125.6, 123.3 (q, $^{1}J_{CF_3}$ = 273.4 Hz), 119.3 (q, $^{2}J_{CF_3}$ =

31.7 Hz), 118.5, 112.9, 67.2, 54.7, 46.3, 36.2, 34.4, 33.2, 31.1, 26.6, 26.3, 24.2, 21.1; HRMS (ESI+): calcd for $C_{29}H_{35}F_3N_5O_4S$ $[M+H]^+$, 606.2356; found, 606.2338.

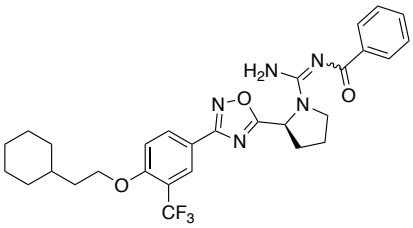

*(*S*)*-N-*(amino(2-(3-(4-(2-cyclohexylethoxy)-3-(trifluoromethyl)phenyl)-1,2,4-oxadiazol-5-yl)pyrrolidin-1-yl)methylene)benzamide* (**3.20n**). Synthesized according to the following protocol: Benzoic acid (1.0 equiv) was dissolved in CH_2Cl_2 (0.2 M solution) and put under an argon gas atmosphere. Next, carbonyldiimidazole (1.5 equiv) was added to the reaction mixture portion wise and left to stir for 2 hours at room temperature. After, (S)-2-(3-(4-(2-cyclohexylethoxy)-3-(trifluoromethyl)phenyl)-1,2,4-oxadiazol-5-yl)pyrrolidine-1-carboximidamide hydrochloride (**3.14**) (1.1 equiv) was added to the reaction mixture followed by TEA (3.0 equiv) and then DMAP (0.1 equiv) and the resulting solution was left to stir at room temperature for 18 hours. The reaction progress was monitored by TLC. Afterward, the reaction was concentrated *via* vacuum and then purified by silica gel chromatography to yield the desired product; 190 mg, 84%, white solid. ^{1}H NMR (400 MHz, $CDCl_3$) δ 8.36-8.01 (m, 4H), 7.39-7.25 (m, 3H), 7.04 (d, J = 8.7 Hz, 1H), 5.66 (br s, 1H), 4.12 (t, J = 6.6 Hz, 2H), 3.79-3.67 (m, 1H), 3.60-3.43 (m, 1H), 2.47-2.31 (m, 2H), 2.25-2.12 (m, 2H), 1.80-1.63 (m, 7H), 1.59-1.48 (m, 1H), 1.32-1.11 (m, 3H), 1.02-0.88 (m, 2H); ^{13}C NMR (101 MHz, $CDCl_3$) δ 180.4, 177.2, 167.4, 159.3, 159.0, 138.3, 132.5, 131.2, 129.2, 127.8, 126.8 (q, $^3J_{CF_3}$ = 5.3 Hz), 123.4 (q, $^1J_{CF_3}$ = 273.8 Hz), 119.5 (q, $^2J_{CF_3}$ = 31.3 Hz), 118.5, 113.0, 67.2, 54.8, 45.5, 36.2, 34.4, 33.3, 31.2, 26.6, 26.3, 24.3; HRMS (ESI+): calcd for $C_{29}H_{33}F_3N_5O_3$ $[M+H]^+$, 556.2530; found, 556.2513.

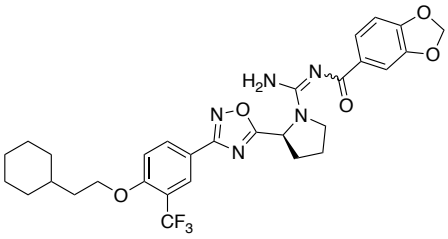

*(*S*)*-N-*(amino(2-(3-(4-(2-cyclohexylethoxy)-3-(trifluoromethyl)phenyl)-1,2,4-oxadiazol-5-yl)pyrrolidin-1-yl)methylene)benzo[*d*][1,3]dioxole-5-carboxamide* (**3.20o**). Synthesized by General Procedure 3A: 194 mg, 79%, tan solid. ^{1}H NMR (400 MHz, CD_3OD) δ 8.17 (s, 1H), 8.06 (d, *J* = 8.7 Hz, 1H), 7.53 (d, *J* = 8.0 Hz, 1H), 7.42 (s, 1H), 7.02 (d, *J* = 9.0 Hz, 1H), 6.60 (d, *J* = 8.0 Hz, 1H), 5.82 (d, *J* = 23.2 Hz, 2H), 5.60-5.46 (m, 1H), 3.99 (t, *J* = 6.4 Hz, 2H), 3.77-3.65 (m, 1H), 3.60-3.47 (m, 1H), 2.48-2.35 (m, 1H), 2.33-2.21 (m, 1H), 2.19-2.06 (m, 2H), 1.74-1.54 (m, 7H), 1.52-1.41 (m, 1H), 1.26-1.09 (m, 3H), 0.95-0.82 (m, 2H); ^{13}C NMR (101 MHz, CD_3OD) δ 182.5, 177.2, 168.3, 160.5, 159.9, 151.6, 148.6, 134.0, 133.7, 127.2 (q, $^{3}J_{CF_3}$ = 5.3 Hz), 125.1, 124.6 (q, $^{1}J_{CF_3}$ = 272.7 Hz), 120.0 (q, $^{2}J_{CF_3}$ = 31.1 Hz), 119.5, 114.4, 110.1, 108.1, 102.6, 68.1, 56.3, 46.9, 37.3, 35.5, 34.2, 32.0, 27.6, 27.3, 25.3; HRMS (ESI+): calcd for $C_{30}H_{33}F_3N_5O_5$ $[M+H]^+$, 600.2428; found, 600.2410.

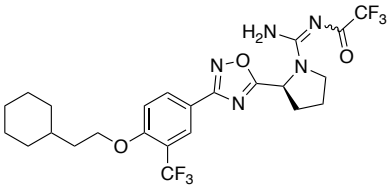

*(*S*)*-N-*(amino(2-(3-(4-(2-cyclohexylethoxy)-3-(trifluoromethyl)phenyl)-1,2,4-oxadiazol-5-yl)pyrrolidin-1-yl)methylene)-2,2,2-trifluoroacetamide* (**3.20p**). Synthesized according to the following protocol: (*S*)-2-(3-(4-(2-cyclohexylethoxy)-3-(trifluoromethyl)phenyl)-1,2,4-oxadiazol-5-yl)pyrrolidine-1-carboximidamide hydrochloride (**3.14**) (1.0 equiv) was dissolved in CH_2Cl_2 (0.2 M solution) and put under a argon gas atmosphere. Next *N*,*N*-diisopropylethylamine (2.0 equiv) was added followed by dropwise addition of 2,2,2-trifluoroacetic anhydride (1.1 equiv). The reaction mixture was stirred at room temperature for 10 minutes. The reaction progress was monitored by TLC. Afterward, the reaction was concentrated *via* vacuum and then purified by silica gel chromatography to yield the desired product; 80 mg, 71%, yellow solid. ^{1}H NMR (400 MHz, CD_3OD) δ 8.22-8.14 (m, 2H),

7.26 (d, J = 8.6 Hz, 1H), 5.58-5.46 (m, 1H), 4.18 (t, J = 6.9 Hz, 2H), 4.01-3.55 (m, 2H), 2.62-2.43 (m, 1H), 2.33-2.11 (m, 3H), 1.82-1.62 (m, 7H), 1.61-1.51 (m, 1H), 1.33-1.14 (m, 3H), 1.04-0.92 (m, 2H); ^{13}C NMR (101 MHz, CD_3OD) δ 181.8, 180.73, 168.4, 160.6, 133.9, 127.1 (q, $^3J_{CF_3}$ = 5.5 Hz), 124.7 (q, $^1J_{CF_3}$ = 271.9 Hz), 120.2 (q, $^2J_{CF_3}$ = 32.4 Hz), 119.7, 114.6, 68.2, 57.0, 56.7, 47.2, 37.4, 35.6, 34.2, 32.4, 27.6, 27.3, 25.0; HRMS (ESI+): calcd for $C_{24}H_{28}F_6N_5O_3$ $[M+H]^+$, 548.2091; found, 548.2088.

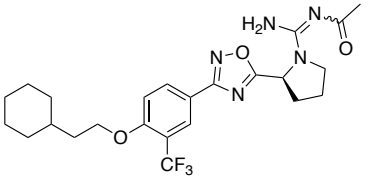

(S)-N-*(amino(2-(3-(4-(2-cyclohexylethoxy)-3-(trifluoromethyl)phenyl)-1,2,4-oxadiazol-5-yl)pyrrolidin-1-yl)methylene)acetamide* (**3.20q**). Synthesized by General Procedure 3A: 128 mg, 63%, yellow solid. ^{1}H NMR (400 MHz, CD_3OD) δ 8.20-8.14 (m, 2H), 7.24 (d, J = 9.4 Hz, 1H), 5.50-5.43 (m, 1H), 4.16 (t, J = 6.4 Hz, 2H), 3.76-3.67 (m, 1H), 3.59-3.49 (m, 1H), 2.49-2.39 (m, 1H), 2.29-2.11 (m, 3H), 1.88-1.62 (m, 10H), 1.61-1.50 (m, 1H), 1.32-1.13 (m, 3H), 1.03-0.92 (m, 2H); ^{13}C NMR (101 MHz, CD_3OD) δ 184.6, 182.3, 168.3, 160.6, 159.9, 133.8, 127.0 (q, $^3J_{CF_3}$ = 5.2 Hz), 124.7 (q, $^1J_{CF_3}$ = 271.6 Hz), 120.2 (q, $^2J_{CF_3}$ = 31.0 Hz), 119.7, 114.6, 68.2, 56.0, 46.8, 37.2, 35.6, 34.2, 32.1, 27.6, 26.9, 25.0; HRMS (ESI+): calcd for $C_{24}H_{31}F_3N_5O_3$ $[M+H]^+$, 494.2374; found, 494.2358.

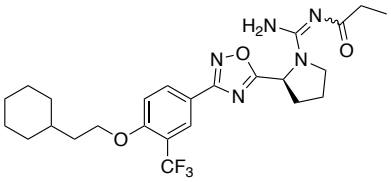

(S)-N-*(amino(2-(3-(4-(2-cyclohexylethoxy)-3-(trifluoromethyl)phenyl)-1,2,4-oxadiazol-5-yl)pyrrolidin-1-yl)methylene)propionamide* (**3.20r**). Synthesized by General Procedure 3A: 61 mg, 30%, yellow solid. ^{1}H NMR (400 MHz, CD_3OD) δ 8.23-8.12 (m, 2H), 7.24 (d, J = 9.9 Hz, 1H), 5.47-5.37 (m, 1H), 4.16 (t, J = 6.5 Hz, 2H), 3.93-3.81 (m, 1H), 3.77-3.66 (m, 1H), 2.57-2.45 (m, 1H), 2.40-2.13 (m, 5H), 1.80-1.61 (m, 7H), 1.60-1.49 (m, 1H), 1.32-1.16 (m, 3H), 1.14-0.98 (m, 3H), 0.96-0.85 (m, 2H); ^{13}C NMR (101 MHz, $CDCl_3$) δ 179.6,

167.4, 159.3, 153.0, 132.5, 126.8 (q, $^{3}J_{CF_3}$ = 5.3 Hz), 123.3 (q, $^{1}J_{CF_3}$ = 272.0 Hz), 119.5 (q, $^{2}J_{CF_3}$ = 30.7 Hz), 118.6, 113.0, 67.2, 56.3, 49.7, 36.2, 34.4, 33.2, 32.3, 31.1, 26.6, 26.3, 24.5, 9.5, 9.2; HRMS (ESI+): calcd for $C_{25}H_{33}F_3N_5O_3$ $[M+H]^+$, 508.2530; found, 508.2529.

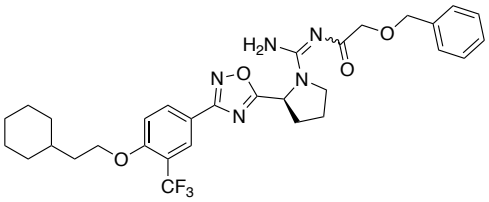

*(*S*)-*N*-(amino(2-(3-(4-(2-cyclohexylethoxy)-3-(trifluoromethyl)phenyl)-1,2,4-oxadiazol-5-yl)pyrrolidin-1-yl)methylene)-2-(benzyloxy)acetamide* (**3.20s**). Synthesized by General Procedure 3A: 153 mg, 62%, white solid. ^{1}H NMR (400 MHz, CD_3OD) δ 8.17-8.05 (m, 2H), 7.27-7.08 (m, 6H), 5.49-5.42 (m, 1H), 4.38 (br s, 2H), 4.13 (t, *J* = 6.4 Hz, 2H), 3.87-3.77 (m, 1H), 3.75-3.65 (m, 2H), 3.56-3.47 (m, 1H), 2.44-2.33 (m, 1H), 2.25-2.05 (m, 3H), 1.79-1.61 (m, 7H), 1.60-1.48 (m, 1H), 1.31-1.12 (m, 3H), 1.02-0.90 (m, 2H); ^{13}C NMR (101 MHz, CD_3OD) δ 182.6, 182.3, 168.3, 160.5, 160.2, 139.2, 133.8, 129.2, 128.8, 128.5, 127.0 (q, $^{3}J_{CF_3}$ = 5.4 Hz), 124.7 (q, $^{1}J_{CF_3}$ = 272.0 Hz), 120.1 (q, $^{2}J_{CF_3}$ = 31.7 Hz), 119.7, 114.6, 73.7, 72.6, 68.2, 56.2, 46.7, 37.3, 35.5, 34.2, 32.1, 27.6, 27.3, 25.0; HRMS (ESI+): calcd for $C_{31}H_{37}F_3N_5O_4$ $[M+H]^+$, 600.2792; found, 600.2773.

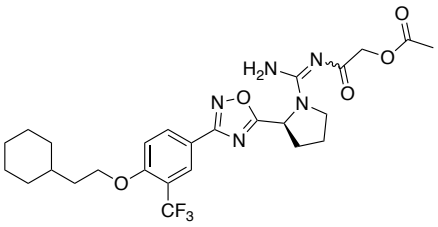

*(*S*)-2-((amino(2-(3-(4-(2-cyclohexylethoxy)-3-(trifluoromethyl)phenyl)-1,2,4-oxadiazol-5-yl)pyrrolidin-1-yl)methylene)amino)-2-oxoethyl acetate* (**3.20t**). Synthesized by General Procedure 3A: 91 mg, 40%, white solid. ^{1}H NMR (400 MHz, $CDCl_3$) δ 8.24 (s, 1H), 8.16 (d, *J* = 8.7 Hz, 1H), 7.06 (d, *J* = 8.8 Hz, 1H), 5.48 (br s, 1H), 4.60-4.29 (m, 2H), 4.14 (t, *J* = 6.6 Hz, 2H), 3.74-3.63 (m, 1H), 3.57-3.41 (m, 1H), 2.44-2.25 (m, 2H), 2.24-2.14 (m, 2H), 2.10 (s, 3H), 1.81-1.61 (m, 7H), 1.59-1.48 (m, 1H), 1.31-1.13 (m, 3H), 1.03-0.91 (m, 2H); ^{13}C NMR (101 MHz, $CDCl_3$) δ 178.9, 171.0, 167.4, 159.4, 158.2, 132.6, 126.9 (q, $^{3}J_{CF_3}$ = 5.2 Hz), 123.4 (q, $^{1}J_{CF_3}$ = 272.9 Hz), 119.5 (q, $^{2}J_{CF_3}$ = 31.5 Hz),

118.4, 113.1, 67.2, 65.3, 54.6, 36.2, 34.4, 33.3, 31.2, 29.8, 26.6, 26.3, 24.1, 20.9; HRMS (ESI+): calcd for $C_{26}H_{32}F_3N_5NaO_5$ $[M+Na]^+$, 574.2248; found, 574.2222.

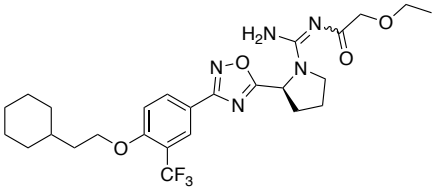

*(*S*)-*N*-(amino(2-(3-(4-(2-cyclohexylethoxy)-3-(trifluoromethyl)phenyl)-1,2,4-oxadiazol-5-yl)pyrrolidin-1-yl)methylene)-2-ethoxyacetamide* (**3.20u**). Synthesized by General Procedure 3A: 85 mg, 38%, white solid. ^{1}H NMR (400 MHz, $CDCl_3$) δ 8.28-8.22 (m, 1H), 8.18-8.12 (m, 1H), 7.06 (d, *J* = 8.2 Hz, 1H), 5.48 (br s, 1H), 4.14 (t, *J* = 6.6 Hz, 2H), 3.94-3.75 (m, 2H) 3.74-3.64 (m, 1H), 3.57-3.39 (m, 3H), 2.45-2.08 (m, 4H), 1.80-1.46 (m, 8H), 1.29-1.12 (m, 6H), 1.03-0.90 (m, 2H); ^{13}C NMR (101 MHz, $CDCl_3$) δ 182.8, 167.4, 159.4, 158.2, 132.5, 126.9 (q, $^3J_{CF_3}$ = 5.3 Hz), 123.4 (q, $^1J_{CF_3}$ = 272.5 Hz), 119.6 (q, $^2J_{CF_3}$ = 31.1 Hz), 118.5, 113.0, 72.8, 67.3, 66.6, 54.5, 45.7, 36.0, 34.4, 33.3, 31.2, 26.6, 26.3, 24.2, 15.3; HRMS (ESI+): calcd for $C_{26}H_{35}F_3N_5O_4$ $[M+H]^+$, 538.2636; found, 538.2634.

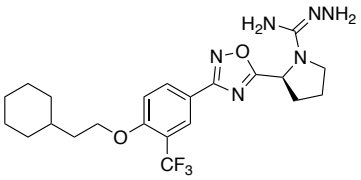

*(*S*)-2-(3-(4-(2-cyclohexylethoxy)-3-(trifluoromethyl)phenyl)-1,2,4-oxadiazol-5-yl)pyrrolidine-1-carbohydrazonamide* (**3.20v**). Synthesized according to the following protocol: (*S*)-2-(3-(4-(2-cyclohexylethoxy)-3-(trifluoromethyl)phenyl)-1,2,4-oxadiazol-5-yl)pyrrolidine-1-carbonitrile (**3.22**) (1.0 equiv) was dissolved in THF (0.2 M solution) and put under an argon gas atmosphere. Next, hydrazine hydrate (2.0 equiv) was added to the reaction mixture followed by addition of Cs_2CO_3 (3.0 equiv). After, the reaction mixture was heated to 65 ºC and stirred for 18 hours. The reaction progress was monitored by TLC. Afterward, the reaction was concentrated *via* vacuum and then purified by silica gel chromatography to yield the desired product; 43 mg, 33%, white solid. ^{1}H NMR (400 MHz, CD_3OD) δ 8.25-8.17 (m, 2H), 7.30 (d, *J* = 8.7 Hz, 1H), 5.38-5.32 (m, 1H), 4.20 (t, *J* = 6.4 Hz, 2H), 3.77-3.68 (m, 1H), 3.61-3.53 (m, 1H), 2.54-2.43 (m, 1H), 2.29-2.14

(m, 3H), 1.82-1.64 (m, 7H), 1.62-1.52 (m, 1H), 1.34-1.15 (m, 3H), 1.06-0.93 (m, 2H); ^{13}C NMR (101 MHz, CD_3OD) δ 181.3, 168.5, 160.7, 160.1, 133.9, 127.0 (q, $^3J_{CF_3}$ = 5.3 Hz), 124.7 (q, $^1J_{CF_3}$ = 271.6 Hz), 120.2 (q, $^2J_{CF_3}$ = 31.4 Hz), 119.6, 114.8, 68.2, 55.7, 48.1, 37.4, 35.6, 34.2, 32.4, 27.6, 27.4, 25.2; HRMS (ESI+): calcd for $C_{22}H_{30}F_3N_6O_2$ $[M+H]^+$, 467.2377; found, 467.2365.

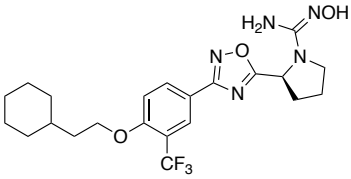

(S)-2-(3-(4-(2-cyclohexylethoxy)-3-(trifluoromethyl)phenyl)-1,2,4-oxadiazol-5-yl)-N′-hydroxypyrrolidine-1-carboximidamide (**3.20w**). Synthesized according to the following protocol: (*S*)-2-(3-(4-(2-cyclohexylethoxy)-3-(trifluoromethyl)phenyl)-1,2,4-oxadiazol-5-yl)pyrrolidine-1-carbonitrile (**3.22**) (1.0 equiv) was dissolved in 200 proof ethanol (0.2 M solution) and put under an argon gas atmosphere. Next, hydroxylamine hydrochloride (2.0 equiv) was added to the reaction mixture followed by addition of Cs_2CO_3 (3.0 equiv). After, the reaction mixture was heated to 85 ºC and stirred for 18 hours. The reaction progress was monitored by TLC. Afterward, the reaction was concentrated *via* vacuum and then purified by silica gel chromatography to yield the desired product; 95 mg, 40%, white solid. ^{1}H NMR (400 MHz, CD_3OD) δ 8.28-8.13 (m, 2H), 7.33-7.22 (m, 1H), 5.28-5.21 (m, 1H), 4.19 (t, *J* = 6.3 Hz, 2H), 3.72-3.63 (m, 1H), 3.56-3.46 (m, 1H), 2.50-2.36 (m, 1H), 2.29-2.05 (m, 3H), 1.82-1.65 (m, 7H), 1.62-1.53 (m, 1H), 1.33-1.18 (m, 3H), 1.05-0.94 (m, 2H); ^{13}C NMR (101 MHz, CD_3OD) δ 182.5, 168.4, 160.6, 160.1, 133.8, 127.0 (q, $^3J_{CF_3}$ = 5.3 Hz), 124.7 (q, $^1J_{CF_3}$ = 272.5 Hz), 120.1 (q, $^2J_{CF_3}$ = 31.6 Hz), 119.8, 114.7, 68.2, 55.2, 47.5, 37.4, 35.6, 34.2, 32.4, 27.6, 27.4, 25.6; HRMS (ESI+): calcd for $C_{22}H_{29}F_3N_5O_3$ $[M+H]^+$, 468.2217; found, 468.2221.

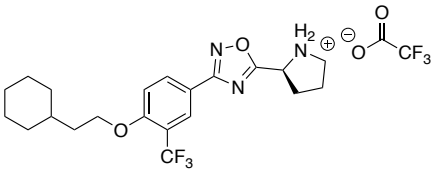

(S)-2-(3-(4-(2-cyclohexylethoxy)-3-(trifluoromethyl)phenyl)-1,2,4-oxadiazol-5-yl)pyrrolidin-1-ium 2,2,2-trifluoroacetate (**3.21**). Synthesized according to the following protocol: To a

solution of dichloromethane (0.2 M) and (*S*)-2-(3-(4-(2-cyclohexylethoxy)-3-(trifluoromethyl)phenyl)-1,2,4-oxadiazol-5-yl)pyrrolidine-1-carboxylate (**3.18**) (1.0 equiv), 1.0 M TFA (10 equiv) was added and then allowed to stir at room temperature for 3 – 12 hours. The reaction progress was monitored by TLC. Next, the reaction was concentrated *in vacuo* followed by addition of diethyl ether to promote TFA salt precipitation. Once the desired intermediate was precipitated as a white solid, the diethyl ether was removed *via* vacuum to afford the corresponding product as a TFA salt; 513 mg, 87%, white solid. ^{1}H NMR (400 MHz, CD_3OD) δ 8.31-8.26 (m, 2H), 7.36 (d, J = 8.5 Hz, 1H), 5.18 (t, J = 7.8 Hz, 1H), 4.23 (t, J = 6.4 Hz, 2H), 3.63-3.48 (m, 2H), 2.72-2.62 (m, 1H), 2.47-2.37 (m, 1H), 2.34-2.19 (m, 2H), 1.83-1.65 (m, 7H), 1.64-1.53 (m, 1H), 1.35-1.15 (m, 3H), 1.07-0.96 (m, 2H); ^{13}C NMR (101 MHz, CD_3OD) δ 176.3, 168.7, 161.0, 134.0, 127.3 (q, $^{3}J_{CF_3}$ = 5.5 Hz), 124.7 (q, $^{1}J_{CF_3}$ = 272.0 Hz), 120.3 (q, $^{2}J_{CF_3}$ = 31.4 Hz), 119.0, 115.0, 68.3, 55.6, 47.4, 37.4, 35.6, 34.3, 30.2, 27.6, 27.4, 24.5; ^{19}F NMR (376 MHz, CD_3OD) δ -64.28 (s, 3F), -76.96 (s, 3F); HRMS (ESI+): calcd for $C_{21}H_{27}F_3N_3O_2$ $[M+H]^+$, 410.2050; found, 410.2056.

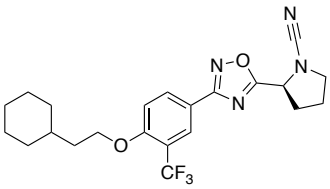

*(*S*)-2-(3-(4-(2-cyclohexylethoxy)-3-(trifluoromethyl)phenyl)-1,2,4-oxadiazol-5-yl)pyrrolidine-1-carbonitrile* (**3.22**). Synthesized according to the following protocol: (*S*)-2-(3-(4-(2-cyclohexylethoxy)-3-(trifluoromethyl)phenyl)-1,2,4-oxadiazol-5-yl)pyrrolidin-1-ium 2,2,2-trifluoroacetate (**3.21**) was dissolved in CH_3CN (0.2 M solution) and put under an argon gas atmosphere. Next, *N*,*N*-diisopropylethylamine (6.0 equiv) was added followed by portion wise addition of cyanic bromide (2.0 equiv). The reaction mixture was then refluxed at 80 ºC for 2 hours. The reaction progress was monitored by TLC. Afterward, the reaction was concentrated *via* vacuum and then purified by silica gel chromatography to yield the desired product; 156 mg,

87%, yellow oil. ^{1}H NMR (400 MHz, $CDCl_3$) δ 8.24 (s, 1H), 8.15 (d, *J* = 9.0 Hz, 1H), 7.05 (d, *J* = 8.7 Hz, 1H), 5.07-4.96 (m, 1H), 4.12 (t, *J* = 6.5 Hz, 2H), 3.79-3.71 (m, 1H), 3.62-3.53 (m, 1H), 2.49-2.37 (m, 1H), 2.37-2.28 (m, 1H), 2.23-2.06 (m, 2H), 1.81-1.58 (m, 7H), 1.57-1.46 (m, 1H), 1.28-1.09 (m, 3H), 1.01-0.87 (m, 2H); ^{13}C NMR (101 MHz, $CDCl_3$) δ 177.5, 167.5, 159.4, 132.6, 126.7 (q, $^{3}J_{CF_3}$ = 5.2 Hz), 123.2 (q, $^{1}J_{CF_3}$ = 272.9 Hz), 119.3 (q, $^{2}J_{CF_3}$ = 32.2 Hz), 117.9, 115.2, 113.0, 67.1, 57.2, 51.4, 36.1, 34.3, 33.1, 31.5, 26.5, 26.2, 24.6; HRMS (ESI+): calcd for $C_{22}H_{26}F_3N_4O_2$ $[M+H]^+$, 435.2002; found, 435.1997.

4.2.4 NMR Spectra

^{1}H spectrum for *4-(2-cyclohexylethoxy)-3-(trifluoromethyl)benzonitrile* (**3.16**).

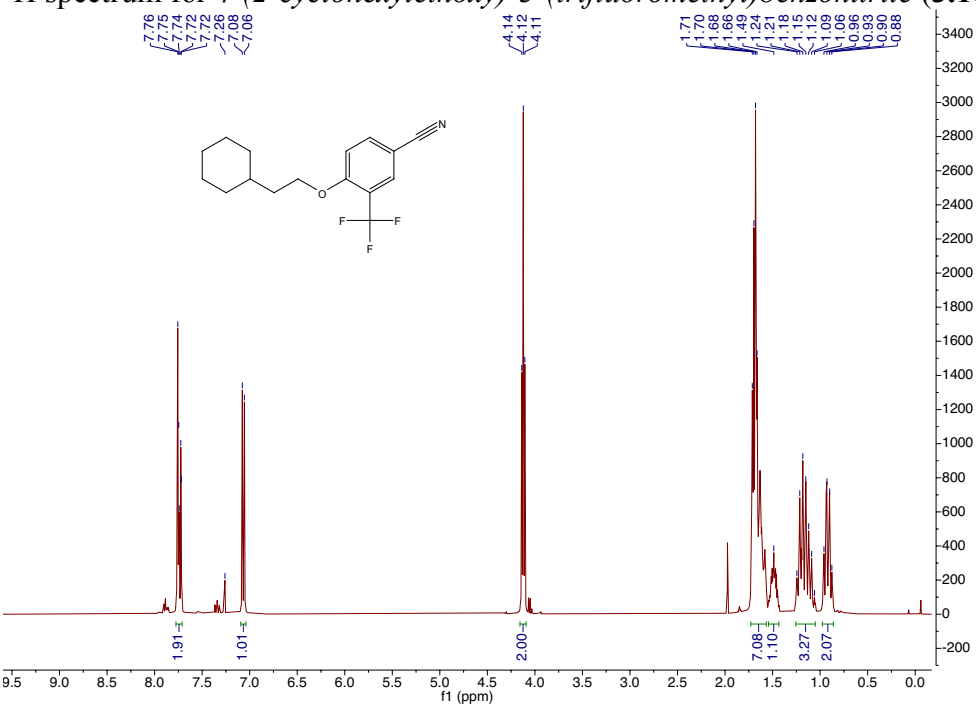

^{13}C spectrum for *4-(2-cyclohexylethoxy)-3-(trifluoromethyl)benzonitrile* (**3.16**).

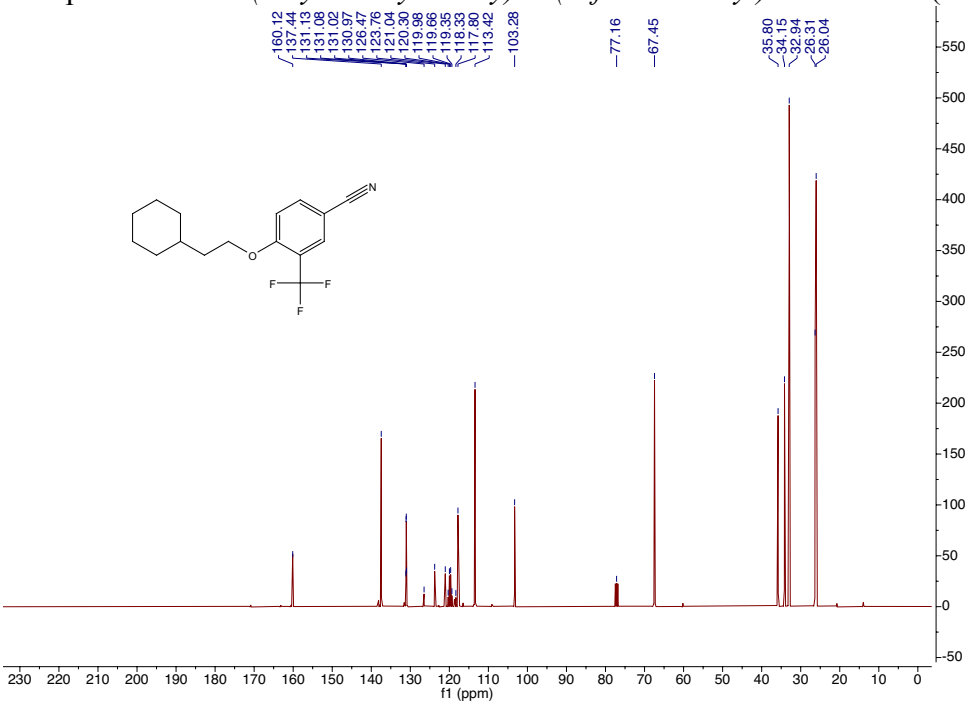

^{1}H spectrum for *4-(2-cyclohexylethoxy)-*N*′-hydroxy-3-(trifluoromethyl)benzimidamide* (**3.17**).

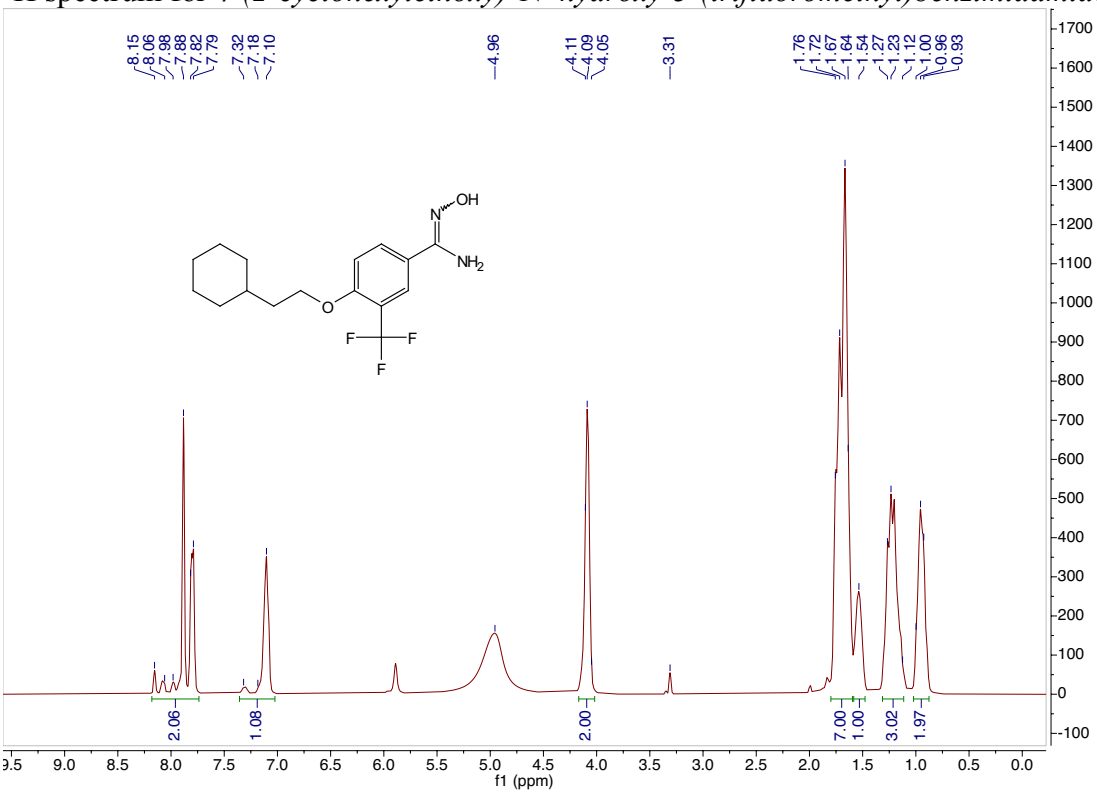

^{13}C spectrum for 4-(2-cyclohexylethoxy)-N'-hydroxy-3-(trifluoromethyl)benzimidamide (**3.17**).

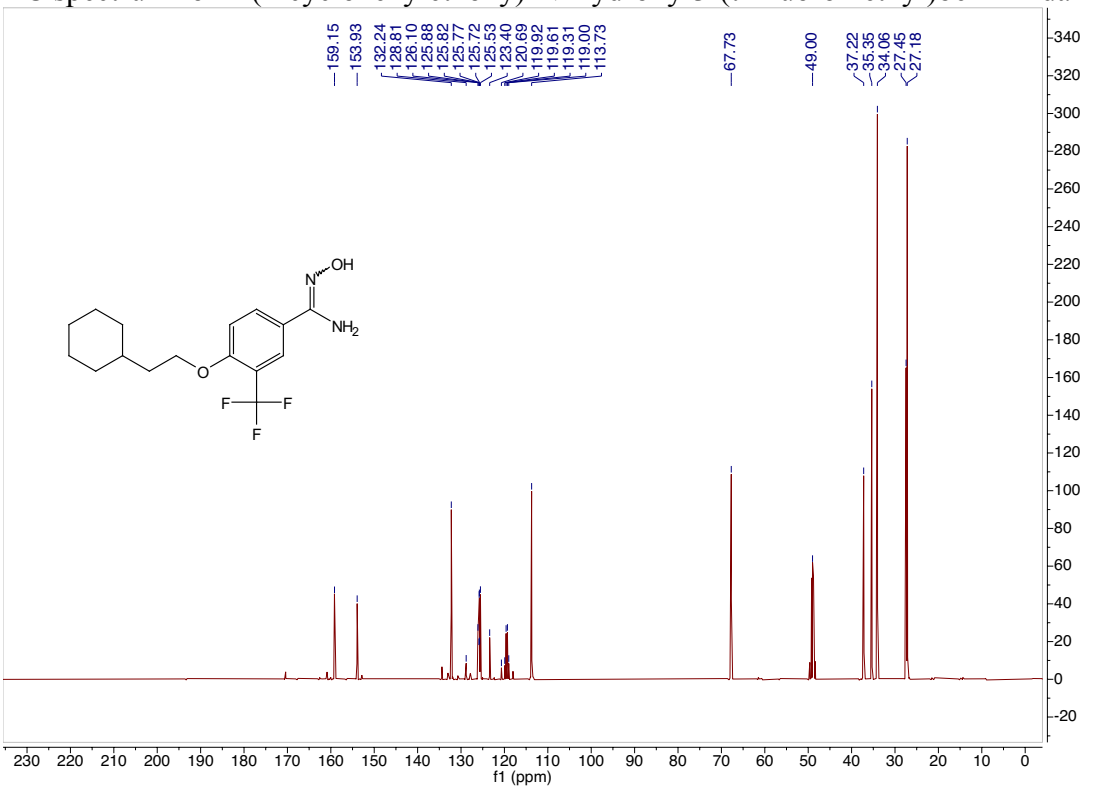

^{1}H spectrum for *tert-butyl (*S*)-2-(3-(4-(2-cyclohexylethoxy)-3-(trifluoromethyl)phenyl)-1,2,4-oxadiazol-5-yl)pyrrolidine-1-carboxylate* (**3.18**).

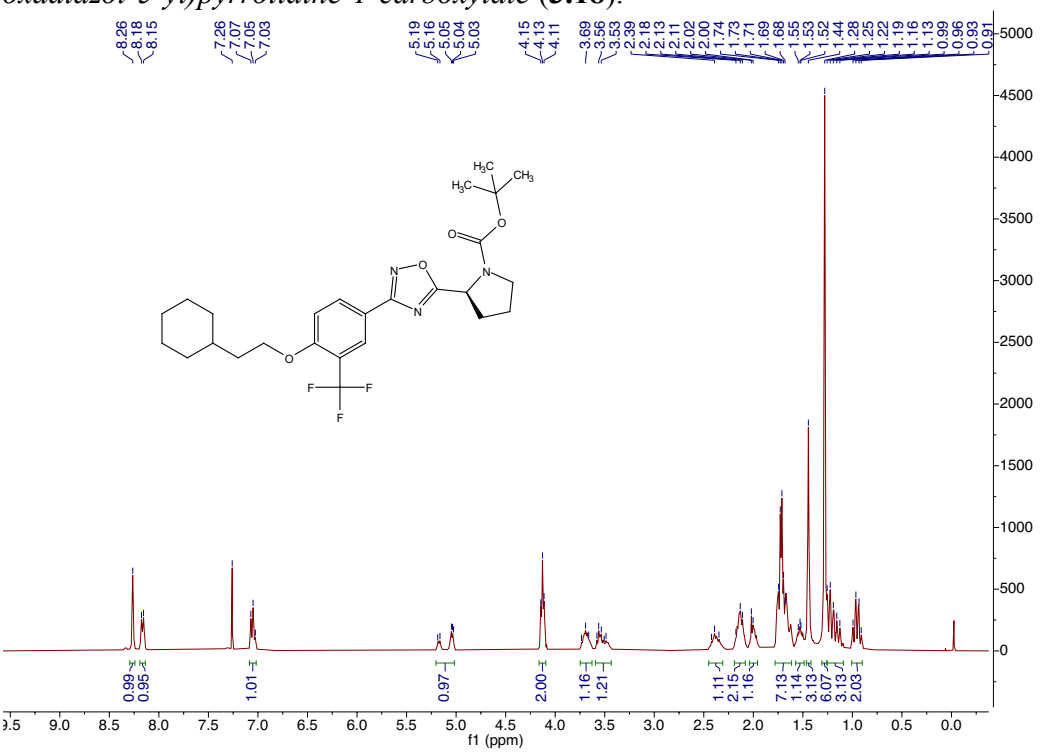

^{13}C spectrum for *tert-butyl (*S*)-2-(3-(4-(2-cyclohexylethoxy)-3-(trifluoromethyl)phenyl)-1,2,4-oxadiazol-5-yl)pyrrolidine-1-carboxylate* (**3.18**).

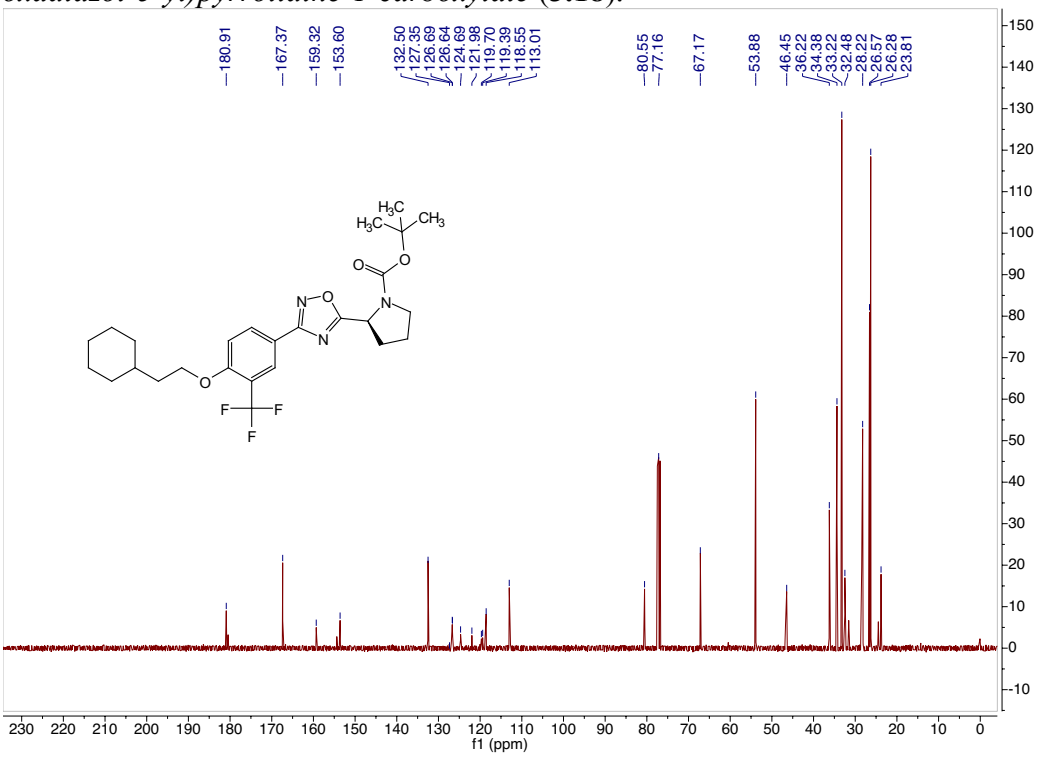

^{1}H spectrum for *(*S*)-2-(3-(4-(2-cyclohexylethoxy)-3-(trifluoromethyl)phenyl)-1,2,4-oxadiazol-5-yl)pyrrolidin-1-ium chloride* (**3.19**)

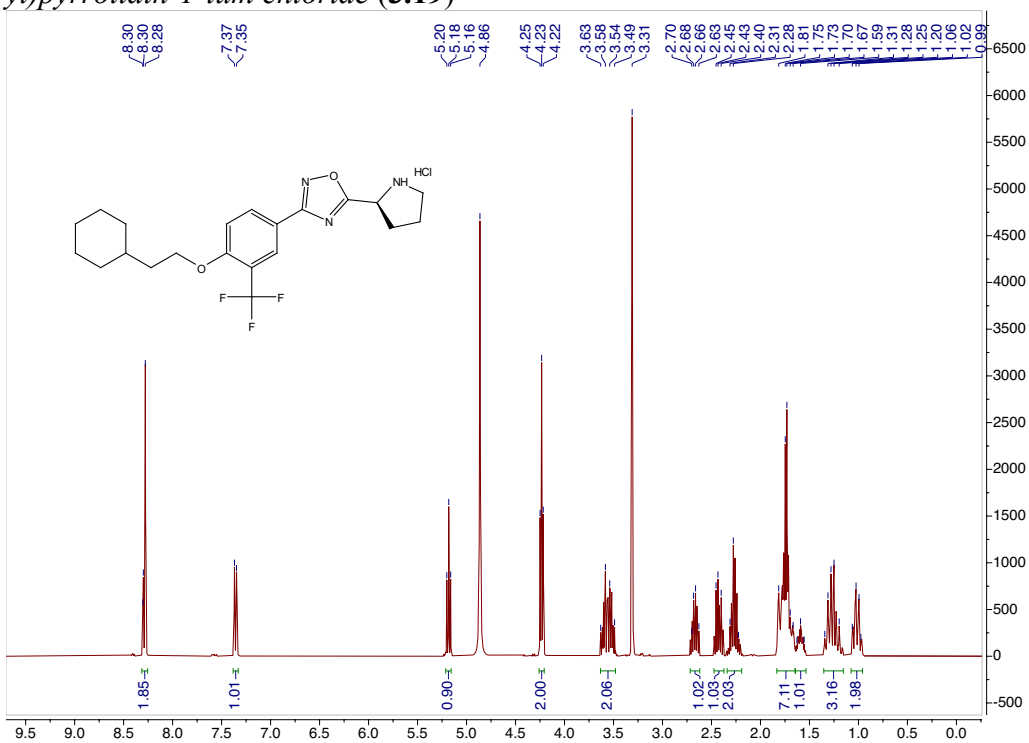

^{13}C spectrum for *(*S*)-2-(3-(4-(2-cyclohexylethoxy)-3-(trifluoromethyl)phenyl)-1,2,4-oxadiazol-5-yl)pyrrolidin-1-ium chloride* (**3.19**)

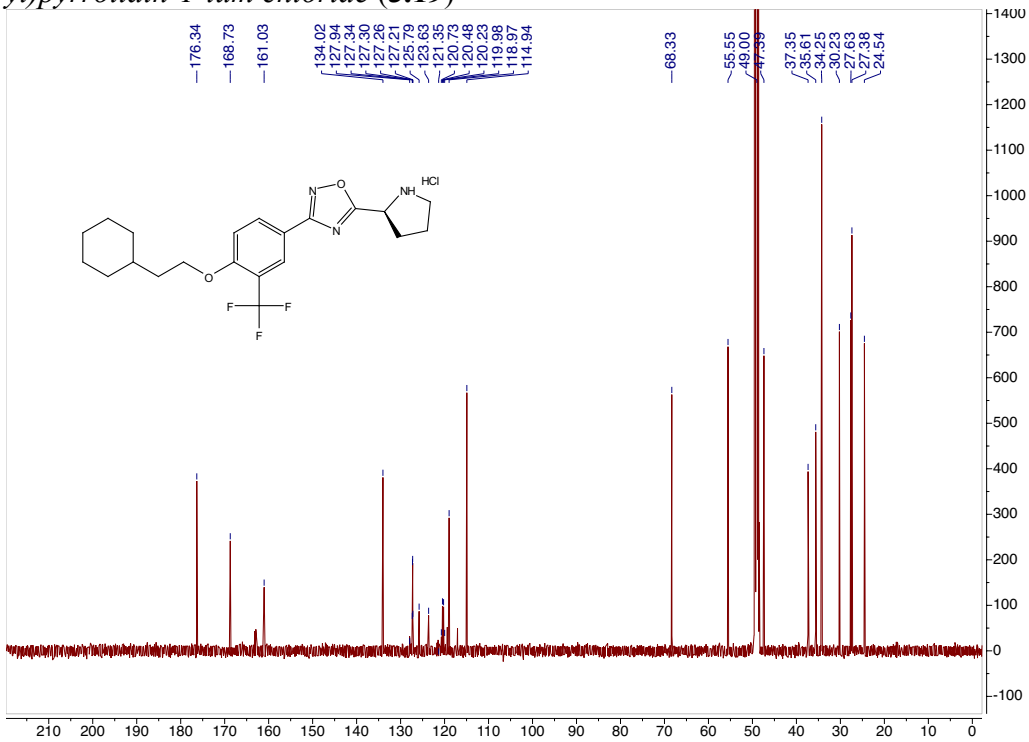

^{1}H spectrum for *(*S*)-2-(3-(4-(2-cyclohexylethoxy)-3-(trifluoromethyl)phenyl)-1,2,4-oxadiazol-5-yl)pyrrolidine-1-carboximidamide hydrochloride* (**3.14**).

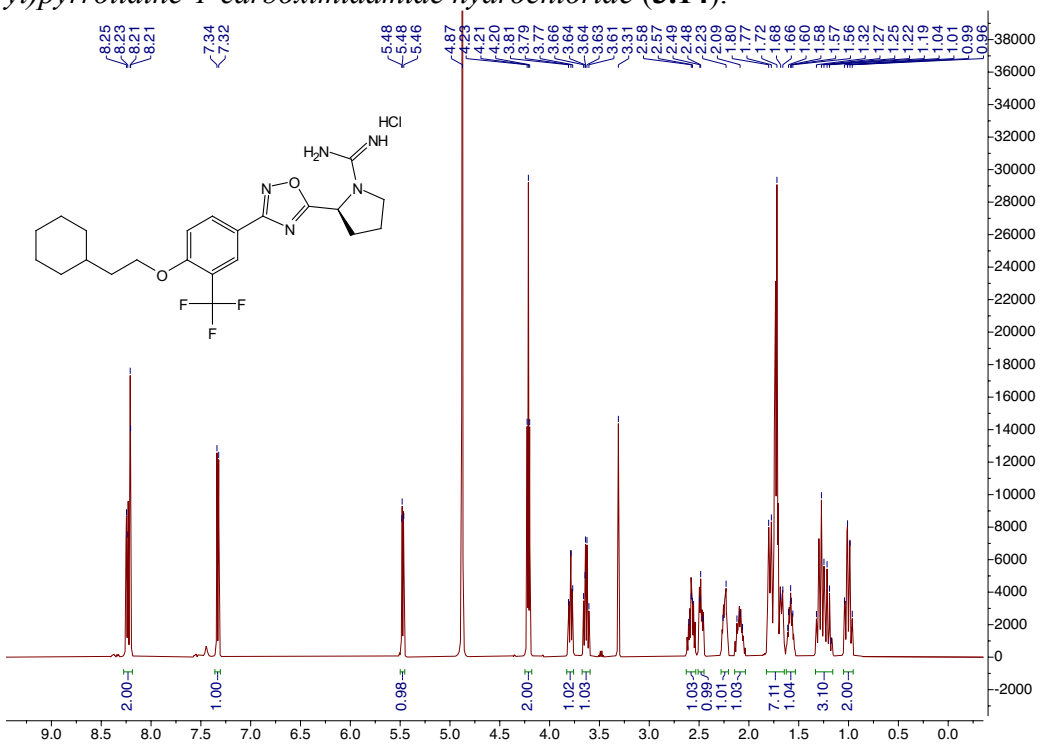

^{13}C spectrum for *(*S*)-2-(3-(4-(2-cyclohexylethoxy)-3-(trifluoromethyl)phenyl)-1,2,4-oxadiazol-5-yl)pyrrolidine-1-carboximidamide hydrochloride* (**3.14**).

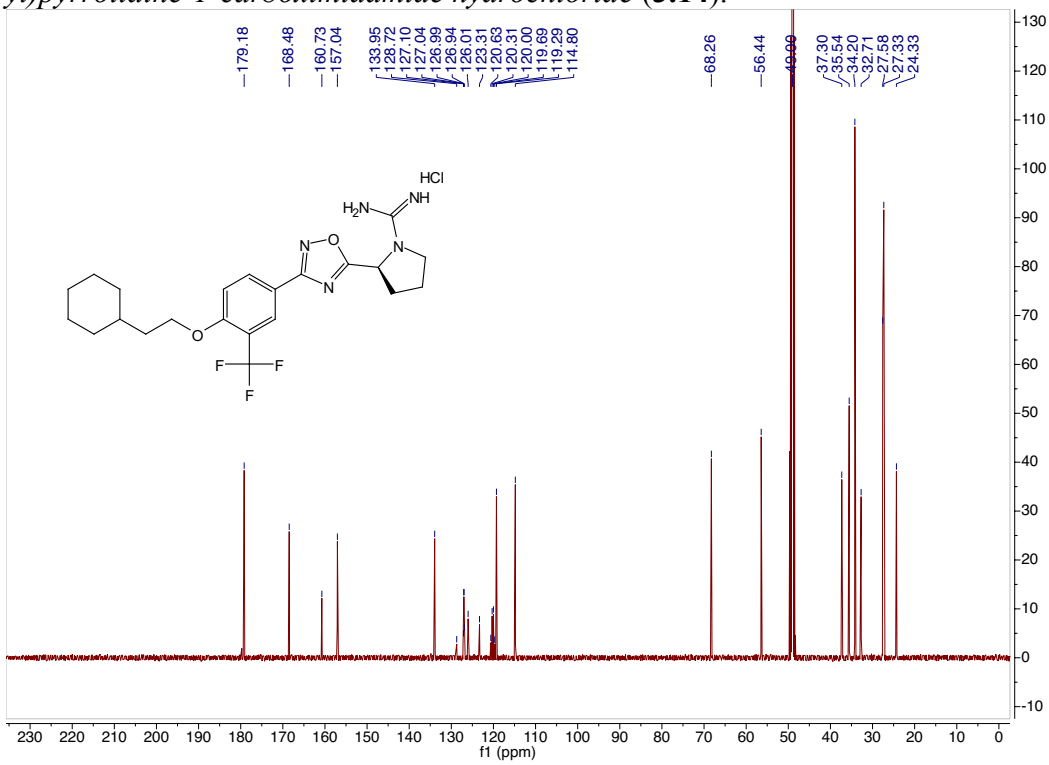

^{1}H spectrum for *(*S*)-2-(3-(4-(2-cyclohexylethoxy)-3-(trifluoromethyl)phenyl)-1,2,4-oxadiazol-5-yl)-*N*′-(dimethylcarbamoyl)pyrrolidine-1-carboximidamide* (**3.20a**).

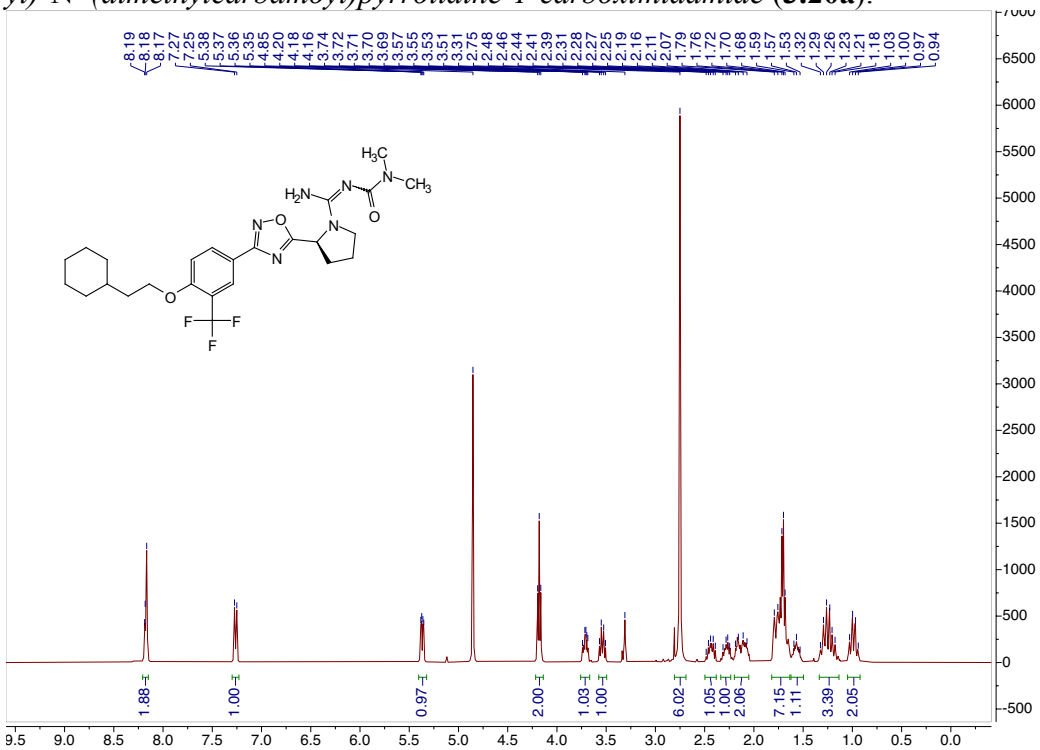

^{13}C spectrum for *(*S*)-2-(3-(4-(2-cyclohexylethoxy)-3-(trifluoromethyl)phenyl)-1,2,4-oxadiazol-5-yl)-*N*′-(dimethylcarbamoyl)pyrrolidine-1-carboximidamide* (**3.20a**).

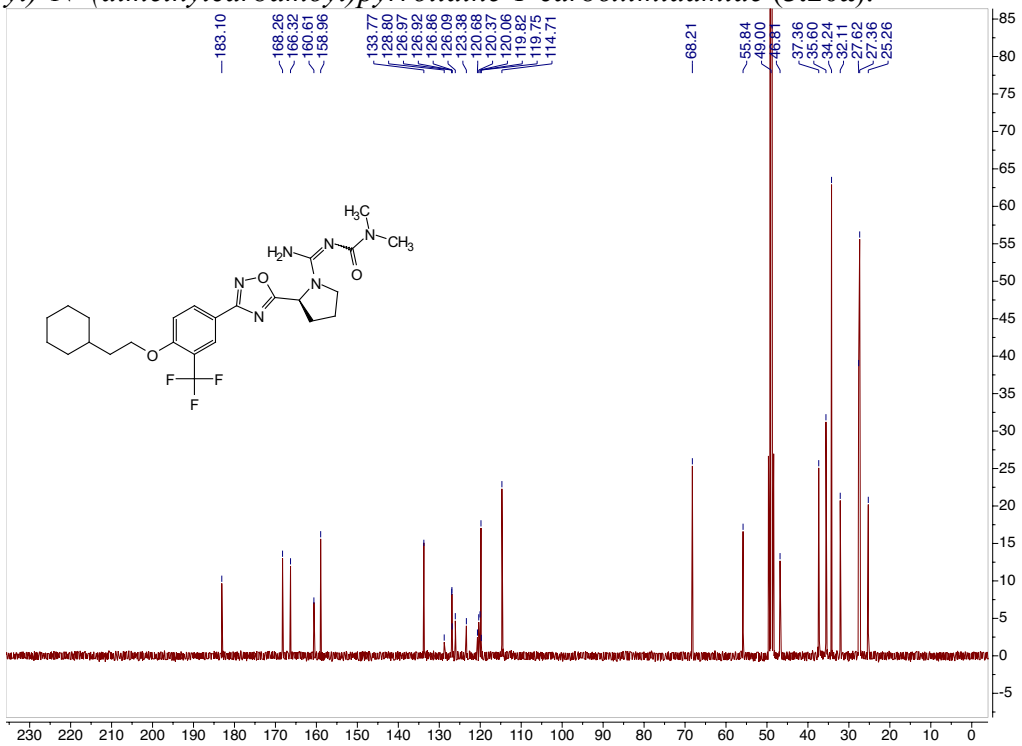

^{1}H spectrum for *(*S*)-2-(3-(4-(2-cyclohexylethoxy)-3-(trifluoromethyl)phenyl)-1,2,4-oxadiazol-5-yl)-*N*′-(methoxy(methyl)carbamoyl)pyrrolidine-1-carboximidamide* (**3.20b**).

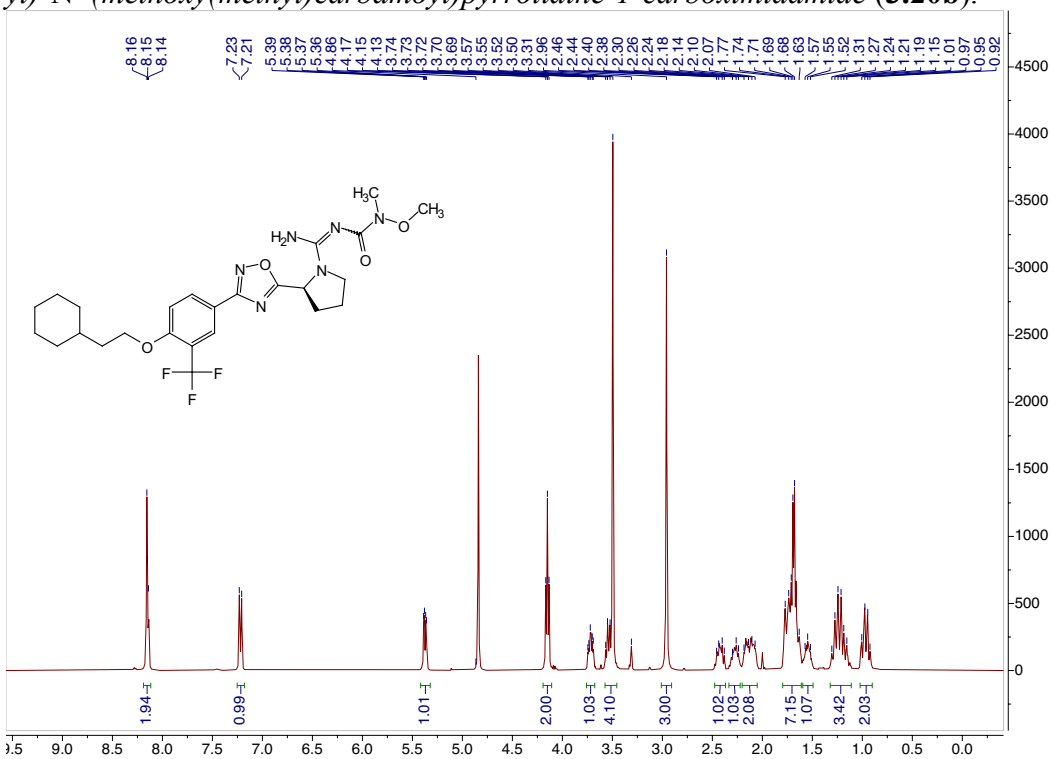

^{13}C spectrum for *(*S*)-2-(3-(4-(2-cyclohexylethoxy)-3-(trifluoromethyl)phenyl)-1,2,4-oxadiazol-5-yl)-*N*′-(methoxy(methyl)carbamoyl)pyrrolidine-1-carboximidamide* (**3.20b**).

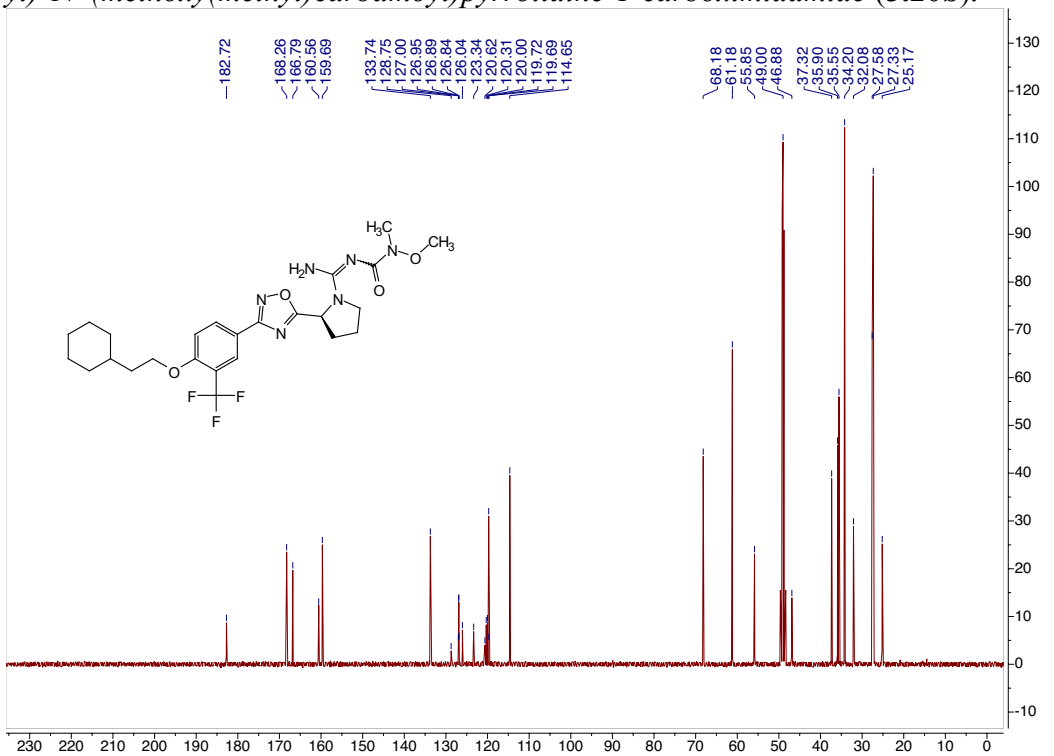

^{1}H spectrum for *(*S*)*-N-*(amino(2-(3-(4-(2-cyclohexylethoxy)-3-(trifluoromethyl)phenyl)-1,2,4 oxadiazol-5-yl)pyrrolidin-1-yl)methylene)morpholine-4-carboxamide* (**3.20c**).

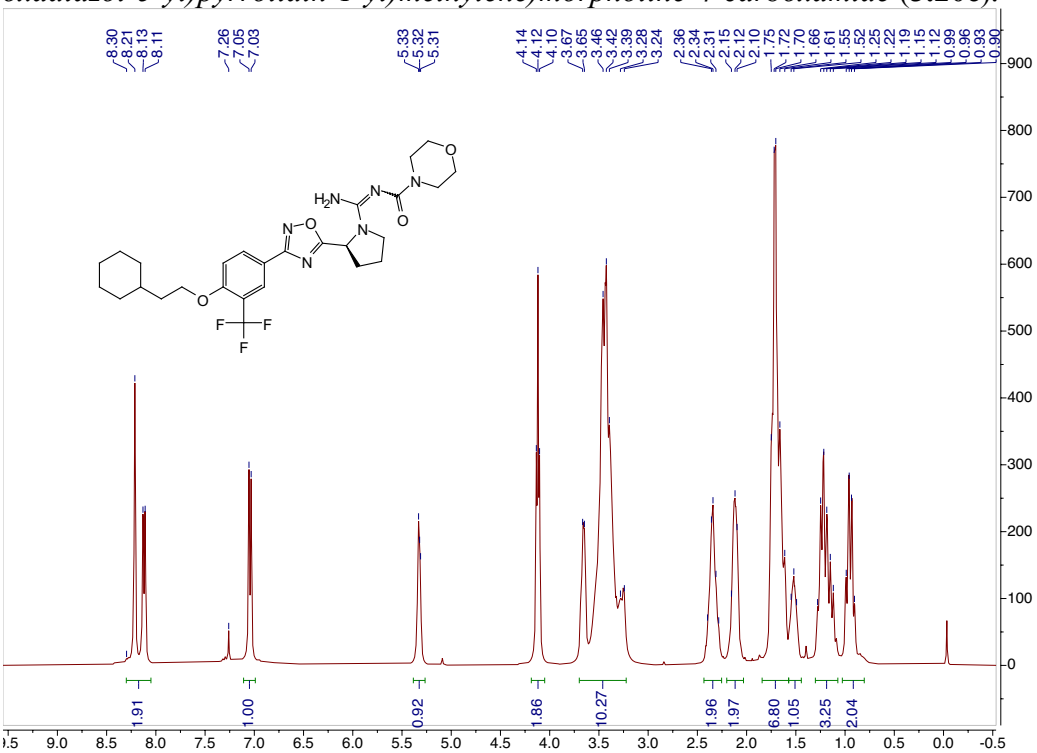

^{13}C spectrum for *(*S*)*-N-*(amino(2-(3-(4-(2-cyclohexylethoxy)-3-(trifluoromethyl)phenyl)-1,2,4 oxadiazol-5-yl)pyrrolidin-1-yl)methylene)morpholine-4-carboxamide* (**3.20c**).

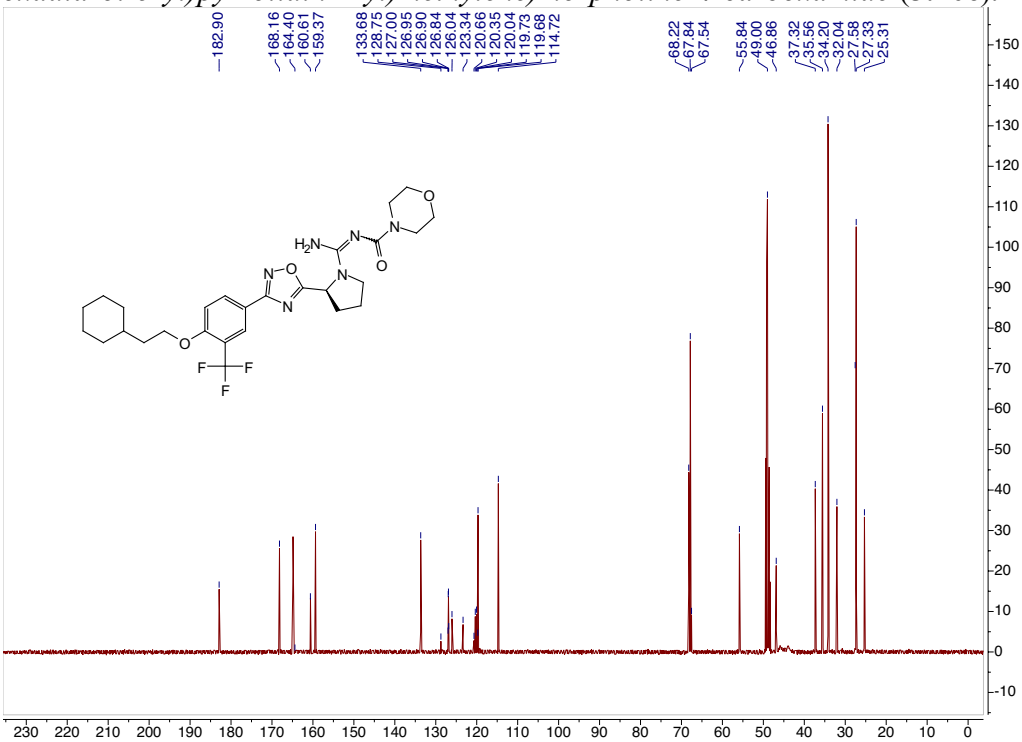

^{1}H spectrum for *phenyl (*S*)-(amino(2-(3-(4-(2-cyclohexylethoxy)-3-(trifluoromethyl)phenyl)-1,2,4-oxadiazol-5-yl)pyrrolidin-1-yl)methylene)carbamate* (**3.20d**).

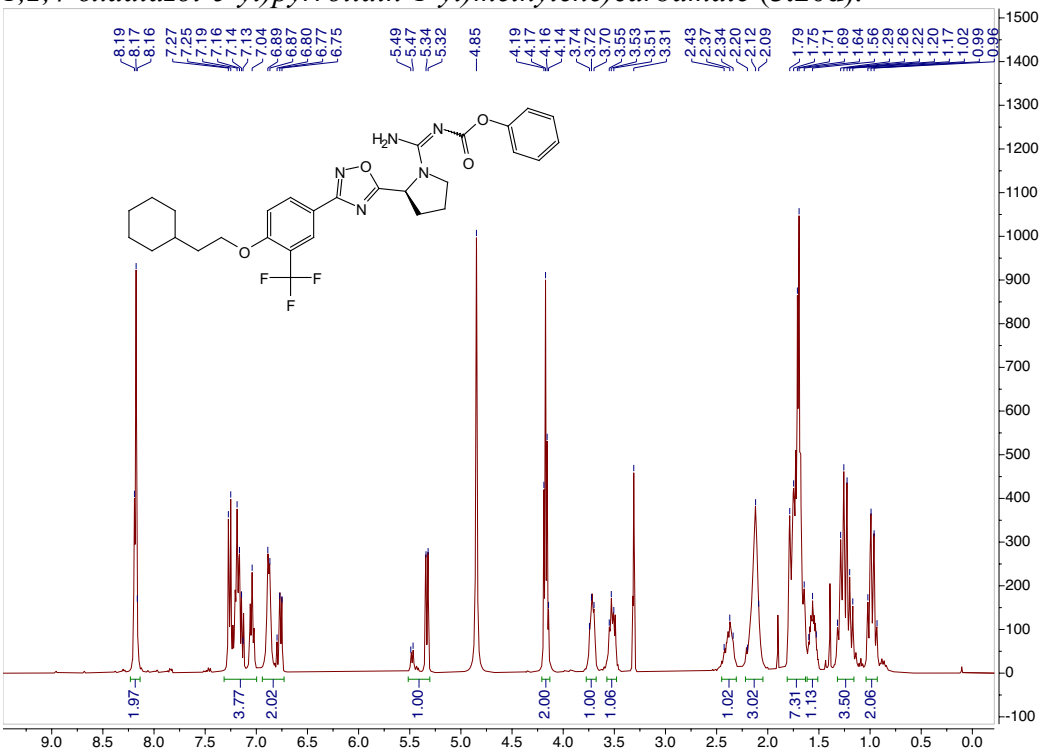

^{13}C spectrum for *phenyl (*S*)-(amino(2-(3-(4-(2-cyclohexylethoxy)-3-(trifluoromethyl)phenyl)-1,2,4-oxadiazol-5-yl)pyrrolidin-1-yl)methylene)carbamate* (**3.20d**).

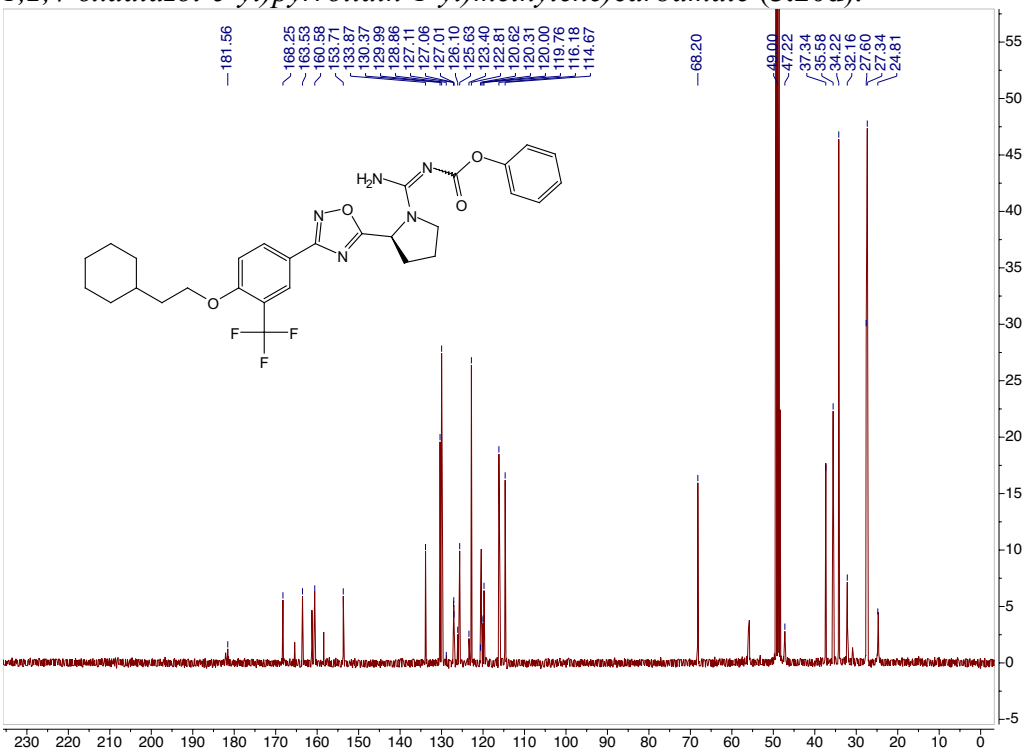

^{1}H spectrum for *methyl (*S*)-(amino(2-(3-(4-(2-cyclohexylethoxy)-3-(trifluoromethyl)phenyl)-1,2,4-oxadiazol-5-yl)pyrrolidin-1-yl)methylene)carbamate* (**3.20e**).

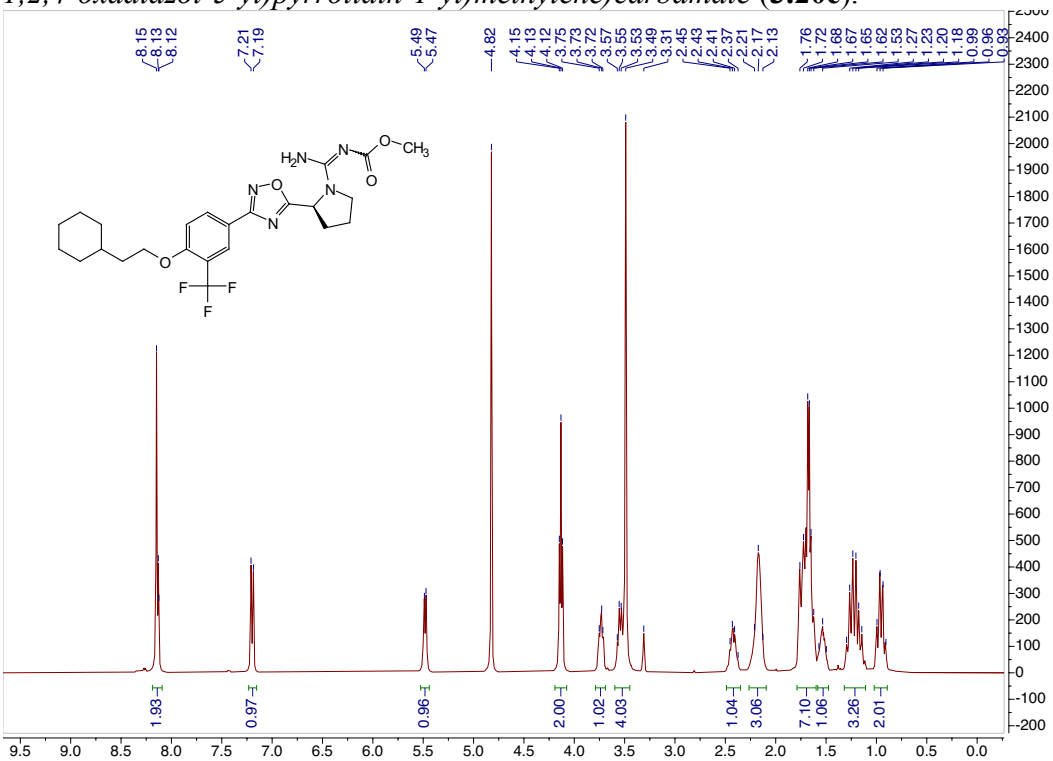

^{13}C spectrum for *methyl (*S*)-(amino(2-(3-(4-(2-cyclohexylethoxy)-3-(trifluoromethyl)phenyl)-1,2,4-oxadiazol-5-yl)pyrrolidin-1-yl)methylene)carbamate* (**3.20e**).

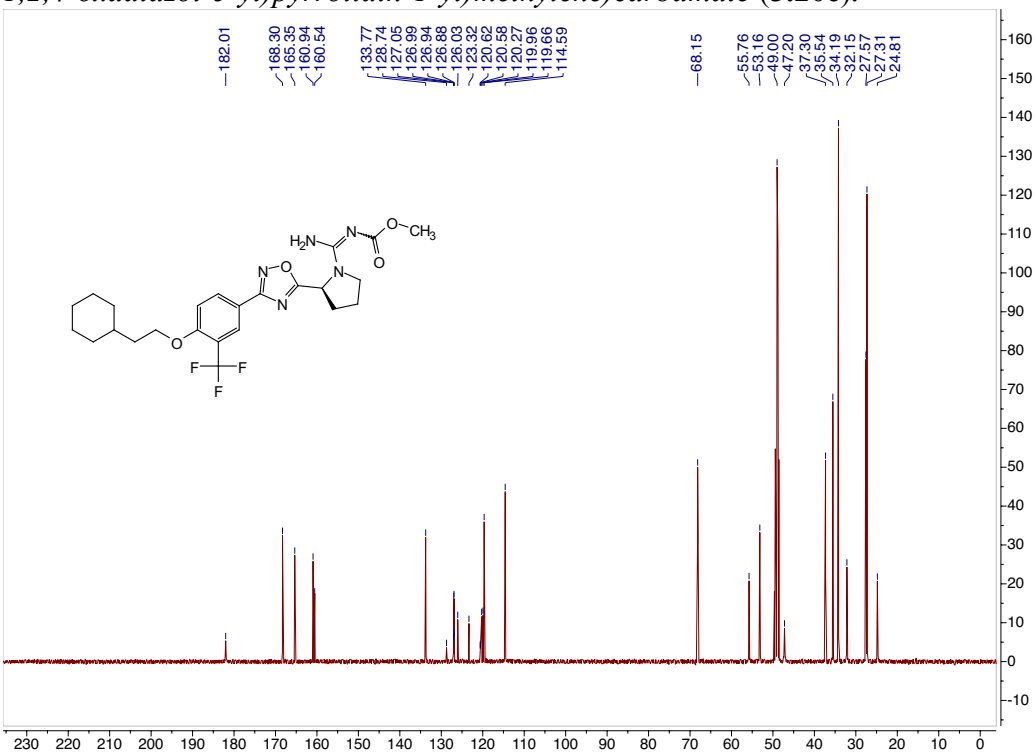

^{1}H spectrum for *ethyl (*S*)-(amino(2-(3-(4-(2-cyclohexylethoxy)-3-(trifluoromethyl)phenyl)-1,2,4-oxadiazol-5-yl)pyrrolidin-1-yl)methylene)carbamate* (**3.20f**).

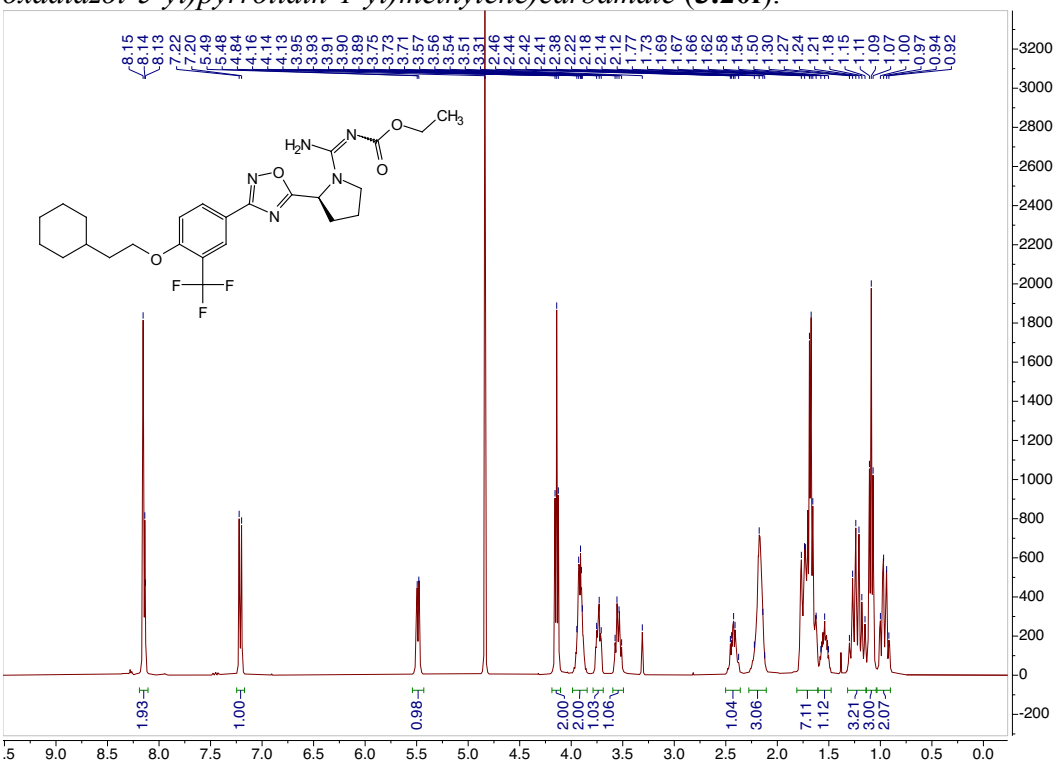

^{13}C spectrum for *ethyl (*S*)-(amino(2-(3-(4-(2-cyclohexylethoxy)-3-(trifluoromethyl)phenyl)-1,2,4-oxadiazol-5-yl)pyrrolidin-1-yl)methylene)carbamate* (**3.20f**).

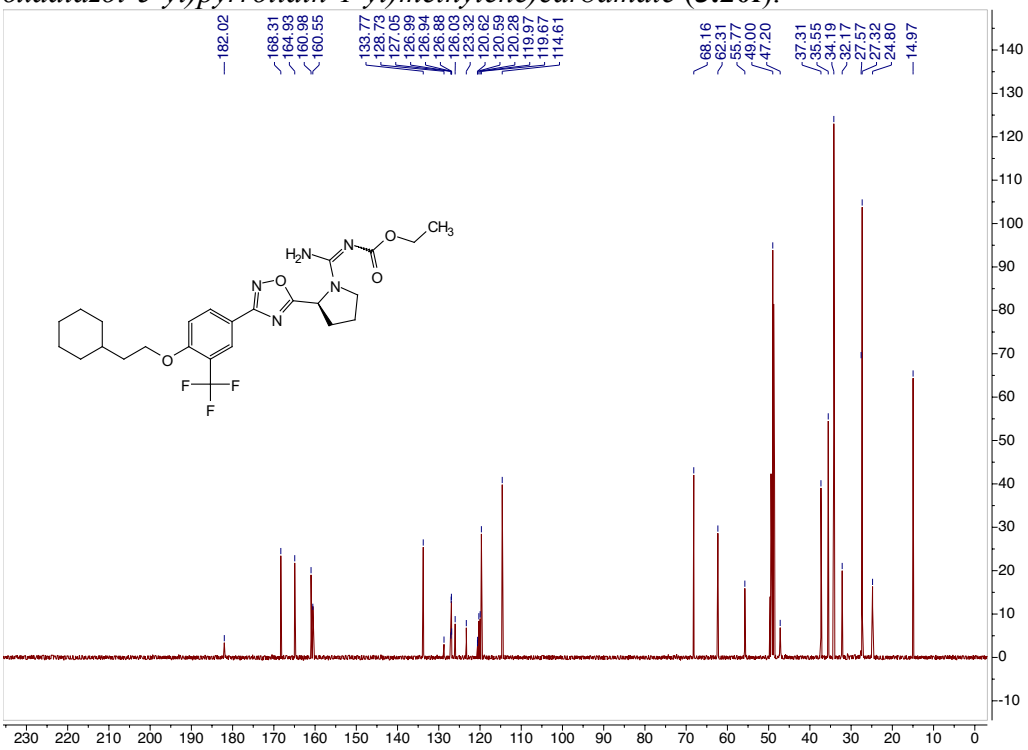

^{1}H spectrum for *benzyl (*S*)-(amino(2-(3-(4-(2-cyclohexylethoxy)-3-(trifluoromethyl)phenyl)-1,2,4-oxadiazol-5-yl)pyrrolidin-1-yl)methylene)carbamate* (**3.20g**).

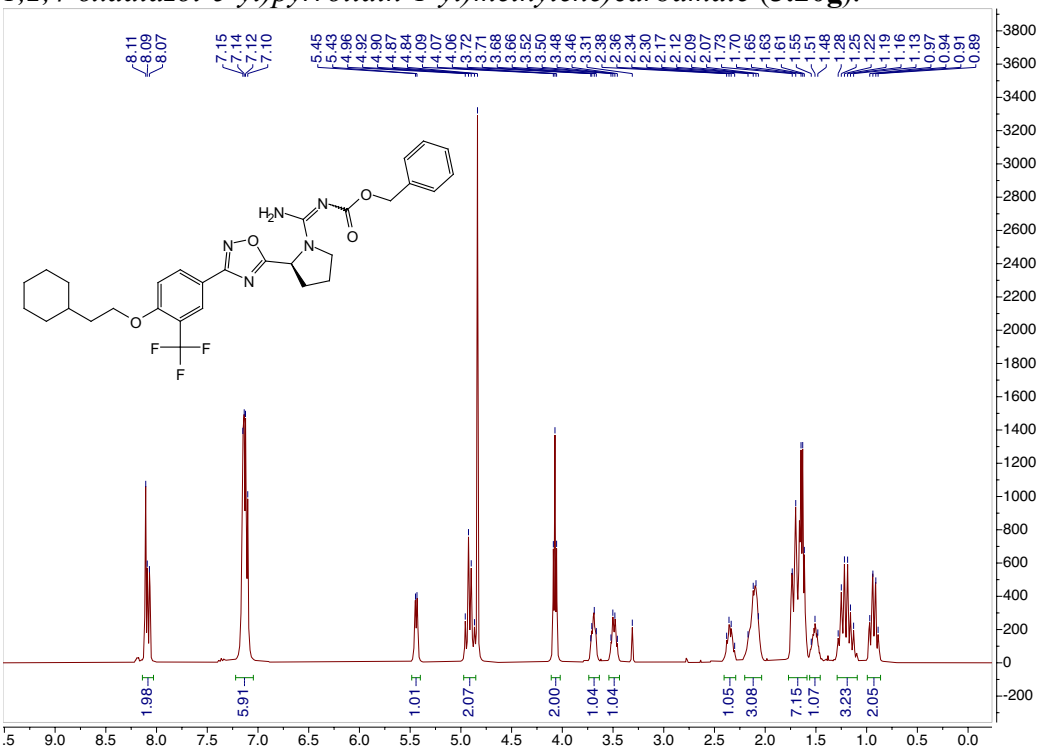

^{13}C spectrum for *benzyl (*S*)-(amino(2-(3-(4-(2-cyclohexylethoxy)-3-(trifluoromethyl)phenyl)-1,2,4-oxadiazol-5-yl)pyrrolidin-1-yl)methylene)carbamate* (**3.20g**).

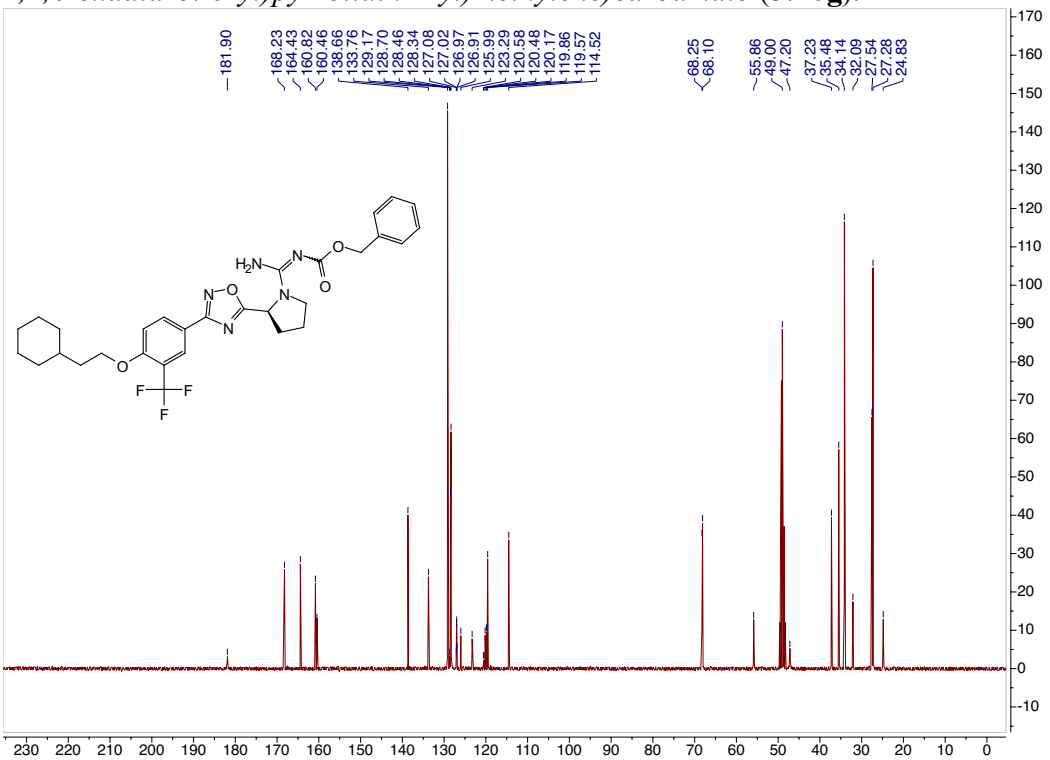

^{1}H spectrum for *allyl (*S*)-(amino(2-(3-(4-(2-cyclohexylethoxy)-3-(trifluoromethyl)phenyl)-1,2,4-oxadiazol-5-yl)pyrrolidin-1-yl)methylene)carbamate* (**3.20h**).

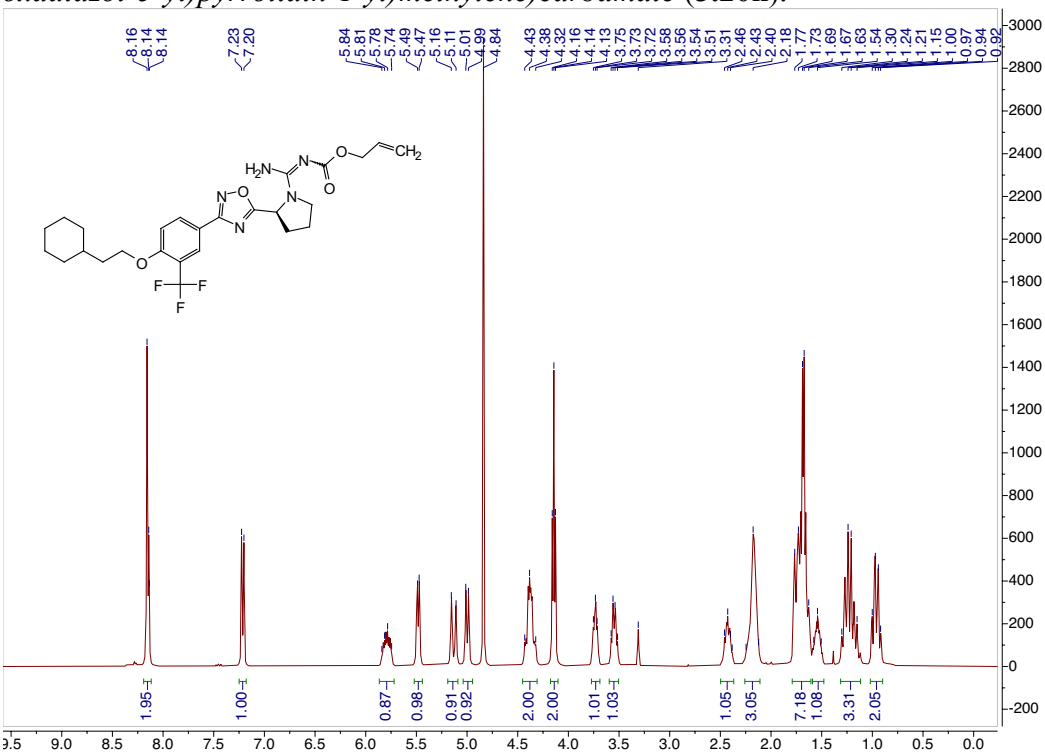

^{13}C spectrum for *allyl (*S*)-(amino(2-(3-(4-(2-cyclohexylethoxy)-3-(trifluoromethyl)phenyl)-1,2,4-oxadiazol-5-yl)pyrrolidin-1-yl)methylene)carbamate* (**3.20h**).

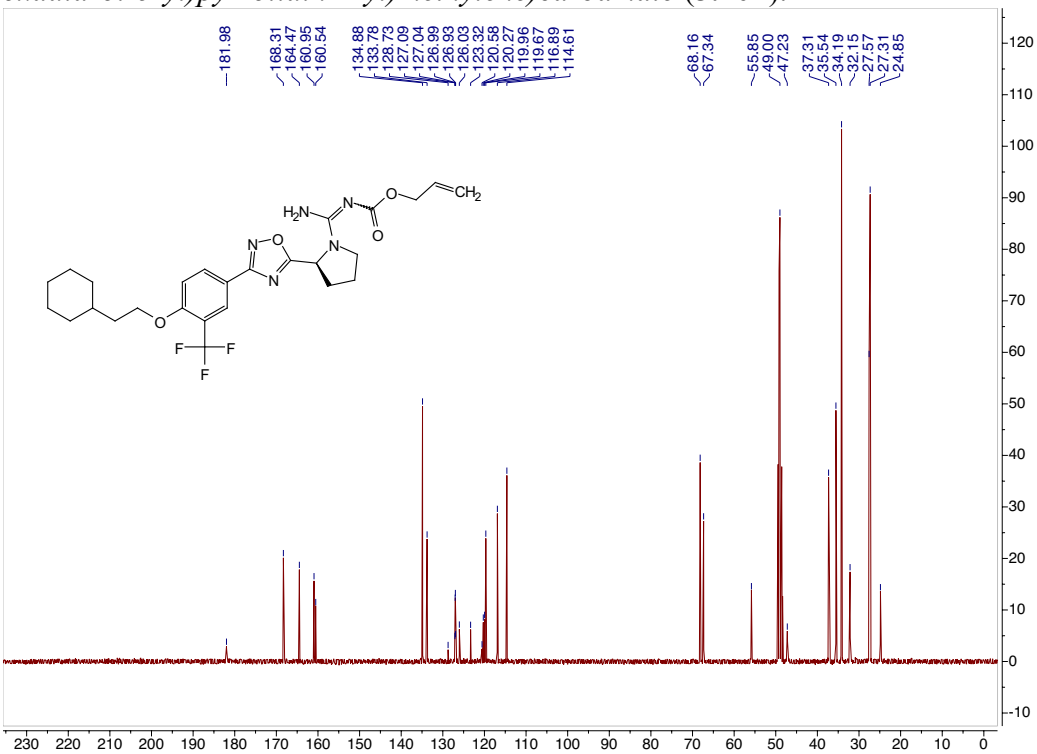

^{1}H spectrum for *2-methoxyethyl (*S*)-(amino(2-(3-(4-(2-cyclohexylethoxy)-3-(trifluoromethyl)phenyl)-1,2,4-oxadiazol-5-yl)pyrrolidin-1-yl)methylene)carbamate* (**3.20i**).

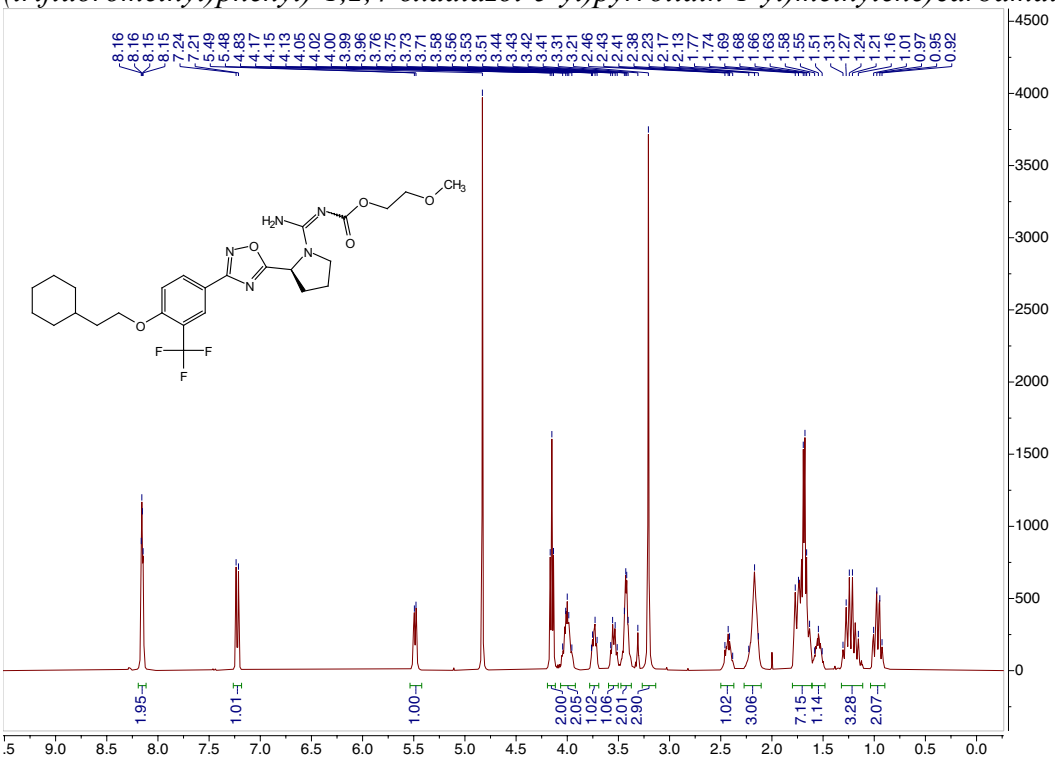

^{13}C spectrum for *2-methoxyethyl (*S*)-(amino(2-(3-(4-(2-cyclohexylethoxy)-3-(trifluoromethyl)phenyl)-1,2,4-oxadiazol-5-yl)pyrrolidin-1-yl)methylene)carbamate* (**3.20i**).

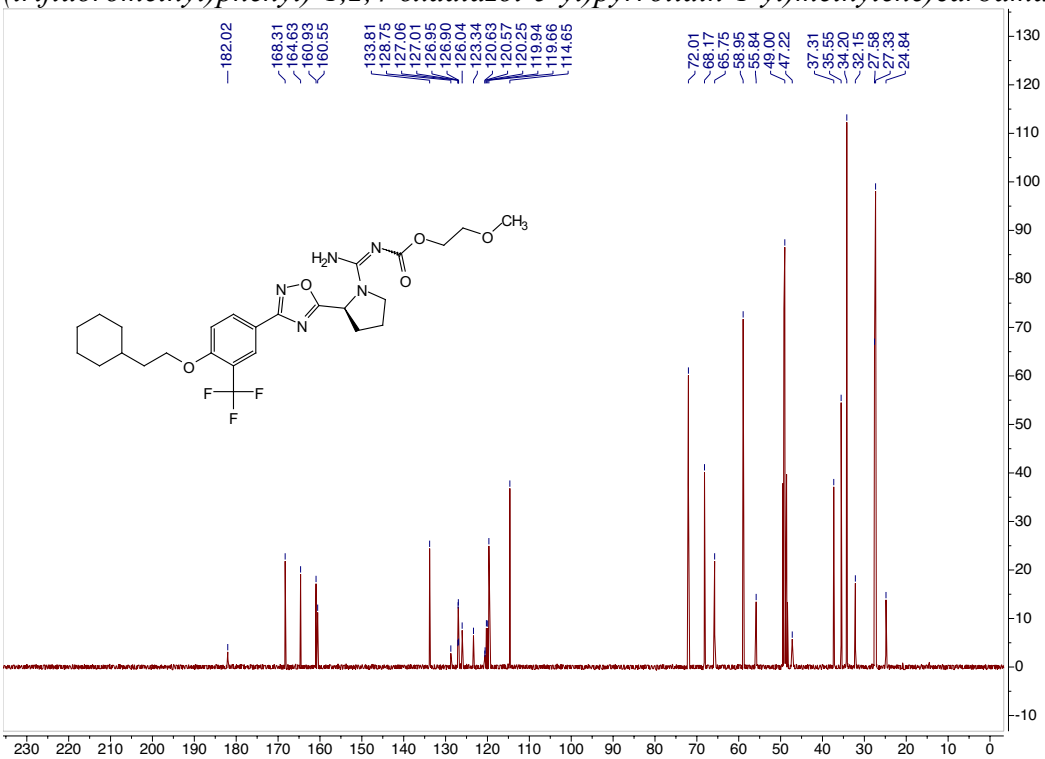

^{1}H spectrum for *(*S*)-*N*′-cyano-2-(3-(4-(2-cyclohexylethoxy)-3-(trifluoromethyl)phenyl)-1,2,4-oxadiazol-5-yl)pyrrolidine-1-carboximidamide* (**3.20j**).

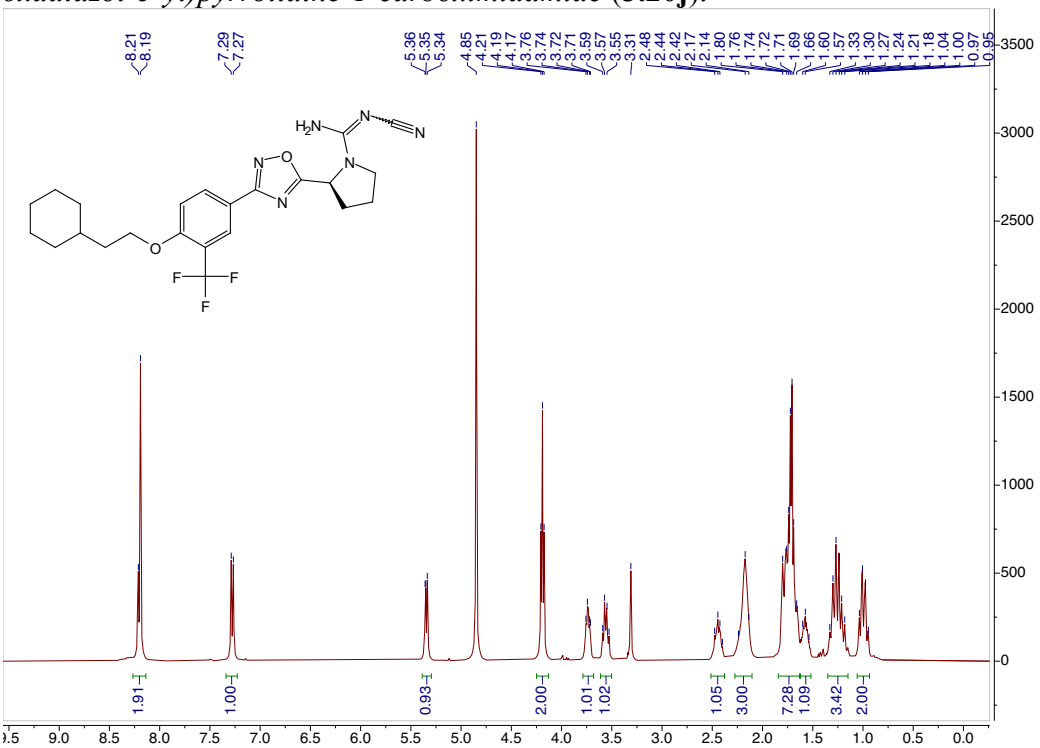

^{13}C spectrum for *(*S*)-*N*′-cyano-2-(3-(4-(2-cyclohexylethoxy)-3-(trifluoromethyl)phenyl)-1,2,4-oxadiazol-5-yl)pyrrolidine-1-carboximidamide* (**3.20j**).

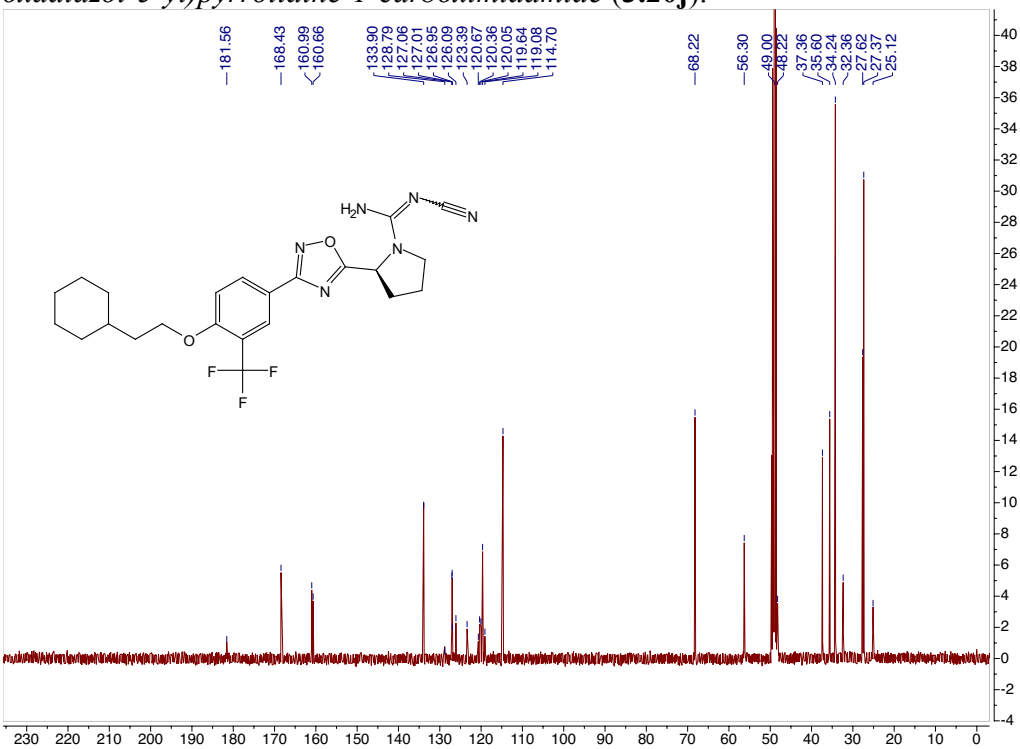

^{1}H spectrum for *(*S*)-2-(3-(4-(2-cyclohexylethoxy)-3-(trifluoromethyl)phenyl)-1,2,4-oxadiazol-5-yl)-*N*′-(methylsulfonyl)pyrrolidine-1-carboximidamide* (**3.20k**).

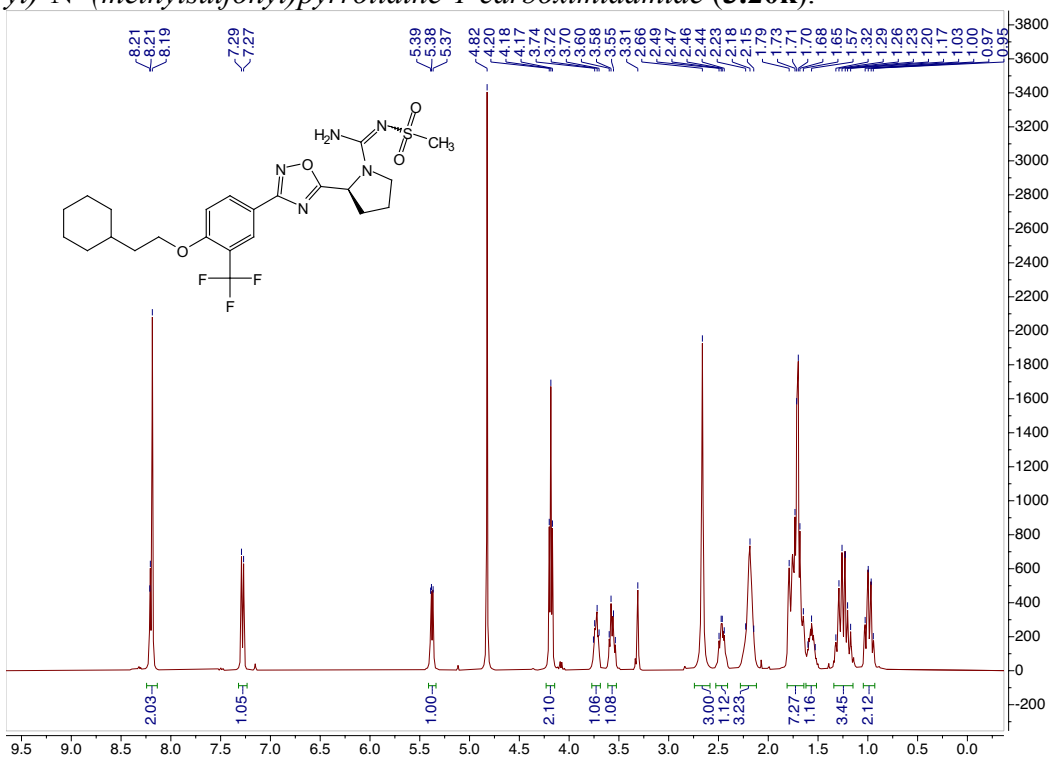

^{13}C spectrum for *(*S*)-2-(3-(4-(2-cyclohexylethoxy)-3-(trifluoromethyl)phenyl)-1,2,4-oxadiazol-5-yl)-*N*′-(methylsulfonyl)pyrrolidine-1-carboximidamide* (**3.20k**).

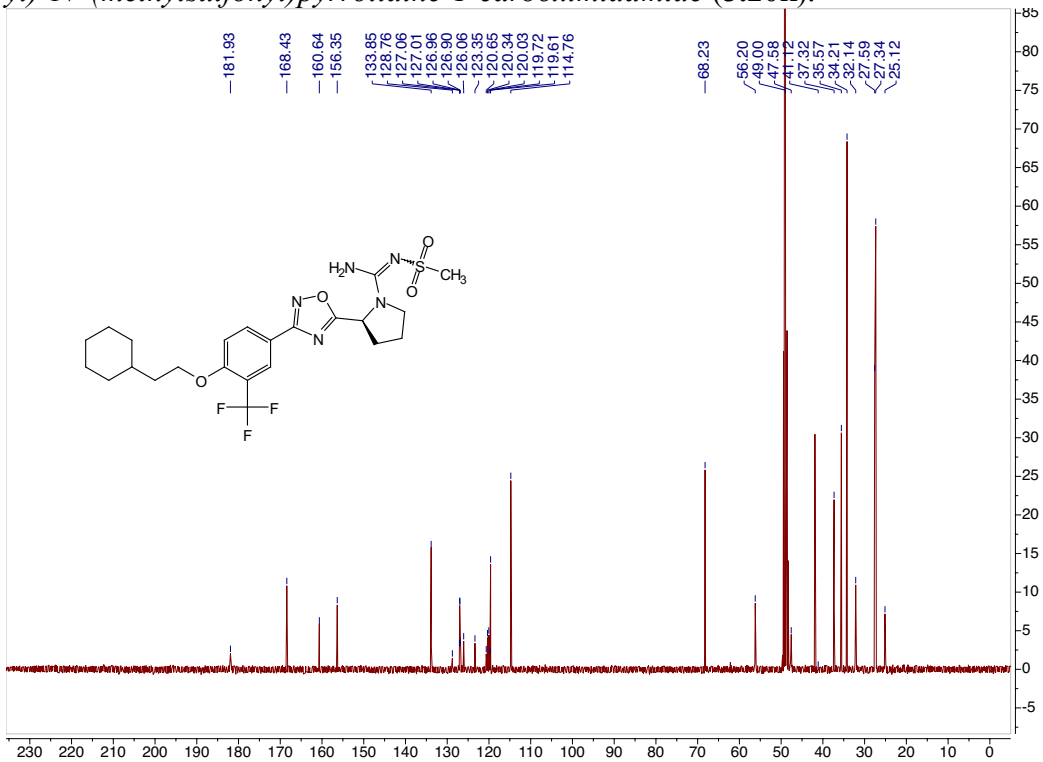

^{1}H spectrum for *(*S*)-2-(3-(4-(2-cyclohexylethoxy)-3-(trifluoromethyl)phenyl)-1,2,4-oxadiazol-5-yl)-*N*′-((trifluoromethyl)sulfonyl)pyrrolidine-1-carboximidamide* (**3.20l**).

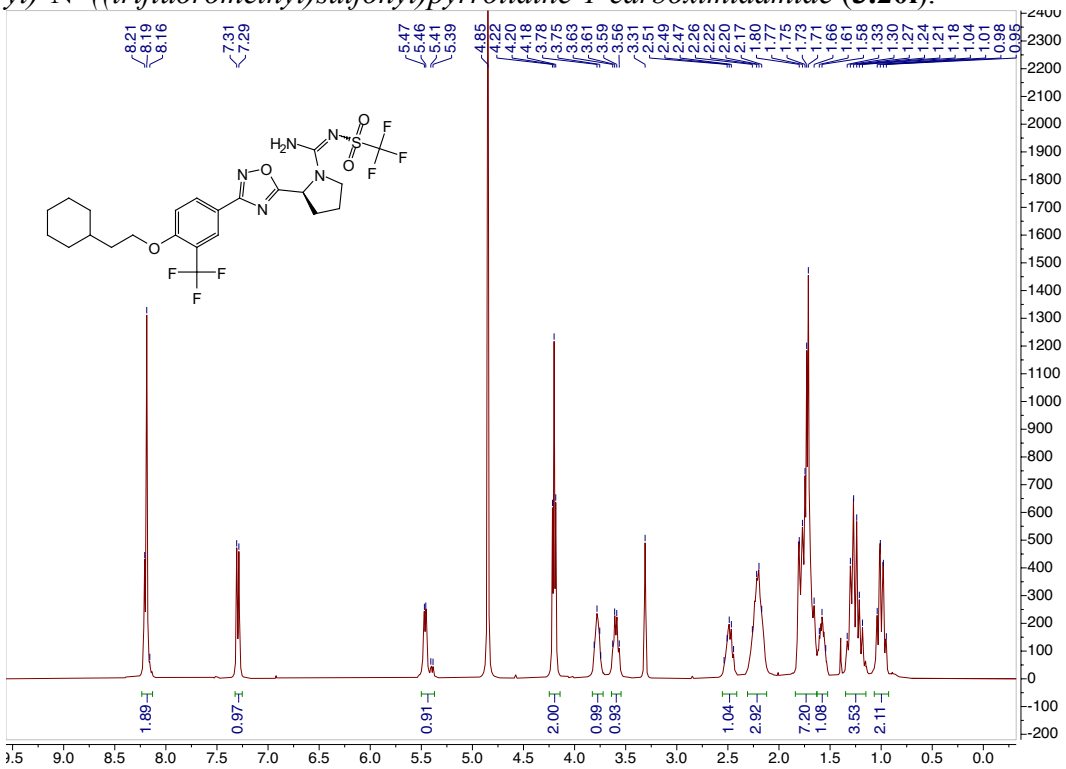

^{13}C spectrum for *(*S*)-2-(3-(4-(2-cyclohexylethoxy)-3-(trifluoromethyl)phenyl)-1,2,4-oxadiazol-5-yl)-*N*′-((trifluoromethyl)sulfonyl)pyrrolidine-1-carboximidamide* (**3.20l**).

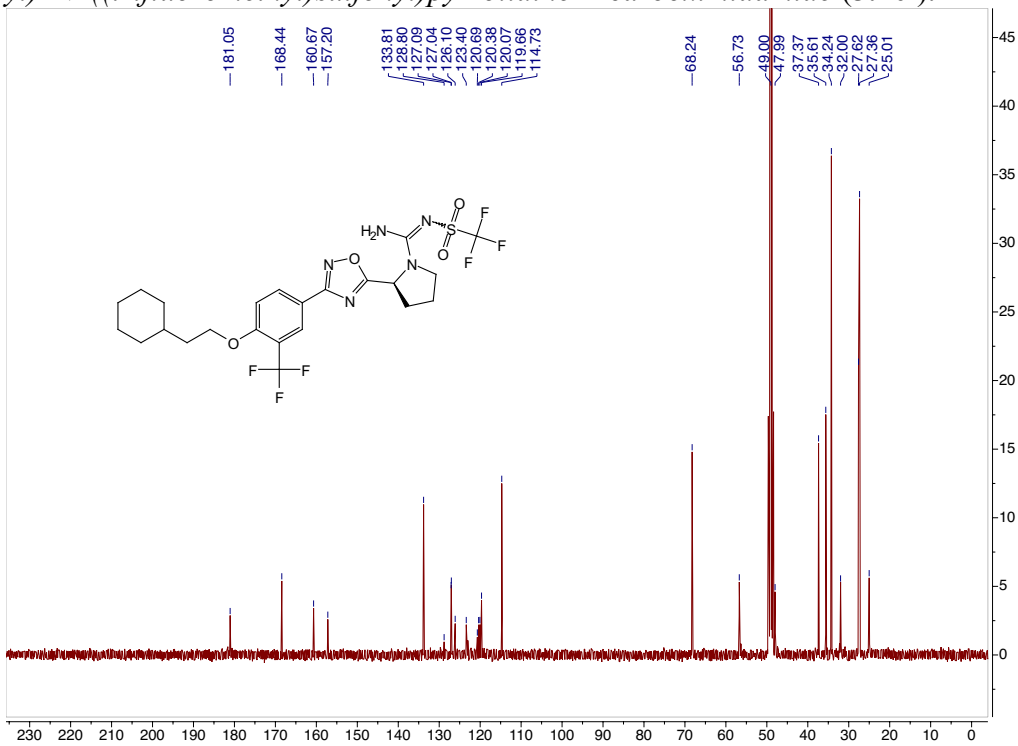

^{1}H spectrum for *(*S*)-2-(3-(4-(2-cyclohexylethoxy)-3-(trifluoromethyl)phenyl)-1,2,4-oxadiazol-5-yl)-*N*′-tosylpyrrolidine-1-carboximidamide* (**3.20m**).

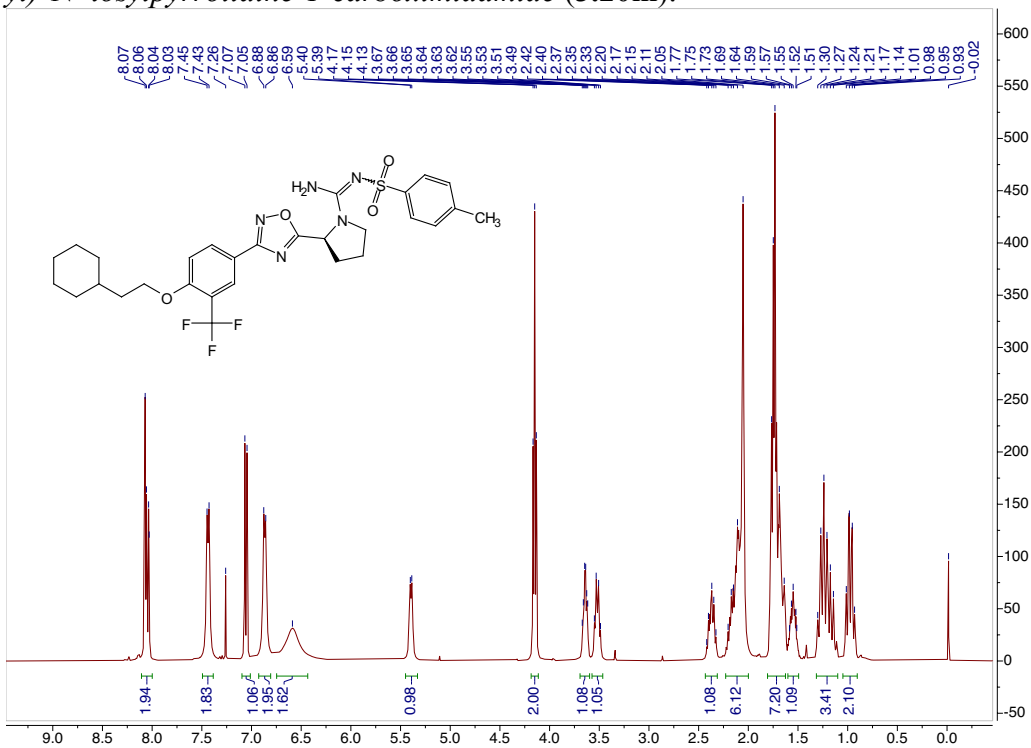

^{13}C spectrum for *(*S*)-2-(3-(4-(2-cyclohexylethoxy)-3-(trifluoromethyl)phenyl)-1,2,4-oxadiazol-5-yl)-*N*′-tosylpyrrolidine-1-carboximidamide* (**3.20m**).

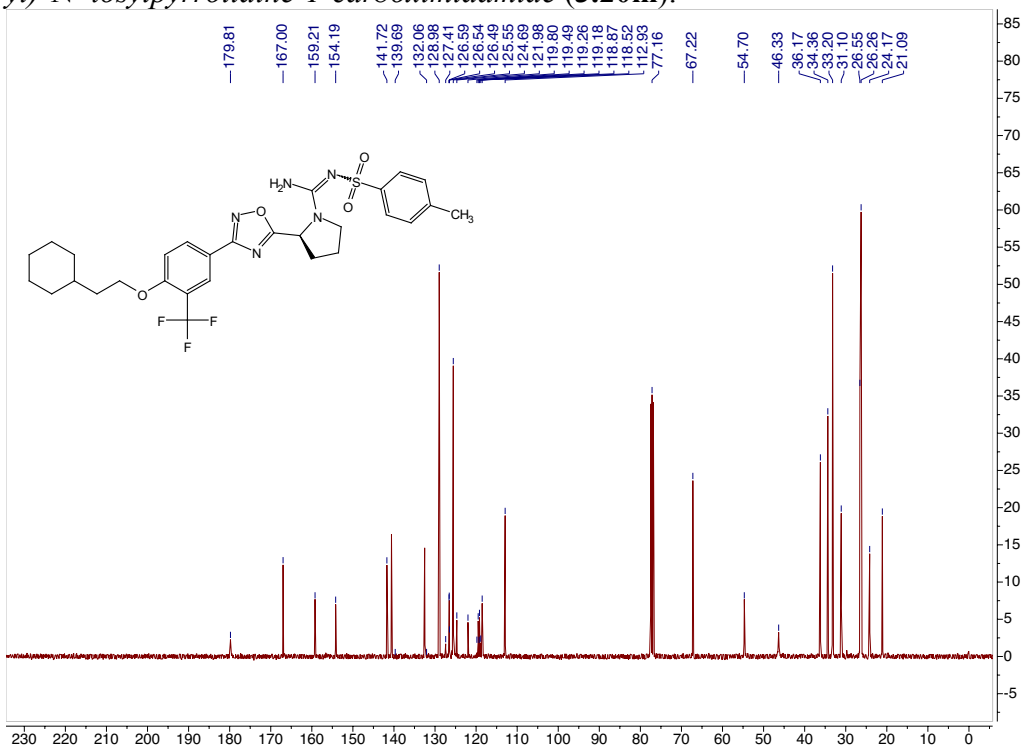

^{1}H spectrum for *(*S*)-N-(amino(2-(3-(4-(2-cyclohexylethoxy)-3-(trifluoromethyl)phenyl)-1,2,4-oxadiazol-5-yl)pyrrolidin-1-yl)methylene)benzamide* (**3.20n**).

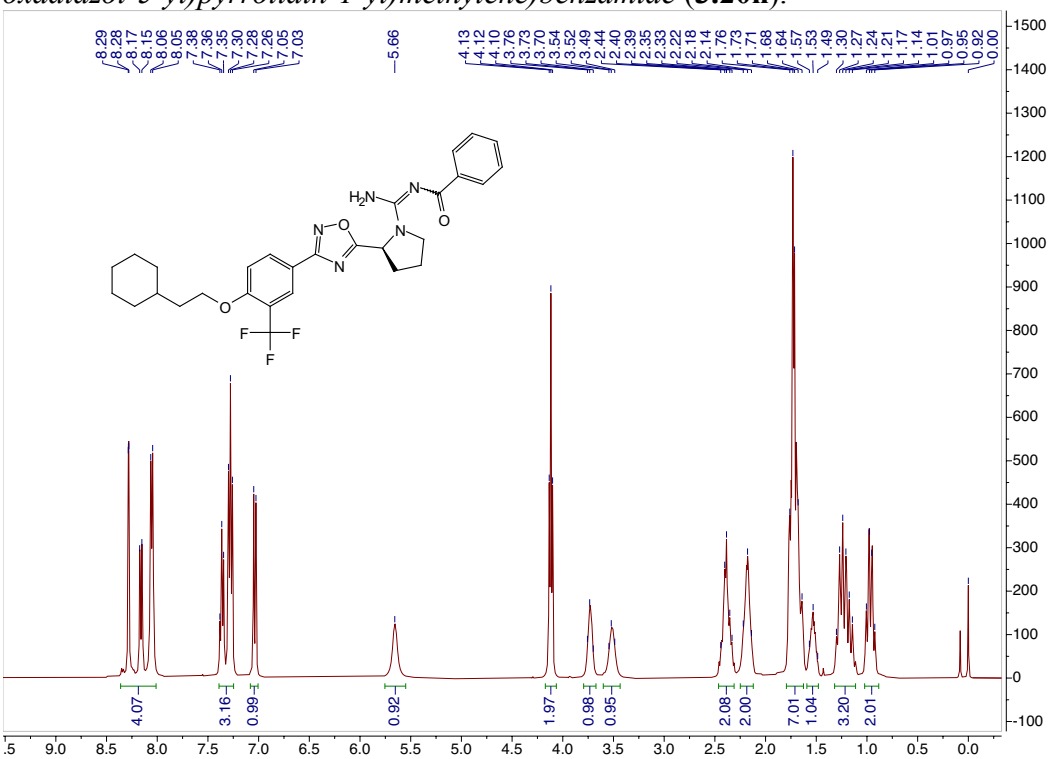

^{13}C spectrum for *(*S*)-N-(amino(2-(3-(4-(2-cyclohexylethoxy)-3-(trifluoromethyl)phenyl)-1,2,4-oxadiazol-5-yl)pyrrolidin-1-yl)methylene)benzamide* (**3.20n**).

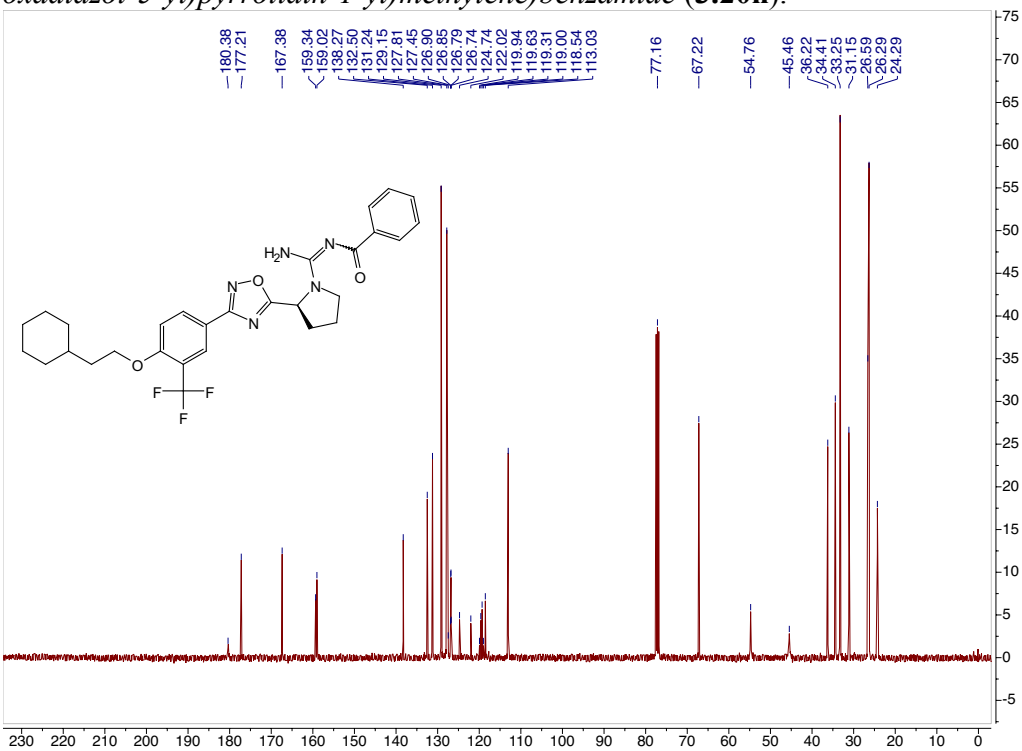

^{1}H spectrum for *(*S*)*-N-*(amino(2-(3-(4-(2-cyclohexylethoxy)-3-(trifluoromethyl)phenyl)-1,2,4-oxadiazol-5-yl)pyrrolidin-1-yl)methylene)benzo[*d*][1,3]dioxole-5-carboxamide* (**3.20o**).

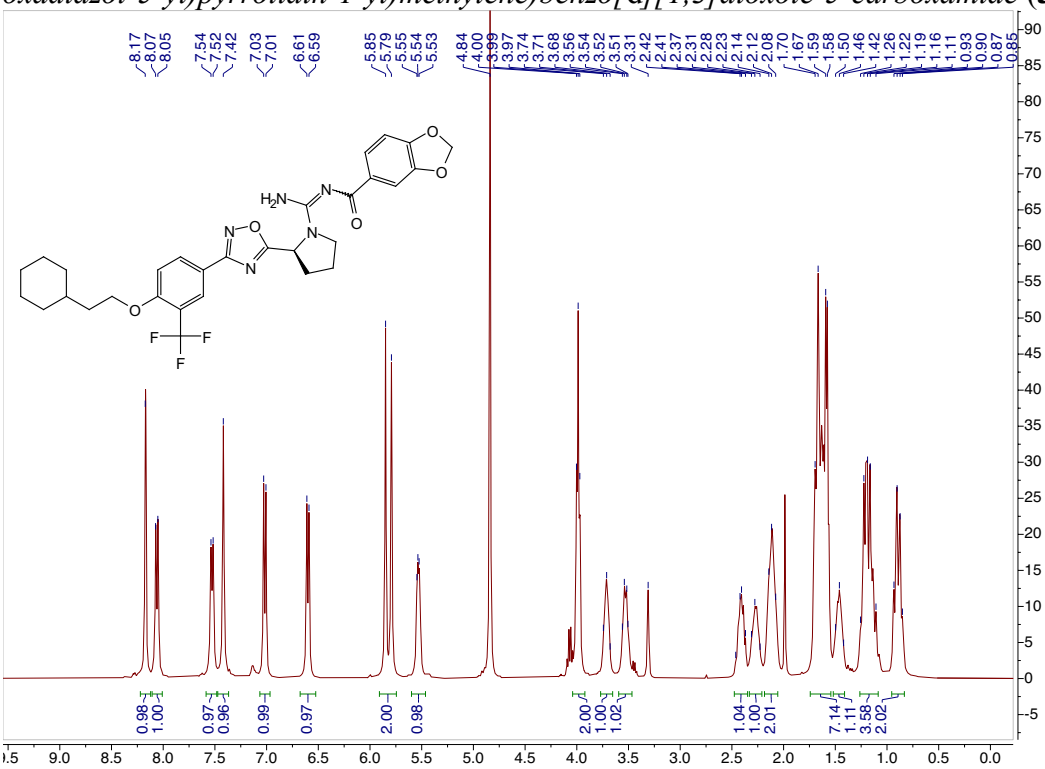

^{13}C spectrum for *(*S*)*-N-*(amino(2-(3-(4-(2-cyclohexylethoxy)-3-(trifluoromethyl)phenyl)-1,2,4-oxadiazol-5-yl)pyrrolidin-1-yl)methylene)benzo[*d*][1,3]dioxole-5-carboxamide* (**3.20o**).

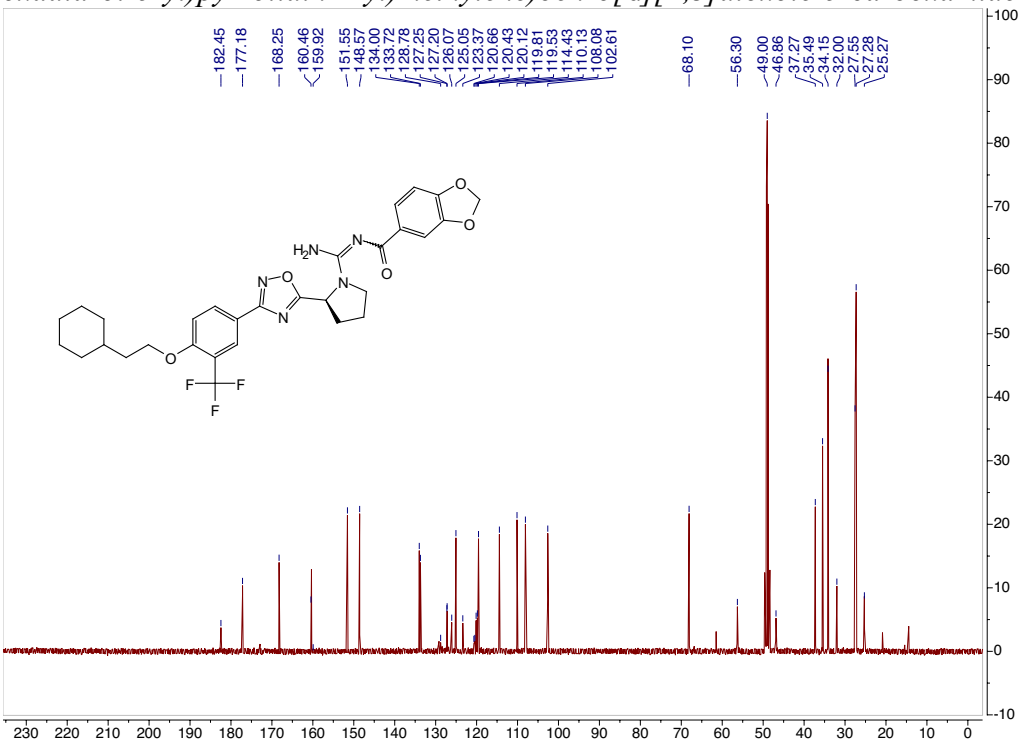

^{1}H spectrum for *(*S*)*-N-*(amino(2-(3-(4-(2-cyclohexylethoxy)-3-(trifluoromethyl)phenyl)-1,2,4-oxadiazol-5-yl)pyrrolidin-1-yl)methylene)-2,2,2-trifluoroacetamide* (**3.20p**).

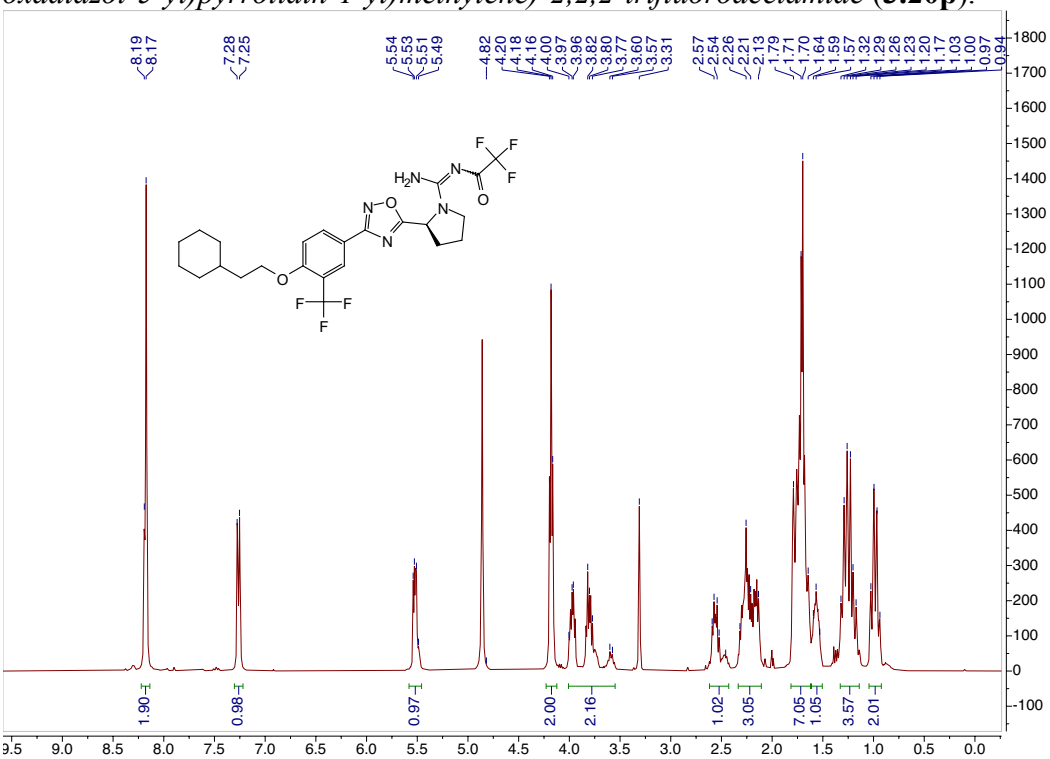

^{13}C spectrum for *(*S*)*-N-*(amino(2-(3-(4-(2-cyclohexylethoxy)-3-(trifluoromethyl)phenyl)-1,2,4-oxadiazol-5-yl)pyrrolidin-1-yl)methylene)-2,2,2-trifluoroacetamide* (**3.20p**).

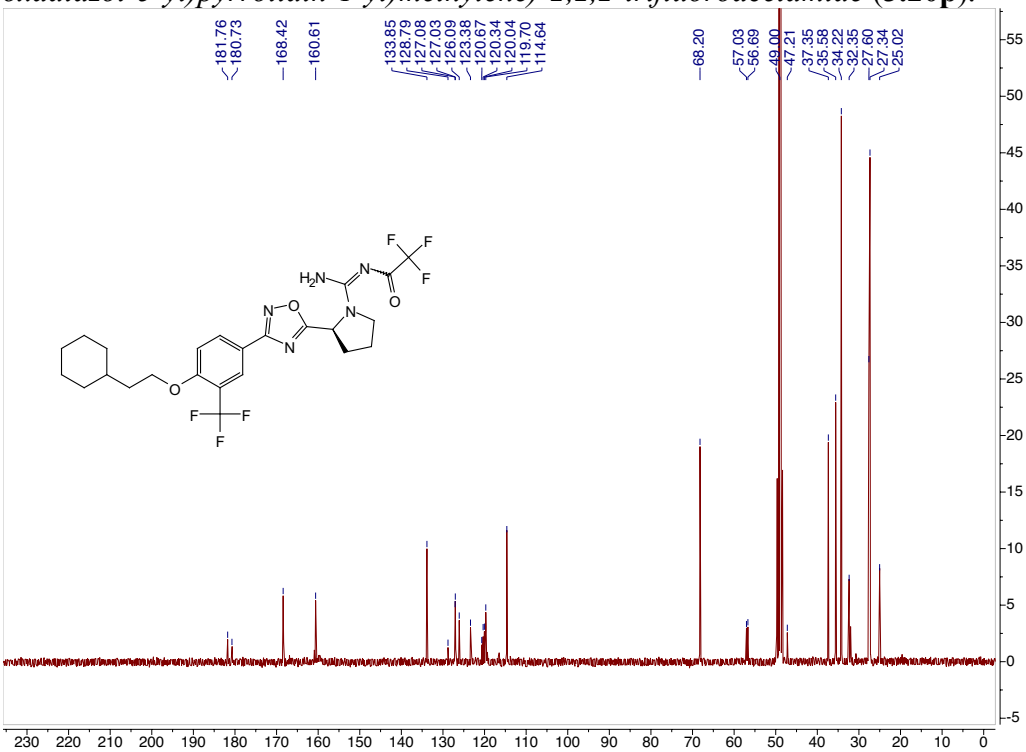

^{1}H spectrum for *(*S*)*-N-*(amino(2-(3-(4-(2-cyclohexylethoxy)-3-(trifluoromethyl)phenyl)-1,2,4-oxadiazol-5-yl)pyrrolidin-1-yl)methylene)acetamide* (**3.20q**).

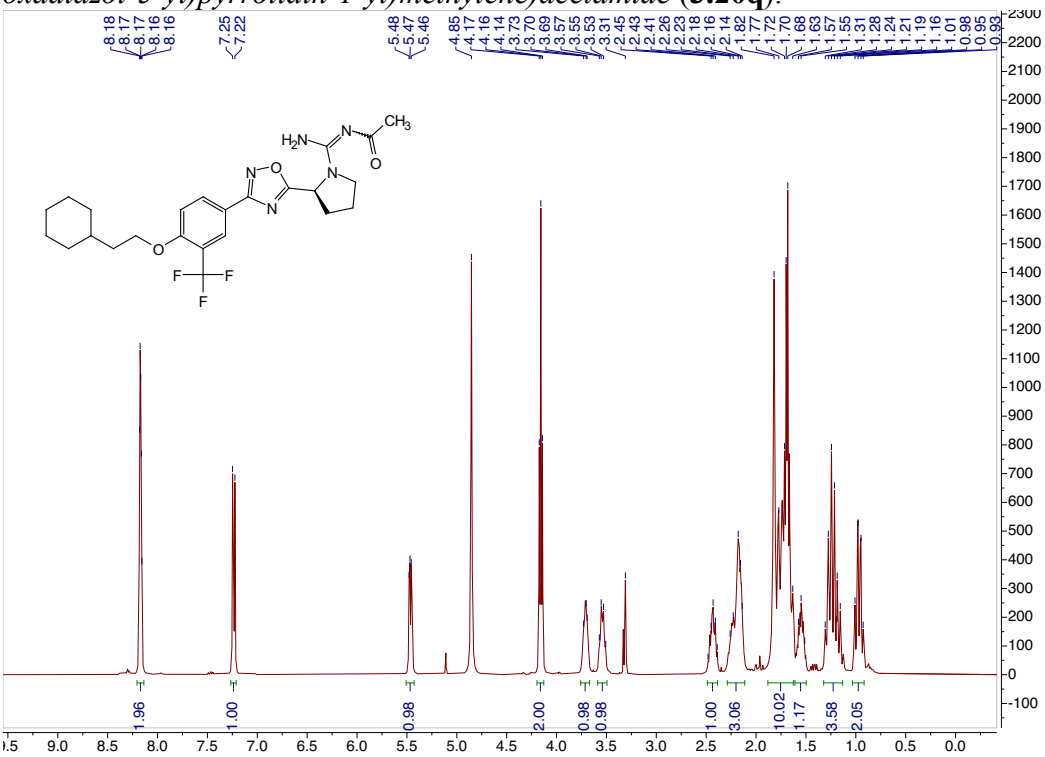

^{13}C spectrum for *(*S*)*-N-*(amino(2-(3-(4-(2-cyclohexylethoxy)-3-(trifluoromethyl)phenyl)-1,2,4-oxadiazol-5-yl)pyrrolidin-1-yl)methylene)acetamide* (**3.20q**).

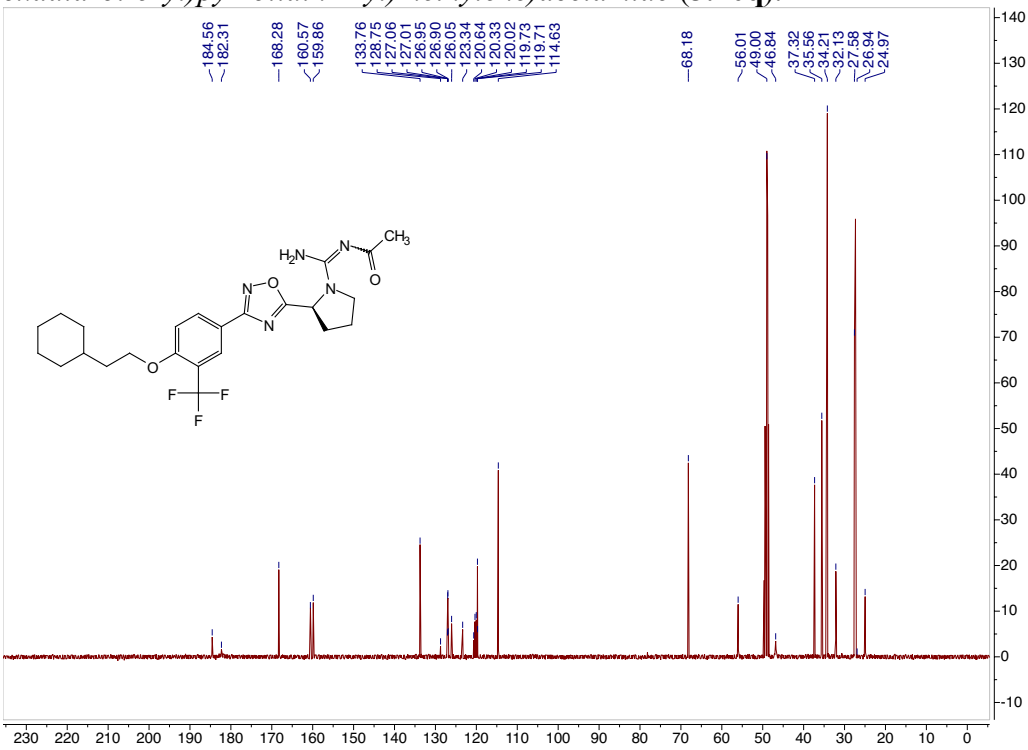

^{1}H spectrum for *(*S*)*-N-*(amino(2-(3-(4-(2-cyclohexylethoxy)-3-(trifluoromethyl)phenyl)-1,2,4-oxadiazol-5-yl)pyrrolidin-1-yl)methylene)propionamide* (**3.20r**).

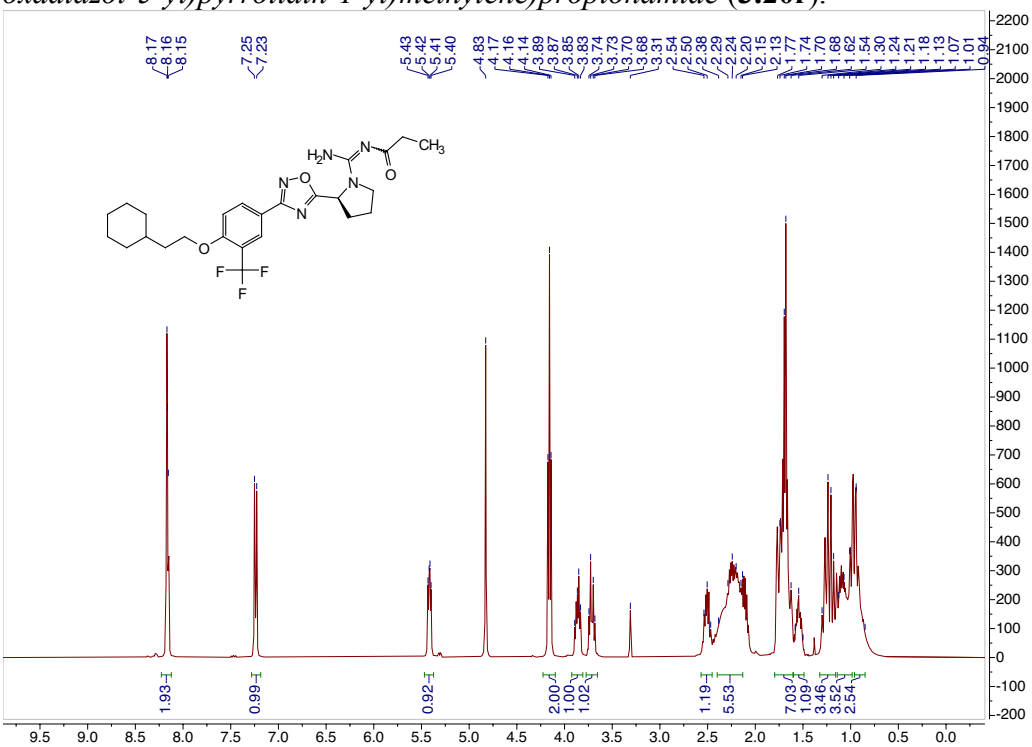

^{13}C spectrum for *(*S*)*-N-*(amino(2-(3-(4-(2-cyclohexylethoxy)-3-(trifluoromethyl)phenyl)-1,2,4-oxadiazol-5-yl)pyrrolidin-1-yl)methylene)propionamide* (**3.20r**).

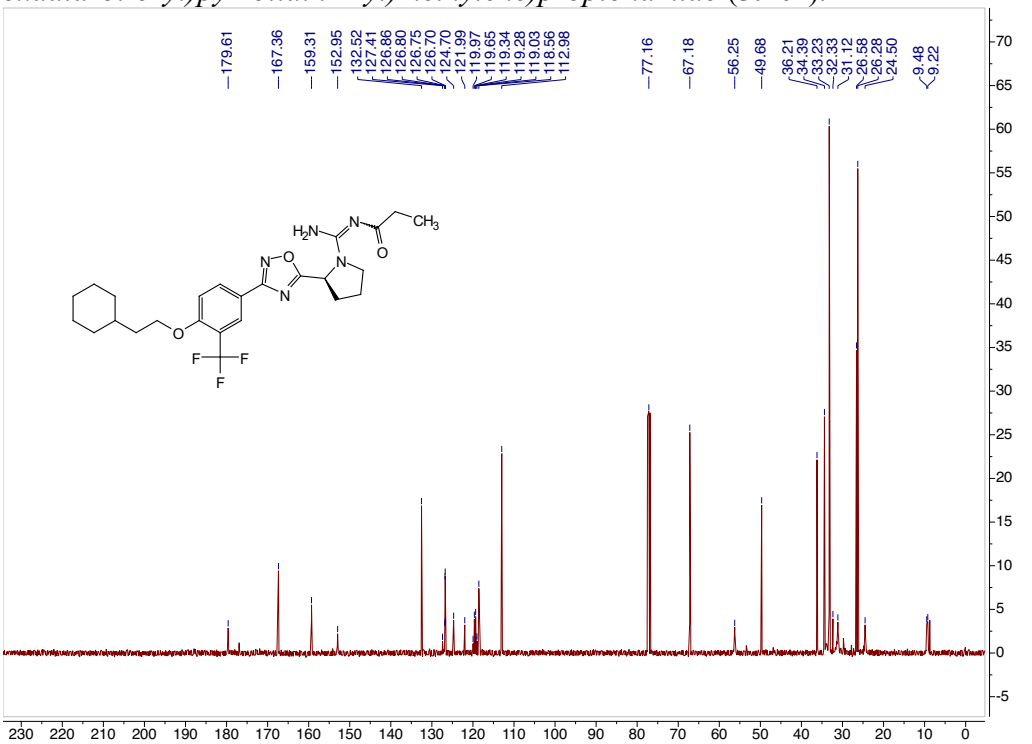

^{1}H spectrum for *(*S*)*-N-*(amino(2-(3-(4-(2-cyclohexylethoxy)-3-(trifluoromethyl)phenyl)-1,2,4-oxadiazol-5-yl)pyrrolidin-1-yl)methylene)-2-(benzyloxy)acetamide* (**3.20s**).

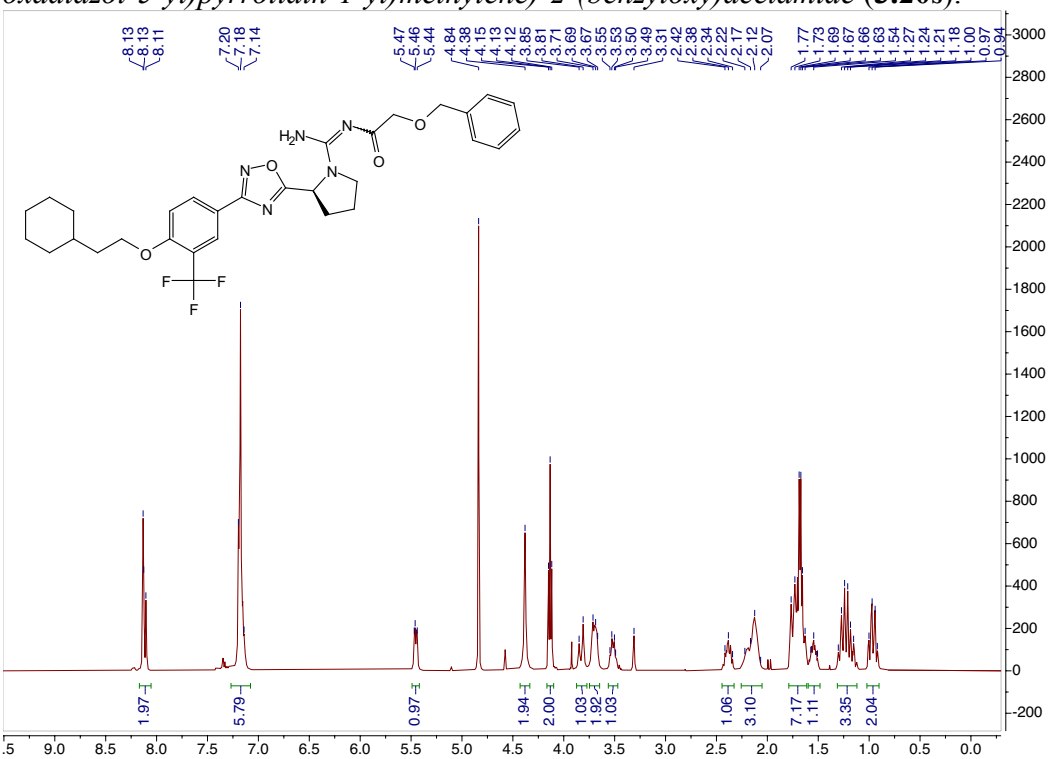

^{13}C spectrum for *(*S*)*-N-*(amino(2-(3-(4-(2-cyclohexylethoxy)-3-(trifluoromethyl)phenyl)-1,2,4-oxadiazol-5-yl)pyrrolidin-1-yl)methylene)-2-(benzyloxy)acetamide* (**3.20s**).

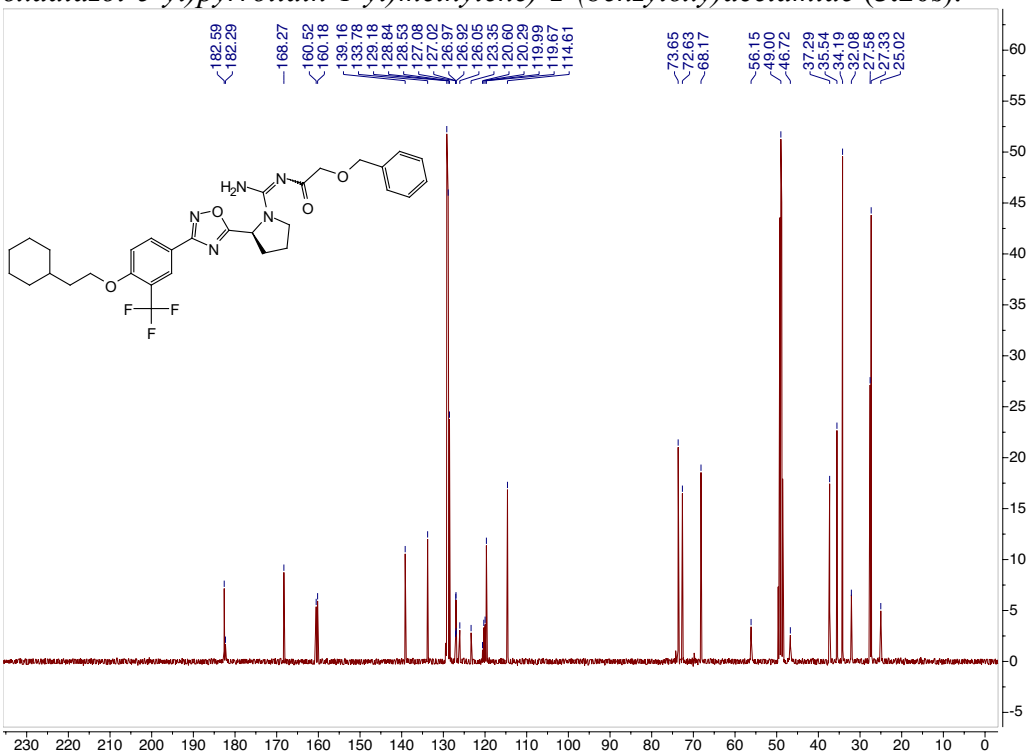

^{1}H spectrum for *(*S*)-2-((amino(2-(3-(4-(2-cyclohexylethoxy)-3-(trifluoromethyl)phenyl)-1,2,4-oxadiazol-5-yl)pyrrolidin-1-yl)methylene)amino)-2-oxoethyl acetate* **(3.20t).**

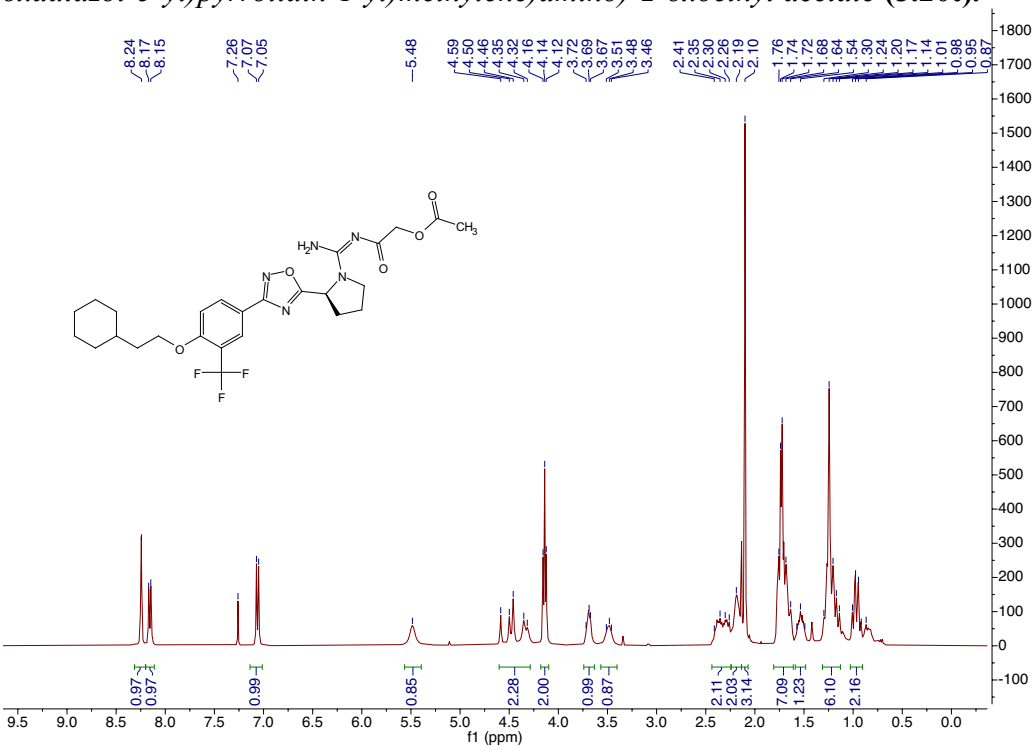

^{13}C spectrum for *(*S*)-2-((amino(2-(3-(4-(2-cyclohexylethoxy)-3-(trifluoromethyl)phenyl)-1,2,4-oxadiazol-5-yl)pyrrolidin-1-yl)methylene)amino)-2-oxoethyl acetate* **(3.20t).**

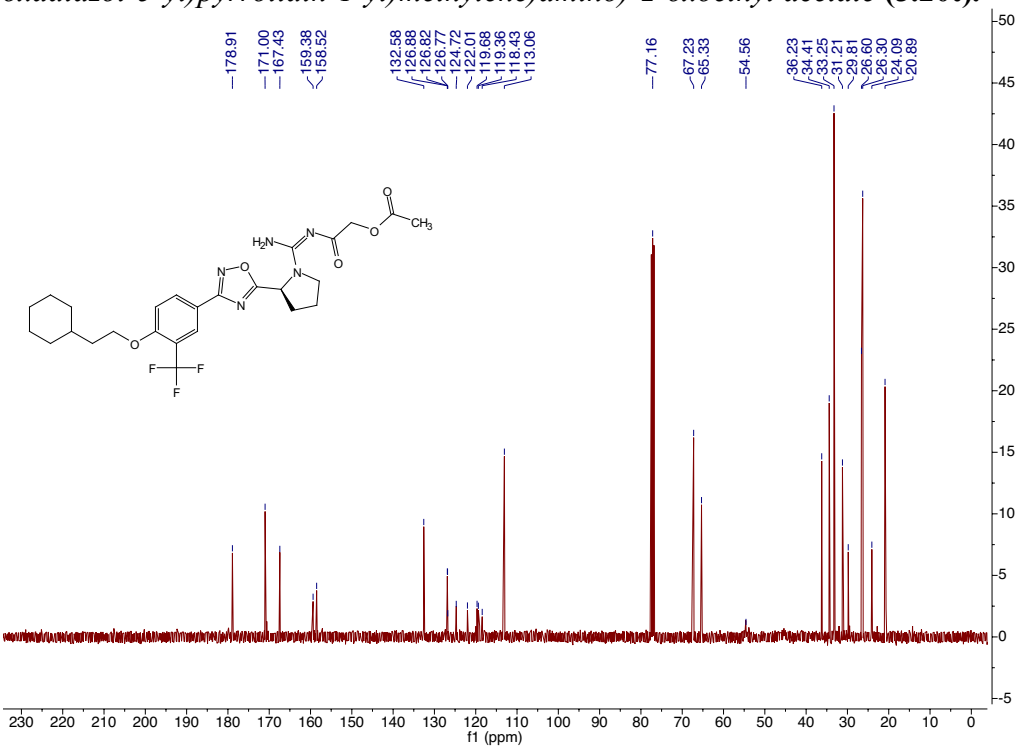

^{1}H spectrum for *(*S*)*-N-*(amino(2-(3-(4-(2-cyclohexylethoxy)-3-(trifluoromethyl)phenyl)-1,2,4-oxadiazol-5-yl)pyrrolidin-1-yl)methylene)-2-ethoxyacetamide* (**3.20u**).

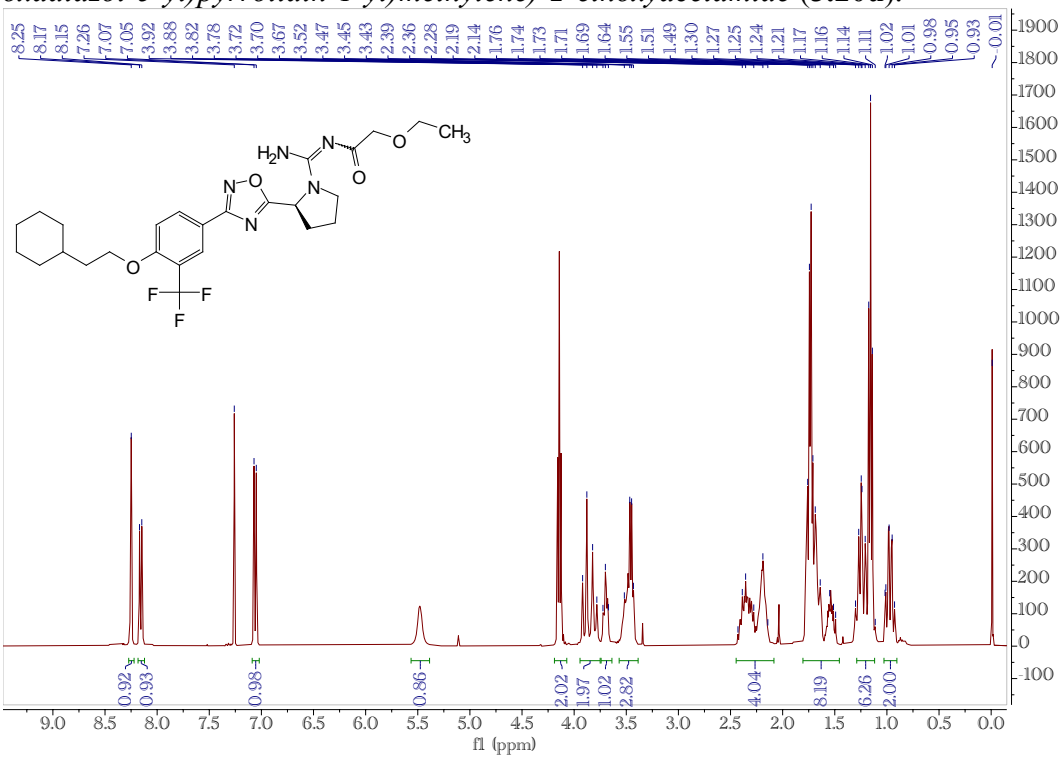

^{13}C spectrum for *(*S*)*-N-*(amino(2-(3-(4-(2-cyclohexylethoxy)-3-(trifluoromethyl)phenyl)-1,2,4-oxadiazol-5-yl)pyrrolidin-1-yl)methylene)-2-ethoxyacetamide* (**3.20u**).

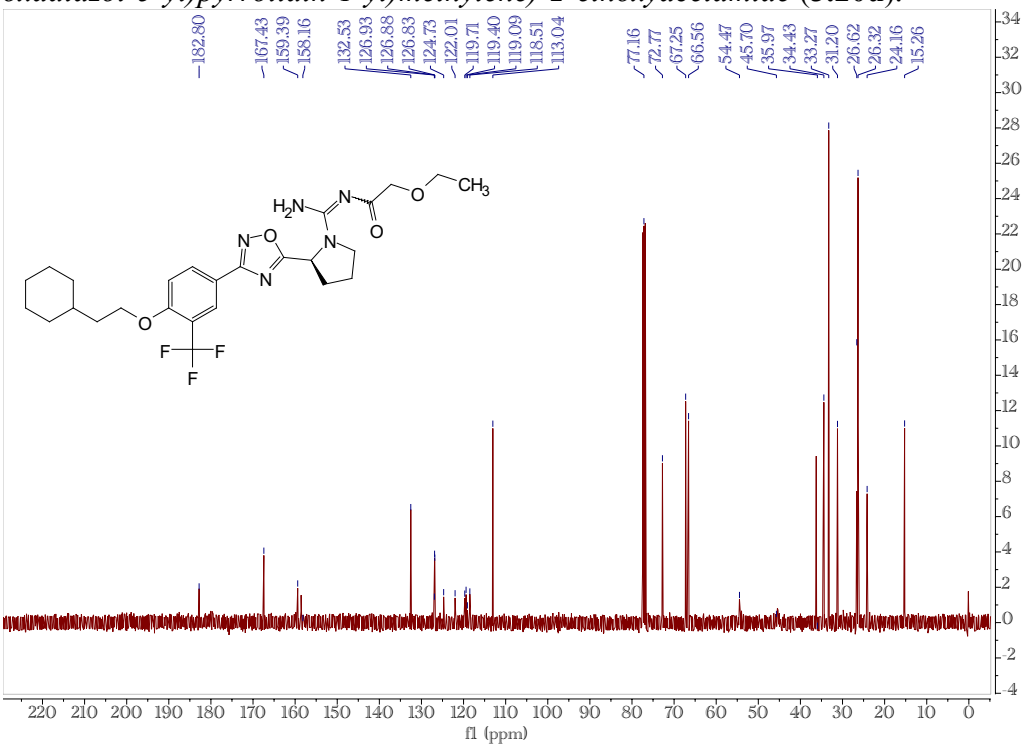

^{1}H spectrum for *(*S*)-2-(3-(4-(2-cyclohexylethoxy)-3-(trifluoromethyl)phenyl)-1,2,4-oxadiazol-5-yl)pyrrolidine-1-carbohydrazonamide* (**3.20v**).

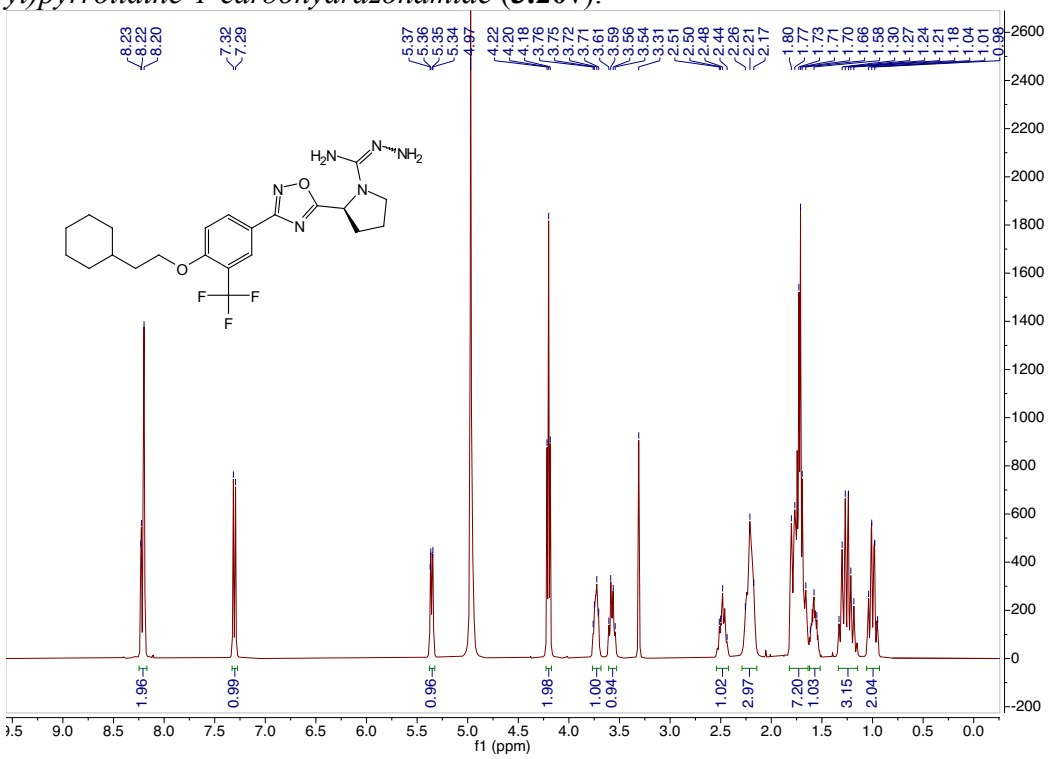

^{13}C spectrum for *(*S*)-2-(3-(4-(2-cyclohexylethoxy)-3-(trifluoromethyl)phenyl)-1,2,4-oxadiazol-5-yl)pyrrolidine-1-carbohydrazonamide* (**3.20v**).

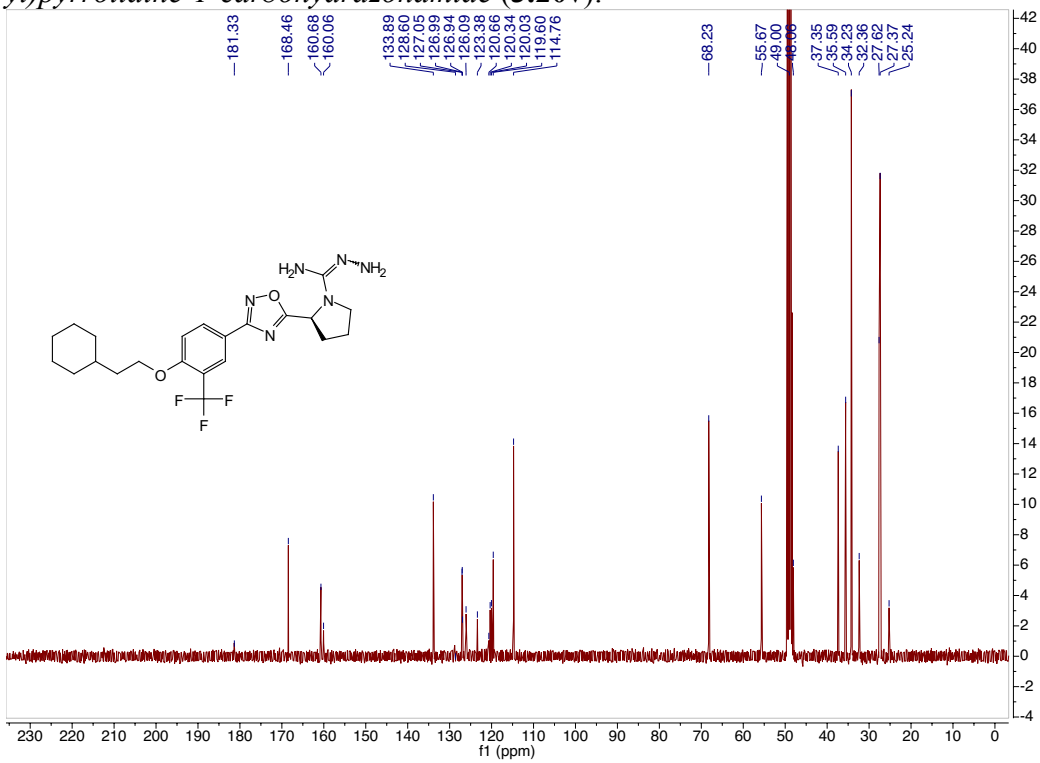

^{1}H spectrum for *(*S*)-2-(3-(4-(2-cyclohexylethoxy)-3-(trifluoromethyl)phenyl)-1,2,4-oxadiazol-5-yl)-*N*′-hydroxypyrrolidine-1-carboximidamide* (**3.20w**).

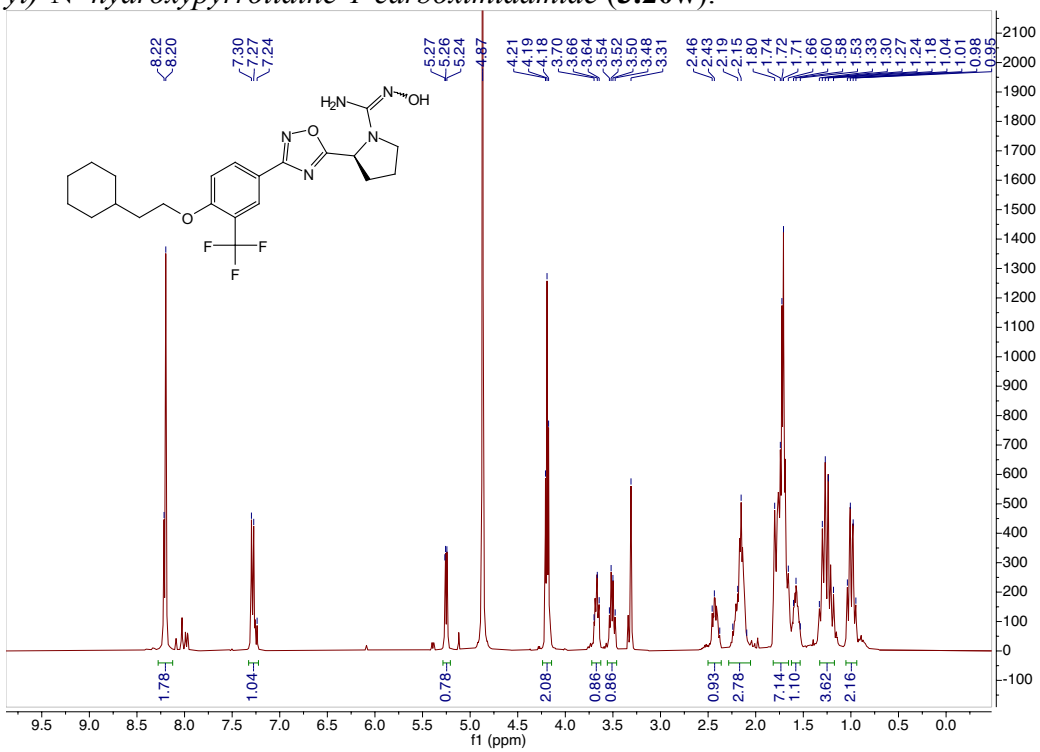

^{13}C spectrum for *(*S*)-2-(3-(4-(2-cyclohexylethoxy)-3-(trifluoromethyl)phenyl)-1,2,4-oxadiazol-5-yl)-*N*′-hydroxypyrrolidine-1-carboximidamide* (**3.20w**).

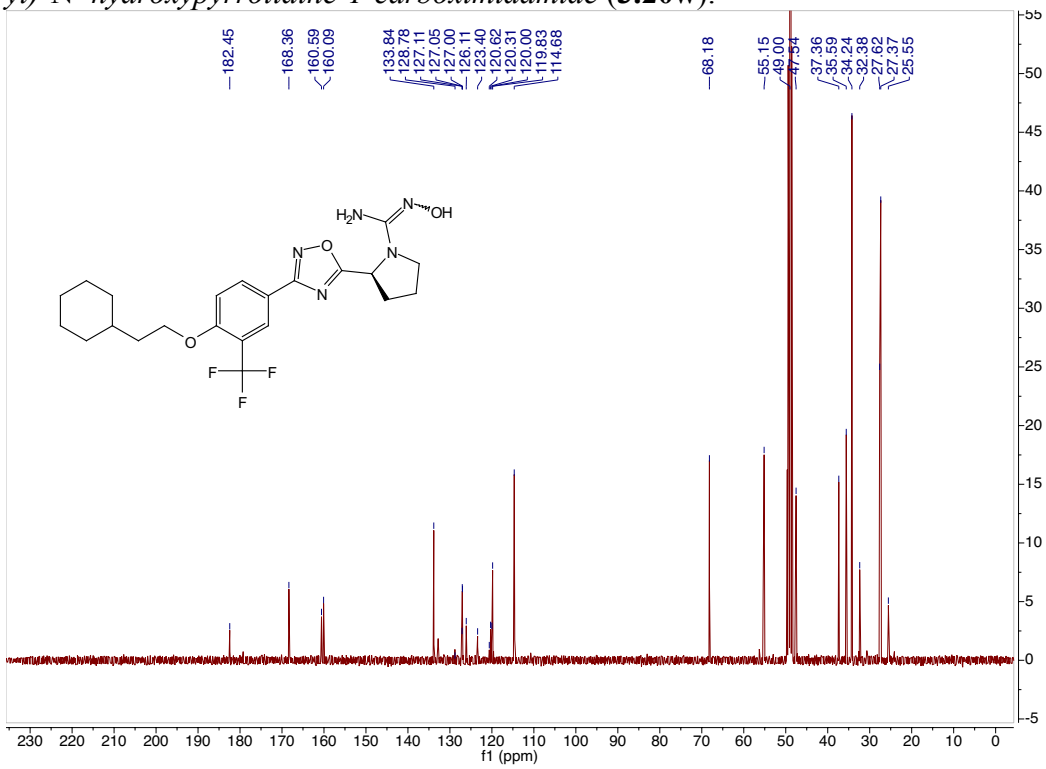

^{1}H spectrum for *(*S*)-2-(3-(4-(2-cyclohexylethoxy)-3-(trifluoromethyl)phenyl)-1,2,4-oxadiazol-5-yl)pyrrolidin-1-ium 2,2,2-trifluoroacetate* (**3.21**).

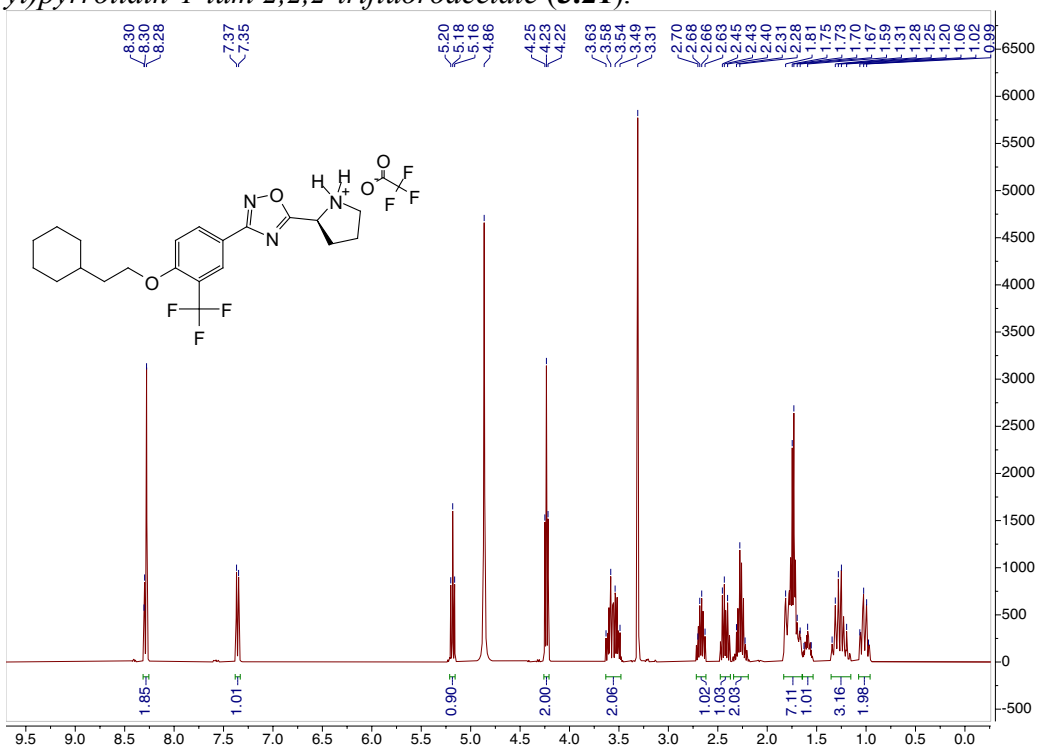

^{13}C spectrum for *(*S*)-2-(3-(4-(2-cyclohexylethoxy)-3-(trifluoromethyl)phenyl)-1,2,4-oxadiazol-5-yl)pyrrolidin-1-ium 2,2,2-trifluoroacetate* (**3.21**).

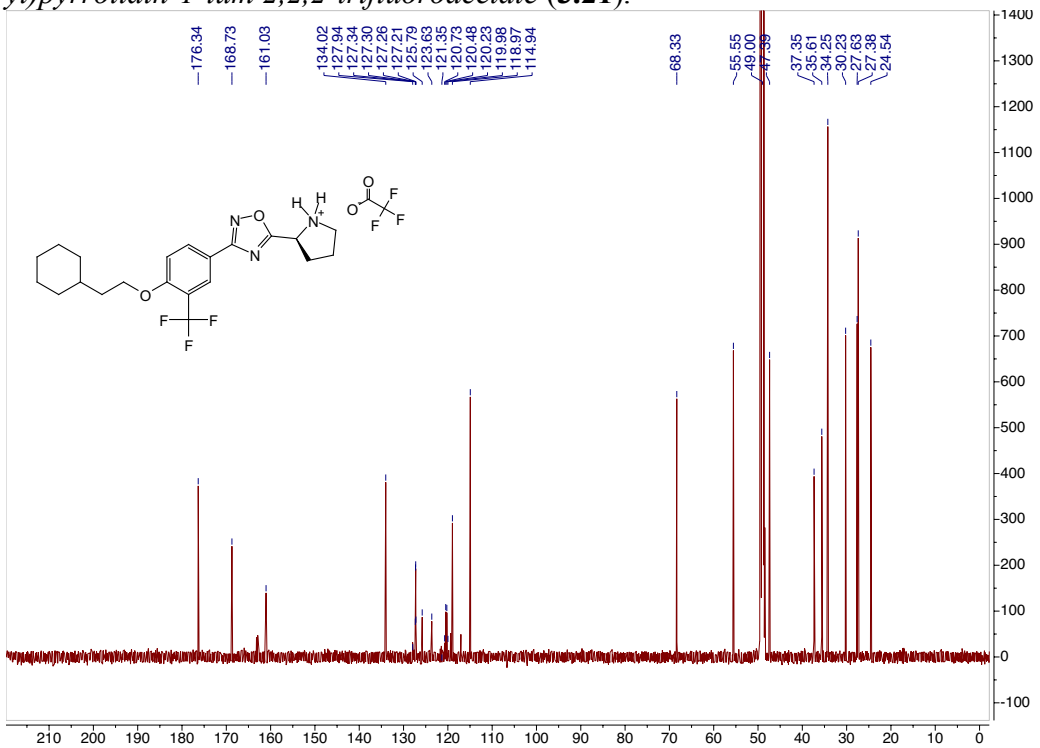

^{19}F spectrum for *(S)-2-(3-(4-(2-cyclohexylethoxy)-3-(trifluoromethyl)phenyl)-1,2,4-oxadiazol-5-yl)pyrrolidin-1-ium 2,2,2-trifluoroacetate* (**3.21**).

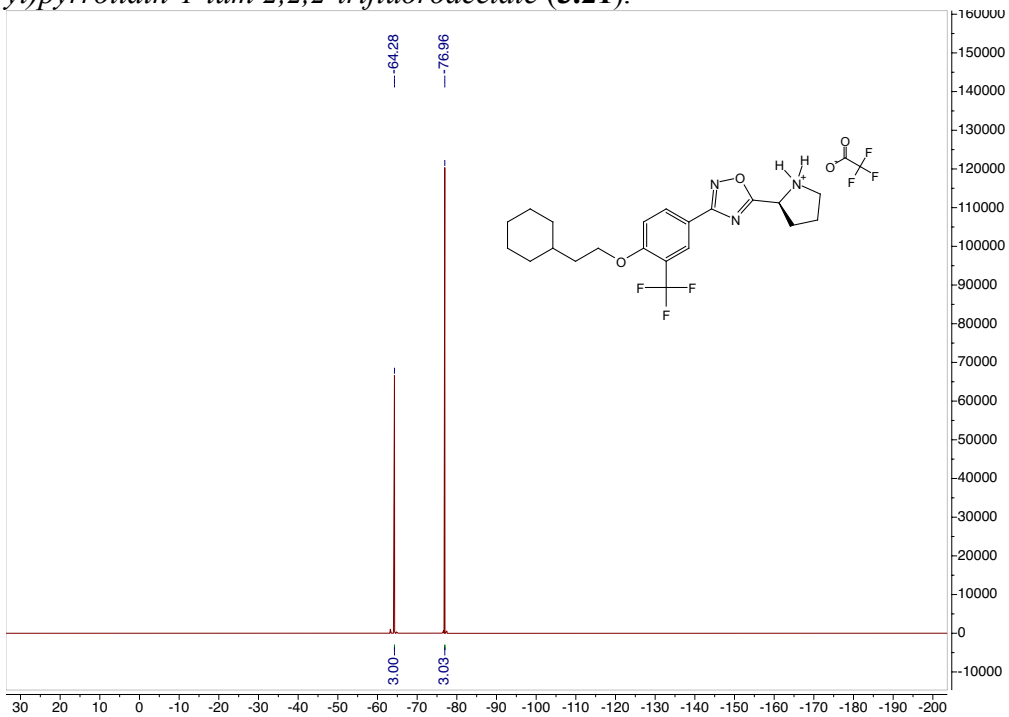

^{1}H spectrum for *(*S*)-2-(3-(4-(2-cyclohexylethoxy)-3-(trifluoromethyl)phenyl)-1,2,4-oxadiazol-5-yl)pyrrolidine-1-carbonitrile* (**3.22**).

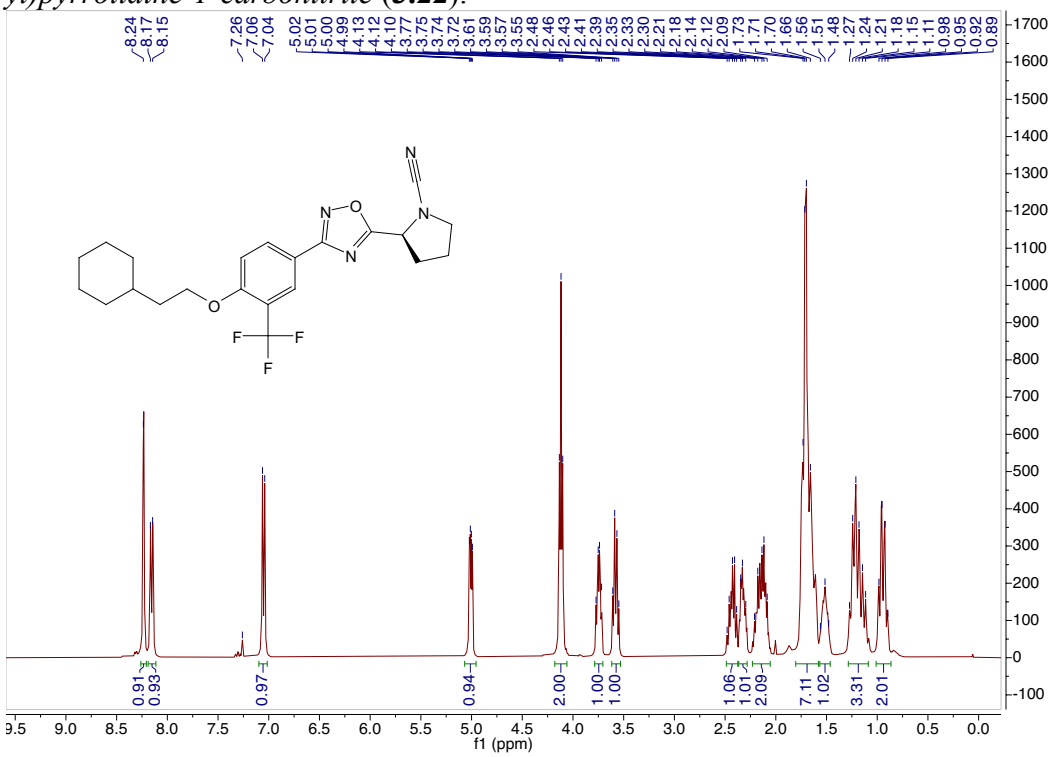

^{13}C spectrum for *(*S*)-2-(3-(4-(2-cyclohexylethoxy)-3-(trifluoromethyl)phenyl)-1,2,4-oxadiazol-5-yl)pyrrolidine-1-carbonitrile* (**3.22**).

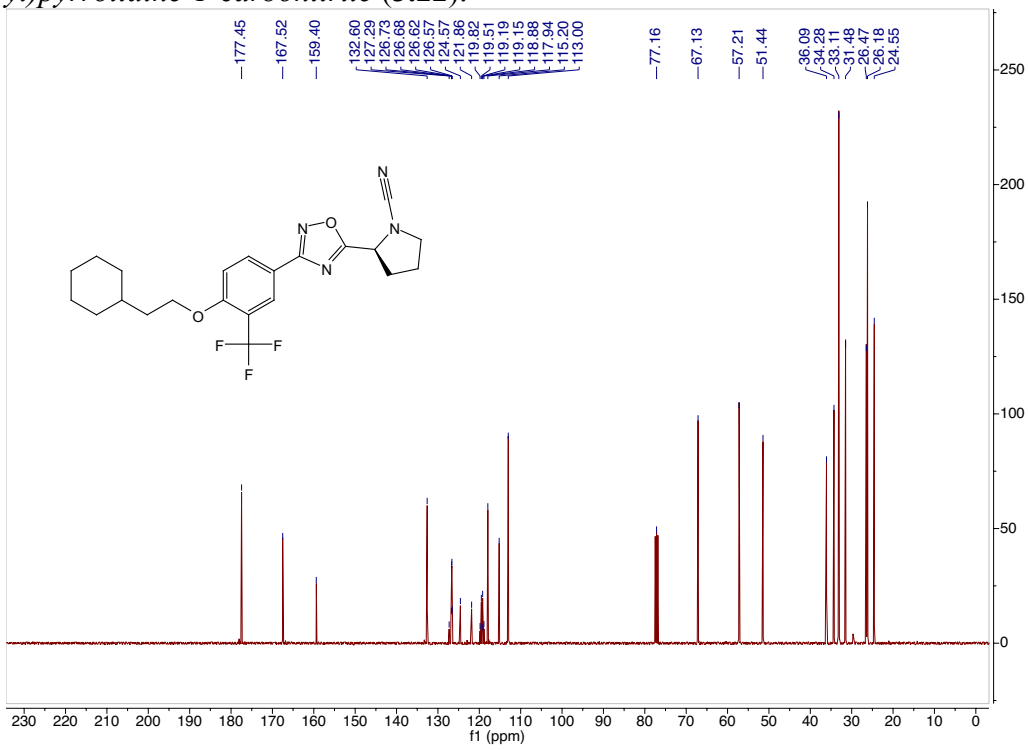

4.4 References

(1) Kharel, Y.; Mathews, T. P.; Kennedy, A. J.; Houck, J. D.; Macdonald, T. L.; Lynch, K. R. A Rapid Assay for Assessment of Sphingosine Kinase Inhibitors and Substrates. *Anal. Biochem.* **2011**, *411*, 230–235.

(2) Patwardhan, N. N.; Morris, E. A.; Kharel, Y.; Raje, M. R.; Gao, M.; Tomsig, J. L.; Lynch, K. R.; Santos, W. L. Structure-Activity Relationship Studies and in Vivo Activity of Guanidine-Based Sphingosine Kinase Inhibitors: Discovery of SphK1- and SphK2-Selective Inhibitors. *J. Med. Chem.* **2015**, *58*, 1879–1899.

(3) Kharel, Y.; Agah, S.; Huang, T.; Mendelson, A. J.; Eletu, O. T.; Barkey-Bircann, P.; Gesualdi, J.; Smith, J. S.; Santos, W. L.; Lynch, K. R. Saccharomyces Cerevisiae as a Platform for Assessing Sphingolipid Lipid Kinase Inhibitors. *PLoS One* **2018**, *13*, e0192179.

(4) Kharel, Y.; Morris, E. A.; Congdon, M. D.; Thorpe, S. B.; Tomsig, J. L.; Santos, W. L.; Lynch, K. R. Sphingosine Kinase 2 Inhibition and Blood Sphingosine 1-Phosphate Levels. *J. Pharmacol. Exp. Ther.* **2015**, *355*, 23–31.

(5) Congdon, M. D.; Kharel, Y.; Brown, A. M.; Lewis, S. N.; Bevan, D. R.; Lynch, K. R.; Santos, W. L. Structure-Activity Relationship Studies and Molecular Modeling of Naphthalene-Based Sphingosine Kinase 2 Inhibitors. *ACS Med. Chem. Lett.* **2016**, *7*, 229–234.

(6) Worrell, B. L.; Brown, A. M.; Santos, W. L.; Bevan, D. R. In Silico Characterization of Structural Distinctions between Isoforms of Human and Mouse Sphingosine Kinases for Accelerating Drug Discovery. *J. Chem. Inf. Model.* **2019**, *59*, 2339-2351.

(7) Morris, G. M.; Huey, R.; Lindstrom, W.; Sanner, M. F.; Belew, R. K.; Goodsell, D. S.;

Olson, A. J. AutoDock4 and AutoDockTools4: Automated Docking with Selective Receptor Flexibility. *J. Comput. Chem.* **2009**, *30*, 2785–2791.

(8) Trott, O.; Olson, A. J. AutoDock Vina: Improving the Speed and Accuracy of Docking with a New Scoring Function, Efficient Optimization and Multithreading. *J. Comput. Chem.* **2010**, *31*, 455–461.

(9) Wang, Z.; Min, X.; Xiao, S.-H.; Johnstone, S.; Romanow, W.; Meininger, D.; Xu, H.; Liu, J.; Dai, J.; An, S.; Thibault, S.; Walker, N. Molecular Basis of Sphingosine Kinase 1 Substrate Recognition and Catalysis. *Structure* **2013**, *21*, 798–809.